Pin1: WW domain ligands, catalytic inhibitors, and the mechanism

By

Ana Y. Mercedes-Camacho

Dissertation submitted to the faculty of the
Virginia Polytechnic Institute and State University
In the partial fulfillment of the requirement for the degree of

Doctor of Philosophy
In
Biochemistry

Felicia A. Etzkorn, chair
David R. Bevan
Peter J. Kennelly
Jianyong Li

May 2011
Blacksburg, VA

Keywords: Pin1, PPIases, Pin1 inhibitors, WW domain ligands, ELEBA, c-Myc, and KIE

Pin1: WW domain ligands, catalytic inhibitors, and the mechanism

by
Ana Y. Mercedes-Camacho

Abstract

The peptidyl prolyl cis/trans isomerase, PPIase, has been the focus of numerous studies in the field of cell cycle regulation since proline-directed phosphorylation is an essential signaling mechanism that might arrest cancer proliferation. Pin1 is the first phosphorylation-dependent PPIase enzyme to be discovered. The Pin1 regulatory mechanism, acting on other mitotic proteins in vivo and in vitro, remains largely unknown. For the study of Pin1 function, two types of assays were used to identity ligands for Pin1: (1) The Enzyme-Linked Enzyme Binding Assay (ELEBA) for the identification of WW domain ligands, (2) a catalytic assay to identified inhibitors of Pin1 catalytic activity. The ELEBA offers a selective approach for detecting ligands that bind to the Pin1 WW domain from chemical libraries. By using the ELEBA, a pSer-Pro peptidomimetic library of 315 ligands was screened, identifying three promising ligands cis-D2, O2, and M18. Competitive K_d values for cis-D2, O2, and M18 were determined to be 263 ± 6.4, 206 ± 3.4, and 130 ± 3.0 μM, respectively. Furthermore, we screened the pSer-Pro peptidomimetic library using a Pin1 discontinuous-catalytic assay to identify inhibitors of Pin1. Ligands D20 and K7 were identified to decrease more than 90% of the Pin1 catalytic activity.

To investigate the nature of the Pin1 interaction with c-Myc, we synthesized and characterized four peptides corresponding to the c-Myc sequence. These peptides were used in NMR isomerization studies of Pin1 by our collaborator Dr. Jeffry Peng (University of Notre Dame). Preliminary work shows that Pin1 binds and isomerizes the Ac–LLPpTPPLSPS–NH_2 peptide at the cMyc pThr58 position.

Finally, we measured a secondary kinetic isotope effect (2º KIE) to study the Pin1 catalytic mechanism of proline isomerization. The ratio of k_H/k_D for unlabeled and [d_3]Ser-labeled substrate gave a SKIE value of 1.34 ± 0.01. The normal 2º KIE value indicates that carbonyl-serine hybridization is not changing from sp^2 to sp^3. This result supports substrate analogue inhibitor studies, and previous solvent and SKIE results on Pin1, that suggest a twisted amide mechanism assisted by a transient hydrogen bond in the transition state.

Acknowledgments

I would like to express my most sincere gratitude to my advisor, Dr. Felicia A. Etzkorn, whose support and expertise were the milestones for this graduate experience. I thank her for sharing with me enormous amount of knowledge and skills in different areas such as science, ethics, and English. I also want to thank Dr. Etzkorn for her assistance in writing research reports, grant proposals, manuscripts, and this dissertation.

I would like to thank members of my committee; Dr. David Bevan, Dr. Erin Dolan, Dr. Richard Helm, Dr. Peter Kennelly, and Dr. Jianyong Li for their scientific input into my projects, and for taking time out from their busy schedules to serve as my committee members during committee meetings, preliminary exam, proposal defense, seminars, and to serve as external readers.

Very special thanks go out to Dr. Ed Smith, for giving me the opportunity to participate in the Post-Baccalaureate Research and Education Program (PREP) and become a PREP-scholar. I would like to thank Dr. Jeffry Peng (University of Notre Dame) for his scientific input into my projects, and NMR experiments. Appreciation also goes out to the administrative group in the biochemistry and chemistry departments, especially Sheila Early and Thomas Bell.

I would like to thank Dr. Etzkorn's graduate students: Xiaodong Wang, Ashley Mullins, Boobalan Pachaiyappan, Guoyan Xu, Song Zhao, Nan Dai, Xingguo Chen, Jennifer Przybyla, Jia Jia Li, Onyi Freeman, Alex Rich, and Keith Sutyak for their contributions and valuable suggestions on my talks and experimental concerns during our weekly group meetings. I also, want to thank Dr. Dennis Dean and his group members, especially, Valerie Cash for teaching me fundamental molecular biology techniques during my research in their labs. In addition, I thank Marlyn Cotty Mas for her unconditional support and valuable suggestions, and Mehdi Ashraf-Khorassani in chemistry department for his help with the LC-MS/MS sample analysis.

I would also like to thank my family and friends for their support during this graduate experience. I must say that without my family's love and encouragement, I would not have finished this path in my education. Finally, the last but not the least, I must thank God because he gives me strength during this exciting graduate experience.

I want to dedicate this dissertation to my family for always believing in me and giving me the support and motivation for me to pursue this path in my education.
with special dedications to:

Ana M. Camacho (my mother), Martin F. Leyva (my husband), and Jakov Y. Leyva (my son)

TABLE OF CONTENTS

LIST OF FIGURES

LIST OF SCHEMES

LIST OF TABLES

List of Abbreviations

Amino acids

Ala, A = Alanine

Asn, N = Asparagine

Asp, D = Aspartic acid

Arg, R = Arginine

Cys, C = Cysteine

Gln, Q = Glutamine

Glu, E = Glutamic acid

Gly, G = Glycine

His, H = Histidine

Ile, L = Isoleucine

Leu, L = Leucine

Lys, K = lysine

Met, M = Methionine

Phe, F = Phenylalanine

Pro, P = Proline

Ser, S = Serine

Thr, T = Threonine

Trp, W = Tryptophan

Tyr, Y = Tyrosine

Val, V = Valine

Xaa, X = Any naturally occurring amino acid

Yaa, Y = Any naturally occurring amino acid

p = phosphoryl

pSer-Pro, pS-P = phosphoSerine-Proline

pThr-Pro, pT-P = phosphoThr-Proline

PTM = post-translational modification

Proteins

APIases = Secondary–amide cis/trans isomerases

APP = Amyloid precursor protein

Bcl-2 = B-cell leukemia/lymphoma 2

BSA = Bovine serum albumin

CAK = cAMP-dependent kinases

CCRPs = Cell cycle regulatory proteins

CDK = Cyclin dependent kinase

Cdc25c = Cell cycle dual-specific phosphatase

CyP = Cyclophilin

ERKs = Extracellular-regulated kinases

FHA = Forkhead-associated domain

FKBPs = FK-506 binding proteins

JNKs = c-Jun N-terminus kinases

HRP = Horseradish peroxidase

Hsp70 = Heat shock 70 kDa protein (DnaK)

I-2 = Phosphatase inhibitor-2 protein

MAPKs = Mitogen activated protein kinases

Myc = Proto-oncogene protein Myc

Myt1 = Myelin transcription factor 1

NIMA = Never in mitosis A

p21, p73, and p53 = proteins related to the p53 tumor suppressor protein

PK-A = Protein kinase A

Pin1 = PPIase interacting with NIMA1

Pin1–HRP = Recombinant human Pin1 chemically conjugated to HRP

Plx1 = Polo-like kinase 1

PP2A = Protein phosphatase-2A

PPIase = Peptidyl-prolyl cis/trans isomerase

SH2/3 = Src homology domain 2 and 3

Wee1 = Wee1-like protein kinase

WW = Pair of tryptophans

PBP = Phosphate-binding pocket

PTB = Phosphotyrosine-binding domain

Cell cycle phases

G_1 = Gap preparation for chromosome replication

S = DNA replication

G_2 = preparation for mitosis

M = Mitosis

Reagents and techniques

Ac = Acetyl

AMC = 7-amino-4-methycoumarin

Bn = Benzyl

Boc = *tert*-butoxycarbonyl

$(Boc)_2O$ = Di-*tert*-butyl dicarbonate

CsA = Cyclosporin A

DCC = *N*, *N*-dicyclohexylcarbodiimide

DIEA = Diisopropylethylamine

DMAP = 4-(dimethylamino)pyridine

DMF = *N*,*N'*-dimethylformamide

EDC = 1-[3-(dimethylammino)propyl]-3-ethylcarbodiimide hydrochloride

Fmoc = 9-fluorenylmethoxy-carbonyl

FK-506 = Tacrolimus, previously known as FK-506, is a macrolide immunosuppressant produced by Streptomyces tsukubaensis

HATU = *O*-(7-azabenzotriazol-1-yl)-*N,N,N′,N′*-tetramethyluronium hexafluorophosphate

HBTU = *O*-(benzotriazol-1-yl)-*N,N,N′,N′*-tetramethyluronium hexafluorophosphate

HEPES = (4-(2-hydroxyethyl)-1-piperazineethanesulfonic acid)

HOAt = 1-hydroxy-7-azabenzotriazole

HOBt = 1-hydroxybenzotriazole

HTS = High-throughput screening

Juglone = 5-hydroxy-1,4-naphthoquinone

LC-MS = Liquid chromatography–mass spectrometry

MBHA, Rink amide = 4-Methylbenzhydrylamine resin

NMP = *N*-methyl-2-pyrrolidone

NMR = Nuclear magnetic resonance

NOS = *N*-oxysuccinimide ester

OD = Optical density

*p*NA = *p*-nitroanilide

Pbf = 2,2,4,6,7-pentamethyldihydrobenzofuran-5-sulfonyl

PBS = Phosphate-buffered saline

RP-HPLC = Reverse-phase high-pressure liquid chromatography

SPPS = Solid-phase peptide synthesis

TBAF = Tetrabutylammonium fluoride

TBS = *tert*-butyldimethylsilyl

THF = Tetrahydrofuran

TFA = Trifluoroacetic acid

TIPS = Triisopropyl silane

TLC = Thin layer chromatography

TMB = 3,3′,5,5′-tetramethylbenzidine

Terms

IC_{50} = Inhibitory concentration, 50%

ED_{50} = Effective dose, 50%

ELISA = Enzyme-Linked ImmunoSorbent Assay

HeLa cell = Immortal cell line derived from cervical cancer taken from a patient named Henrietta Lacks.

k_{cat} = Catalytic rate constant

K_d = Binding dissociation constant

K_m = Michaelis-Menten constant

k_{cat}/K_m = enzyme catalytic efficiency

k_3 = Non enzymatically catalyzed isomerization

$[M+H]^+$ = Parent molecular ion

$[M+H]^{2+}$ = Doubly charged parent molecular ion

M_r = Relative molecular mass, is the ratio of the mass of that molecule to 1/12 of the mass of carbon-12.

Chapter 1

Introduction and Background

1.1 Peptidyl–Amide Isomerization

Peptide bonds populate two distinct conformations: the cis and the trans [1]. The trans conformation has 99.9% abundance, and it is energetically favorable with the omega torsion angle (ω) of 180° for the αCn–αCn'+1 (n' = any amino acid (Xaa), except proline) [1, 2]. When n' is a proline, the cis conformation has 10-40% abundance. The cis conformation (ω = 0°) and the trans conformation (ω = 180°) are both thermodynamically stable with a Gibbs free energy difference (ΔG) of ca. 1.5 kcal-mol^{-1} [1, 3].

Peptidyl–amide cis-trans isomerization is the rate-determining step for polypeptide unfolding with a relaxation time of 1-100 sec^{-1} [4, 5]. In vitro, the kinetics of prolyl isomerization is influenced by physical and chemical variables, such as acidic pH and temperature. However, in vivo at pH 7.3 and 37 °C, the peptidyl–amide cis-trans isomerization is catalyzed enzymatically.

1.2 Peptidyl cis-trans isomerases in biology

The peptidyl cis-trans isomerases specifically catalyze secondary amide isomerization, thereby restoring the thermodynamic equilibrium in a system in which the equilibrium has been upset [6]. Peptidyl isomerases leave unaltered the chemical constitution of the peptide bond, demonstrating the difficulty of peptidyl–amide isomerization as a spontaneous process in protein folding [6, 7]. Peptidyl isomerases are classified in two super-families: 1) the secondary–amide cis-trans isomerases (APIases), and 2) the peptidyl–prolyl cis-trans isomerases (PPIases). The primary function of APIases is to catalyze the cis-trans isomerization of peptidyl–nonprolyl

peptide bonds [8]. The heat-shock 70 kDa protein, DnaK, was the first member of this novel class of enzymes, which was discovered by Schiene-Fischer et al. in 2002 [8].

The second category of peptidyl isomerases is the peptidyl–prolyl cis-trans isomerases (PPIases) that catalyze the cis-trans isomerization of the peptidyl–prolyl peptide bond (Scheme 1.1) [6]. Fischer et al. identified the first member of this family, cyclophilin A (CyPA), in 1984 using a cyclosporin (CsA)-affinity column. Shortly thereafter, two independent groups identified FK506 binding protein (FKBP)-12, and more recently Pin1 [6, 9, 10, 11].

Scheme 1.1. The peptidyl–prolyl cis-trans isomerization catalyzed by PPIase.

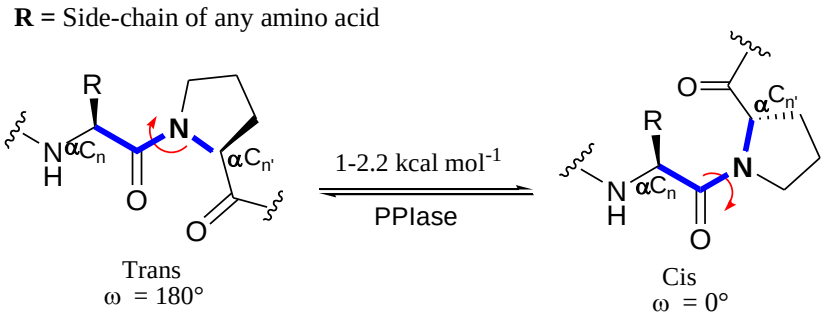

The PPIases are divided in three subfamilies: (1) the cyclosporin A (CsA)-binding proteins, cyclophilins (CyP) [6], (2) the FK506 binding proteins (FKBPs) [9], and (3) the parvulins, which do not bind immunosuppressant drugs [10, 11]. The FKBP12-FK506 and the CyP18-CsA immunosuppressant complexes share a common inhibition target, the Ser/Thr-protein phosphatase calcineurin, which dephosphorylates substrates in the signal transduction pathway leading to T-cell activation [12, 13, 14]. The FKBP12-FK506 and the CyP18-CsA complex inhibition of calcineurin are independent of their isomerase activity [15].

PPIases are redundant enzymes with a wide range of substrates, unique reaction profiles (multiple Xaa-Pro sites in a single substrate), and domain compositions. PPIases share a high

degree of conservation in their 3D structure rather than in their linear sequence of amino acids (Fig. 1.1). Moreover, it is difficult to assigned specific cellular functions to them because of their poorly defined mechanisms of catalysis. Despite the enigmatic role of PPIases, research confirms their participation in numerous cellular processes, such as immune responses, protein folding, cell cycle progression, apoptosis, neurological changes associated with Alzheimer's disease, and other cellular changes (Table 1.1) [7, 11, 16, 17, 18]. In eukaryotes, multiple gene copies are present, which indicate their cellular relevancy [19, 20]. In yeast, the knockout of the twelve PPIase genes, eight corresponding to cyclophilins and four to FKBPs, do not generate a particular phenotype [14]. Humans have 33 genes that encode PPIases; 16 genes for cyclophilins, 15 genes for FKBPs, and 2 genes for parvulins—the latter being in low frequency in comparison with CyPs and FKBPs [19]. Parvulins appear to have evolved from the same ancestral gene of CyPs and FKBPs about 3.5 billion years ago [17].

Table 1.1. PPIases identified in the three kingdoms of life, and their different cellular functions[11, 19, 20, 21].

PPIase	Functions	Kingdom
Cyclophilins	Apoptosis, ion channel, folding, virulence, T-cell activation	Eukaryotic
FKBPs	Hormonal response, ion channel, folding	Eukaryotic
Pin1, ESS1	Apoptosis, Alzheimer disease, immunoresponse, asthma	Eukaryotic
RanBP2, Nup358	Nuclear pore transport	Eukaryotic
NinaA	Folding	Eukaryotic
Trigger Factor	Folding	Prokaryotic
MIP	Virulence	Prokaryotic
HcCyP19, MbtCyP15	Environmental stress tolerance	Archaea

```
P62937|7-163    ---FFDIAVDGEPLG-RVSFELFADKVPKTAENFRALS----------------------T 35   Human-CyPA
tr|O50586|      --MPVDATVHTS-EG-EFDIELYDERAPRTVENFLNLARHEPAADADPAPDTVTWEDPES 56   H. cutirubrum.–CyP19
P0A850|161-246 -----EDRVTIDFTG-SVDGEEFEG--GKASDFVLAMG---------------------- 30   E.coli-trigger factor
Q02790|50-138   -----GDRVFVHYTGWLLDGTKFDSSLDRKDKFSFDLG---------------------- 33   human-FK506
Q13526|52-163   PARVRCSHLLVKHSQSRRPSSWRQEKITRTKEEALELIN---------------------- 39   Human-Pin1

P62937|7-163    GEKGFG--YKGSCFHRIIPGFMCQGGDFTRHNGTGGKSIYGEKFEDENFILKHTGPGILS 93   Human-CyPA
tr|O50586|      GEIRGDSLYAGVSFHRIIEGFMIQGGDPTGTGRGGPGYEFADEFHDD---LTHDGPGVLS 113  H. cutirubrum.–CyP19
P0A850|161-246 ---------QG----RMIPGF--EDG--IKGHKAGEEFTIDVTFPEE-----YHAENLK- 67   E.coli-trigger factor
Q02790|50-138   ---------KG----EVIKAWDIAIATMKVGEVCHITCKPEYAYGSA-----GSPPKIP- 74   human-FK506
Q13526|52-163   -----GYIQKIKSGEEDFESLASQFSDCSSAKARGDLGAFSRGQMQKP--FEDASFALRT 92   Human-Pin1

P62937|7-163    MANAGPNTNGSQFFICTAKTEWLDGKHVVFGKVKEGMNIVEAMERFGS-RNGKTSKKITI 152  Human-CyPA
tr|O50586|      MANSGPDTNGSQFFITLDAQPHLDGRHAVFGAVTDGMDVVETIGDVETDANDAPASEITI 173  H. cutirubrum.–CyP19
P0A850|161-246 ----G---KAAKFAINLKK---VEERELP------------------------------- 86   E.coli-trigger factor
Q02790|50-138   --------PNATLVFEVEL---FEFK---------------------------------- 89   human-FK506
Q13526|52-163   GEMSGPVFTDSGIHIILRTEHUMANFKBP------------------------------- 121  Human-Pin1

P62937|7-163    ADCGQ-- 157                                                    Human-CyPA
tr|O50586|      DRVEIHE 180                                                    H. cutirubrum.–CyP19
P0A850|161-246 -------                                                        E.coli-trigger factor
Q02790|50-138   -------                                                        human-FK506
Q13526|52-163   -------                                                        Human-Pin1
```

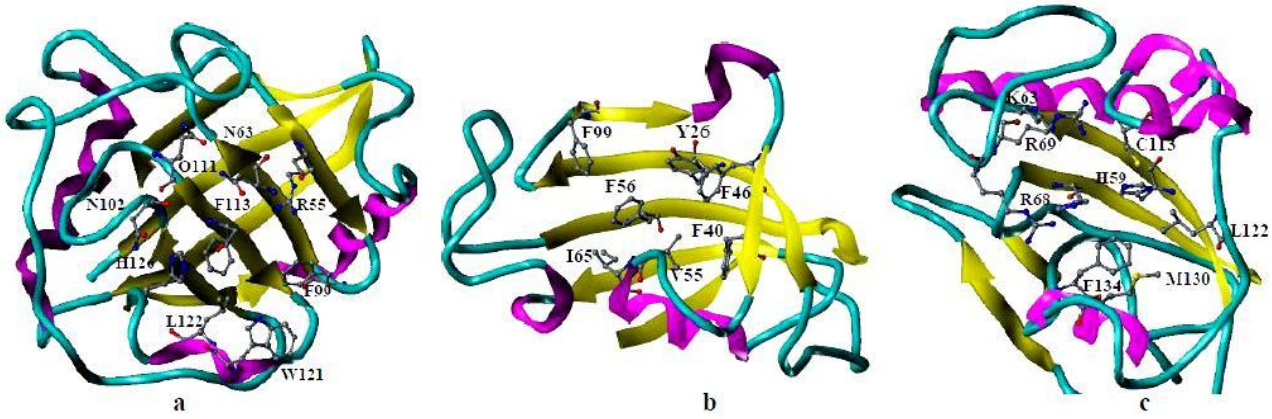

Fig. 1.1. Sequence alignment of PPIase domains and 3D structures. Top: multiple sequence alignment of PPIase domains in some PPIase members show a small degree of amino acid conservation among members, a high degree of amino acid conservation (blue), and a low degree of amino acid conservation (yellow). Bottom: a) 3D structures of CyPA (3K0N, 18 kDa) [22], b) FKBP-12 (2PPN, 12 kDa) [23], and c) Pin1 (1PIN, 18 kDa) [24] show a higher degree of homology in 3D-fold than in their linear sequence of amino acids. The residues involved during substrate recognition are displayed via the ball and stick model, random coils (blue), α-helixes (magenta), and β-sheets (yellow). (Prepared with UnitPro- CLUSTAL 2.0.10 and Sybyl 8.1.)

1.3 Pin 1: a new switch for proline isomerization

Protein interacting with NIMA-1 (Pin1) is a member of the parvulin family. Parvulins are noted for their two conserved histidine motifs (**His**–Xaa–Val/Leu–Xaa–Lys and Gly–Xaa–Ile–**His**–Ile/Val–Leu) (Fig. 1.2) [5]. Pin1 was discovered in a yeast-two hybrid screen while

searching for NIMA substrates [11] in *A. nidulans*, an important fungal system used in molecular biology.

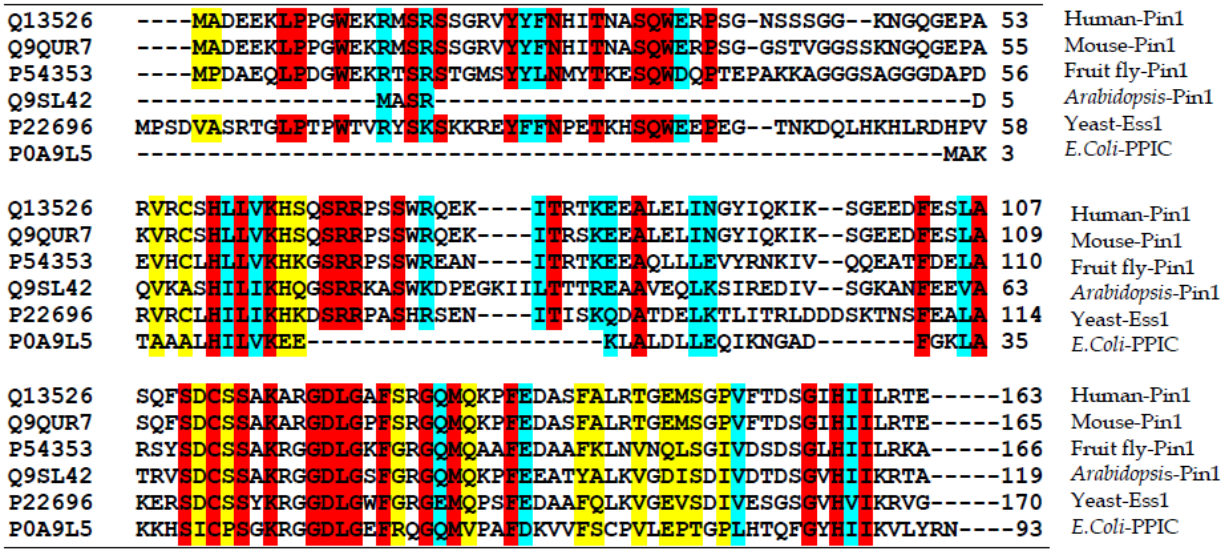

Fig. 1.2. Multiple sequence alignment of Pin1 homologues in some model organisms shows a high degree of amino acid conservation. Conserved residues are shown in red, a high degree of amino acid conservation is shown in blue, and a low degree of amino acid conservation is represented by yellow. (Prepared with UnitPro- CLUSTAL 2.0.10)

Pin1 is a two-domain protein in a single polypeptide of 163 amino acid residues (NCBI accession #: AAC50492). Pin1 catalyzes the cis-trans isomerization of the pSer/pThr–Pro motif (Scheme 1.2). The sterically hindered pSer/pThr decreases the rate of cis-trans isomerization of the prolyl-amide bond by approximately 4- to 8-fold [5, 25]. The Pin1 catalytic site is located at the C-terminus (PPIase domain, residues 45-163) connected by a random coil of 11 amino acids to a protein-protein binding domain at the N-terminus (WW domain, residues 1-39) (Fig. 1.3) [11, 24, 26]. In solution, no inter-domain interaction is observed, together, the domains create a cavity of ca. 22Å [24]. Peng and co-workers have shown that a Pin1 ligand from Cdc25, EQPLpTPVTDL, affects the dynamics of Pin1 side chains at the hydrophobic interface between the WW domain and the catalytic domain [27]. Upon ligand binding, however, a conformational change of Pin1 occurs that brings both domains in close proximity with weak interactions [28].

Scheme 1.2. The pSer–prolyl cis-trans isomerization catalyzed by Pin1.

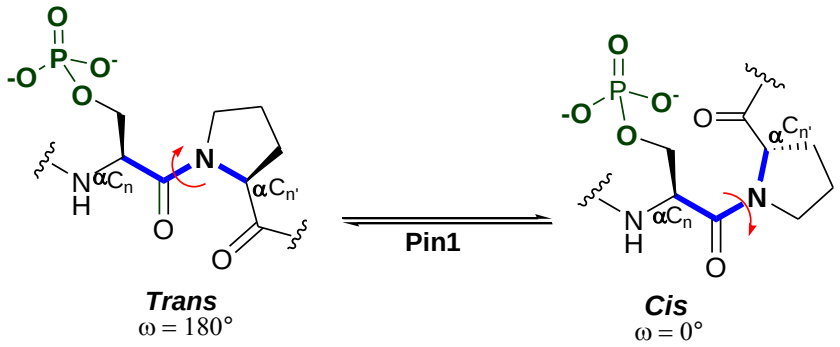

1.4 Pin1 PPIase domain

The PPIase domain folds into four anti-parallel β-sheets, four α-helixes, and a β-barrel, forming a deep cavity capable of accommodating the pSer/pThr–Pro-containing substrates [24]. A hydrophobic cluster containing Leu122, Met130, His157, and Phe134 creates the proline-binding pocket, which is flanked at opposite ends with basic and acidic residues (Fig. 1.3) [24, 29]. The presence of an unstructured loop (the catalytic loop, residues 66-77) plays a critical role in recognizing the pSer/pThr, and in Pin1 cellular distribution [30]. The basic cluster contains Lys63, Arg68, and Arg69 and acts as an active-site gateway for entry of the negatively charged phosphorylated substrates [24, 29]. The mutation of Lys63 to Ala weakens the strength of the Pin1 interaction with phosphorylated peptide, while mutations of Arg68 or Arg69 deactivate Pin1 specificity for the phosphate moiety of pSer/pThr without compromising enzymatic activity [31]. In addition, mutations of either Arg68 or Arg69 prevent Pin1 from entering into the cell nucleus by blocking Pin1 interaction with Importin-α5, which facilitates nuclear import [30]. This nuclear import was independent of Pin1 PPIase activity [30]. A second hydrophobic cluster containing Ile96, Phe103, Met146, and Leu160 is on the back of the PPIase domain, creating a hydrophobic patch capable of interacting with hydrophobic molecules [24].

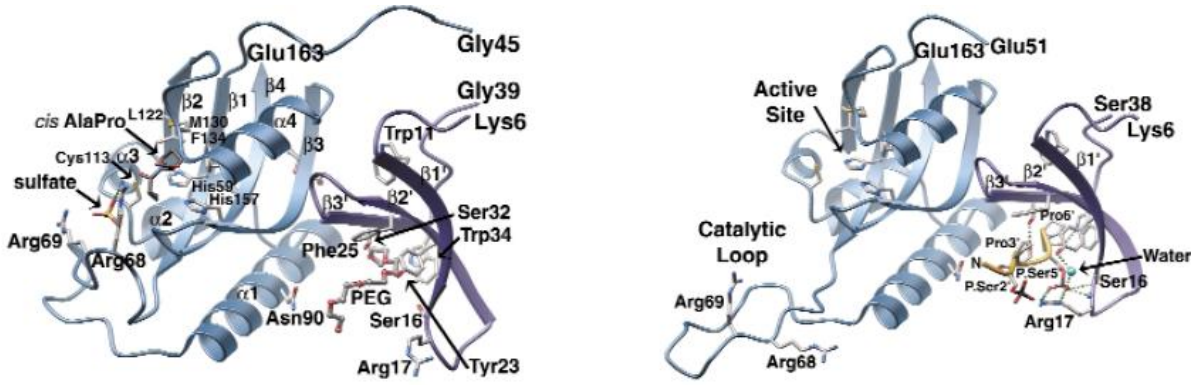

Fig. 1.3. Pin1 crystal structure, showing the two-domains. The catalytic site is located at the PPIase domain, residues 45-163 and connected by a random coil of 11 amino acids to the WW domain, residues 1-39 (right). The Pin1 WW domain fold creates two hydrophobic clusters in opposite β-strands capable of binding ligands. Reprinted by permission from Macmillan Publishers Ltd: Nature Structural Biology (7, 639-43, 2000), copyright (2000) [32].

1.5 Pin1 WW domain

WW domains are stretches of 38-40 amino acid residues that fold in a stable triple-stranded anti-parallel β-sheet, and participate in protein-protein interactions [33]. WW domains are named after two conserved tryptophan (W) residues that are 20-23 amino acid residues apart from each other (Fig. 1.3) [34]. More than 5886 WW domains have been identified in approximately 3139 proteins; in some cases the WW domain is repeated up to four times in a single protein [35]. WW domains are classified in six groups according to their ligand-binding specificity [36, 37]: Group I binds the Pro–Pro–Xaa–Yaa motifs, where Xaa and Yaa are any amino acid [38]. Group II binds Pro–Pro–Leu–Pro motifs [39]. Group III binds Pro–Gly–Met motifs [40]. Group IV binds pSer/pThr–Pro motifs [41]. Group V binds Pro–Arg motifs, and Group VI binds Pro–Pro–Tyr–pTyr motif [37].

The Pin1 WW domain (Group IV) binds and regulates phosphorylated proteins at different stages of the cell cycle [32, 42]. This binding appears to occur throughout a conserved phosphate-binding pocket present among Pin1 and its homologues (Fig. 1.3) [32]. In the absence

of ligands, the Pin1 WW domain fold creates two hydrophobic clusters in different β-strands. Cluster 1 contains Leu7, Trp11, Tyr24, and Pro37; and Cluster 2 contains Arg17, Tyr23, and Phe25 [32]. When the two clusters come in close proximity, they form a phosphate-binding pocket in the presence of a ligand [32]. The phosphate-binding pocket is capable of interacting with up to five consecutive amino acid residues in small phospho-peptides, and interactions occur with Ser16, Arg17, and Tyr23. In some cases, water facilitates hydrogen bond formation between the oxygen of the phosphate and the hydroxyl group of Tyr23 (Fig. 1.3) [32]. Trp34 keeps the aliphatic side chain of proline well positioned in the trans conformation by van der Waals interactions, which is essential for ligand binding [41, 43].

One attractive feature of the human Pin1 WW domain is its folding stability of ca. 4 kJ mol^{-1} compared to similar WW domains in other parvulins [44]. This stability is due to favorable ionic interactions between the negatively charged side chains of Asp3, Glu4, and Glu5 at the N-terminus, and the positively charged side chain of Lys13 [45]. Both the Lys13 side chain and the negatively charged side chains of amino acid residues at the N-terminus are capable of participating in the ligand binding process [44, 45].

1.6 Postulated mechanisms of prolyl isomerization catalyzed by Pin1

The enzymatic mechanism of prolyl isomerization catalyzed by PPIases remains unknown. Due to the low degree of amino acid similarity in members of the PPIase family, different catalytic mechanisms are possible for each member (Fig. 1.1). Four primary mechanisms for human Pin1 prolyl isomerization have been proposed based on site-directed mutagenesis and various crystallography studies of Pin1 in complexes with inhibitors. These studies have provided a better understanding of the Pin1 active site organization and domain interactions [24, 26, 28, 32, 46].

The first mechanism to be proposed was based on the Pin1 crystal structure in complex with Ala–*cis*–Pro, and a sequestered SO_4^{2-} ion [24]. The short distance between the Cys113 and the carbonyl of the prolyl–amide bond suggested nucleophilic attack on the carbonyl in alanine by the thiolate anion (Fig.1.3). The mechanism associated with the nucleophilic attack of Cys113 was supported by the irreversible inactivation of Pin1 by juglone. Specifically, the Michael addition of juglone at Cys41, Cys69, and Cys113 partially denatures and changes the Pin1 active site, which indicates a difference in reactivity of the electrostatic environment near the Cys113 [47, 48]. Nevertheless, several studies involving the site-directed mutagenesis of C113A, C113S, and C113D mutants decrease k_{cat}/K_m only 123-, 20-, and 6-fold, respectively [24, 31]. In addition, Xu et al. showed that ketoamide inhibitors of Pin1, which are highly electrophilic ketones, and designed for the ideally nucleophilic attack of Cys113 to the ketone group were poor Pin1 catalytic inhibitors with IC_{50} values of 100-200 μM, which suggested that the nucleophilic attack mechanism of Pin1-Cys113 is unlikely to occur during proline-amide isomerization[49].

The second mechanism associated with Pin1-catalyzed prolyl isomerization postulated that either Pin1 or the substrate participates as a hydrogen-bond donor for a twisted-amide or twistase mechanism [50]. Furthermore, the conserved His59 or His157 was suggested to participate as a hydrogen-bond donor to the proline nitrogen, and decrease the double bond character of the peptidyl prolyl-amide to enable it to freely rotate.[ref] A Pin1 mutant of H157L was able to catalyze cis-trans isomerization using the pintide substrate [51]. For CyP18, the twistase mechanism with a transient hydrogen bond is likely to be mediated by Arg55, as evidenced by the fact that a mutation of Arg55 for Ala abolished 95-99% of CyP18 enzymatic activity [15, 52, 53].

The third mechanism suggests that the hydrophobic cavity containing Leu122, Met130, and Phe134 in the Pin1 active site creates a hydrophobic environment with the appropriate dimensions to accommodate the proline side chain [24], in addition to facilitating the twisting of the prolyl–amide bond by electrostatic stabilization [54]. This mechanism was demonstrated for FKBPs, which indicates that the site of the PPIase cavity constitutes the main element for prolyl–amide isomerization [55].

1.7 Pin1: a cell cycle regulator

The eukaryotic cell cycle is controlled by the activation and deactivation of a subset of proteins, often called cell cycle regulatory proteins (CCRPs) [56, 57]. Cyclin-dependent kinases (CDKs) are major proteins that control cell cycle progression, and their activities and levels are regulated by phosphorylation and dephosphorylation [57]. Pin1 plays an important role in cell cycle progression by direct association with CDKs and a subset of CCRPs (Table 1.2.); which direct to the identification of a new post-phosphorylation regulatory mechanism facilitated by Pin1[58, 59, 60].

Table 1.2. Cell cycle regulatory proteins identified as Pin1 binding targets.

Protein	Function	Reference
β-Catenin	Cadherin-associated protein	Pang, et al. 2004 [61]
Bcl-2	Adapter molecular protein	Basu, et al. 2001 [62]
Bcl-xL	Adapter molecular protein	Pathan, et al. 2001 [63]
Cdc2	Cell cycle kinase	Pathan, et al. 2001 [63]
Cdc25c	Cell cycle phosphatase	Shen, et al. 1998 [42]
Cdc27	Cell cycle phosphatase	Shen, et al. 1998 [42]
CENP-F	Centromere protein-F	Lu, et al. 2006 [64]
Che-1	RNA Pol. binding protein	De Nicola, et al. 2007 [65]
CK2	Protein kinase	Messenger, et al.2002 [66]
CyclinD	Cell cycle regulator	Lu, et al. 2002 [60]
CyclinE-Cdc2	Cell cycle regulator	Stanya, et al. 2008 [67]
Daxx	Transcriptional regulator	Ryo, et al. 2007 [68]
I-2	Phosphatase inhibitor	Li, et al. 2007 [69]
Myt1	Cdc2 inhibitory kinase	Shen, et al. 1998 [42]
NFAT	Nuclear factor	Lui, et al. 2001 [70]
NHERF-1	Mitotic rreceptor	He, et al. 2001 [71]
NIMA	Cell cycle kinase	Lu, et al. 1996 [11]
Myc	Transcription factor	Yeh, et al. 2004 [72]
P53 family	Pro/onco-proteins	Lu, et al. 2002 [60]
Pim-1	Ser/Thr kinase	Ma, et al. 2007 [73]
Plk1	Cell cycle Kinase	Lu, et al. 2002 [74]
PML	Cell cycle regulator	Reineke, et al. 2008 [75]
Rab4	Small GTPase	Lu, et al. 2002 [60]
Raf1	Signaling protein	Dougherty, et al. 2005 [76]
RARα	Transcrition factor	Brondani, et al. 2005 [77]
RNaP-II	Transcritional machinary	Verdecia, et al. 2000 [32]
SMRT	Mediator protein	Stanya, et al. 2008 [67]
Survivin	Cell cycle protein	Dourlen, et al. 2007 [78]
Top-II	Cell cycle protein	Xu ,et al. 2007 [79]
Wee1	Cell cycle kinase	Lavoie, et al. 2003 [80]

More than 134 proteins have been identified as Pin1 substrates. Among these proteins, 78% are cell cycle proteins, 14% are transcription factors, 6% are neuronal proteins, and 2% are immune-mediator proteins [35]. The significant number of Pin1 substrates is related to the fact that multiple Ser/Thr–Pro-directed kinases, including the mitogen activator protein kinases (MAPKs), the cyclin dependent kinases (CDKs), and the extracellular-regulated kinases (ERKs) are capable of creating binding sites for Pin1.

Pin1 binds and isomerizes the pSer/pThr–Pro motif in substrate proteins, thus altering their conformation. This conformational change can generate different forms of isomeric-native proteins with different functions, locations, and stabilities [21, 60]. Conversely, specific isomeric-proteins could prevent or be coupled to a sequential post-translational modification (PTM) that could activate or deactivate substrate proteins (Scheme 1.3) [21, 81].

Scheme 1.3. Pin1 regulatory mechanisms. Phosphorylation can acts as an ON/OFF regulatory mechanism by (1) changing protein conformation, (2) altering protein-protein interactions, and (3) modulating steric or charge effects in proteins[82]. After phosphorylation, some proteins can exist in two different conformational native states. The shift from one conformation to another could result in an alternative protein native state with a different cellular function, location, and stability [82]. The interconversion from the cis-trans isomeric forms is catalyzed by Pin1 in living cells [83].

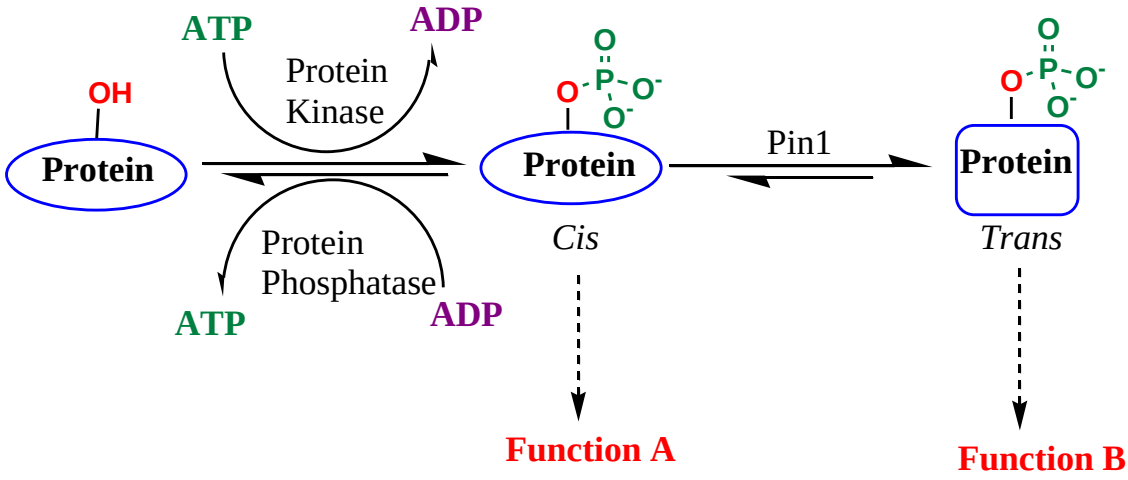

1.8 Pin1 interaction with Cdc25c

To elucidate the nature of Pin1 interactions with phosphoproteins, cyclin D and the dual-specific phosphatase (Cdc25c) have been extensively studied as Pin1-binding partners. Cdc25c is the key activator for the Cdc2/cyclin B heterodimer, which is significant since the activation of this heterodimer is the event that marks the onset of mitosis. During the G_2-to-M transition, Cdc2/cyclin B complex is sequestered in the cytoplasm by Myt1 [58], and it is negatively

regulated by the phosphorylation of Thr14 and Tyr15. Wee1 and Myt1 are the two kinases responsible for these phosphorylations, and therefore Cdc2/cyclin B inhibition, which prevents the early onset of mitosis [84]. Pin1 inhibits Wee1 by binding the pThr186–Pro187 motif [85], and Pin1 binds Myt1 at the C-terminal domain, affecting its interaction with Cdc2/cyclin B [58]. Cdc2/cyclinB becomes active through the removal of inhibitory phosphates by Cdc25c, and the phosphorylation of Thr161 by the cAMP-dependent kinases (CAK) [58]. Furthermore, when levels of active Cdc2/cyclin B decrease in the cell, Cdc25c is feedback-activated by phosphorylation via the polo-like kinase (Plx1) (Fig. 1.4) [58].

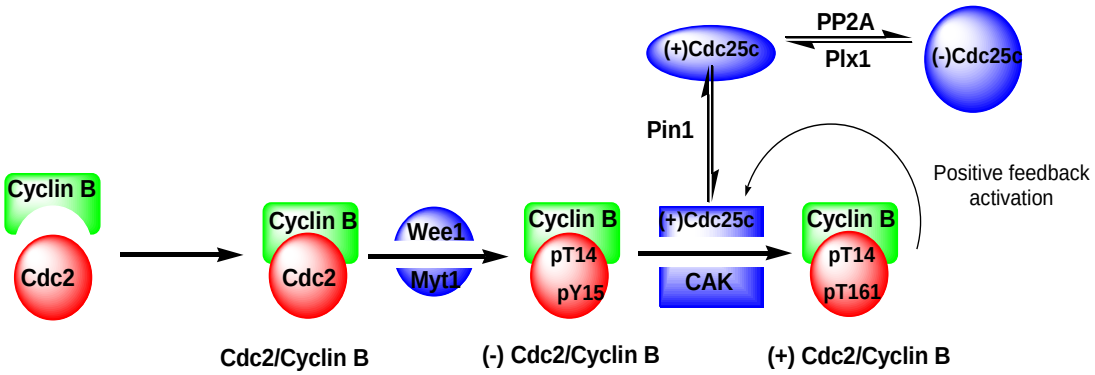

Fig. 1.4. Cdc2 associates with cyclin B forming a Cdc2/Cyclin B complex. The resulting Cdc2/Cyclin B complex is phosphorylated at a pair of inhibitory sites by Wee1 and Myt1 kinases. Then, inactive (-) Cdc2/Cyclin B complex is activated by the phosphatase Cdc25c and CAK. Cdc2/Cyclin B and Plx1 provide positive feedback to activate (+) Cdc25c by phosphorylation[58]. Pin1 binds Cdc25c at different phosphorylation sites altering the Cdc25c conformation, and either facilitating the Cdc25c dephosphorylation by PP2A, or enhancing its phosphatase activity[42, 86].

The N-terminus of human Cdc25c (isoform 1) becomes phosphorylated at six distinct Ser/Thr–Pro motifs [35]; five separate interactions with human Pin1 have been confirmed at pThr48–Pro49, pThr67–Pro68, pThr138–Pro139, pSer168–Pro169, and pSer214–Pro215 motifs [27, 32, 42, 87, 88, 89, 90]. Pin1 binds Cdc25c in a catalytic manner and induces a change in its conformation [42, 86]. Pin1 either enhances or inhibits Cdc25c phosphatase activity depending on its phosphorylation state [42, 86]. In addition, Pin1 enhances the ability of Cdc25c to become

phosphorylated by the Cdc2/cyclin B complex [86], and facilitates the dephosphorylation of Cdc25c via the conformation-specific protein phosphatase-2A (PP2A) (Fig. 1.4) [91]. Understanding the nature of Pin1 interactions with Cdc25c could facilitate the search for new anti-cancer treatments.

1.9 Pin1 in carcinogenesis

Understanding cell growth and controlled cell death by apoptosis is vitally important for advancing cancer treatments, since many forms—such as breast and prostate cancer—demonstrate a high rate of recurrence even after clinical interventions [92, 93, 94]. Cancer cells can undergo a variety of transformations in response to extracellular stress, genetoxic agents, or irradiation. Phosphorylation and dephosphorylation are the most profound mechanisms for signal cascade amplification in response to cellular transformations. Pin1 is linked to cellular events such as cell cycle progression, transcriptional regulation, and cell proliferation by its direct association with multiple proteins that can trigger or block apoptosis (Table 1.2). Moreover, about 52% of human cancers show a high expression of Pin1, and many types of cancers are positively linked to the metastatic stage [93]. In addition, high levels of Pin1 correlate with the overexpression and stability of proteins frequently found in a variety of tumors. They are well documented as oncoproteins, such as c-jun/AP-1, β-catenin/TCF, Bcl-2 antiapototic members, c-Myc, Rab4, Ras, cyclin E, and cyclin D1 [95, 96].

Nearly 15 years ago, Lu et al. (1996) demonstrated Pin1's association with cancer cells by proving that, when Pin1 was depleted in HeLa cells, mitotic arrest ensued, followed by apoptosis [11]. Pin1 was found to be essential for the transition from G_2 through M in *Xenopus laevis* extracts [97]. Research has also shown that mice with a Pin1 knock-out are viable, but developed similar phenotypes to cyclin D deficient mice [94]. Specifically, mice with low levels

of cyclin D showed premature aging, retinal atrophy, and inconsistent neuronal regulation of amyloid disposition [64, 94]. Because Pin1 binds cyclin D1 at the pThr286–Pro287 site, thereby stabilizing cyclin D1 in the nucleus and preventing its degradation in the cytoplasm [64, 98], it is hypothesized that Pin1 might be associated with aberrant-cell proliferation.

Since mutation of the *PIN1* gene has not been identified in either normal or cancer cells, Pin1 is considered to be an oncogenic-signaling activator, rather than an oncogene [99]. Functionally, Pin1 activation is needed for maintaining DNA integrity in response to cell stress by activating and stabilizing pro-oncoproteins such as Che-1, p21, p73, and p53 [64, 65, 78, 100, 101]. Pin1 binds p53 at pSer33–Pro34 and pSer46–Pro47 motifs, thereby altering its conformation and preventing p53 degradation by the E3-ubiquitin ligase [100]. An accumulation of p53 activates the transcription of several pro-oncogenes that arrest uncontrolled cell growth, and triggers the signal for apoptosis [100]. The ways in which Pin1 can participate as either an oncogenic-activator or an oncogenic-suppressor in different cancer cells are not clear and need to be studied in greater detail.

1.10 Pin1 in Alzheimer's disease

Pin1 appears to have a protective role in neuronal development and neuronal integrity. Specifically, Pin1 is down-regulated in the neuronal cells of patients with Alzheimer's disease [102]. In addition, Pin1 binds several important neuronal proteins—such as the Tau protein, which has been the focus of several studies (Table 1.3). Tau is a neuronal protein responsible for microtubule polymerization and stability [102]. Aberrant phosphorylation of Tau is a hallmark of neurodegenerative diseases, such as Alzheimer's, Parkinson's, and dementia [103]. Pin1 has been shown to be capable of binding the Tau protein at the pThr231–Pro232 motif, thereby facilitating Tau dephosphorylation by the protein phosphatase 2A (PP2A) [102]. Pin1 catalyzes

the cis-trans isomerization of pThr231-Pro232; PP2A then recognizes the trans isomer, removes the phosphate, and restores Tau's ability to bind microtubules [102]. Pin1 also interacts with the Amyloid precursor protein APP at pThr668–Pro669, reducing proteolytic cleavage and thereby preventing the production of amyloidogenic peptides. This is notable since amyloid-β (Aβ) deposits play a fundamental role in neurodegenerative diseases. The exact mechanism by which Pin1 prevents a hypherphosphorylated form of Tau from forming intraneuronal aggregates, and thus the accumulation of amyloidogenic peptides associated with Alzheimer's disease is currently not well understood.

Table 1.3. Neuronal proteins identified as Pin1 substrates

Protein	Function	Reference
Amyloid precursor protein	synapse formation	Lee, et al. 2009 [104]
Tau	microtubule stability	Lu, et al. 1999 [102]
Gephyrin	glycine receptors modulator	Zita, et al. 2007 [105]
TIPS21	Receptor	Hong, et al. 2005 [106]
NF-H	neurofilament protein	Rudrabhatla, et al. 2008 [107]

1.11 Significance of Pin1 inhibition

Pin1 inhibition has been extensively studied as a viable approach for treating a large number of diseases, such as cancer and Alzheimer's disease, as well as organ transplant rejection, allergies, and asthma [92, 93, 94, 108, 109, 110, 111, 112]. In efforts to identify potential inhibitors of Pin1, different approaches have been used including the screening of combinatorial libraries, molecular modeling, chemical synthesis, and bioassays [29, 46, 113, 114, 115, 116, 117]. The first identified Pin1 inhibitor was the natural product 5-hydroxy-1,4-naphthoquinone (juglone). This compound binds irreversibly exposed cysteine residues Cys41, Cys69, and Cys113 producing thioether adducts that cause Pin1 to partially unfold [118]. Inhibition of Pin1 with juglone was thought to be a promising approach to addressing organ transplant rejection since it works differently from the commonly used immunosuppressant drugs

cyclosporine A and FK506. These immunosuppressant are leading drugs in the treatment of organ rejection, both of which induce numerous unwanted side effects due to the high dosage levels needed to make them effective [94, 109]. Treating Pin1 with juglone was found to regulate the stability of TGF-β1, which promotes fibrosis in asthmatic mice [94]. However, the use of juglone is currently not viewed as a feasible way of producing therapeutic drugs because it demonstrates poor specificity, and it irreversibly binds multiple protein kinases and phosphatases[109, 119].

Structural studies of the Pin1 active site have revealed two key elements that can be used in the design of novel drug therapies. First, the positively charged loop of Pin1 binds a phosphate moiety or a dianionic group in the target inhibitor [24, 29]. Second, the Pin1 proline-binding pocket can accommodate five- or six-membered aliphatic rings, facilitating important hydrophobic interactions with a ligand [24, 29, 116]. Based on this knowledge of the Pin1 active-site structure, reversible peptidomimetic and non-peptidomimetic compounds have been synthesized that display moderate to potent levels of Pin1 inhibition (Fig. 1.5). Unfortunately, a significant number of compounds with effective Pin1 inhibition in vitro have also shown low cell permeability in vivo due to the negatively charged phosphate moiety [29].

In 2004, Wang et al. synthesized conformationally locked isosteres of the cis-trans pSer–Pro motif and inserted them into short peptides [114]. These isosteres demonstrated moderate inhibition of Pin1 catalytic activity and antiproliferative activity in the ovarian cancer cell line A2780 [114]. Shortly thereafter, the cell permeability and the antiproliferative activity in ovarian cancer cell line A2780 of the isosteres was improved by masking the negatively charged phosphate with bis-pivaloyloxymethyl (POM) phosphate [117].

Pin1 shares some structural similarities with FKBP, which binds to the cyclic immunosuppressant drug FK506 [54]. In an effort to develop effective Pin1 inhibitors, a library of more than 200 FKBP-12 inhibitors was screened against Pin1. However, no viable candidates were identified [29]. Tricyclic and tetracyclic benzofuranones were synthesized and tested—also with poor inhibition of Pin1[120]. More recently, a library of cyclic peptides containing a phospho-(D)-Thr–Pip–Nal core were modified by incorporating polyarginines, which facilitated membrane permeability and anti-proliferation properties [121]. In another study, aryl indole ketones were synthesized and used as twisted-amide transition state analogs, which also showed moderate inhibition of Pin1 [122]. Bivalent-inhibitors containing a ligand with an affinity for both domains, and covalently linked by rigid polyproline linkers, were tested. The results revealed a 305-fold increase in the inhibitory constant in comparison to the individual building blocks [123].

In addition to the Pin1 catalytic site (PPIase domain), the Pin1 WW domain also represents a target site for the inhibition of Pin1. In 2002, Lu et al. showed that in healthy tissues, the phosphorylation of Ser16 located in the WW domain reduced the Pin1 binding affinity for its target substrates, essentially inactivating Pin1 [74]. In 2005, Smet et al. reported that small dipeptide analogues were able to abolish the interaction between the Pin1 WW domain and phosphopeptides [124]. Therefore, either the Pin1 catalytic site or the WW domain represents a viable approach for the inactivation of Pin1.

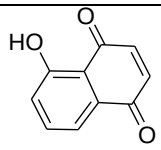

Juglone
Hennig et al. 1998
~ 2 µM

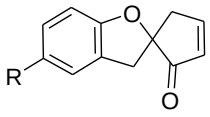

Benzofuranones
Braun et al. 2008
63 µM

Ac-Phe-Phe-**p**Ser- [(E)CH=C]Pro-Arg-NH_2 and
Ac-Phe-Phe-**p**Ser- [(Z)CH=C]Pro-Arg-NH_2,

Conformationally locked isosteres
Wang et al. 2004
1.4 and 40 µM

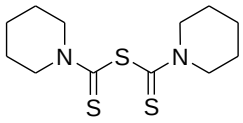

Thiuram monosulfide
Tarata et al. 2009
4.1 µM

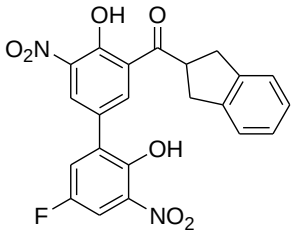

Aryl indanyl ketones
Daum et al. 2006
0.2 µM

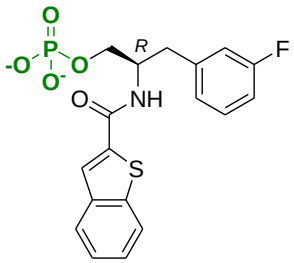

3-Fluoraphenylalanine devivated
Guo et al. 2009
6 nM

Ac-Lys(N-biotinoyl)-Ala-Ala-Phe-D-**p**Thr-Pip-Nal-Gln-NH_2

Nonproteinogenic peptide
Wildemann et al. 2006
4.8 nM

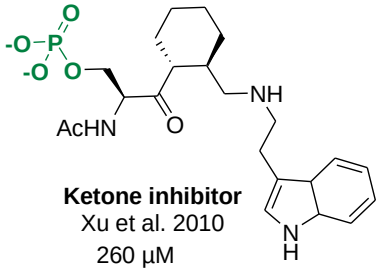

Ketone inhibitor
Xu et al. 2010
260 µM

Fmoc-(bisPOM)-**p**Ser-Psi[(Z)CHC]-Pro-(2)-N-(3)-ethylaminoindole

phosphorylated prodrug
Zhao et al. 2007
~27 µM

Ac-Phe-DGlu-Pip-Nal-Gln-$(Pro)_n$-Ala-Bth-**p**Thr-Pro-Cha-Gln-NH_2

Bivalent Pin1 inhibitors
Daum et al. 2007
n = 3-6, K_d = 10-0.4 µM

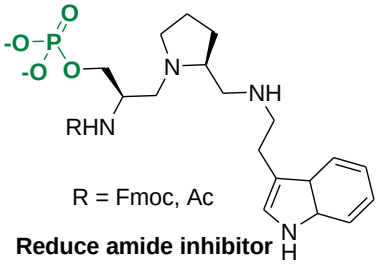

R = Fmoc, Ac

Reduce amide inhibitor
Xu et al. 2010
6.3-12 µM

Fig. 1.5. Compounds with potent to moderate inhibition of Pin1.

1.12 Current research goals

The overall aims of this research are to explore the impact of Pin1 on cell cycle regulation by screening organic molecules from compound libraries, and by using peptide substrates to study Pin1 catalytic mechanism of proline cis/trans isomerization.

Aim 1: To design an enzyme-linked enzyme binding assay (ELEBA) for the identification of Pin1 WW domain ligands from a compound library. Hypothesis: By using a peptide-core (-VPRpTPV-, 7.7 μM) derived from the sequence of Cdc25c [32] and specific for the Pin1 WW domain, a competitive binding-assay can be designed for the selective identification of ligands that bind at the Pin1 WW domain from chemical libraries. The identification of ligands that selectively block the Pin1 WW domain association with phosphoproteins represents a promising approach for the study of Pin1 in cell cycle regulation and a rational drug design for cancer treatment.

Aim 2: To utilize a proteolytic-discontinuous assay for the identification of Pin1 catalytic inhibitors. Hypothesis: By adapting the traditional Pin1 continuous-catalytic assay to a discontinuous assay in a 96/384-microplate format, organic molecule libraries can be screened in parallel against the Pin1 catalytic activity. The identification organic molecules that affect Pin1 catalytic activity will provide the groundwork for rational design of potent and specific Pin1 inhibitors.

Aim 3: To identify the site/or sites of cis-trans isomerization on c-Myc peptides catalyzed by Pin1. Hypothesis: By varying the position of the phosphorylation in four small peptides corresponding to the c-Myc sequence, the site of Pin1 interaction with c-Myc can be identified

using NMR isomerization studies. The results of these experiments will provide the necessary evidence for the understanding of Pin1 effects in c-Myc degradation.

Aim 4: To use peptide substrates for the study of Pin1 catalytic mechanism by measuring the kinetic isotopic effect. Hyphothesis: By synthesizing efficient chromogenic substrates, Ac–Phe–Phe–pSer–Pro–Arg–*p*NA (unlabeled) and the Ac–Phe–Phe–p[d_3]Ser–Pro–Arg–*p*NA (labeled), analogues to pintide (H–Trp–Phe–Tyr–pSer–Pro–Arg–*p*NA, k_{cat}/K_m = 20,160 $mM^{-1}s^{-1}$). The secondary kinetic isotopic effect (2° KIE) catalyzed by Pin1 can be measured. The ratio of k_H/k_D for unlabeled and [d_3]-labeled substrate will provide evidence for the Pin1 catalytic mechanism of cis-trans isomerization. Results of this experiment will facilitate the rational design of transition-state-analogue Pin1 catalytic inhibitors.

Chapter 2

This chapter is an article titled Enzyme-linked enzyme-binding assay for Pin1 WW domain ligands, published in the journal of Analytical Biochemistry, Elsevier License # 2441121102930 for dissertation use of the full article. I wrote the first draft of the manuscript, and Dr. Felicia Etzkorn edited and rewrote portions of the manuscript in close consultation with me.

Reproduced with permission from Mercedes-Camacho, A.Y. and F.A. Etzkorn, Enzyme-linked enzyme-binding assay for Pin1 WW domain ligands. Anal Biochem. 2010, 402(1): p. 77-82.

Enzyme-linked enzyme-binding assay for Pin1 WW domain ligands

Ana Y. Mercedes-Camacho [a,b] and Felicia A. Etzkorn,[a]
[a]Department of Chemistry, Virginia Tech, Blacksburg, VA 24061, USA
[b]Department of Biochemistry, Virginia Tech, Blacksburg, VA 24061, USA

2.1 Abstract

Peptidyl prolyl *cis-trans* isomerase (PPIase) interacting with NIMA-1 (Pin1) catalyzes the *cis-trans* isomerization of pSer/pThr–Pro amide bonds. Pin1 is a two-domain protein that represents a promising target for the treatment of cancer. Both domains of Pin1 bind the pSer/pThr–Pro motif; PPIase enzymatic activity occurs in the catalytic domain, and the WW domain acts as a recognition module for the pSer/pThr–Pro motif. An assay we call an enzyme-linked enzyme-binding assay (ELEBA) was developed to measure the K_d of ligands that bind selectively to the WW domain. A ligand specific for the WW domain of Pin1 was covalently immobilized in a 96-well plate. Commercially available Pin1 conjugated to horseradish peroxidase was used for chemiluminescent detection of ligands that block the association of the WW domain with immobilized ligand. The peptide ligands were derived from the cell cycle regulatory phosphatase, Cdc25c, residues 45–50. The K_d values for Fmoc–VPRpTPVGGGK–NH_2 and Ac–VPRpTPV–NH_2 were determined to be 36 ± 4 and 110 ± 30 μM, respectively. The ELEBA offers a selective approach for detecting ligands that bind to the Pin1 WW domain, even

in the presence of the catalytic domain. This method may be applied to any dual specificity, multidomain protein.

Keywords: Pin1; WW domain assay; PPIase; HRP; Chemiluminescent binding assay; Pin1 ligands

2.2 Background

Pin1 is a two-domain protein that catalyzes the *cis-trans* isomerization of pSer/pThr–Pro motifs through its PPIase (peptidyl prolyl isomerase)[1] catalytic domain[11, 24]. Pin1 also contains a WW domain, so called because it has two invariant Trp residues [41]. The WW domain binds pSer/pThr–Pro motifs in target ligands, but does not catalyze cis-trans proline isomerization [11, 41]. The Pin1 WW domain interaction with ligands occurs through a conserved phosphate-binding pocket, present in Pin1 and its homologues [11, 32]. The Pin1 WW domain binds and regulates phosphorylated proteins at different stages of the cell cycle [26, 32, 42], and the WW domain is the site of Pin1 regulation by protein kinase A [74]. Pin1 phosphoprotein-binding activity is abolished by phosphorylation of Ser16, located in the WW domain [74]. Peng and co-workers have shown that a Pin1 ligand from Cdc25, EQPLpTPVTDL, affects the dynamics of Pin1 side chains at the hydrophobic interface between the WW domain and the catalytic domain [27]. The possibility of a tight-binding WW domain ligand that blocks Pin1 association with its physiological substrates represents an alternative approach for inactivation of Pin1, a potential strategy for cancer therapy [125].

In previous efforts to identify Pin1 WW domain ligands with prospective clinical applications, several focused compound libraries have been screened by a variety of methods: fluorescence anisotropy, nuclear magnetic resonance (NMR), Förster resonance energy transfer

(FRET), and virtual screening [32, 87, 88, 126, 127]. However, for screening larger libraries, these techniques have various limitations, such as the requirement for fluorescent labeling of ligands, the amount of protein needed, the use of isolated WW domain, isotopic labeling of protein, or the time for data acquisition and interpretation [32, 87, 88, 126, 127]. We now describe an assay to screen for ligands that bind to the Pin1 WW domain. The enzyme-linked enzyme-binding assay (ELEBA) is simple to use compared with other protein–ligand interaction techniques. This assay can be adapted to screen compound libraries with multiple domains, or multimeric proteins with different ligand affinities and specificities in each domain or protein subunit, such as proteins containing Src homology (SH2 and SH3) domains [128], phosphotyrosine-binding (PTB) domains, or other protein-interacting modules. The major requirement for the assay is to identify a selective ligand with moderate affinity, but high specificity, for the site of interest. This is already known for the Pin1 WW domain [32].

For the ELEBA, we synthesized peptides containing the VPRpTPV core of the dual-specificity phosphatase Cdc25c at the pThr48–Pro49 position. Fluorescence anisotropy has shown that the Pin1 WW domain is highly selective for the VPRpTPV sequence, with an affinity of 7.7 μM for the WW domain, and no detectable binding to the catalytic domain [32]. Synthetic H–GGGGVPRpTPVGG–NH_2 was covalently immobilized to a 96-well microtiter plate, and commercially available Pin1 (residues 2–163) conjugated to horseradish peroxidase (Pin1–HRP) was used for chemiluminescent detection of binding. Full-length Pin1 is more stable than the isolated WW domain [32]. WW domain ligands in solution that have similar or better affinity than the immobilized ligand block the binding of the WW domain with the immobilized ligand on the plate. Therefore, WW domain ligands in complex with Pin1–HRP are removed during washing, and produce little or no colorimetric signal after the addition of peroxidase substrate.

Materials and Methods

2.3 Peptide synthesis

Peptides were synthesized using manual solid-phase peptide synthesis (SPPS) in disposable polypropylene columns (Thermo Scientific) with standard 9-fluorenylmethoxy-carbonyl (Fmoc) chemistry. All Fmoc amino acids were purchased from Novabiochem. 4-Methylbenzhydrylamine (MBHA, Rink amide) resin (100 mg, 0.66 meq/g, 0.064 meq) was swelled in CH_2Cl_2 (3 mL) for 20 min, and the Fmoc protecting group was removed with 20% piperidine in *N*-methyl-2-pyrrolidone (NMP) (2 × 3 mL). The resin was washed twice with NMP (ca. 8 mL). The first amino acid in the sequence (3 eq) was coupled to the resin using 2-(1*H*-benzotriazol-1-yl)-1,1,3,3-tetramethyluronium hexafluorophosphate (HBTU) (70 mg, 0.19 mmol), *N*-hydroxybenzotriazole (HOBt) (29 mg, 0.19 mmol), and diisopropylethylamine (DIEA) (67 μL, 0.38 mmol) in NMP (2 mL), and the mixture was double-coupled (2 × 2 h). Completion of coupling was monitored by the Kaiser test for primary amines, and by the *p*-chloranil test for prolines [129, 130]. The reaction mixture was washed with NMP (2 × 6 mL), and a solution of acetic anhydride (0.2 mL, 1.1 mmol), DIEA (0.2 mL, 2.1 mmol), and CH_2Cl_2 (1.6 mL) was added and shaken for 10 min to cap any uncoupled amines. The Fmoc group was removed with 20% piperidine in NMP (2 × 3 mL). The following amino acids were added one at a time in the same manner: Fmoc–Gly–OH (59 mg, 0.19 mmol), Fmoc–Val–OH (65 mg, 0.19 mmol), Fmoc–Pro–OH (65 mg, 0.19 mmol), Fmoc–Thr(PO_2H(OBzl))–OH (98 mg, 0.19 mmol), Fmoc–Lys(Boc)–OH (93 mg, 0.19 mmol), and Fmoc–Arg(Pbf)–OH (125 mg, 0.19 mmol), Fmoc–Leu–OH (68 mg, 0.19 mmol), and Fmoc–Ser(tBu)–OH (74 mg, 0.19 mmol). The peptide resins were cleaved with a mixture of 95% CF_3CO_2H, 2.5% H_2O, 2.5% triisopropylsilane for 4 h at 30 °C. With exceptions noted, crude peptides were precipitated with cold diethyl ether (3 × 10 mL), and purified using reverse-phase high-pressure liquid chromatography (RP-HPLC), using a Waters

C18 XBridge 5 μm, 19 × 100 mm semipreparative column (unless otherwise noted) on a Varian Pro-Star 218 HPLC with linear gradients as noted, flow rate 10 mL/min, λ = 210 nm. CH_3CN was removed under vacuum, and the water was removed by lyophilization. Analytical HPLC were obtained on a Beckman HPLC with linear gradients as noted, flow rate 1.0 mL/min, λ = 210 nm. Peptides were characterized by ^1H NMR on an INOVA-400 MHz, and by liquid chromatography–mass spectrometry (LC-MS) on an Agilent 1100 LC-ThermoFinnigan TSQ MS with electrospray ionization (ESI+) for molecular ion identification (Supplementary Material).

H–GGGGVPRpTPVGG–NH_2 (**1**) was purified by RP-HPLC with 0.1% ammonium formate in 5 to 60% CH_3CN/H_2O gradient over 7 min. The desired peak was collected at 6 min to give 8 mg (11% yield). Analytical HPLC using a Waters C18 XBridge 2.5 μm, 4.6 × 50 mm column, with 5% CH_3CN/H_2O for 2 min and then 5 to 50% gradient over 15 min showed a major peak at 14.2 min, 91.2% pure. LC-MS 13.25 min, calcd. for $C_{42}H_{74}N_{16}O_{16}P$ $[M+H]^+$ *m/z* = 1089.5, found *m/z* = 1089.7 (Supplementary Material, Figs. S1-S5).

Fmoc–VPRpTPVGGGK–NH_2 (**2**) was purified by RP-HPLC with 0.1% CF_3CO_2H in 20 to 70% CH_3CN/H_2O gradient over 8 min. The desired peak was collected at 6.5 min to give 38 mg (47% yield). Analytical HPLC using an XBridge BET130 3.5 μm C18 4.6 × 50 mm column, with 5% CH_3CN/H_2O for 2 min and then 5 to 80% gradient over 5 min, showed a major peak at 4.3 min, 96.2% pure. LC-MS 14.04 min, calcd. for $C_{57}H_{87}N_{15}O_{16}P$ $[M+H]^+$ *m/z* = 1268.6, found *m/z* = 1268.7 (Supplementary Material, Figs. S6-S9).

Ac–VPRpTPV–NH_2 (**3**) was purified by RP-HPLC with 5 to 60% CH_3CN/H_2O gradient over 18 min. The desired peak was collected at 11 min to give 9 mg (18% yield). Analytical HPLC using a Waters C18 XBridge 2.5 μm, 4.6 × 50 mm column, with 5% CH_3CN/H_2O for 2

min, 5 to 60% gradient over 5 min, and then 60% for 4.5 min, showed a major peak at 5.48 min, 91.7% pure. LC-MS 15.32 min, calcd. for $C_{32}H_{58}N_{10}O_{11}P$ $[M+H]^+$ *m/z* = 789.4, found *m/z* = 789.4 (Supplementary Material, Figs. S10-S13).

Ac–LPTPPLSPS–NH_2 (**4**) was purified by RP-HPLC, using a Varian Polaris 10 μm, C18 100 × 212 mm semipreparative column, with 0.1% CF_3CO_2H in 10 to 60% CH_3CN/H_2O gradient over 15 min, λ = 220 nm. The desired peak was collected at 7 min to obtain 9.4 mg (16% yield). Analytical HPLC using a Varian Polaris 5 μm C18 4.4 × 100 mm column, with 0.1% CF_3CO_2H in 10 to 40% CH_3CN/H_2O gradient over 15 min, showed a major peak at 8.5 min, 84.5% pure. LC-MS 14 min, calcd. for $C_{44}H_{73}N_{10}O_{13}$ $[M+H]^+$ *m/z* = 949.5, found *m/z* = 949.6 (Supplementary Material, Figs. S14-S17).

2.4 Immobilization of ligands to the 96-well plate

H–GGGGVPRpTPVGG–NH_2, ligand **1** (100 μL, 2.8 mM), in phosphate-buffered saline (PBS), 15 mM sodium phosphate, 2 mM potassium phosphate buffer, and 150 mM NaCl at pH 9.2, was added to each well of a DNA-BIND microtiter plate (Corning Life Sciences, Wilkes Barre, PA). The plate was sealed with clear tape (Corning Costar Corporation), and incubated for 2 h at 37 °C with shaking. The uncoupled ligand was decanted and the wells were washed (3 × 150 μL/well). The wash buffer contained 10 nM imidazole, and 0.05% Tween 20 in PBS at pH 7.3. The plate was shaken in air and inverted on a paper towel until dry ca. 30 min, and the remaining active sites were blocked with PBS buffer containing 5% sucrose, 0.05% NaN_3, 2% bovine serum albumin (BSA), Fraction V, ELISA grade (Calbiochem) at pH 7.3 (100 μL/well). The plate was sealed with tape, and incubated overnight at 0°C. The solution was decanted via pipet, and the plate was rinsed 3 times with a squeeze bottle of wash buffer, and inverted on a paper towel to drain excess buffer.

Fmoc–VPRpTPVGGGK–NH_2, ligand **2** (100 μL, 0.1 mM), was covalently attached to the 96-well plate through the ε-amino group of the Lys side chain at pH 11.0, otherwise as described above.

2.5 ELEBA procedure

Competitive binding with the Pin1 WW domain of ligands **2** and **3** with plate-linked GGGGVPRpTPVGG–NH_2 **1** was measured. UV–vis spectroscopy was used for accurate determination of ligand **2** concentration using the Fmoc ε value of 3981 cm^{-1} M^{-1} at 256 nm. Ligand **3** was dried over P_2O_5 for 2 days prior to assay, weighed (4.3 mg) to determine the

concentration, and dissolved in 200 mM phosphate, 30 mM NaCl, pH 7.0 (1.0 mL, 5.4 mM). Recombinant human Pin1–HRP (R&D Systems, Minneapolis, MN) was diluted to a final concentration of 200 pM in PBS buffer containing 2% BSA at pH 7.3 (Fig. S18). For ligand **2**, the concentrations were 1.1, 3.3, 7.7, 15, 44, 95, 146, 230, 460, and 730 μM; for ligand **3**, 2, 6, 12, 25, 40, 120, and 180 μM; for ligand **4**, 7.7, 95, 460, 1000, and 2000 μM; for ligand **5**, 7.7, 95, and 460 μM; and for ligand **6**, 7.7, 95, 460, and 1000 μM. For ligand **2** against ligand **2** linked to the plate, the concentrations were 1.1, 4.0, 10, 33, 62, 102, 345, and 550 μM.

The Pin1–HRP solution was incubated at room temperature for 1 h with orbital shaking in the plate with ligands **2**-**6** in a total volume of 100 μL/well. The solutions were decanted, and the wells were washed with wash buffer (3 × 150 μL/well). Hydrogen peroxide and 3,3′,5,5′-tetramethylbenzidine (TMB, R&D Systems, Minneapolis, MN) were added to the plate in a 1:1 ratio (100 μL/well), and incubated at room temperature for 20 min in the dark. The stop solution, 2 N H_2SO_4 (50 μL/well), was added to the 96-well plate. The optical density (OD) of each well was determined immediately, using a plate reader (Spectra Max 340 PC) with UV absorbance detection at 450 nm. The 96-well plate with covalently attached ligand is reusable after appropriate washing steps and storage (Supplementary Material, Fig. S19).

Results

2.6 Design, synthesis, and immobilization of ligand 1

The Cdc25c-T48 peptide of Verdecia et al. [32] was modified with the addition of two glycine residues at the C-terminus to avoid diketopiperazine formation [131], and four glycine residues at the N-terminus as an additional spacer between the ligand and the 96-well plate surface to give H–GGGGVPRpTPVGG–NH_2 **1**. Computer modeling was used to evaluate the

interactions of ligand **1** with the Pin1 WW domain-binding pocket. All of the glycine residues extended outside of the Pin1 contact region (Supplementary Material, Fig. S20).

Peptides were synthesized using standard Fmoc chemistry on a Rink amide resin to produce amidated C-termini. During purification of phosphopeptides, improved recovery from HPLC was obtained without acid in the mobile phase, which we have observed to cause β-elimination of phosphate from pSer or pThr. Ligand **4**, that is not phosphorylated, was purified with CF_3CO_2H in the mobile phase.

2.7 ELEBA validation with conjugated Pin1–HRP

Ligand **1** was covalently bound to the 96-well plate, which contained an *N*-oxysuccinimide ester (NOS)-activating group that was reacted with the peptide primary amine at pH 9.2 to capture the ligand covalently on the solid surface (Fig. 2.1) [132]. The effects of the buffers we used in the ELEBA assay were tested at pH values ±1 of their respective pK_a values, and with and without 150 mM NaCl (Supplementary Material, Figs. S21 and S22). For the ELEBA, the most suitable buffer to prevent Pin1–HRP nonspecific binding with the plate surface was PBS at pH 7.3 with 150 mM NaCl. Two specific WW domain ligands Fmoc–VPRpTPVGGGK–NH_2 **2** and Ac–VPRpTPV–NH_2 **3** were used as positive controls for ELEBA validation (Table 2.1). Commercially available recombinant human Pin1, residues 2–163, chemically conjugated via a peptide linker to horseradish peroxidase (Pin1-HRP) was used with varying concentrations of **2** and **3** to measure affinity (Fig. 2.2). As the concentrations of **2** and **3** were increased, they competed with ligand **1** on the plate for binding to the Pin1 WW domain, leaving unbound Pin1–HRP which was washed away.

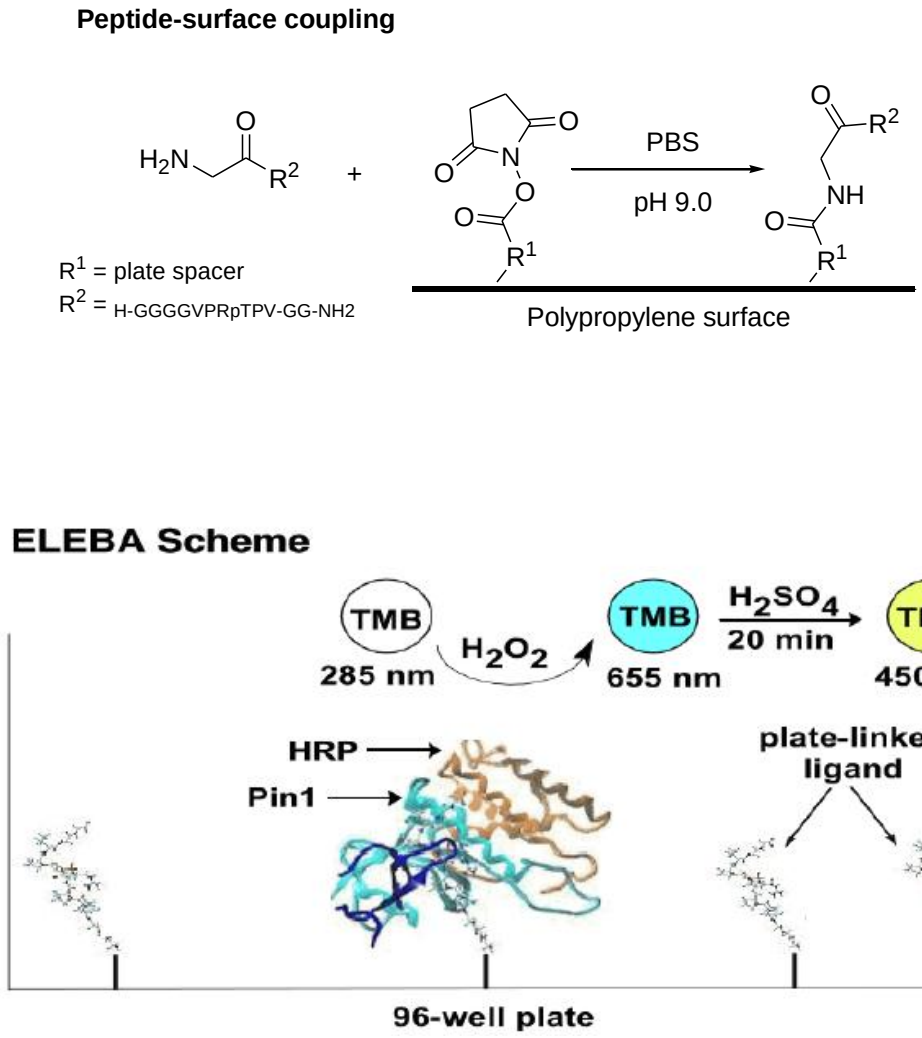

Fig. 2.1. ELEBA methodology. (a) At alkaline pH, the free N-terminus of H–GGGGVPRpTPVGG–NH_2 1 was coupled to an N-oxysuccinimide ester becoming covalently linked to the plate surface. (b) Pin1–HRP-conjugated enzyme bound to immobilized ligand 1 in the absence of ligands that block the WW domain-binding site. The amount of Pin1–HRP bound to the plate was measured by oxidation of the HRP-substrate. (Prepared with ChemBioDraw Ultra and Canvas 8.)

Table 2.1. Binding affinities (K_d) for ligands used in ELEBA. The pT/S–P motif is shown in bold.

Ligand	Structure	K_d	Pin1 PPIase IC_{50}
1	H-GGGGVPR**pTP**VGG–NH_2	N.A.[a]	N.A.[a]
2	Fmoc-VPR**pTP**VGGGK–NH_2	36 ± 4 μM	N.A.[a]
3	Ac-VPR**pTP**V–NH_2	110 ± 30 μM	N.A.[a]
4	Ac-LPTPPL**SP**S–NH_2	> 2 mM[b]	N.A.[a]
5	Fmoc-**pS–Ψ[CH_2N]–P**–2-(3-indolyl)-ethylamine	> 0.5 mM[b]	6.3 ± 0.4 μM[133]
6	Ac–**pS–Ψ[(Z)CH=C]–Pip**–2-(2-naphthyl)-ethylamine	> 1 mM[b]	141 ± 18 μM [134]

[a] Not applicable. [b] No detectable binding.

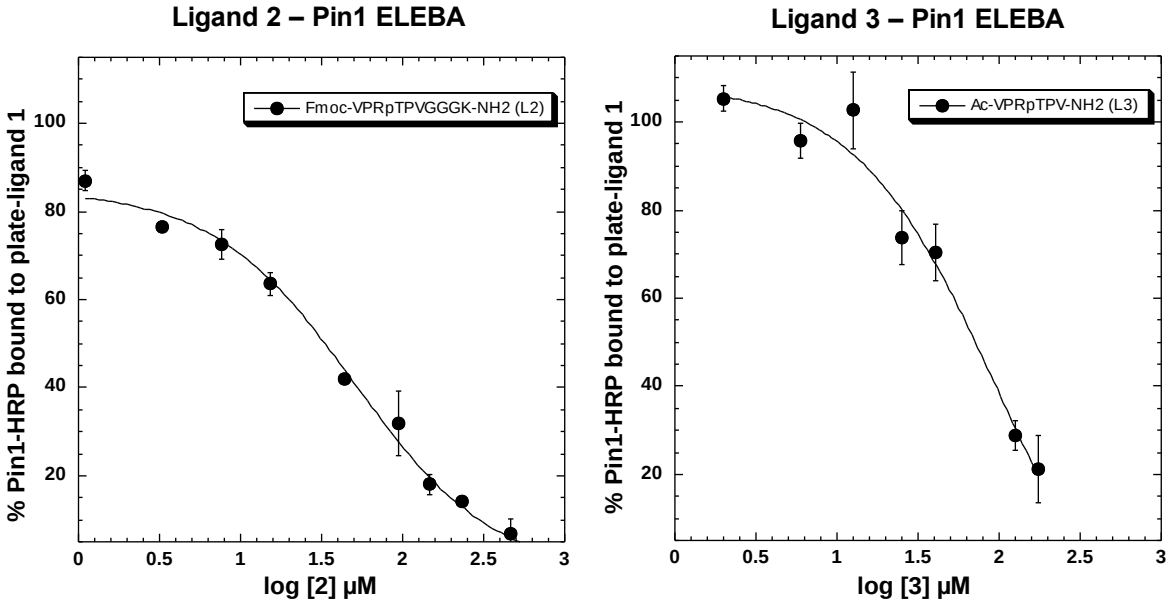

Fig. 2.2. Binding curves showing the percentage of Pin1–HRP bound to plate-linked GGGGVPRpTPVGG–NH_2 **1** at varying concentrations of ligands **2** and **3**. Data are an average of N = 3 with standard deviations shown in the error bars; the data were fitted to (Eq.1), using KaleidaGraph 4.3. Left: binding curve for ligand **2**. Right: binding curve for ligand **3**. The calculated K_d values were 36 ± 4 μM for **2** and 110 ± 30 μM for **3**. (Prepared with Kaleidagraph 4.3.)

The data for ligands **2** and **3** were fitted to a dose–response binding curve, using Kaleidagraph v. 4.3,

$$\%\ \text{of binding} = a + \frac{(b - a)}{(1 + 10^{(c - [L])})} \qquad (1)$$

where [L] is the concentration of the ligand in solution. The dose–response binding curve measures the binding constant at a single concentration of Pin1–HRP in the presence of varying concentrations of competing ligands **2** and **3** [135]. We normalized the data to percentage Pin1–HRP bound to the plate-linked ligand by setting the lowest concentration of competitive ligand in solution to 100% binding. The top of the curve is a plateau represented by the value of *a*. The highest concentration of ligand in solution was set to 1% binding, which is represented by the bottom of the curve as a plateau, corresponding to the value of *b*. The log of the concentration at zero is undefined. Instead, we entered very low competitor concentration values of 1.1 and 2 μM for ligands **2** and **3**, respectively. The *c* value corresponds to the response halfway between *a* and *b* values. This variable is sometimes called ED_{50} (effective dose, 50%), or IC_{50} (inhibitory concentration, 50%). The competitive K_d values were calculated by solving for log [L] when % binding (y) = 50%. The values, $a = 85 \pm 2$, $b = -2.6 \pm 3$, and $c = 1.7 \pm 0.07$ with $R^2 = 0.9966$, were fitted for ligand **2**. The K_d value of 36 ± 4 μM was determined from three data sets (Table 2.1, Fig. 2.2). The values, $a = 108 \pm 6$, $b = -29 \pm 20$, and $c = 2.0 \pm 0.2$ with $R^2 = 0.9877$, were fitted for ligand **3**. The K_d value of 110 ± 30 μM was determined from three data sets (Table 2.1 and Fig. 2.2).

2.8 ELEBA selectivity for WW domain ligands

To study the specificity of the assay for phosphopeptides, an unphosphorylated, proline-rich peptide, c-Myc 56-64, Ac–LPTPPLSPS–NH_2 **4**, was assayed. Pin1 is known to regulate turnover of transcription factor c-Myc that is dependent on phosphoThr-58 [72]. Varying concentrations of **4** were used as described above. Ligand **4** was not able to compete with plate-linked ligand **1**, even at a concentration of 2 mM, and Pin1–HRP remained fully bound to the plate after washing (Fig. 2.3).

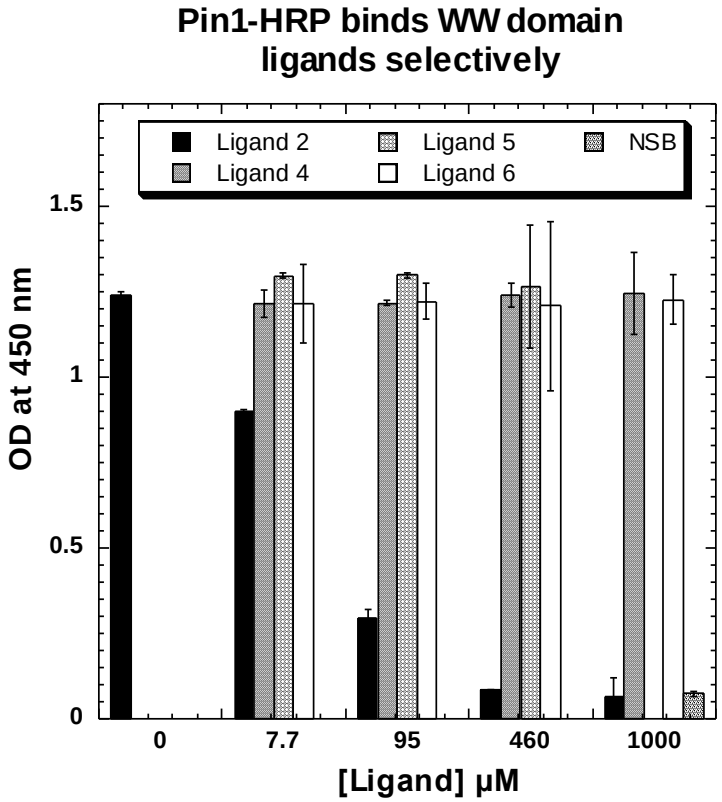

Fig. 2.3. Pin1–HRP was incubated with varying concentrations of ligands **2**–**6** (Table 2.1), to detect the ability of the ligands to block Pin1 WW association with immobilized ligand **1**. Pin1–HRP-binding with ligand 1 on the plate decreased with increasing concentration of 2 in solution. Ligands **4**, **5**, and **6** did not show any decrease in binding of Pin1–HRP to the plate. The last column shows Pin1–HRP nonspecific binding (NSB) when ligand **1** was not linked to the plate. Mean of N = 3 was used for data analysis with standard deviations shown as error bars. (Prepared with Kaleidagraph 4.3.)

To further investigate the site of ligand binding to Pin1, two of our Pin1 PPIase inhibitors, Fmoc–pSer–ψ[CH_2N]–Pro–2-(3-indolyl)ethylamine **5** and Ac–pSer–ψ[(*Z*)CH=C]–Pip–2-(2-naphthyl)ethylamine **6** [133, 134], were assayed. Both PPIase catalysis inhibitors were unable to prevent Pin1 WW domain binding with ligand **1**, even at high concentrations (Table 2.1 and Fig. 2.3). Nonspecific binding of Pin1–HRP to the plate surface was reduced by blocking any residual NOS sites with the noninterfering protein, BSA. The affinity of Pin1–HRP for bound ligand **1** was tested in the presence and absence of ligand **1** attached to the 96-well plate surface. In the presence of ligand **1**, Pin1–HRP was detected at high levels on the plate after

washing (OD 1.2–2.7). However, in the absence of ligand **1**, only 0.89–2.5% nonspecifically bound Pin1–HRP was detected on the plate after washing (Fig. 2.3).

2.9 Effect of the plate-linked ligand in the competitive ELEBA

Fmoc–VPRpTPVGGGK–NH_2, ligand **2**, was covalently attached to the 96-well plate via the Lys side chain ε-amine. Pin1–HRP was incubated with different concentrations of ligand **2** in solution, in competition with ligand **2** bound to the plate. The variable values fitted were $a = 99 \pm 3$, $b = -10 \pm 4$, and $c = 1.8 \pm 0.1$ with $R^2 = 0.9976$. The K_d value of 66 ± 10 μM was determined from two data sets (Fig. 2.4).

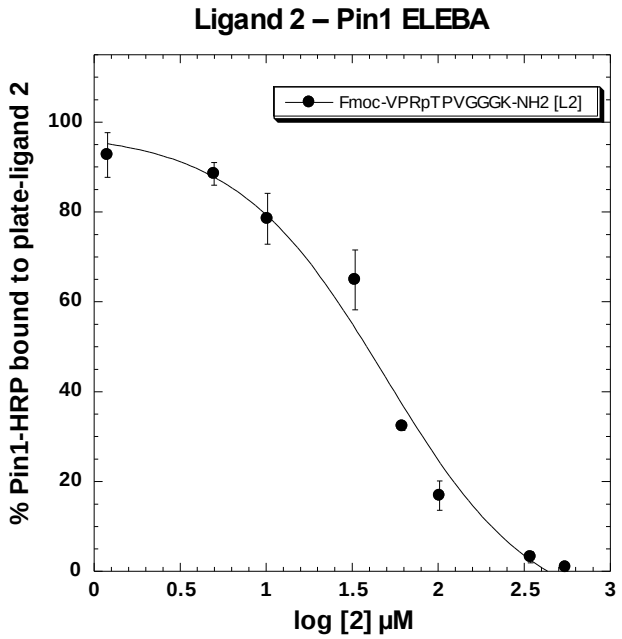

Fig. 2.4. The effect of plate-linked ligand **2** in the competitive ELEBA. The K_d value for Pin1–HRP was calculated to be 66 ± 10 μM for N = 3 with standard deviations shown as error bars. (Prepared with Kaleidagraph 4.3.)

2.10 Discussion

Pin1 contains catalytic (PPIase) and regulatory (WW) domains within the same polypeptide chain. Both domains have specificity for the pSer/pThr–Pro motif, but with different

binding affinities and specificities [26, 32]. The study of ligand-binding site preference with full-length Pin1 is challenging because high concentrations of ligands that bind at the Pin1 catalytic site can mask binding to the Pin1 WW domain. Therefore, the isolated domains are often used in the identification of ligand-binding site preference [32, 126, 127].

We designed the enzyme-linked enzyme-binding assay to selectively identify ligands that bind at the Pin1 WW domain using full-length Pin1 (Fig. 2.1). The ELEBA was intended to measure only Pin1 WW domain affinities, not PPIase inhibition constants. The availability of Pin1-HRP-conjugated protein allowed us to develop a high-throughput assay, similar to an ELISA, without the requirement for antibodies. Such covalent protein–HRP conjugates have been used to date in Western blots with Protein A and Protein G HRP conjugates [136], and in a viral protease assay with Gag precursor substrate–HRP conjugate [137] The labeled peptide sequence from Cdc25c 45–50, rhodamine–VPRpTPV, is highly selective for the WW domain (7.7 μM), with no detectable binding to the PPIase domain [32]. We used peptides with the sequence VPRpTPV covalently linked to 96-well plates for the selective identification of ligands that compete for the Pin1 WW domain.

Glycine residues were added at either the N- or the C-termini of ligands **1** and **2**, with the objective of extending the peptide at least 12 or 15 atoms away from the 96-well plate surface to avoid Pin1–HRP absorption on the plate surface (Fig. 2.1). Computer modeling indicated that the additional Gly residues do not affect Pin1 binding with the VPRpTPV core (Fig. S20), in agreement with published results that the WW domain phosphate-binding pocket is capable of interacting with up to five consecutive amino acid residues, and polar residues do not affect the peptide affinities [32, 126].

Binding affinities for ligands **2** and **3** with the Pin1 WW domain were measured by the ELEBA in a concentration-dependent manner (Table 2.1 and Fig. 2.2). Both ligands **2** and **3** effectively competed with ligand **1** on the plate surface for the Pin1 WW domain. The affinity of Pin1–HRP for Fmoc–VPRpTPVGGGK–NH_2 **2** was 3-fold tighter than for Ac–VPRpTPV–NH_2 **3** (Table 2.1). A similar binding affinity has been measured for EQPLpTPVTDL (120 μM), lacking a hydrophobic label, by NMR [27, 87, 88]. Since ligand **3** exhibited weaker affinity than ligand **2** for the Pin1 WW domain, the Fmoc group contributed to the binding affinity. The Fmoc derivative **2** was more similar in hydrophobicity to the original rhodamine-VPRpTPV ligand used in the fluorescence assay, which may explain the higher affinity [32]. This demonstrates the utility of the ELEBA in differentiating the affinities of two similar ligands.

Fmoc–VPRpTPVGGGK–NH_2 **2** showed a 2-fold tighter Pin1–HRP-binding affinity in competition with ligand **1** covalently linked to the plate, than it did in competition with ligand **2** covalently linked to the plate (Fig. 2.4). This also suggests that the hydrophobic Fmoc group of ligand **2** improves the affinity for the Pin1 WW domain in comparison with ligand **1** [32, 41, 126]. Either ligand **1** or ligand **2** attached to the plate gives a suitable assay for screening libraries to obtain hit compounds with affinity for the WW domain in the micromolar or better range.

The ELEBA was developed as a method for high-throughput screening, rather than as an absolute measure of binding affinity. Since our method is competitive with ligand linked to a plate, it is not to be taken as a direct measurement of binding affinity. We chose to compare the affinities of several different ligands primarily to permit flexibility in the choice of plate-linked ligand. In some cases, it makes more sense to have a weak ligand on the plate so that a high-throughput assay would not miss weaker potential hits. On the other hand, if the high-throughput

assay gave too many hits, it might be necessary to make the screening more stringent with a tighter binding ligand bound to the plate.

An unphosphorylated, proline-rich peptide, Ac–LPTPPLSPS–NH_2, showed no detectable binding to the Pin1 WW domain, in agreement with published data that the Pin1 WW domain does not interact with unphosphorylated peptides [32, 41]. Two of our small molecule inhibitors of the Pin1 catalytic activity, **5** and **6**, respectively, were used as negative controls [133, 134]. Neither compound showed any competition with ligand **1**, indicating that the inhibitors were unable to block the Pin1 WW domain-binding site, and that Pin1–HRP was fully capable of interacting with ligand **1** covalently linked to the plate (Table 2.1). These experiments demonstrated the selectivity of the ELEBA for phosphorylated ligands that bind to the WW domain.

2.11 Conclusions

The ELEBA is a noncatalytic binding assay for the identification of ligands that bind to the Pin1 WW domain. The assay is fast, selective, and amenable to screening ligand libraries, with the potential for automation. The assay is advantageous over existing methods, because it selectively identifies compounds that bind to the Pin1 WW domain, it uses small quantities of reagents, and no antibodies, fluorescent labels, or radioactive labels are required.

2.12 Acknowledgments

We thank the NIH for support of this work (R01 CA110940), and for the LC-MS (1S10RR16658). We thank Guoyan G. Xu and Xingguo R. Chen for samples of compounds **5** and **6**, and Mehdi Ashraf-Khorassani for LC-MS analysis.

2.13 References

[1] K.P. Lu, S.D. Hanes and T. Hunter, A human peptidyl-prolyl isomerase essential for regulation of mitosis, *Nature* **380** (1996), pp. 544–547.

[2] R. Ranganathan, K.P. Lu, T. Hunter and J.P. Noel, Structural and functional analysis of the mitotic rotamase Pin1 suggests substrate recognition is phosphorylation dependent, *Cell* **89** (1997), pp. 875–886.

[3] P. Lu, X.Z. Zhou, M. Shen and K.P. Lu, Function of WW domains as phosphoserine- or phosphotheonine-binding modules, *Science* **283** (1999), pp. 1325–1328

[4] M.A. Verdecia, M.E. Bowman, K.P. Lu, T. Hunter and J.P. Noel, Structural basis for phosphoserine–proline recognition by group IV WW domains, *Nat. Struct. Biol.* **7** (2000), pp. 639–643

[5] M.B. Yaffe, M. Schutkowski, M. Shen, X.Z. Zhou, P.T. Stukenberg, J.U. Rahfeld, J. Xu, J. Kuang, M.W. Kirschner, G. Fischer, L.C. Cantley and K.P. Lu, Sequence-specific and phosphorylation-dependent proline isomerization: a potential mitotic regulatory mechanism, *Science* **278** (1997), pp. 1957–1960.

[6] M. Shen, P.T. Stukenberg, M.W. Kirschner and K.P. Lu, The essential mitotic peptidyl-prolyl isomerase Pin1 binds and regulates mitosis-specific phosphoproteins, *Genes Dev.* **12** (1998), pp. 706–720.

[7] P.J. Lu, X.Z. Zhou, Y.C. Liou, J.P. Noel and K.P. Lu, Critical role of WW domain phosphorylation in regulating phosphoserine binding activity and Pin1 function, *J. Biol. Chem.* **277** (2002), pp. 2381–2384.

[8] A.T. Namanja, T. Peng, J.S. Zintsmaster, A.C. Elson, M.G. Shakour and J.W. Peng, Substrate recognition reduces side-chain flexibility for conserved hydrophobic residues in human Pin1, *Structure* **15** (2007), pp. 313–327.

[9] G.G. Xu and F.A. Etzkorn, Pin1 as an anticancer drug target, *Drug News Perspect.* **22** (2009), pp. 399–407.

[10] R. Wintjens, J.M. Wieruszeski, H. Drobecq, P. Rousselot-Pailley, L. Bue´e, G. Lippens and I. Landrieu, ^{1}H NMR study on the binding of Pin1 Trp-Trp domain with phosphothreonine peptides, *J. Biol. Chem.* **276** (2001), pp. 25150–25156.

[11] D.M. Jacobs, K. Saxena, M. Vogtherr, P. Bernado, M. Pons and K.M. Fiebig, Peptide binding induces large scale changes in inter-domain mobility in human Pin1, *J. Biol. Chem.* **278** (2003), pp. 26174–26182.

[12] C. Smet, J.F. Duckert, J.M. Wieruszeski, I. Landrieu, L. Buée, G. Lippens and B. Déprez, Control of protein-protein interactions: structure-based discovery of low molecular weight inhibitors of the interactions between Pin1 WW domain and phosphopeptides, *J. Med. Chem.* **48** (2005), pp. 4815–4823.

[13] B. Wu, M.F. Rega, J. Wei, H. Yuan, R. Dahl, Z. Zhang and M. Pellecchia, Discovery and binding studies on a series of novel Pin1 ligands, *Chem. Biol. Drug Des.* **73** (2009), pp. 369–379.

[14] W.Q. Liu, M. Vidal, N. Gresh, B.P. Roques and C. Garbay, Small peptides containing phosphotyrosine and adjacent alphaMe-phosphotyrosine or its mimetics as highly potent inhibitors of Grb2 SH2 domain, *J. Med. Chem.* **42** (1999), pp. 3737–3741

[15] E. Kaiser, R.L. Colescott, C.D. Bossinger and P.I. Cook, Color test for detection of free terminal amino groups in the solid-phase synthesis of peptides, *Anal. Biochem.* **34** (1970), pp. 595–598.

[16] T. Vojkovsky, Detection of secondary amines on solid phase, *Pept. Res.* **8** (1995), pp. 236–237.

[17] S. Steinberg and J.L. Bada, Diketopiperazine formation during investigations of amino acid racemization in dipeptides, *Science* **213** (1981), pp. 544–545.

[18] J.K. Wang, J.L. Li, M.L. Li, D. Hua and H.M. Chen, Assay of DNA-binding proteins with a dsDNA-coupled plate, *Clin. Biochem.* **39** (2006), pp. 167–175.

[19] P.J. Munson, LIGAND: a computerized analysis of ligand binding data, *Methods Enzymol.* **92** (1983), pp. 543–576.

[20] E. Yeh, M. Cunningham, H. Arnold, D. Chasse, T. Monteith, G. Ivaldi, W.C. Hahn, P.T. Stukenberg, S. Shenolikar, T. Uchida, C.M. Counter, J.R. Nevins, A.R. Means and R. Sears, A signalling pathway controlling c-Myc degradation that impacts oncogenic transformation of human cells, *Nat. Cell Biol.* **6** (2004), pp. 308–318.

[21] G.G. Xu, F.A. Etzkorn, Design and synthesis of amine and ketone inhibitors of Pin1, Abstract of Papers, 235th ACS National Meeting, New Orleans, LA, USA, April 6–10, 2008, BIOL-057.

[22] X.R. Chen, F.A. Etzkorn, Three stereoisomers of Ac-pSer-ψ[(*Z*)CH=C]-Pip-2-(2-naphthyl)ethylamine as inhibitors of Pin1, Abstracts of Papers, 238th ACS National Meeting, Washington, DC, USA, August 16–20, 2009 ORGN-286.

[23] A. Lal, S.R. Haynes and M. Gorospe, Clean Western blot signals from immunoprecipitated samples, *Mol. Cell. Probes* **19** (2005), pp. 385–388.

[24] D. Horáková, M. Rumlová, I. Pichová and T. Ruml, Luminometric method for screening retroviral protease inhibitors, *Anal. Biochem.* **345** (2005), pp. 96–101.

Chapter 3

Enzyme-Linked Enzyme Binding Assay (ELEBA) screen of a combinatorial pSer–Pro peptidomimetic library

3.1 WW domain affinity for pSer/pThr–Pro motif

The Pin1 WW domain interacts with a large number of mitotic phosphoproteins suggesting that Pin1 could play a role in cell cycle control in addition to its role in isomerization (Table 3.1) [32]. The Pin1 WW domain and the PPIase domain both recognize and bind the pSer/pThr–Pro motif. One important difference, however, is that the WW domain displays a higher affinity for the pThr–Pro than the pSer–Pro motif in small peptides; this difference likely results from the longer retardation time for the prolyl cis/trans isomerization of the pThr–Pro bond. In short peptides, the amount of the pThr–*cis*–Pro bond is dependent on the dianionic state of the phosphate moiety, which is not the case for the pSer–*cis*–Pro [45]. The Pin1 WW domain appears to have a stronger interaction for pThr than pSer, and that affinity increases when the consensus sequence is (pThr–Pro–Pro) [45]. Our molecular model of Pin1 in complex with H–GGGGVPRpTPVGG–NH_2 **1** also revealed the methyl side chain of pThr inserted into a small hydrophobic pocket, which probably enhances the affinity of the WW domain for pThr (Fig. 3.1). Crystallography and NMR studies revealed the preference of the WW domain for binding ligands in the trans conformation [32, 87, 114]. Molecular modeling of peptides in the cis conformation resulted in ligands with no binding affinity [32].

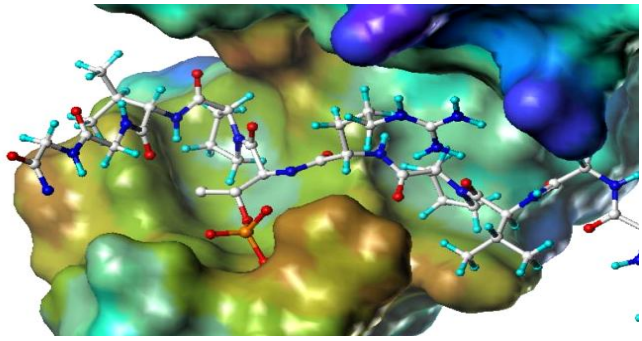

Fig. 3.1. Molecular model showing the Pin1 WW domain binding pocket in complex with H–GGGGVPRpTPVGG–NH_2 **1**, and minimized using Sybyl 8.1.1 (Tripos, Inc.). The electrostatic potential of Pin1 surface indicates sites of attractive interactions with ligand **1** by matching opposite colors, red (most positive) to purple (most negative). The model showed the presence of a methyl side chain of pThr inserted into a small hydrophobic pocket, which probably enhances the affinity of the WW domain for pThr.

The Pin1 PPIase domain is capable of binding both the cis- and trans-substrates—while the Pin1 WW domain is only capable of binding the trans conformation—suggesting a possible role for the WW domain in the stabilization of trans-ligands for the downstream dephosphorylation by protein phosphatases [138].

Table 3.1. Binding affinities (K_d) by fluorescence polarization for peptide fragments identified as Pin1 substrates from cell cycle regulatory proteins. The pT/S–P motif is shown in bold [32].

Peptides	**Full-length Pin1 K_d (μM)**	**WW domain K_d (μM)**	**PPIase domain K_d (μM)**
[a]Rh–VPR**pTP**V (Cdc25c)	4.9 ± 1.1	7.7 ± 3.3	N.B. [b]
[a]Rh–PPA**pTP**P (Myt1)	12 ± 2.1	15 ± 4.7	N.B. [b]
[a]Rh–PPG**pSP**P (Myt1)	80 ± 18	126 ± 21	N.B. [b]
[a]Rh–STS**pTP**R (Myt1)	46 ± 6.5	39 ± 12	N.B. [b]
[a]Rh–Y**pSP**TSPS (CTD)	61 ± 6.3	110 ± 26	N.B. [b]

[a]Rh = rhodamine

[b]No detectable binding (N.B).

3.2 WW domain ligands in drug discovery

Ligands that block the Pin1 WW domain have several advantages compared to Pin1 catalytic inhibitors. First, catalytic inhibitors of enzymes are frequently associated with both high drug tolerance and dependence, since enzyme active sites evolve after drug treatments, eventually leading to drug resistance [139]. Second, enzyme active sites are more likely to be conserved among protein homologues, making it very difficult to achieve drug selectivity for a single member of a protein family [139, 140, 141]. Third, once a drug is bound to a receptor in a regulatory site (i.e., a binding site other than the active site) and saturation occurs, no further changes will take place. This makes allosteric drugs a safer choice for avoiding a drug overdose [139]. Fourth, Pin1 is the only PPIase in humans that has a type IV WW domain. This feature facilitates desired drug selectivity without affecting other essential cellular proteins containing pSer/pThr binding modules [37, 138]. Our objective is to identify ligands that bind selectively the Pin1 WW domain from a combinatorial pSer-Pro dipeptide library. The identification of ligands that block the Pin1 WW domain association with phosphoproteins represents a promising approach for the study of Pin1 in cell cycle regulation and a rational drug design for cancer treatment.

3.3 Combinatorial pSer–Pro dipeptide library for Pin1 WW domain

To identify potent inhibitors of Pin1, the synthesis of a compound library with substrate analogues, and an efficient high-throughput screening (HTS) assays were used. Developing a combinatorial library involves the efficient and timely generation of a large number of ligands that are different, but related in their core structure. Dr. Etzkorn proposed the design and synthesis of small combinatorial libraries targeted to bind at the Pin1 WW domain. Accordingly,

the combinatorial synthesis of a pSer–Pro dipeptide library was achieved by solid-phase peptide synthesis using a Wang resin linked via a phosphoester bond to a phosphorylating reagent developed by Xingguo R. Chen. The incorporation of 21 diverse amines at the C-terminus and 15 diverse carboxylic acids at the N-terminus of the pSer–Pro core generated a combinatorial library of 315 ligands (Fig. 3.2). The substituent amines and carboxylic acids were selected with different structural and chemical properties in order to determine the Pin1 WW domain binding preference (Fig. 3.3a-b).

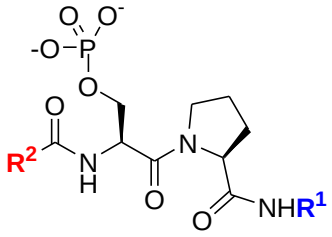

pSer-Pro as the core structure
R^1NH2 = 21 amines, including some secondary amines
R^2COOH = 17 carboxylic acids

Fig. 3.2. pSer–Pro core structure used for the synthesis of a combinatorial library of dipeptides.

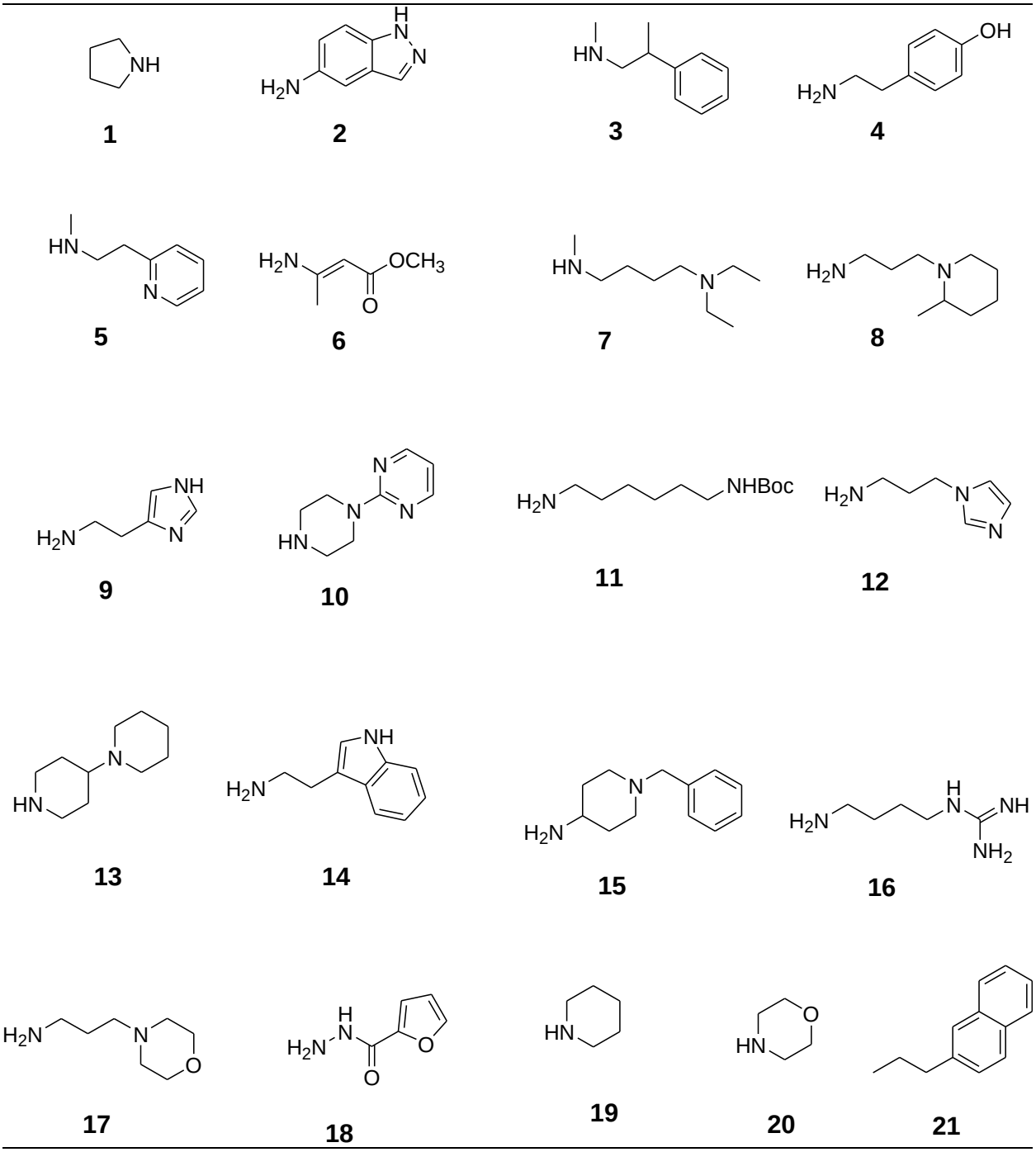

Fig. 3.3a. Structures of the 21 diverse amines to be incorporated at the C-terminus of the pSer–Pro core.

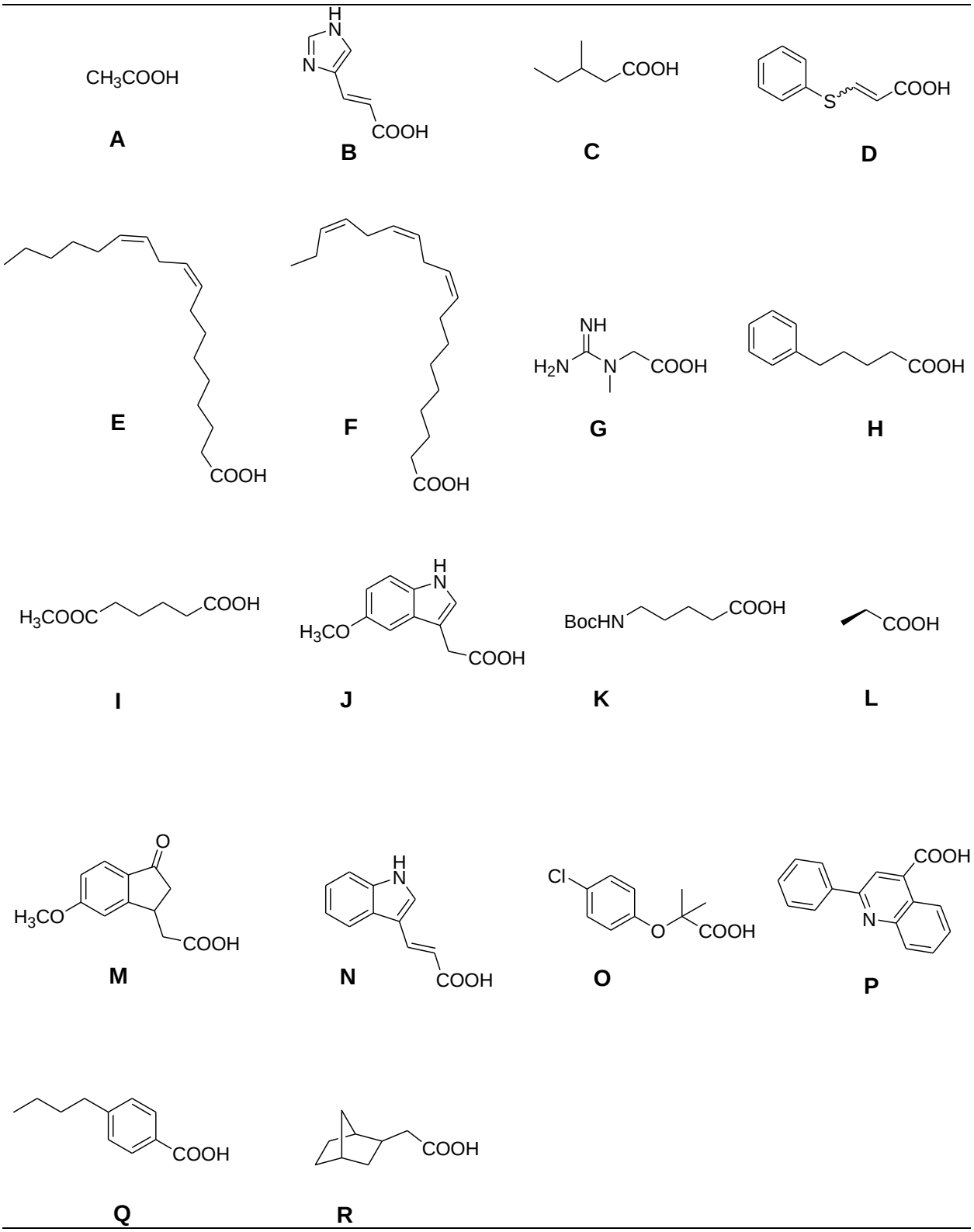

Fig. 3.3b. Structures of the 17 diverse acids to be incorporated at the N-terminus of the pSer–Pro core. Acids N and P did not couple during ligand synthesis.

Material and Methods

3.4 Screening of the pSer–Pro dipeptide library using ELEBA

Fmoc–VPRpTPVGGGK–NH_2, (100 µL/well, 245 µM stock solution) was covalently attached to a 96-well plate through the ε-amino group of the Lys side chain at pH 11.0, as published [90]. Ligands were dissolved in DMSO at stock concentrations of ca. 50 mM by weight. Competitive binding with plate-linked Fmoc–VPRpTPVGGGK–NH_2 (L1) of pSer–Pro dipeptides was measured at ca. 600 µM (Table 3.2) for primary screening. Competitive dissociation constants (K_d) were determined after the large-scale synthesis, HPLC purification, and quantification of cis-D2, trans-D2, O2, and M18 ligands that proved to be good hits during a secondary screening. Ligand stock concentrations were 88 mM by weight, and the final concentrations for competitive dissociation constants (K_d) were 2000, 1000, 700, 500, 300, 200, 100, 50, 30, 10, and 5.0 µM. Recombinant human Pin1–HRP (R&D System) was diluted to a final concentration of 200 pM in a PBS buffer containing 2% BSA at a pH of 7.3. The Pin1–HRP in the ligand solution was pre-incubated with ligand for 30 min with orbital shaking. The resulting solutions containing 100 µL/well of Pin1–HRP and ligand were added to the 96-well plate and incubated for one additional hour. The solutions were decanted, and the wells were washed with wash buffer containing 10 nM imidazole, and 0.05% Tween 20 in PBS at pH 7.3 (3 × 150 µL/well). The substrates hydrogen peroxide and 3,3’,5,5’-tetramethylbenzidine (R&D System) were added to the plate in a 1:1 ratio (100 µL/well), and incubated at room temperature for 20 minutes in the dark. The stop solution, 2 N H_2SO_4 (50 µL/well), was then added to the 96-well plate in order to ensure similar kinetics among the samples. The optical density (OD) of each well was immediately determined using a plate reader (Spectra Max 340 PC) with UV absorbance detection at 450 nm.

Table 3.2. ELEBA screening of the pSer–Pro dipeptide library.

Groups	No. of ligands	No. of positive hits	Retest
A and B	42	1	1
C and D	42	3	1
E, F, G, and H	83	2	1
I, J, and K	63	4	1
M, N, O, and P	84	6	1
Q and R	42	0	0

Primary screening of library ligands was performed at ca. 600 µM by weight. Positive hits were ligands that blocked 50% or more of the Pin1–HRP association with plate-linked ligand (L1).

3.5 Screening results of the pSer–Pro dipeptide library

In total, we screened a library of 356 pSer–Pro ligands (Appendix B). Acid N and P did not couple during the synthesis, which made the assay results useless for group N and P. We developed the ELEBA for the screening of ligand libraries. From the screen, we identified seven ligands that were capable of blocking 50% or more of the Pin1–HRP association with plate-linked ligand (L1), confirming the efficacy of ELEBA in identifying ligands that bind at the WW domain from a compound library[90]. Competitive dissociation constants (K_d) for the best ligands: trans-D2, cis-D2, O2, and M18 were measured. K_d values were normalized to percentage Pin1–HRP bound to the plate-linked ligand by setting the lowest concentration of competitive ligand in solution to 100% binding (eq.1)[90]. The K_d values were 820 ± 6.4 µM (trans-D2), 263 ± 6.4 µM (cis-D2), 206 ± 3.4 µM (O2), and 130 ± 3.0 µM (M18) (Table 3.3, Fig. 3.4-3.5).

$$\%\ \text{of binding} = a + \frac{(b - a)}{(1 + 10^{(c - [L])})} \qquad (1)$$

The **a** value represents the top of the fitted curve, the **b** value represent the bottom of the curve, the **c** value corresponds to the response halfway between a and b values. The competitive K_d values were calculated by solving for log [**L**] when % binding (y) = 50% (Eq. 1)[90].

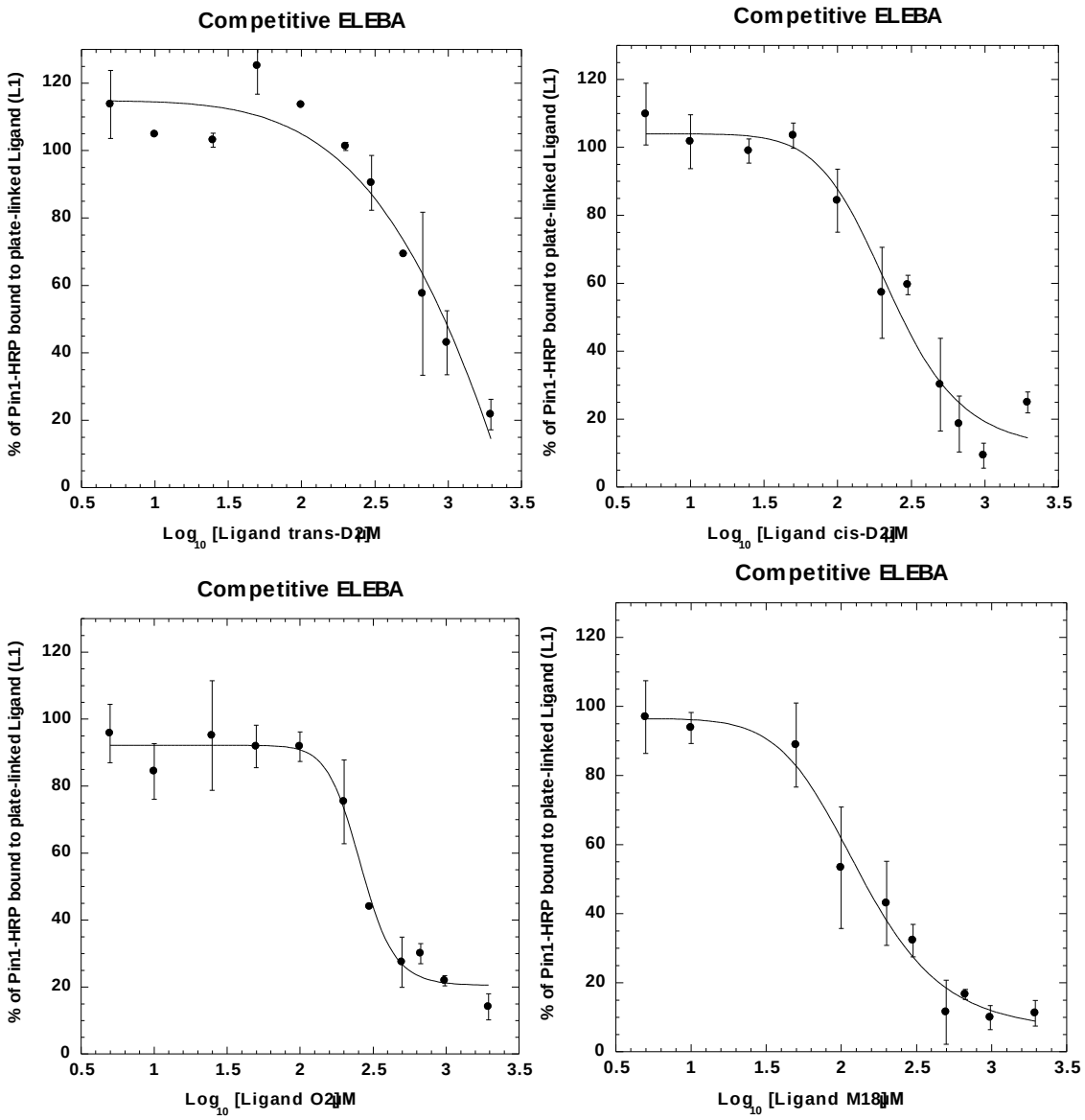

Fig. 3.4. Binding curves showing the % of Pin1–HRP bound to plate-linked ligand L1 at varying concentrations of ligands cis-D2 (top left), trans-D2 (top right), O2 (bottom left), M18 (bottom right). Data are an average of N = 2 with standard deviations shown in the error bars; the data were fitted to Eq. (1), using KaleidaGraph 4.3. The estimated competitive K_d values were 820 ± 6.4µM for D2 trans, 263 ± 6.4 µM for D2 trans, 206 ±3.4 µM for O2, and 130 ± 3.0 µM for M18 respectively. (Prepared with Kaleidagraph 4.3.)

Table 3.3. Variable values fitted for ligand binding curves.

Ligand	a	b	c	R^2	K_d value
Trans-D2	109 ± 2	-32 ± 17	3.1 ± 0.1	0.996	820 ± 6.4
Cis-D2	110 ± 7	1.4 ± 12	2.3 ± 0.2	0.976	263 ± 6.4
O2	93 ± 4	6.3 ± 6	2.3 ± 0.1	0.994	206 ± 3.4
M18	101 ± 4	0.06 ± 5	2.1 ± 0.1	0.993	130 ± 3.0

Table 3.4. Competitive dissociation constants (K_d) for the best ligands identified as the best hits during a secondary screening.

Ligand	Structure	K_d value µM
Trans-D2	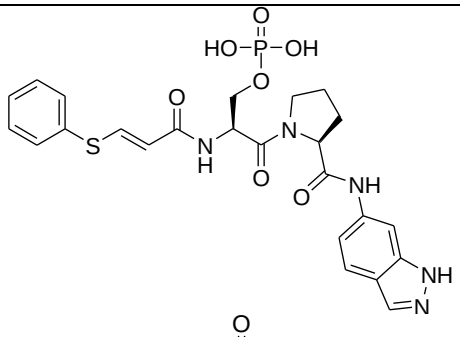	820 ± 6.4
Cis-D2	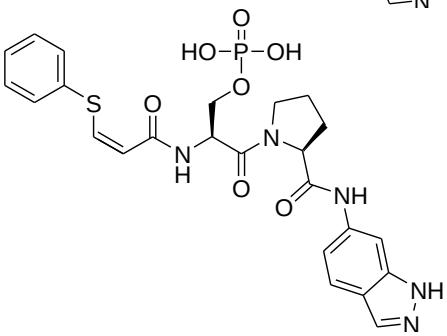	263 ± 6.4
M18	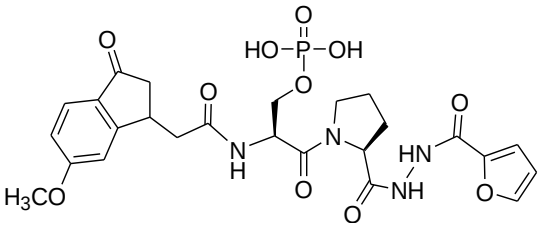	130 ± 3.0
O2	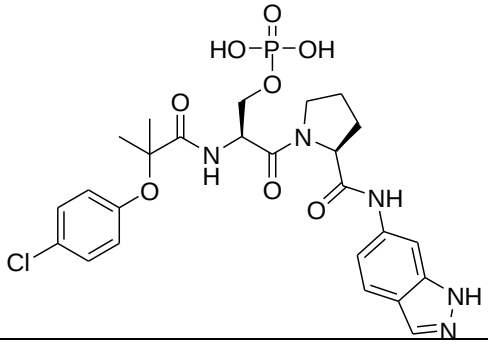	206 ± 3.2

The K_d values provide the basis for a structure-activity relationship (SAR) for the WW domain. We identified two major structural features of ligands that enhance the Pin1 WW

domain affinity for ligands. Polar aromatic acids appear to be the best building blocks at the N-terminus, and polar hydrophobic amines were the best substituents at the C-terminus. It appears that the acid and amine structures at each side of the pSer–Pro motif are not additive for the WW domain binding of ligands. For example, from the screening, ligands M18 and O2 have the higher affinity for the WW domain, K_d values of 130 and 206 μM, respectively (Table 3.4). An additive structure would result in ligands O18 and M2 being as good or better than M18 and O2. However, ligands O18 had lower affinity for the WW domain than M18, and M2 was worse than O2 (Fig. 3.5). We hypothesize that the WW domain binding-pocket could not accommodate simultaneously two large bulky-hydrophobic substituents at each side of the pSer-Pro motif.

The ELEBA was developed as a method for high-throughput screening, rather than as an absolute measure of binding affinity. Since our method is competitive with a potent ligand linked to a plate (L1), it is not to be taken as a direct measurement of binding affinity [90]. The K_d values for cis-D2, O2, and M18 with the Pin1 WW domain were measured another way by NMR (Jill Bouchard and Jeffrey Peng, University of Notre Dame). The K_d values were determined to be 88 ± 8 (cis-D2), 175 ± 21 (O2), and 108 ± 20 μM (M18). NMR titration studies were performed using the full-length Pin1 at different concentrations of ligands (Appendix, 2. Fig S.27-S28). The chemical shift perturbations demonstrate localized binding of ligands to the WW domain of Pin1. Eleven residues from the WW domain (K13, R14, M15, S16, G20, R21, A31, S32, Q33, W34, and E35) consistently reported perturbations upon ligand binding, versus three residues located at the PPIase domain (S114, K132, and V150). Interestingly, chemical shift perturbations of Pin1 catalytic residues (H59, C113, S116, and H157) were not observed during the titration studies, which indicates that ligands bind selectively at the Pin1 WW domain.

Molecular models of trans-D2, cis-D2, O2, and M18 at the Pin1 WW domain, under investigation by Xingguo R. Chen, will provide additional evidence for ligand binding modes in the WW domain. The ELEBA proved crucial for the rapid detection of ligands that bind at the WW domain from a pSer–Pro ligand library, and the measurement of competitive binding affinities (K_d) for hit ligands. The K_d values provide structural activity relationship (SAR) that could serve in the rational design of a specific tight-binding WW domain ligand. Such a ligand could block the Pin1 association with its physiological substrates.

We observed an apparent enhanced signal in comparison to the negative control (DMSO), for some ligands that do not block the Pin1 WW domain association with the plate-linked ligand (L1), i.e. ligand B20 (Fig. 3.5). B20 could be an agonist for WW domain binding L1 on the plate. But, we did not investigate this further. It is likely, therefore, that some ligands bind at the PPIase domain, since all ligands contain the pSer–Pro motif, which is also recognized by the PPIase domain. Once ligands are bound to the PPIase domain, the free WW domain may become more stably folded and bind tightly to the plate-linked ligand L1. Verdecia et al. showed that full-length Pin1 binds phosphorylated ligands more tightly than the isolated Pin1 domains; these findings can be attributed to the folding stabilization of the whole protein [32].

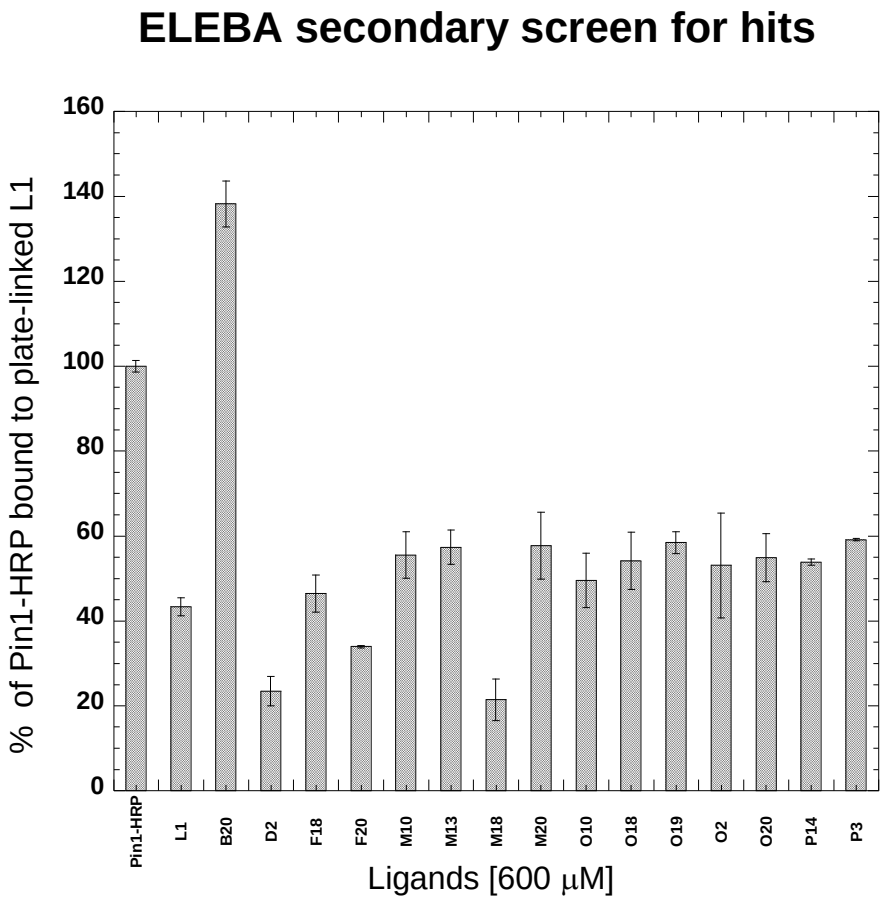

Fig. 3.5. Secondary screening of pSer-Pro dipeptide ligands. Fifteen pSer–Pro dipeptide ligands (600 μM) were screened again using ELEBA, DMSO was used as negative control, and Fmoc–VPRpTPVGGGK–NH_2 (L1) (60 μM) was used as positive control. (Prepared with Kaleidagraph 4.3.)

3.6 Screening of proteins with ELEBA

Application of the ELEBA was extended to proteins that bind at the Pin1 WW domain[32, 69]. We performed ELEBA with protein phosphatase inhibitor-2 (I-2) as the WW domain ligand. I-2 is a small protein of 205 amino residues containing a single pThr72–Pro73 motif, which is a known Pin1 binding partner [69]. To study the nature of the Pin1 interaction with I-2, we assayed six I-2 protein homologues obtained from Dr. David Brautigan (University of Virginia) using ELEBA (Table 3.5). These proteins were diluted in PBS at pH 7.3 to make equal concentration stock solutions of ca. 65 μM. We assayed concentrations ranging from 0.1-

10 μM for each protein, in accord with an identified dissociation constant of 1 μM for an I-2 wild type (wt) in complex with Pin1 [69]. BSA as the negative control was used at the same concentration as the I-2 proteins. Fmoc-VPRpTPVGGGK-NH_2 (L1) (100 μL/well, 245 μM stock solution) was used as the plate-linked ligand, and as the positive control (78 μM).

Table 3.5. ELEBA for I-2 proteins.

Protein	M_r	concentrations
Xenopus laevis I-2	21470	0.1,1, and 10 μM
Drosophila melanogaster I-2	22968	0.1,1, and 7.3 μM
Truncated I-2 (14-197)	20523	0.1,1, and 6.6 μM
GLC	ND	1 and 6.6 μM
I-2 wt	23015	0.1,1, and 10 μM
pThr-I-2	23095	0.1,1, and 10 μM
BSA	69293	0.1, 1, and 10 μM

Concentration of I-2 proteins used based in an identified K_d of 1 μM, ND = no-determined [69].

3.7 Result of protein screening with ELEBA

None of the I-2 proteins appeared to block the Pin1–HRP WW domain association with plate-linked ligand (WW1) at an assay concentration of 0.1-10 μM (Fig. 3.6). Interestingly, the binding of the I-2 protein to Pin1 appears to be independent of the I-2 phosphorylation state, but rather depends of the phosphorylation state of Pin1 [69]. These findings confirm a prior report that the binding of I-2 proteins to Pin1 requires the phosphorylation of Pin1 at Ser16 [69]. In conducting the ELEBA, we used commercially available recombinant Pin1–HRP expressed in *E. coli;* therefore, not phosphorylated Ser16.

The Pin1 WW domain is phosphorylated at Ser16 (pS16-Pin1) by the protein kinase-A (PK-A), a cAMP-dependent kinase, which hinders Pin1's ability to bind phosphoproteins during interphase and during the onset of mitosis [69, 74]. Specifically, during interphase and entry into mitosis, the binding of Pin1 to the protein I-2 restores the pS16-Pin1 binding affinity for phosphoproteins [69]. The binding of pS16-Pin1 to I-2 is likely to alter the Pin1 conformation

and facilitate the formation of a ternary complex with some (but not all) phosphoproteins identified as Pin1 substrates [69].

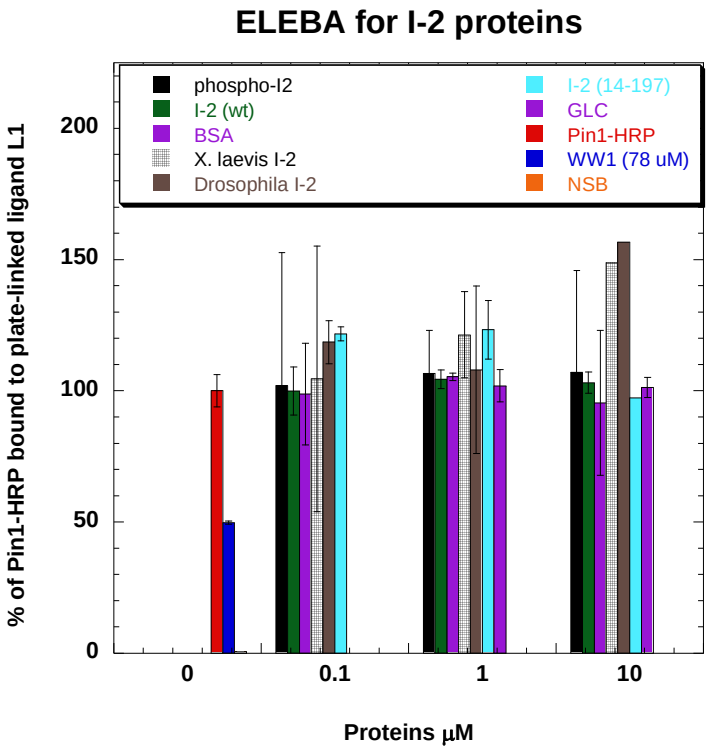

Fig. 3.6. I-2 proteins were screened using ELEBA, BSA was used as negative control, and Fmoc–VPRpTPVGGGK–NH_2 (L1) was used as positive control. (Prepared with Kaleidagraph 4.3.).

3.8 Summary of library screening using ELEBA

We would like to extend the use of ELEBA to full-length phosphoproteins identified as Pin1 WW domain ligands, such as Cdc25c, Wee1, CTD, and Myt1. Quantitative K_d values of Pin1 interactions with phosphoproteins can be easily identified and compared to known peptide ligands [32]. Our study of Pin1 with I-2 was inconclusive because wt Pin1 was used. Therefore, an in vitro kinase phosphorylation of Pin1 at Ser16 using pK-A will be used to produce the desired pSer16-Pin1 for a better understanding of Pin1 interactions with I-2 proteins.

Chapter 4

PPIase catalytic assay for the identification of Pin1 inhibitors

4.1 Inhibitors of Pin1 catalysis

Research evidence suggests that Pin1 regulates the activity, location, and function of other proteins and plays a critical role in the activation of various oncogenic pathways [26, 60, 72, 93]. To identify Pin1 inhibitors with therapeutic properties, a number of approaches have been used, including the following: the screening of combinatorial libraries, molecular modeling, chemical synthesis, and bioassays [29, 46, 49, 113, 114, 115, 116, 117, 125, 133]. Because of these efforts, several molecules have been broadly identified as Pin1 inhibitors [29, 46, 49, 113, 114, 115, 116, 117, 125, 133]—not all of which function in the same way. Some of these molecular inhibitors lack selectivity and potency for Pin1, which limit their use as therapeutic drugs (Chapter 1). Previously, we developed an Enzyme-Linked Enzyme-Binding Assay (ELEBA), which was designed to identify ligands that bind at the Pin1 WW domain (Chapter 2) [90]. In this chapter, I describe our efforts to identify inhibitors of Pin1 from a compound library using the Pin1 catalytic discontinuous assay (PPIase assay).

4.2 Pin1 PPIase assay

The catalytic activity of PPIases is detected by the hydrolysis of a chromophore from the trans-amide isomer by a serine protease [114, 142, 143]. We used α-chymotrypsin, which hydrolyzes only the trans conformation of the Suc–Ala–Glu–Pro–Phe–chromophore when proline occupies the P2 position of the C-terminus in a peptide chain [142]. In aqueous solution, only 10% of the assay substrate adopts the cis conformation and often, 0.5 M LiCl/TFE is used

to increase the amount of cis substrate from 10 to 30-70% (Fig. 4.1) [143]. In addition, the suppression of non-enzymatically catalyzed, or thermal isomerization (k_3) is necessary by careful control of the assay temperature at ca. 2-5 °C [114, 143]. For the Pin1 assay automation and library screening, assay conditions such as temperature, the ratio of cis to trans substrate, and the concentrations of enzymes must be carefully controlled.

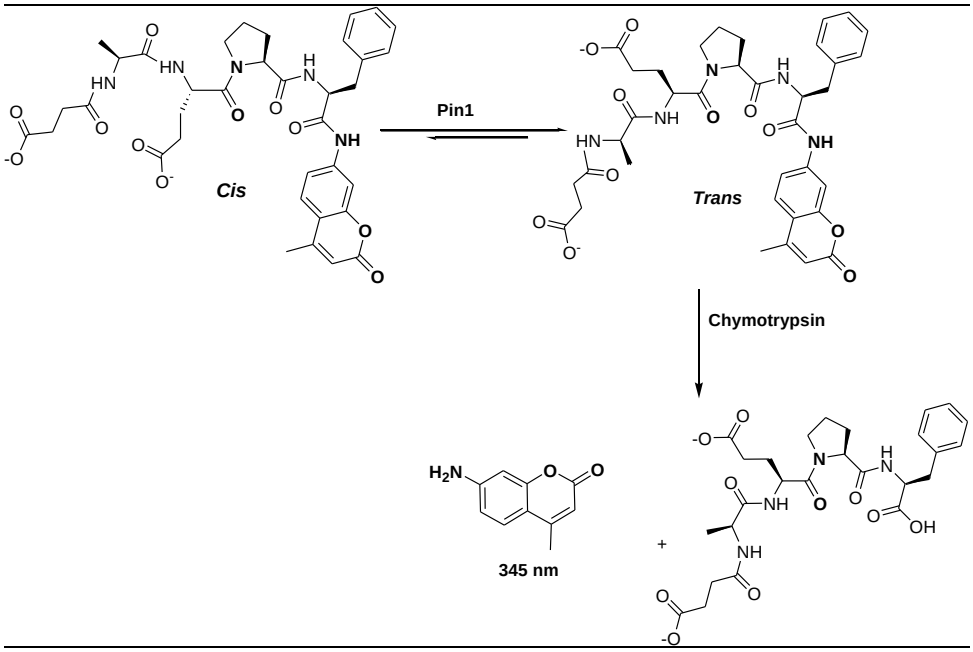

Fig. 4.1. Pin1 proteolytic coupled assay: The enzymatic activity of Pin1 is coupled with α-chymotrypsin hydrolysis of a chromophore.

4.3 Assay substrate

Traditionally, *p*-nitroanilide (*p*NA) substrates are the preferred chromogenic substrates used to monitor PPIase activity in the presence of serine proteases [26, 114, 143]. During a preliminary assay, we observed *p*NA precipitation at high substrate concentration 150-200 µM. Therefore, we replaced the *p*NA moiety in the peptide substrate with a 7-amino-4-methylcoumarin (AMC) chromophore [113]. The resulting AMC fluorescent product was shown to increase assay sensitivity approximately 700-fold after chymotrypsin hydrolysis [144]. The Suc–Ala–Glu–Pro–Phe–AMC is analogous to the *p*NA-substrate. The negatively charged, long,

and flexible side chain of the glutamic acid mimics the phosphate. In addition, previous experiments have shown that Suc–Ala–Glu–Pro–Phe–*p*NA has a K_m of 120 µM [113], which makes the Suc–Ala–Glu–Pro–Phe–AMC a good substrate to screen for weak hits from the library. Since large quantities of substrate were required for high-throughput screening, a solution phase synthesis was performed (Scheme 4.1).

Scheme 4.1. Synthesis of Suc–Ala–Glu–Pro–Phe–AMC, **6**.

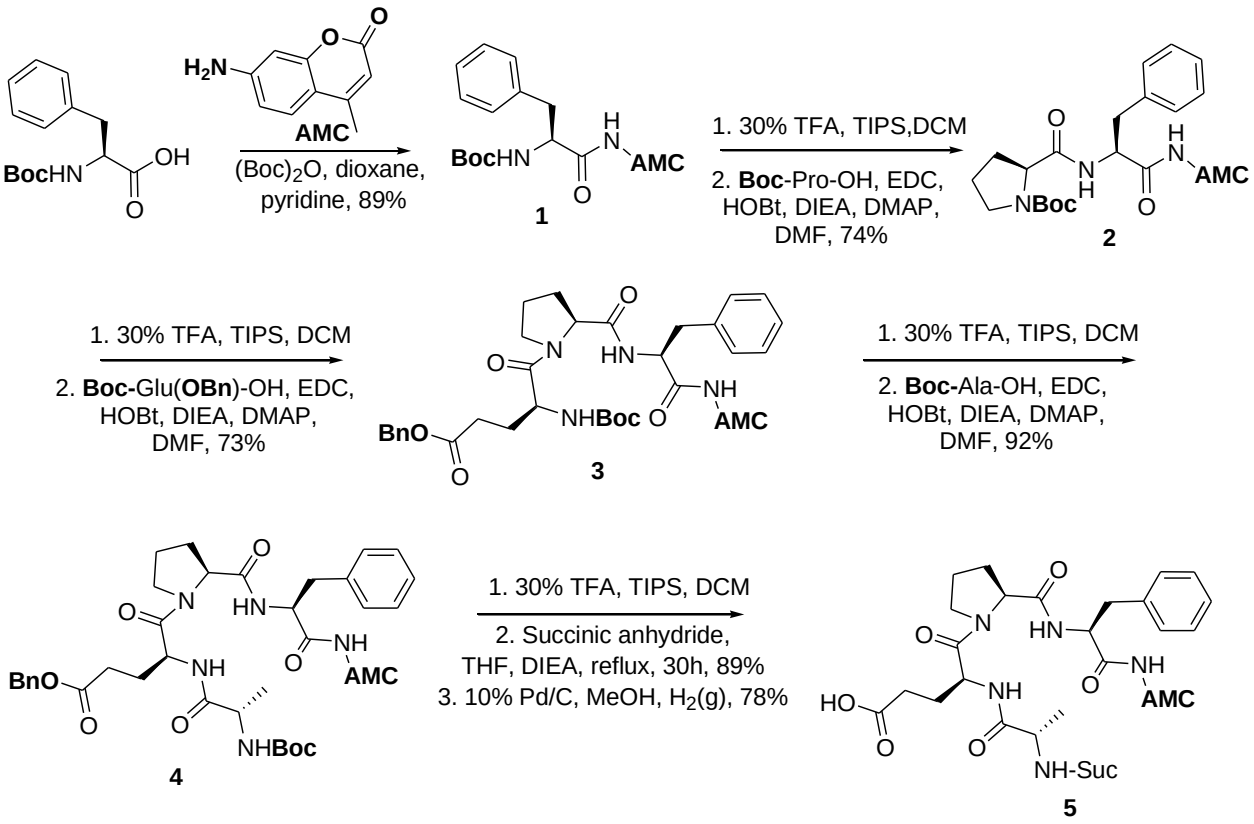

Material and Methods

4.4 Synthesis of Suc–Ala–Glu–Pro–Phe–AMC

Boc–Phe–AMC, 1. Boc–Phe–OH (859 mg, 3.31 mmol), pyridine (0.27 mL, 3.4 mmol), and $(Boc)_2O$ (732 mg, 3.35 mmol) were dissolved in dioxane (10 mL). Excluding from the light to protect the AMC, the AMC (500 mg, 2.79 mmol) was dissolved in dioxane (5 mL), THF (5

mL) was added as a co-solvent to increase the poor solubility of the AMC. The reaction mixture was stirred at 25°C for 24 h [145],and quenched by the addition of EtOAc (30 mL). The mixture was washed three times with 1M aq. $KHSO_4$ (3 × 60 mL), H_2O (60 mL), saturated aqueous $NaHCO_3$ (60 mL), H_2O (60 mL), and brine (60 mL). The organic layer was then dried with $MgSO_4$ and concentrated in vacuum. The crude product was recrystallized from CH_2Cl_2 (20 mL) at rt (1.1 g, 89%). 1H NMR (400 MHz, CDCl3) δ 8.8 (br s, 1H), 7.6 (br s, 1H), 7.4 (d, *J* = 8.0 Hz, 2H), 7.36-7.19 (m, 7H), 7.1 (br s, 1H), 6.1 (s, 1H), 5.2 (br s, 1H), 4.6 (s, 1H), 3.1 (dd, *J* = 8.0, 7 Hz, 2H), 2.4 (s, 3H), 1.4 (s, 9H), (Appendix C, Fig. S29).

Boc–Pro–Phe–AMC, 2. Compound **1** (1.1 g, 2.51 mmol) was dissolved in TFA (4.0 mL), CH_2Cl_2 (12.0 mL), and triisopropyl silane (TIPS) (0.98 mL). The reaction mixture was stirred at 25 °C for 30 min; residual solvent was evaporated in vacuum. A mixture containing Boc–Pro–OH (1.1 g, 5.0 mmol), DIEA (4.5 mL, 25.2 mmol), HOBt (0.77 g, 5 mmol), 1-[3-(dimethylammino)propyl]-3-ethylcarbodiimide hydrochloride (EDC·HCl) (0.96 g, 5 mmol), and 4-(dimethylamino)pyridine (DMAP) (6.9 mg, 0.05 mmol) in DMF (20 mL) was stirred at 0°C for 10 min. Crude H–Phe–AMC·TFA salt in DMF (20 mL) was added to the mixture and stirred at 25 °C for 24 h. The reaction was quenched with EtOAc (60 mL). The mixture was washed with H_2O (3 × 60 mL), 1N HCl (3 × 60 mL), NaH_2CO_3 (3 × 60 mL), and saturated NaCl (3 × 60 mL). The organic layer was dried with $MgSO_4$ and concentrated under vacuum, which resulted in crude **2** (0.95 g, 74%). ^{1}H NMR (400 MHz, $CDCl_3$) δ 8.93 (br s, 1H), 7.82 (s, 1H), 7.67 (d, *J* = 8 Hz, 1H), 7.48 (d, *J* = 9.0 Hz, 1H), 7.34-7.11 (m, 8H), 7.04 (s, 1H), 6.41 (d, *J* = 8.5 Hz, 1H), 6.17 (s, 1H), 4.88 (s, 1H), 4.23 (d, *J* = 5.0 Hz, 1H), 3.56-2.81 (m, 5H), 2.38 (s, 3H), 1.99 (m, 6H), 1.27 (s, 9H), 1.04 (s,1H) (Appendix C, Fig. S30).

Boc–Glu(OBn)–Pro–Phe–AMC, 3. Boc–Pro–Phe–AMC **2** (0.95 g, 1.8 mmol) was dissolved in TFA (4.0 mL), CH_2Cl_2 (12.0 mL), and TIPS (0.98 mL, 6.2 mmol) for deprotection similar to compound **1**. A mixture containing Boc–Glu(OBn)–OH (1.2 g, 3.6 mmol), DIEA (3.10 mL, 18.4 mmol), HOBt (0.56 g, 3.6 mmol), EDC·HCl (0.69 g, 3.6 mmol), and DMAP (5.5 mg, 0.04 mmol) was stirred at 0 °C for 10 min. Crude H–Pro–Phe–AMC·TFA salt in DMF (20 mL) was added to the mixture and stirred at 25 °C for 26 h. The reaction was quenched and worked up as for **2**. Silica gel flash chromatography with a 1:9 ratio of hexane and ethyl acetate was used for separation of the two apparent isomers in a 2:1 ratio. A major isomer (625 mg, 47%) and a minor isomer (343 mg, 26%) were obtained. Both isomers were independently synthesized to final products. Major isomer: ^{1}H NMR (400 MHz, $CDCl_3$) δ 8.77 (s, 1H), 7.80 (s, 1H), 7.68 (d, *J* = 7.8 Hz, 1H), 7.49 (d, *J* = 8.7 Hz, 1H), 7.39-7.14 (m, 16H), 6.86 (d, *J* = 9.1 Hz, 1H), 6.18 (s, 1H), 5.19 (d, *J* = 7.7 Hz, 1H), 5.08 (dd, *J* = 12.1, 12.2 Hz, 2H), 4.90 (dd, *J* = 5.6, 8.6 Hz, 1H), 4.51 (m, 3H), 3.64 (s, 1H), 3.52 (s, 1H), 3.42-3.29 (m, 1H), 3.26-3.12 (m, 1H), 3.05 (m, 1H), 2.39 (s, 3H), 2.18-1.55 (m, 9H), 1.44 (s, 9H), 1.26 (t, *J* = 7.1 Hz, 1H) (TMS ref.) (Appendix C, Fig. S31). Minor isomer: ^{1}H NMR (400 MHz, $CDCl_3$) δ 8.88 (s, 1H), 7.79 (s, 1H), 7.65 (d, *J* = 7.02 Hz, 1H), 7.41 (d, *J* = 8.7 Hz, 1H), 7.35–7.12 (m, 13H), 6.80 (s, 1H), 6.14 (s, 1H), 5.24 (s, 1H), 5.14 (br s, 2H), 4.82 (dd, *J* = 6.5, 5.0 Hz, 1H), 4.39 (t, *J* = 6.0 Hz, 1H), 4.29 (s, 1H), 3.29 (m, 4H), 2.34 (s, 3H), 2.29 (d, *J* = 6.5 Hz, 1H), 2.21–1.55 (m, 9H), 1.36 (s, 9H) (Appendix C, Fig. S32).

Boc–Ala–Glu(OBn)–Pro–Phe–AMC, 4. The major isomer **3** (0.63 g, 0.85 mmol) was dissolved in TFA (2.0 mL), CH_2Cl_2 (6.0 mL), and TIPS (0.49 mL, 3.1 mmol) and reacted as in **2**. A mixture containing Boc–Ala–OH (0.32 g, 1.7 mmol), DIEA (1.5 mL, 10.2 mmol), HOBt (0.26

g, 1.7 mmol), EDC·HCl (0.33 g, 1.7 mmol), and DMAP (2.3 mg, 0.02 mmol) was stirred at 0 °C for 10 min. Crude H–Glu–Pro–Phe–AMC·TFA salt in DMF (12 mL) was added to the mixture and stirred at 25 °C for 24 h. The reaction was quenched with EtOAc (30 mL), and worked up as for **2**. The crude major isomer **4** (0.64 g, 92%) was obtained. ^{1}H NMR (400 MHz, $CDCl_3$) δ 8.90 (s, 1H), 7.98 (d, *J* = 7.9 Hz, 1H), 7.75 (s, 1H), 7.54 (d, *J* = 8.7 Hz, 1H), 7.39 - 7.13 (m, 18H), 6.84 (d, *J* = 8.8 Hz, 1H), 6.20 (s, 1H), 5.46 (s, 1H), 5.04 (dd, *J* = 34.6, 12.3 Hz, 2H), 4.89 (dd, *J* = 13.9, 9.1 Hz, 2H), 4.72 (dd, *J* = 9.3, 4.8 Hz, 1H), 4.36-4.30 (m, 1H), 4.18-4.08 (m, 1H), 3.69-3.51 (m, 2H), 3.44 (q, *J* = 6.3, 6.2, 6.4 Hz, 1H), 3.23 (dd, *J* = 4.6, 9.6 Hz, 1H), 2.51-2.30 (m, 7H), 2.19-1.64 (m, 9H), 1.39 (d, *J* = 7.2 Hz, 3H), 1.36 (s, 10H), 1.07 (s, 1H) (Appendix C, Fig. S33). Minor isomer **4**, ^{1}H NMR (400 MHz, $CDCl_3$) δ 8.94 (s, 1H), 7.72 (s, 3H), 7.47 (d, *J* = 9.3 Hz, 2H), 7.39–7.18 (m, 31H), 6.86 (s, 1H), 6.70 (s, 1H), 6.17 (s, 1H), 5.14 (s, 3H), 4.82 (s, 1H), 4.57 (s, 1H), 4.32 (s, 1H), 4.12 (m, 1H), 3.42–3.16 (m, 7H), 2.38 (s, 3H), 2.25–1.66 (m, 15H), 1.60 (s, 8H), 1.41 (s, 9H), 1.29 (d, *J* = 7.1 Hz, 5H), 1.06 (d, *J* = 1.7 Hz, 1H) (Appendix C, Fig. S34).

Suc–Ala–Glu(OBn)–Pro–Phe–AMC, 5. Boc–Ala–Glu(OBn)–Pro–Phe–AMC **4** (0.64 g, 0.79 mmol) was dissolved in TFA (4.0 mL), CH_2Cl_2 (12.0 mL), and TIPS (0.98 mL, 6.2 mmol) and reacted as for **2**. The crude H–Ala–Glu(OBn)–Pro–Phe–AMC·TFA salt was dissolved in dry THF (20 mL) with DIEA (0.6 mL, 4.2 mmol), and succinic anhydride (78 mg, 0.7 mmol). The mixture was then heated at reflux (70 °C) in an oil bath for 30 h protected from light? [146]. After cooling to rt, the THF was evaporated in vacuum, and CH_2Cl_2 (40.0 mL) was added. The reaction mixture was washed with 1N HCl (2 × 50 mL) and the organic layers were dried with $MgSO_4$, and concentrated under vacuum. The crude peptide **5** (0.5 g, 89%) was obtained.

Suc–Ala–Glu–Pro–Phe–AMC, 6. Suc–Ala–Glu(OBn)–Pro–Phe–AMC **5** (0.5 g, 0.68 mmol) and 10% Pd/C (73 mg) were combined under vacuum avoiding moisture, after which anhydrous CH_3OH (18 mL) and a balloon filled with H_2(g) were added. The reaction mixture was stirred at 25 °C for 21 hours, the Pd/C was removed by filtration through Celite, and the solvent was evaporated under vacuum to obtained compound **6** (380 mg, 78%). Major isomer **6:** ^{1}H NMR (400 MHz, DMSO) δ 12.23 (s, 1H), 10.33 (S, 1H), 8.36 (d, *J* = 7.5 Hz, 1H), 8.15 (d, *J* = 7.1 Hz, 2H), 7.90 (s, 1H), 7.82 (d, *J* = 8.3 Hz, 1H), 7.60 (d, *J* = 8.8 Hz, 1H), 7.43-7.28 (m, 5H), 7.31 (m, 1H), 6.39 (s, 1H), 4.72 (m, 1H), 4.63 (m, 1H), 4.47-4.33 (m, 2H), 3.69 (m, 3H), 3.49 (s, 3H), 3.33-3.00 (m, 2H), 2.62 (s, 3H), 2.50 (s, 4H), 2.41 (m, 3H), 2.19-1.75 (m, 5H), 1.28 (d, *J* = 7.1 Hz, 2H) (Appendix C, Fig. S35). Minor isomer **6:** ^{1}H NMR (400 MHz, DMSO) δ 12.23 (s, 1H), 10.33 (S, 1H), 8.36 (d, *J* = 7.5 Hz, 1H), 8.15 (d, *J* = 7.1 Hz, 2H), 7.90 (s, 1H), 7.82 (d, *J* = 8.3 Hz, 1H), 7.60 (d, *J* = 8.8 Hz, 1H), 7.43-7.28 (m, 5H), 7.31 (m, 1H), 6.39 (s, 1H), 4.72 (m, 1H), 4.63 (m, 1H), 4.47-4.33 (m, 2H), 3.69 (m, 3H), 3.49 (s, 3H), 3.33-3.00 (m, 2H), 2.62 (s, 3H), 2.50 (s, 4H), 2.41 (m, 3H), 2.19-1.75 (m, 5H), 1.28 (d, *J* = 7.1 Hz, 3H) (Appendix C, Fig. S36).

FAB+ molecular ion detection calcd. for $C_{36}H_{41}N_5O_{11}$ $[M + H]^+$ *m/z* = 719.3, found *m/z* = 720.3 for both isomers (Appendix C, Fig. S37-S38). Analytical HPLC in an X-Bridge C18 column, 2.5 µM (4.6 × 50 mm), 10% ACN for 2.5 min, 60% B over 19 min, 210 nm. One single broad peak with a retention time of 12.0 min for the major isomer (Appendix C, Fig. S39), and 11.3 min for the minor isomer (Appendix C, Fig. S40) were observed.

4.5 Expression and Purification of Pin1

The plasmid pET28C that expresses a recombinant form of human His6–Pin1 was a generous gift from Professor Joseph Noel at the Salk Institute. The plasmid pET28C (2 µL) was

transfected in competent *E. coli* cells BL21-DE3 in $CaCl_2$ 0.1 M (20 min on ice, heat-shocked 2 min at 42°C). The cells were then plated on LB kanamycin-50 agar plates (Sigma-Aldrich, L0543) for 15 h, after which they were cultivated in LB media (50 mL) containing 40 µg/mL kanamycin (Sigma-Aldrich, K0254) for 2 h until an OD of 0.8 was reached. The cells were then induced with 1% lactose at 30 °C for 4 h, and then centrifugated at 5,000 rpm at 4 °C for 10 min. The supernatant was subsequently poured out, and the cell pellet was stored at –20°C for one week. The cell pellet (3.5 g) was resuspended in 10 mL of buffer (5 mM imidazole, 500 mM NaCl, 20 mM Tris at pH 7.9) containing a protease inhibitor cocktail (100 µL, Thermo Scientific, # 78410), after which it was sonicated (Branson Sonifier®, S-450D) at the 60% level (1 min in, 1 min out) for 8 min, with cooling in an ice bath. The supernatant was collected after centrifuging the cells at 20,000 rpm at 4 °C for 20 min. The resulting protein was purified on a cobalt (Co^{2+}) metal-chelating 6% agarose resin slurry (1.5 mL, Thermo Scientific, # 89964) in a disposable polypropylene tube (Thermo Scientific). The eluted fractions (3 of 5 mL) were dialyzed overnight in dialysis tubing with a 10,000 MWCO (Fisher Scientific, 08667B) in 20 mM HEPES, 100 mM NaCl at pH 7.5, 1L at 4 °C, and concentrated via membrane filtration (Vivascience, VS0601). The protein was analyzed by SDS-PAGE, and a single band of ca. 22 kDa was identified (Appendix C, Fig. S41). A protein concentration of 1.2 mg/mL was determined by Bradford assay (Appendix C, Fig. S42).

4.6 Determination of k_{cat}/K_m for Suc–Ala–Glu–Pro–Phe–MCA

HEPES buffer pH 7.5 (880 µL, 35 mM stock) and chymotrypsin (100 µL, 60 mg/mL in 0.001 N HCl) were added to the 1.5 mL, 1 cm quartz cuvette, and pre-equilibrated for 20 min at 2 °C. Pin1 in 20 mM Tris·HCl, pH 7.8 (5 µL, 1.7 µM stock) was added. The thermal isomerization rate constant k_3 was determined in the absence of Pin1 at 2 °C. Substrate in dry

0.47 M LiCl/TFE (15 μL, 6.8 mM stock for major isomer, 5.8 mM for minor isomer, determined by absorbance at 325 nm, ε_{390nm} = 7700 M^{-1} cm^{-1}) was added via syringe, and mixed vigorously by inversion three times, with a total time delay of 3-5 sec. The progress of the reaction was monitored at 370 nm for 90 s. The concentrations of the cis component of the major isomer (56%) and minor isomer (25%) substrates were determined by the UV-Vis absorbance after complete cleavage of the AMC by chymotrypsin after 2 min.

4.7 Pin1 PPIase discontinuous-assay optimization

Suc–Ala–Glu–Pro–Phe–MCA (1.0 mM stock, 3.4 μL), and varying Pin1 (1 mM stock, 5-30 nM final) in 50 mM HEPES buffer at pH 7.5 for a total volume of 34 μL were mixed. DMSO was used as negative control (2 μL). The mixture was incubated in an ice bath to reduce the thermal background reaction rate k_3, and then initiated with ice-cold α-chymotrypsin in 0.001 N HCl (4 μL, 60 mg/mL). After 10-50 seconds, the reaction was quenched with HOAc:MeOH (1:1, 40 μL) to obtain a total volume of 80 μL. The absorbance was monitored using a plate reader (Spectra Max 340 PC) at discrete wavelengths from 345-370 nm to identify the most suitable wavelength for the assay.

4.8 Plate reader PPIase assay for screening of the pSer–Pro ligand library

Ligands (10 μL, 500 μM stock solution) were added to a 96-well microplate (Corning Costar 3690, ½ area), DMSO (10 μL) was used as a negative control. The Fmoc-pSer–Ψ[CH_2N]–Pro–2-(3-indolyl)-ethylamine was used as a positive control inhibitor (100 μM, IC_{50} 6.3 μM)[133]. HEPES buffer pH 7.8 (50 mM stock) containing Pin1 (25 nM stock) and Suc–Ala–Glu–Pro–Phe–AMC (250 μM stock), for a total volume of 20 μM, were pre-mixed and incubated with the ligands in an ice bath to reduce the k_3. The reaction was initiated with α-chymotrypsin in HEPES buffer (8 mg/mL stock, 20 μL). After 30 seconds, the reaction was quenched with HOAc:MeOH

(1:1, 50 μL) to obtain a total volume of 100 μL in the presence and absence of Pin1. A Synergy-Biotek microplate reader in the laboratory of Dr. Sakiko Okumoto, (Department of Plant Pathology of Virginia Tech) was used to monitor the relative fluorescence unit (RFU) using an excitation λ 365 and emission λ 460 nm.

Results and discussion

4.9 Synthesis results of Suc–Ala–Glu–Pro–Phe–MCA

Two Suc–Ala–Glu–Pro–Phe–MCA isomers with similar chemical properties were obtained in a 2:1 ratio. HPLC co-injection of both isomers revealed an overlapping peak that split at the crest (Appendix C, Fig. S43). Both isomers displayed similar UV-Vis spectra, which indicated that there was no decomposition of the AMC moiety (Appendix C, Fig. S44). To explain this outcome, we hypothesized that during glutamic acid coupling, epimerization could take place. We assume that the major product was an all L-amino acid peptide, which was used in screening the library. The rate constants of Pin1 with substrates confirmed that both isomers are good for subsequent assays with k_{cat}/K_m = 3.6 $M^{-1}sec^{-1}$ for the major isomer, and k_{cat}/K_m = 3.0 M^{-1} sec^{-1} for the minor isomer. The difference in catalytic rates can likely be attributed to the percentage of cis component in each isomer—which was 56% for the major isomer and 26% for the minor isomer. We obtained 0.76 g of the major isomer and 0.99 g of the minor isomer. It should be noted that a portion of the major isomer was lost during the O-benzyl deprotection. The new Pd/C catalyst was highly active, and after contact with wet MeOH a fire took place. In addition, HPLC re-purification for the major isomer was necessary after we observed three methylated-side products (Appendix C, Fig. S45), which indicated that the use of MeOH should be avoided during O-benzyl deprotection and HPLC purification.

Table 4.1. Summary of the synthesis results

	Major isomer	**Minor isomer**
calcd. $[M + H]^+ = 719.3$	720.3	720.3
Analytical HPLC t_R	12.0 min	11.3 min
k_{cat}/K_m	3.6 $M^{-1}Sec^{-1}$	3.0 M^{-1} Sec^{-1}
Yield	0.76 g	0.99 g

4.10 High-throughput screening assay of Pin1 inhibitors

We perform a preliminary Pin1 proteolytic-catalytic assay to investigate the difference in signal between the enzymatically-catalyzed reaction k_{obs} and the non-enzymatically-catalyzed isomerization k_3 (Fig. 4.2a) for high-throughput screening (HTS). The most significant difference was observed at 10 seconds, and 20 nM of Pin1. However, at 20 and 30 seconds, the reactions gave more consistent results (Fig. 4.2b).

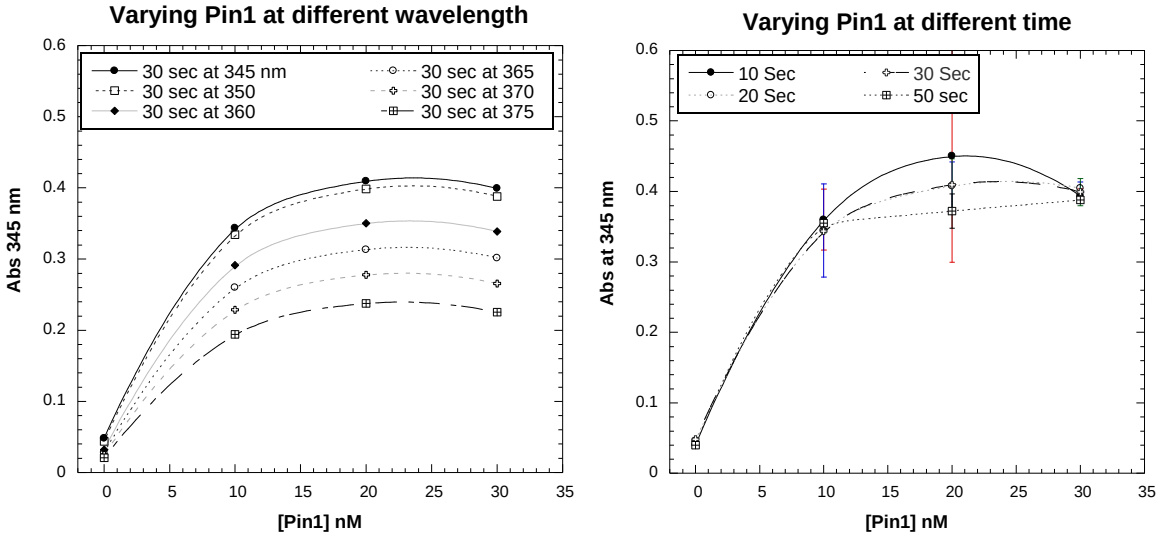

Fig 4.2. Assay optimization. a) Varying Pin1 concentrations with 100 µM of Suc–Ala–Glu–Pro–Phe–MCA substrate at different wavelengths from 345-375 nm. b) Determination of the best time for quenching at discrete time points from 10-50 sec. (Prepared with Kaleidagraph 4.3.)

We sought to automate the assay to screen 165,000 small molecules at the High Throughput Screening Resource Center (HTSRC) at Rockefeller University, which features a

real-time fluorescence instrument that measures fluorescence using a CCD camera in 96 or 384 microplates. Peptidyl–MCA is an excellent substrate for fluorescence assay, since a large enhancement in fluorescence can be observed. We used similar screening conditions as reported for hCyPA by Mori et al. [147]. Mrs. Onyi Freeman (Etzkorn Lab Specialist at Virginia Tech), and Dr. Fraser Glickman (Rockefeller University) conducted the preliminary assays. Data results were not interpretable, revealing a higher signal for Pin1 with the inhibitor Fmoc-pS–Ψ[CH_2N]–P–2-(3-indolyl)-ethylamine (50 µM, IC_{50} 6.3 µM) [133], and without Pin1 than with Pin1 alone (Fig. 4.3). For successful automation of the Pin1 catalytic assay, we discovered that it was essential to suppress the non-enzymatically-catalyzed isomerization (k_3), and short instrumentation delay, as reported for hCyPA of 4s. Regrettably, it was difficult to identify a HTS facility that featured robotic dispensers housed in a cold room, which was essential for our assays.

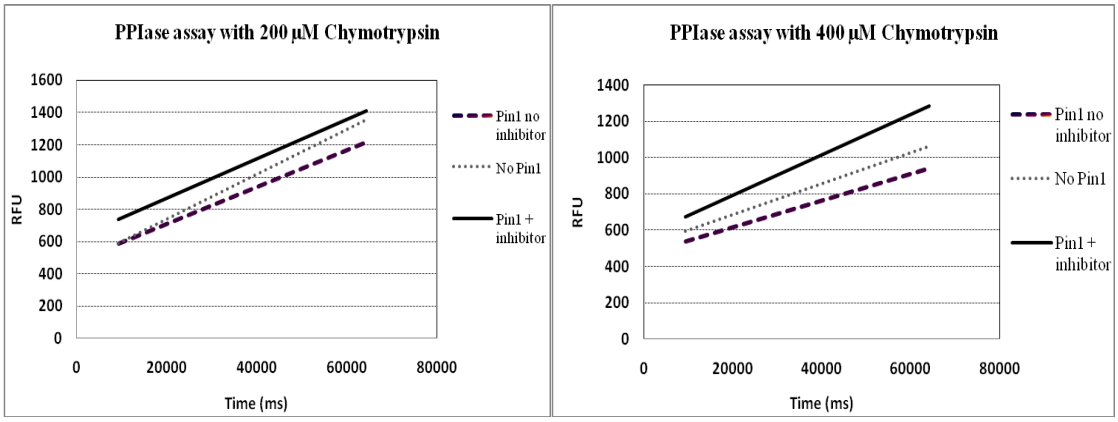

Fig. 4.3. Preliminary screening for assay automation. Pin1 with Fmoc-pS–Ψ[CH_2N]–P–2-(3-indolyl)-ethylamine inhibitor (black line), no Pin1 (dotted line), and Pin1 (dashed line) with different chymotrypsin concentrations. Data was obtained at the High Throughput Screening Resource Center (HTSRC) at Rockefeller University by Onyi Freeman (Virginia Tech).

4.11 Results of the pSer–Pro ligand library screening

During our search for Pin1 WW domain ligands from a combinatorial library of 315 pSer–Pro ligands (Chapter 3), we observed an enhancement in the association between Pin1–

HRP with the plate-linked ligand L1 (Fig. 3.5). Based on this observation, we hypothesized that some ligands might be binding the PPIase domain, because ligands containing the pSer–Pro motif are also recognized by the PPIase domain. To investigate our hypothesis, we screened the combinatorial library of 315 pSer–Pro ligands using the PPIase discontinuous assay (Table 4.2).

Table 4.2. PPIase screening of the pSer–Pro dipeptide library.

Groups	No. of ligands	No. of positive hits	Retest for False positives
A and B	42	0	2
C and D	42	1	5
E and F	42	0	0
G and H	42	1	1
I, J, and K	63	2	2
M, and O	42	0	3
Q and R	42	0	0

Primary screening of library ligands was performed at 100 μM by weight.
Positive hits were ligands that decreased the release of the AMC 50% or more.
Ligands were re-tested with and without Pin1.

The intensity of the signal (I) was determined using (eq. 2), where $RFU_{(Pin1+L)}$ represents the amount of AMC cleaved in the presence of Pin1 and ligand, $RFU_{(no\ Pin1)}$ represents the amount of peptide cleaved in the absence of Pin1(background thermal isomerization), and [Pin1] represents the final Pin1 concentration for the assay [148]. Data were normalized to percent of active Pin1 using the ratio of RFU in the presence of ligand (L) to the RFU of the negative control (DMSO) using (eq. 3).

$$I = \frac{(RFU_{(Pin1+L)} - RFU_{(no\ Pin1)}}{[Pin1]} \qquad (2)$$

$$\%\ of\ active\ Pin1 = \frac{I(Ligand)}{I(DMSO)} \times 100 \qquad (3)$$

We classified as positive hits the ligands capable of decreasing the catalytic rate of Pin1 by more than 50%. From the primary screening, ligands D20, H16, K7, and K19 appeared to

affect the Pin1 catalytic activity (Table 4.2). However, we observed a great deal of data inconsistency for some ligands and the positive control Fmoc-pS–Ψ[CH_2N]–P–2-(3-indolyl)-ethylamine (Appendix C, Fig. S44-47). To investigate the source of the data inconsistency, and re-test hit ligands, and ligands with aromatic moieties for the measurement of possible signal interference at Em_{365}/Ex_{460} nm. Ligands D20 and K7 decreased Pin1 catalytic activity by 90% or more, consistent with the primary screen. In addition, we observed that some ligands have an effect on the intensity of the RFU of the substrate, but the data variability remained unclear (Appendix C, Fig. S48). We quenched the assay with 2 mM phenylmethanesulfonyl fluoride (PMSF) in 100% 2-propanol to ensure the complete inactivation of α-chymotrypsin after quenching. PMSF is a suicide inhibitor of serine protease. In our continuous-kinetic assay, PMSF inactivated α-chymotrypsin within four seconds with proper mixing of the sample by inversion of the cuvette three times. However, pipetting the PMSF quenching solution up and down in the well was not sufficient for the complete inactivation of α-chymotrypsin (Appendix C, Fig. S49). We believe that the source of the data inconsistency for our bench-top PPIase discontinuous assay could be the mixing technique of pipetting the sample up and down using the micropipettor with either HOAc:MeOH (1:1) or PMSF.

4.12 PPIase assay summary

The traditional Pin1 continuous, proteolytic assay was adapted to a discontinuous assay in a 96/384-well microplate format to identify inhibitors of Pin1. Despite our efforts, it was difficult to identify a HTS facility that featured robotic dispensers housed in a cold room, which was essential for automation of our assay. We manually screened a small, focused library of 315 pSer-Pro ligands, and two potential ligands were identified. Because our manual screening was in aqueous solution, the 10 % *cis*-substrate conversion had low sensitivity for the detection of

weak ligands with IC_{50} values greater than 10 μM [127, 148]. In addition, the manual screening assay results were ambiguous with a great deal of data variability, due to the poor mixing technique. For the success of manual screening, a future approach will be to use 0.5 M LiCl/TFE substrate solution to give a higher cis/trans ratio, and a 96-well plate shaker to the quench the assay, which has been proven essential in HTS for the identification of PPIase inhibitors from chemical libraries [29, 113, 147, 148, 149]. Results from these studies will lead to a deeper understanding of the role of Pin1 in regulating mitosis.

Chapter 5

Synthesis and characterization of peptide substrate to elucidate the Pin1 interaction with c-Myc

5.1 Pin1 interaction with c-Myc

Pin1 associates with Cdc25c, Tau, and c-Myc in a manner that facilitates their dephosphorylation by protein phosphatase 2A (PP2A) [48, 72, 73, 80, 150, 151]. c-Myc is a transcription factor involved in cell cycle regulation and apoptosis, and it is a Pin1 substrate. c-Myc undergoes phosphorylation of Ser62 and Thr58 at the trans-activation domain via the extra-cellular signal-regulated kinases (ERKs) and glycogen synthase kinase-3β (GSK-3β), respectively [72, 151]. The phosphorylation that occurs at these two sites influences c-Myc stability and degradation differently. Specifically, phosphorylation of Ser62 stabilizes c-Myc, thereby promoting the phosphorylation of Thr58, which is essential for c-Myc degradation [72, 150, 151]. Pin1 plays an essential role in c-Myc stability by facilitating the dephosphorylation of Thr58 by PP2A. Moreover, the Axin1 scaffold protein creates the platform for the formation of a protein complex essential for the signal cascade that promotes c-Myc ubiquitination [72, 151] (Fig. 5.1). Our collaborator, Prof. Jeffry W. Peng at the University of Notre Dame, is interested in conducting NMR dynamics studies of the Pin1 interaction with c-Myc using small peptides. To examine the catalytic activity of Pin1 towards differentially phosphorylated peptides by NMR, we synthesized four peptides corresponding to the c-Myc sequence to investigate the effect of phosphorylation on the Ser62 and Thr58 sites on Pin1 interactions with c-Myc (Fig. 5.2).

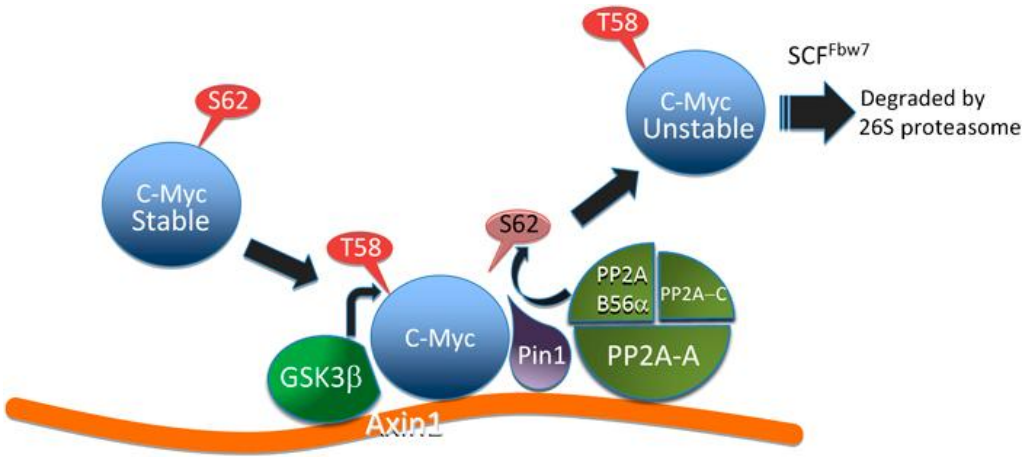

Fig. 5.1 A model showing the formation of a protein complex essential for c-Myc ubiquitination. c-Myc is phosphorylated at S62 by ERK, creating a stable form of c-Myc protein capable of binding a scaffold protein, Axin1. Axin1 binds GSK3 that consequently phosphorylates c-Myc at pT58. Pin1 recognizes the pT58-P motif and isomerizes P63. PP2A associates with Axin1, and dephosphorylates S62 creating an unstable form of c-Myc that is destined for ubiquitination and degradation. Reprinted by permission from Nature Publishing Group: The EMBO Journal (28, 500-12, 2009), copyright (2009)[151].

1. Ac–LLPTPPLSPS–NH_2
2. Ac–LLPTPPL**pSP**S–NH_2
3. Ac–LLP**pTP**PLSPS–NH_2
4. Ac–LLP**pTP**PL**pSP**S–NH_2

Fig. 5.2 c-Myc peptides: the position of phosphorylation was varied to study the Pin1 interactions with non-, mono- and di-phosphorylated peptides; the pS/pT-Pro motif is highlighted in bold.

Material and Methods

5.2 Peptide synthesis

Four c-Myc peptides were synthesized using manual solid-phase peptide synthesis (SPPS) in disposable polypropylene columns (Thermo Scientific) via standard 9-fluorenylmethoxy-carbonyl (Fmoc) chemistry. All Fmoc amino acids were purchased from Novabiochem. MBHA resin (300 mg, 0.192 mol/g) was swelled in DMF (3 mL) for 1 hour, and the Fmoc protecting group was removed with 20% piperidine in DMF (2 × 5 mL, 5 and 15 min). The resin was washed twice with DMF (ca. 8 mL). The Fmoc-Ser(*t*-Bu)-OH (221 mg, 0.57) was coupled to the resin using HBTU (219 mg, 0.58 mmol), HOBt (78 mg, 0.58 mmol), and DIEA (200 μL, 1.15

mmol) in DMF (4 mL), and the mixture was double-coupled (2 × 2 h). The completion of coupling was monitored by the Kaiser test for the primary amines[129], and by the p-chloranil test for the prolines and [130]. The reaction mixture was washed with DMF (2 × 8 mL), after which a solution of Ac_2O (0.2 mL, 1.1 mmol), DIEA (0.2 mL, 1.1 mmol), and CH_2Cl_2 (1.6 mL) was added and shaken for 10 min to cap any uncoupled amines. The Fmoc group was removed with 20% piperidine in DMF (2 × 5 mL). Batch syntheses were performed for two peptides simultaneously. At the desired elongation point, the resin was split in half, and the reagent added was reduced by half. The following amino acids were added one at a time in the same manner: Fmoc–Pro–OH (194 mg, 0.58 mmol), Fmoc–Thr(PO_2H(OBzl))–OH (511 mg, 0.58 mmol), Fmoc–Thr(tBu)–OH (229 mg, 0.58 mmol), Fmoc–Ser(PO_2H(OBzl))–OH (221 mg, 0.58 mmol), and Fmoc–Leu–OH (204 mg, 0.58 mmol). The peptide were cleaved from the resin with a mixture of 2.5% H_2O, 2.5% TIPS, and 95% TFA, (5 mL) for 3 h at 30 °C. Crude peptides were precipitated with cold Et_2O (15 mL) for 15-17 h, centrifuged, and decanted. Peptides were purified via reverse-phase high-pressure liquid chromatography (RP-HPLC), using a Varian Polaris (100 × 50 mm RP C18) semi-preparative column on a Varian Pro-Star 218 HPLC with linear gradients of 0.1% TFA in CH_3CN/H_2O as noted, flow rate 10 mL/min, λ 220 nm. CH_3CN was removed under vacuum, and the water was removed by lyophilization. Analytical HPLC were obtained on a the Varian HPLC using a Polaris C18 column 5 μm, (250 × 4.4 mm RP C18) with linear gradients as noted, flow rate 1.0 mL/min, λ 220 nm. Peptides were characterized by ^1H NMR with water-suppression in (D_2O:H_2O 1:1) on an INOVA-400 MHz, and FAB^+ and by liquid chromatography–mass spectrometry (LC-MS) on an Agilent 1100 LC-ThermoFinnigan TSQ MS with electrospray ionization (ESI^+) for molecular ion identification (Appendix D).

Ac–LLPTPPLSPS–NH_2 (**1**) was purified by RP-HPLC with 0.1% TFA in 10 to 35% CH_3CN/H_2O gradient over 15 min. The desired peak was collected at 8.5 min to give 3.5 mg (1.7% yield). FAB+, calcd. for $C_{50}H_{84}N_{11}O_{14}$ $[MH]^+$ *m/z* = 1063.3, found *m/z* = 1063.2 (Appendix D, Figs. S53-S54).

Ac–LLPTPPLpSPS–NH_2 (**2**) was purified by RP-HPLC with 0.1% TFA in 10 to 55% CH_3CN/H_2O gradient over 26 min. The desired peak was collected at 17 min to give 2.6 mg (2.3% yield). LC-MS calcd. for $C_{50}H_{84}N_{11}O_{17}P$ [M] *m/z* = 1142.3, found *m/z* = 1142.6; for $C_{50}H_{86}N_{11}O_{17}P$ $[MH_2]^{2+}/2$ *m/z* = 571.1, found *m/z* = 571.9; for $C_{50}H_{84}N_{11}O_{17}P$ Na [M·Na] calcd *m/z* = 1164.3, found *m/z* = 1164.5, (Appendix D, Figs. S55-S57).

Ac–LLPpTPPLSPS–NH_2 (**3**) was purified by RP-HPLC with 10 to 30% CH_3CN/H_2O gradient over 12 min. The desired peak was collected at 11.1 min to give 5.4 mg (5.4 % yield). FAB+, calcd. for $C_{50}H_{85}N_{11}O_{17}P$ $[MH]^+$ *m/z* = 1143.2, found *m/z* = 1143.3 (Appendix D, Figs. S58-S60).

Ac–LLPpTPPLpSPS–NH_2 (**4**) was purified by RP-HPLC with 0.1% TFA in 10 to 55% CH_3CN/H_2O gradient over 26 min. The desired peak was collected at 15.1 min to give 2.6 mg (1% yield). LC-MS calcd. for $C_{50}H_{85}N_{11}O_{20}P_2$ [M] *m/z* = 1222.5, found *m/z* = 1222.7, *m/z* = $[M·Na]^+$ calcd *m/z* = 1244.5, found *m/z* = 1244.6, $[MH]^{2+}/2$ calcd. *m/z* = 611.3, found *m/z* = 611.3 (Appendix D, Figs. S61–S62).

Results

5.3 Synthesis results

Four c-Myc peptides were synthesized using standard Fmoc chemistry on a Rink amide resin to produce amidated C-terminus. During purification of the phosphopeptides, low recovery

from HPLC was obtained. We believe this resulted from the addition of TFA during the mobile phase, which causes β-elimination of phosphate from pSer or pThr. All four peptides were sent to Dr. Jeffrey Peng for NMR analysis of Pin1 interactions with c-Myc (unpublished results). One example of experimental of double-selective EXchange Spectroscopy (EXSY) at 400 ms for Ac–LLpPTPPLSPS–NH_2 (1 mM) with labeled N15-H2 Pin1 (50 µM) is shown in Figure 5.3. Data was collected on a 700 MHz NMR spectrophotometer at 295 K. The chemical shift perturbation of the two cross peaks of the peptide in complex with Pin1 was measured. Additionally, the prolyl-cis-trans isomerization of the Thr58–Pro methyl side chain was observed. Precipitation of Pin1 was observed in experiments with Ac–LLPpTPPLpSPS–NH_2. Therefore, we synthesized more Ac–LLPpTPPLpSPS–NH_2 and sent the peptide to Dr. Peng for the NMR experiment. Results from these experiments will help the elucidate the Pin1 interactions with the various phosphorylation states of c-Myc.

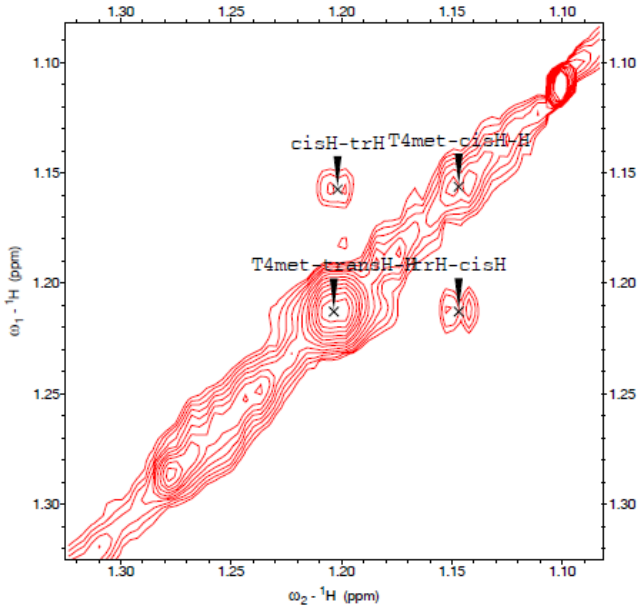

Fig. 5.3. Double-selective EXchange Spectroscopy (EXSY) at 400 ms of Ac–LLpPTPPLSPS–NH_2 (1 mM) with N15-H2 labeled Pin1 (50 µM). Cis-trans isomerization is shown by the two cross peaks of the Thr58 side chain methyl.

5.4 Flexibility-activity studies of Pin1 with ligands

This section is part of an article titled *Toward Flexibility-Activity Relationships by NMR Spectroscopy: Dynamics of Pin1 Ligands*, published in the Journal of the American Chemical Society, Elsevier Licence # 2442850117821 for dissertation use of less than 50% of original article. Reproduced with permission from Namanja, A.T;[†] Wang, X.J;[‡] Xu, B; [‡] Mercedes-Camacho, A.Y;[‡] Wilson, B. D;[†] Wilson, K. A;[†] Etzkorn, F.A;[‡] and Peng, J.W, Toward Flexibility-Activity Relationships by NMR Spectroscopy: Dynamics of Pin1 Ligands. J. Am. Chem. Soc. 2010, 132, 5607-5609. My contribution in this work was the synthesis and characterization of the Ac–FFpSPR–NH_2 peptide.

5.5 Synthesis of Ac–FFpSPR–NH_2

Ac–FFpSPR–NH_2 was synthesized manually with 3 equiv Fmoc-protected amino acids on a Rink-amide resin, coupling with HBTU, HOBt, and DIEA in NMP (2 × 20 min), and deprotecting with 20% piperidine/NMP. Fmoc–Ser(PO(OBzl)OH)–OH was obtained from Novabiochem. The peptide was acetylated with 10% Ac_2O/10% DIEA/CH_2Cl_2 (2 × 10 min), cleaved with 2.5% H_2O/2.5% triisopropylsilane/TFA for 4 h, and purified by HPLC with 10% CH_3CN (2 min) to 90% CH_3CN over 17 min, holding at 90% CH_3CN for 4 min, on a Waters X-Bridge 5μm C18 1.9 × 10 cm column. LC-MS (ESI+) $[MH]^+$ calcd. 774.3, found 774.4 [89](Appendix D, Figs. S63–S65).

5.6 Binding affinities of Ac–FFpSPR–NH_2

To investigate interactions between human Pin1, a peptidyl-prolyl isomerase, and structurally similar, but flexibility differentiated, ligands. A truncated Pin1 construct (Pin1-

PPIase) that omits the WW domain was used. 2-D $^{1}H-^{1}H$ EXSY experiments [152] on Ac–FFpSPR–NH_2 confirmed the cis−trans isomerase activity of Pin1-PPIase, and fits of Pin1-PPIase $^{15}N-^{1}H$ chemical shift perturbations during ligand titrations gave binding affinities of K_d, Ac–FFpSPR–NH_2 = 203 ± 46 μM (Fig 5.4). Our results reveal how structural variations among the ligands alter the millisecond dynamics relevant for their interactions with the Pin1-PPIase domain. Our results suggest flexibility-activity studies can provide FAR, in complete analogy to traditional structure-activity relationships (SAR).

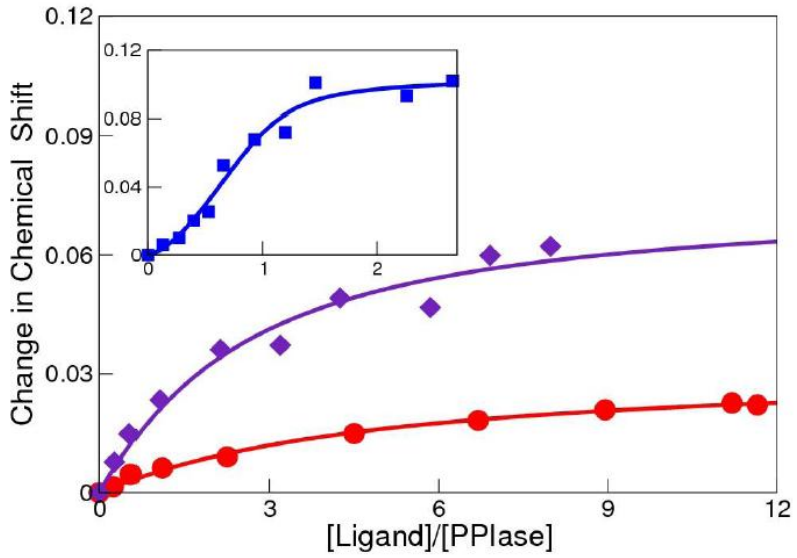

Fig. 5.4. Examples of ligand titrations as monitored by $^{15}N/^{1}H$ chemical shift perturbations of Pin1-PPIase at 295 K. The chemical shift of S72 of the Pin1-PPIase catalytic loop vs. the [ligand]/[PPIase] ratio is shown for the substrate Ac–FFpSPR–NH_2 (●), cis-locked (■), and trans-locked (♦) inhibitors [89].

Chapter 6

Toward understanding the Pin1 catalytic mechanism using kinetic isotopic effect studies

6.1 Kinetic isotopic effects

The determination of kinetic parameters is a good starting point for the understanding of the Pin1 catalytic mechanism, and the rational design of Pin1 inhibitors [15, 24, 51, 53]. One hypothesized mechanism is that the prolyl-amide nitrogen is hydrogen-bonded with either His59 or His157 in the transition state [50]. These highly conserved residues cluster at a nearby distance of the pSer/pThr-Pro motif of the substrate, with the potential to participate as hydrogen-bond donors (Fig. 6.1)[153].

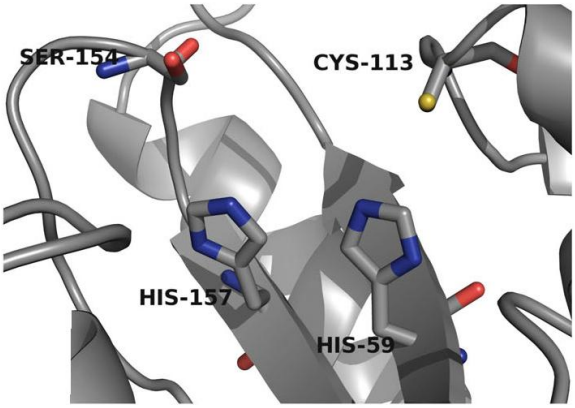

Fig. 6.1. Catalytic residues located at the Pin1 active site. Reprinted by permission from Heikkinen et al; license BioMed Central Ltd., copyright (2009)[153].

We employed kinetic isotopic effect (KIE) studies to investigate the formation of a twisted-amide transition state facilitated by a transient hydrogen-bond to the proline nitrogen. KIE measurement involves the determination of the ratio of catalytic efficiencies (k_{cat}/K_m) of an unlabeled and labeled substrate for a particular reaction [154, 155]. There are two types of KIE, primary and secondary isotopic effects. In a primary isotopic effect (1º KIE), an isotopically labeled atom is in a chemical bond that is broken or created during the rate-limiting step; as a

result, the ratio in k_H/k_D values vary between 2 and 7[154]. In a secondary kinetic isotopic effect (2º KIE), the isotopically labeled atom is not involved in the bond that is breaking or forming during the rate-limiting step, but involves the C–H bond relaxation or tightening in the transition state. In this case, the ratio of k_H/k_D is less than 2 [154, 155, 156]. The 2º KIE are called α, β, γ, δ. or ε, depending on the distance between the isotope-labeled atom and the reacting center, with values between 0.7-1.5 [154, 155, 156]. The 2º KIE is sub-divided into normal 2º KIE or inverse 2º KIE. In a normal 2º KIE, the value for the ratio of k_H/k_D is between 1 and 2. In an inverse 2º KIE, the value for the ratio of k_H/k_D is less than 1, indicating that the labeled substrate reacts faster than the unlabeled substrate.

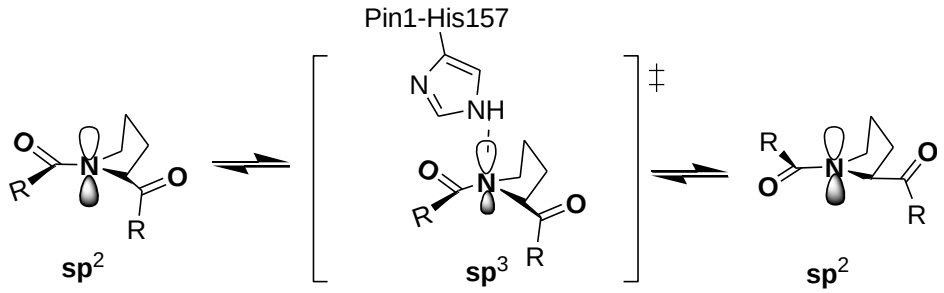

Fig. 6.2. Proposed twisted-amide transition state mechanism.

To measure the secondary kinetic isotope effects, we adapted the assay substrate from a peptide developed by Yaffe et al. Similar substrates have k_{cat}/K_m values ranging from 9,300 to 20,160 mM^{-1} Sec^{-1} [26]. Peptide Ac–Phe–Phe–pSer–Pro–Arg–*p*NA was synthesized using natural L-Ser and deuterated d_3-L-Ser using a combination of solution and solid phase peptide synthesis (Scheme 6.1-6.3). The ratio of k_H/k_D of unlabeled (Ac–Phe–Phe–pSer–Pro–Arg–*p*NA) and labeled (Ac–Phe–Phe–p[d_3]Ser–Pro–Arg–*p*NA) substrates from k_{cat}/K_m was measured as described by Kofron et al [114, 142, 143]. Results from the kinetic isotope effect studies provide evidence of whether the peptidyl-proline amide carbonyl rehybridizes from sp^2 to sp^3 or not.

*6.2. Ac–Phe–Phe–pSer–Pro–Arg–*p*NA substrates*

Previously, Matthew Mason successfully achieved the synthesis and purification of unlabeled Ac–Phe–Phe–pSer–Pro–Arg–*p*NA and labeled Ac–Phe–Phe–pSer–[d_7]Pro–Arg–*p*NA substrates (unpublished results). Ashley Mullins collected kinetic data using these substrates, varying the Pin1 concentration. The kinetic data indicates an inverse-secondary kinetic isotopic effect value of 0.85 ± 0.03 (unpublished results), establishing that the prolyl-amide nitrogen proceeds through a pyramidal transition state during the rate-limiting step [157]. However, we sought to prove that pyramidalization occurs at the prolyl-amide nitrogen, and not at serine-carbonyl, which can also rehybridize from sp^2 to sp^3 forming a tetrahedral transition state during the rate-limiting step, and faciliting free rotation of the prolyl-amide (Fig. 6.3). The Ac–Phe–Phe–pSer–Pro–Arg–*p*NA was deuterium labeled at the α- and β-carbons of serine.

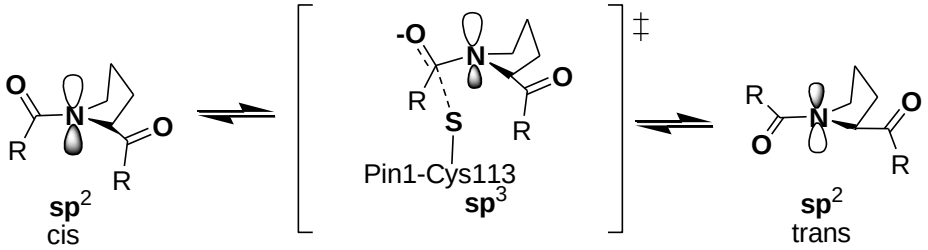

Fig. 6.3. Proposed tetrahedral transition state mechanism.

Material and Methods

*6.3 Synthesis of Fmoc–Orn(Boc)–*p*NA*

Fmoc–Orn(Boc)–OH (2.3 g, 5 mmol) was dissolved in pyridine (0.48 mL, 6 mmol), and $(Boc)_2O$ (1.3 g, 3.35 mmol) was dissolved in dioxane (15 mL). The *p*-nitroaniline (500 mg, 6 mmol) was dissolved in dioxane (5 mL), and the reaction mixture was stirred for 20.5 h at rt [145]. The reaction mixture was quenched by addition of EtOAc (30 mL). The mixture was washed with 1M $KHSO_4$, H_2O, saturated aqueous $NaHCO_3$ (3 × 60 mL), H_2O(3 × 60 mL), and brine (3 × 60 mL). The organic layer was dried with $MgSO_4$, and concentrated in vacuum (1.3 g,

57% yield). ^{1}H NMR (400 MHz, $CDCl_3$) δ 9.4 (s, 1H), 8.5 (d, J = 7.4, 2H), 7.89 (m, 4H), 7.73 (m, 2H), 7.43-7.37 (m, 5H), 5.7 (s, 1H), 4.23 (m, 3H), 3.91 (m, 1H), 3.0 (s, 1H), 1.61 (m, 1H), 1.50 (m, 1H), 1.37 (s, 9H). (Appendix E, Fig. S66). The crude Fmoc-Orn(Boc)-OH (700 mg,1.2 mmol) was dissolved in TFA (6.0 mL), CH_2Cl_2 (14 mL), and TIPS (0.49 mL, 3.1 mmol). The reaction mixture was stirred for 30 min at rt, and solvents were evaporated in vacuum.

*6.4 Solid phase synthesis of Ac–Phe–Phe–pSer–Pro–Arg–*p*NA peptides*

Both peptides Ac–Phe–Phe–pSer–Pro–Arg–*p*NA and Ac–Phe–Phe–p[d_3]Ser–Pro–Arg–*p*NA were treated under identical conditions unless otherwise noted. 2-chlorotritylchloride resin (500 mg, 0.8-1.6 mmol/g) was swollen for 20 min in DCM using a polypropylene disposable column. The Fmoc–Orn(NH_3^+)–*p*NA·TFA salt (552 mg, 1.2 mmol) and DIEA (730 µL 4.2 mmol) were dissolved in NMP (2 mL). The mixture was added to the 2-chlorotritylchloride resin and reacted for 4 h. The Fmoc protecting group was removed with 50% morpholine in NMP (2 × 5 mL). The resin was washed with NMP (2 × 8 mL). The Fmoc-Pro-OH (700 mg, 2.1 mmol) was coupled to the resin using HBTU (797 mg, 2.1 mmol), HOBt (284 mg, 2.1 mmol), and DIEA (730 µL, 4.2 mmol) in NMP (5 mL), and the mixture was double coupled (2 × 20 min). The peptide was dried under high vacuum overnight, and split in two batches of 282 mg. The peptide on resin (282 mg) was elongated by adding the following amino acids one at the time: Fmoc–Ser(TBS)–OH (150 mg, 0.35 mmol), HOBt (142 mg, 1.1 mmol), HBTU (399 mg, 1.1 mmol), and DIEA (365 µL, 2.1 mmol) were coupled for 20 min, and Fmoc–Phe–OH (400 mg, 1.05 mmol) was double coupled for 20 min each. For the labeled substrate; L-[d_3]Serine was purchased from Cambridge Isotope Laboratories, and modified by the addition of Fmoc at the N-terminus, and TBS on the hydroxyl-side chain by Guoyan G. Xu. Fmoc–[d_3]Ser(TBS)–OH (150 mg, 0.35 mmol) was coupled for 20 min. After elongation, the final Fmoc protecting group was

removed using 50% morpholine/NMP (5 mL, 2 × 20 min) and the free N-terminus was acetylated using a mixture of 10% DIEA and 10% Ac_2O in DCM for 10 min (3 mL). The peptide was dried under vacuum overnight. The resin was suspended in DMF (6 mL), to which tetrabutyl ammonium fluoride (0.15 M, 2.5 mL) and 0.4% H_2O were added, and mixture was shaken for 4 h. The resin was then washed with DMF (5 mL, 3 × 30 sec), DCM (5mL, 3 × 30 sec), MeOH (5 mL, 3 × 30 sec), and dried in vacuo overnight.

6.5 Global phosphorylation of substrates

The (N,N-diisopropyl)dibenzylphosphoramidite (345 µL, 1.05 mmol) was dissolved in anhydrous DMF (5 mL) containing 5-ethylthio-1-tetrazole (365 mg, 2.8 mmol). This solution was transferred to a 10 mL conical bottom flask containing the peptide using dry techniques under Ar, and reacted for 6 h. The resin was then covered with DMF 1 mL, tBuOOH (5 M in decane, 3 mL), and agitated for 45 min. The resin was transfered to a polypropylene disposable column, and washed with DMF(5 mL, 3 × 30 sec), DCM (5 mL, 3 × 30 sec), MeOH (5 mL, 3 × 30 sec), and dried in vacuum overnight.

The dried resin was then treated with 95% TFA, 2.5% TIPS, and 2.5% H_2O for 4 h, the resin was removed by filtration, and the peptide was collected by filtration. The resin beads were washed with MeOH (5 mL, 3 × 1 min), and DCM (5 mL, 3 × 1 min), and the filtrates were combined and concentrated. Diethyl ether (15 mL) was added to remove any remaining TFA. Ac–Phe–Phe–pSer–Pro–Orn–*p*NA (31.7 mg) and Ac–Phe–Phe–p[d_3]Ser–Pro–Orn–*p*NA (24.3 mg) crude were obtained. Peaks were identified by LC-MS as the Ac–Phe–Phe–pSer–Pro–Orn–*p*NA for $C_{39}H_{49}N_8O_{12}P$ $[MH]^+$ *m/z* = 853.3, found *m/z* = 853.4, and Ac–Phe–Phe–p[d_3]Ser–Pro–Orn–*p*NA for $C_{39}H_{46}D_3N_8O_{12}P$ $[MH]^+$ *m/z* = 857.2, found *m/z* = 857.2.

Scheme 6.1. Synthesis of Fmoc-Orn(Boc)-*p*NA.

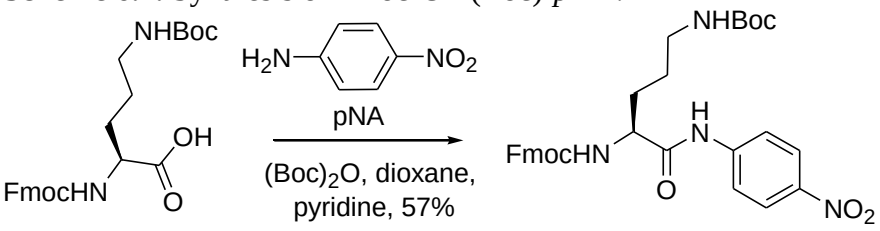

Scheme 6.2. Solid phase peptide synthesis of Ac–Phe–Phe–pSer–Pro–Orn–*p*NA.

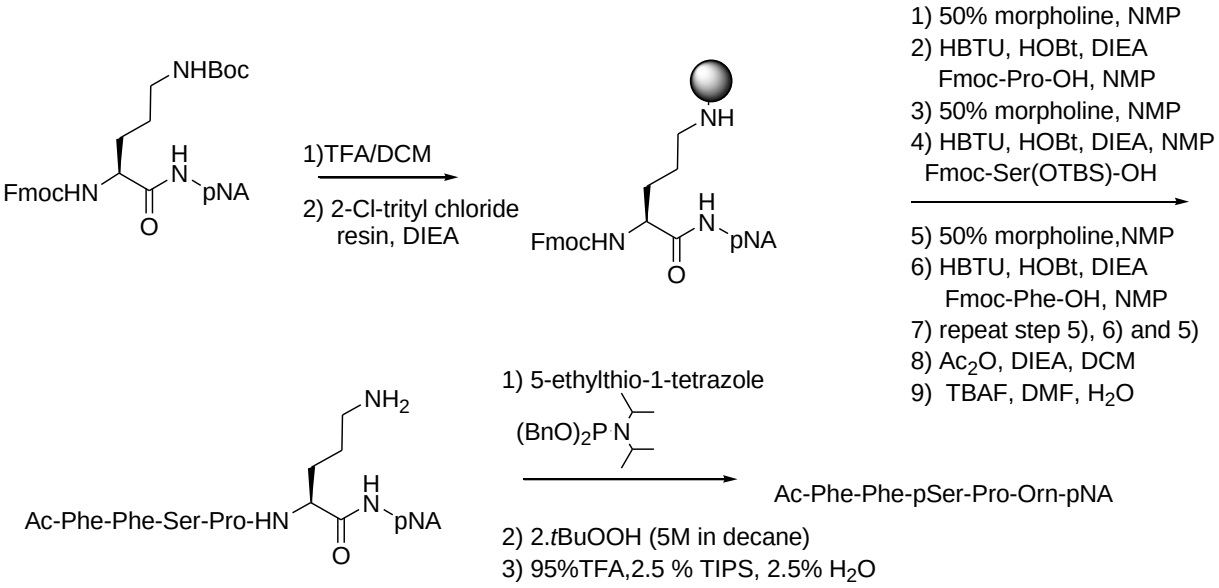

6.6 Guanidinylation of ornithine side chain

The crude Ac–Phe–Phe–p[d_3]Ser–Pro–Orn–*p*NA (24.3 mg, 0.03 mmol) was dissolved in DMF (2.0 mL) and DMSO (2.0 mL). Dimethyl-1H-pyrazole carboxamidine nitrate (41.0 mg, 0.2 mmol) and DIEA (0.06 mL, 0.34 mmol) were added, and the mixture was heated to 45 ^{o}C for 24 h. The reaction was quenched with water (30 mL), frozen, and lyophilized overnight to remove the solvent mixture. CH_3CN precipitation (12 mL) was used to remove excess impurities. The dried white precipitate contained 21.4 mg of crude peptide. Analytical HPLC using an XBridge^{TM} BET130 3.5 µm C18 4.6 × 50 mm column, with a linear gradient of 60% over 15 min and hold for 7 min, showed a peak at 11.7 min, identified by LC-MS as the Ac–Phe–Phe–

p[d_3]Ser–Pro–Arg–*p*NA for $C_{39}H_{46}D_3N_8O_{12}P$ $[M + H]^+$ *m/z* = 898.4, found *m/z* = 898.3. Similar conditions were used for the guanidinylation of unlabeled.

Scheme 6.3. Guanidinylation of ornithine side chain.

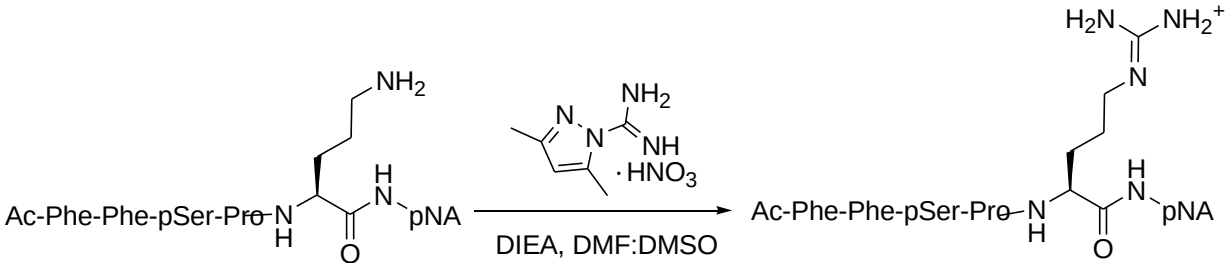

Peptides were purified by RP-HPLC, using a Waters C18 XBridge 5 μm, 19 × 100 mm semi-preparative column on a Varian Pro-Star 218 HPLC with linear gradient of 0 to 40% CH_3CN/H_2O over 16.5 min. The desired peaks were collected at 12.6 min, flow rate 10 mL/min, λ = 210 nm. CH_3CN was removed under vacuum, and the water was removed by lyophilization to give Ac–Phe–Phe–pSer–Pro–Arg–*p*NA (3 mg, 0.84% yield). ^{1}H NMR (500 MHz, CD_3OD) for Ac–Phe–Phe–pSer–Pro–Arg–*p*NA δ 8.2 (d, *J* = 9.1 Hz, 2H), 8.1 (d, *J* = 9.2 Hz, 2H),7.3-7.2 (m, 10H), 5.0 (br s, 1H), 4.7 (q, *J* = 5.6, 2.3 Hz, 1H), 4.6 (q, *J* = 5.7, 3.8 Hz, 1H), 4.4 (m, 2H), 4.2 (m, 1H), 4.1(m, 1H), 4.0 (q, *J* = 11.4, 10.2, 2H), 3.4-3.2 (m, 4H), 3.0 (dd, *J* = 18, 5.5 Hz, 2H), 2.8(m, 2H), 2.2-1.7 (m, 10H). LC-MS 12.55 min, calcd. for $C_{39}H_{49}N_8O_{12}P$ $[MH]^+$ *m/z* = 895.4, found *m/z* = 895.3. Ac–Phe–Phe–p[d_3]Ser–Pro–Arg–*p*NA (1.9 mg, 0.53% yield). ^{1}H NMR (500 MHz, CD_3OD) δ 8.2 (d, *J* = 9.4 Hz, 2H), 8.1 (d, *J* = 9.4 Hz, 2H),7.5-7.2 (m, 10H), 4.7-4.5 (m, 3H), 4.4 (m, 2H), 4.1 (s, 1H), 3.9 (s, 1H), 3.5 (m, 2H), 3.1-2.9 (dd, *J* = 5.2,5.5, 4H), 2.62 (s, 3H), 2.8 (dd, *J* = 23.1, 4.8 Hz, 2H), 2.35 (m, 2H), 2.2-1.7 (m, 12H). Calcd. for $C_{39}H_{46}D_3N_8O_{12}P$ $[MH]^+$ *m/z* = 898.4, found *m/z* = 898.3. (Appendix E, Figs. S67-S72).

6.7 Measurement of k_{cat}/K_m

HEPES buffer pH 7.0 (35 mM stock, 1.05 µL) and trypsin (60 mg/mL in 0.001 N HCl, 120 µL) were added to a 1 mL, 1 cm, polypropylene cuvette, and pre-equilibrated to 2 °C. Varying Pin1, from 5-20 nM in 20 mM Tris·HCl, pH 7.0 (200 nM stock, 10 µL) was added. The thermal isomerization rate constant k_3 was determined in the absence of Pin1 at 2 ºC. Substrate concentrations were determined by UV absorbance at 390 nm, ε_{390nm} = 12,500 M^{-1} cm^{-1}. Substrate in dry 0.48 M LiCl/TFE (2.9 mM stock, 10 µL) was added via syringe, and mixed vigorously by inversion three times with a time delay of 3-5 sec. The progress of the reaction was monitored at 390 nm for 90 s. The concentrations of the cis component of the unlabeled (44%) and labeled (54%) substrates were determined by the UV-Vis absorbance after complete cleavage of the *p*NA by trypsin in 3 min.

6.8 Results of kinetic data

Pin1 binds reversibly to the cis-substrate (cis-S) to form a Pin1::cis-substrate complex (Pin1::cis-S). Then, the product, the trans-substrate (trans-S), is cleaved by trypsin, releasing free *p*NA monitoring at 390 nm (Scheme 6.4). To enhance the amount of the cis-substrate, a dry solution of 0.5 M LiCl/TFE was used as the substrate solvent, which increased the cis-substrate concentration from 10-15% to 30-70% depending in the amount of moisture present[143]. When the substrate concentration [cis-S] is much less than K_m ([cis-S] << K_m), the Michaelis-Menten equation (Eq. 5) is directly proportional to the concentration of substrate [cis-S], and the substrate concentration does not have a considerable effect on K_m (Eq.6).

Scheme 6.4. Kinetics of Pin1 catalytic reaction.

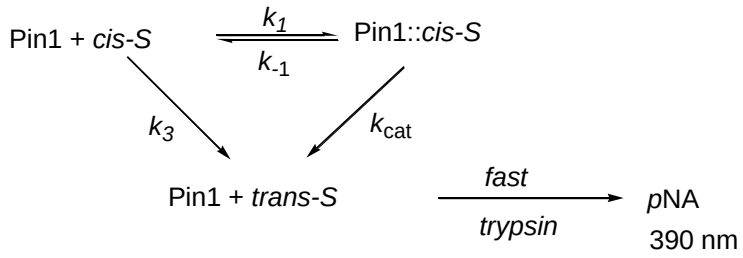

$$\upsilon_o = \frac{V_{max}[S]}{K_m + [S]} \quad (5)$$

$$\upsilon_o = \frac{V_{max}[S]}{K_m} \quad (6)$$

K_m shows how tightly the enzyme binds to the substrate, and it is a constant for the particular enzyme with a particular substrate. K_m is defined as the substrate concentration at which the velocity is half of the maximum velocity (V_{max}). However, the speed of any particular reaction being catalyzed by a particular enzyme can only reach a certain maximum value. This rate is known as V_{max}. The V_{max} depends on the total amount of total enzyme ($[E]_T$) used for the assay (Eq. 7), for a purified enzyme with known molecular weight, like Pin1 MW = 22 kDa, $V_{max}[S]$ can be expressed as a fundamental constant that is called the maximum turnover number, or catalytic constant (k_{cat}) (Eq.8).

$$[E]_T = [E]_0 + [ES] \quad (7)$$

$$V_{max} = k_{cat}[E]_T \quad (8)$$

Rearrangement of (Eq. 6) and (Eq. 8) yields (Eq. 9)

$$\upsilon_o = \left(\frac{k_{cat}}{K_m}\right)[E]_T[S] \qquad (9)$$

When [S] << K_m, the amount of free enzyme $[E]_0$ approximates the amount of total enzyme $[E]_T$. Therefore, k_{cat}/K_m behaves as a second-order rate constant for the reaction between substrate and free enzyme.

The experimental absorbance was monitored by following the progress of the reaction for 90 s. The data was analyzed by nonlinear least-squares fit using TableCurve software V5.2 for the measurement of k_{obs}, which is equal the rate of the [ES] complex converted to product over the progress of the reaction. To find the value of k_{cat}/K_m, the k_{obs} versus enzyme concentration was plotted to fit to the form of Eq.10. This ratio shows what the enzyme can accomplish when abundant enzyme sites are available, and it allows direct comparison of the effectiveness of an enzyme toward different substrates (Eq.10).

$$k_{obs} - k_3 = \frac{k_{cat}}{K_m}[E] \qquad (10)$$

Eq.10 is a straight-line equation in the form of y = mx + b, and the slope of the line is the catalytic efficiency (k_{cat}/K_m) for Pin1. The ratio of catalytic efficiencies for unlabeled and labeled substrates was measured at varying Pin1 concentrations and calculated using (Eq. 11)

$$\text{ratio} = \frac{\left(\frac{k_{cat}}{K_m}\right)unlabeled}{\left(\frac{k_{cat}}{K_m}\right)labeled} \qquad (11)$$

A k_{cat}/K_m value of 4,230 mM^{-1} sec^{-1} was measured for the Ac–Phe–Phe–pSer–Pro–Arg–*p*NA, and 3,150 mM^{-1} sec^{-1} for Ac–Phe–Phe–p[d_3]Ser–Pro–Arg–*p*NA (Fig.6.4). The ratio of k_{cat}/K_m for the unlabeled and labeled substrates gave a value of 1.34 ± 0.01 for a duplicated set of data. The magnitude of the SKIE value indicates that the carbonyl-serine hybridization does not change from sp^2 to sp^3. However, the 2º KIE at proline of 0.85 ± 0.03 measured by Ashley Mullins indicated that the proline nitrogen rehybridizes from sp^2 to sp^3.

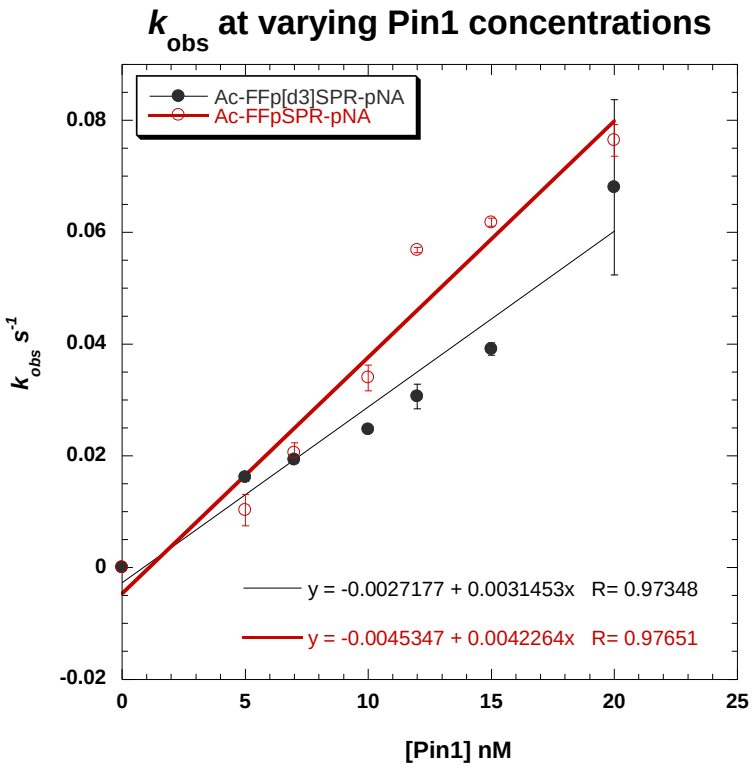

Fig. 6.4. k_{obs} at varying Pin1 concentrations. A calculated k_{cat}/K_m values of 4,230 mM^{-1} sec^{-1} for Ac–Phe–Phe–pSer–Pro–Arg–*p*NA (Red line) and 3,150 mM^{-1} sec^{-1} for Ac–Phe–Phe–p[d_3]Ser–Pro–Arg–*p*NA (Black line). The ratio of k_{cat}/K_m values for the unlabeled and labeled substrates gave a 2° KIE value of 1.34 ± 0.01 for a duplicated set of data. (Prepared with Kaleidagraph 4.3.)

6.9 Discussion

The ß-secondary isotope effect is strongly dependent on molecular geometric and steric hindrance factors. We believe that the large magnitude 1.34 ± 0.01 of our observed 2º KIE could be the result of a steric hindrance factor. The deuterium-labeled atom was at the β-position of the postulated nitrogen proline that undergoes from sp^2 to sp^3 hybridization, during the rate limiting step transition state formation. During the cis-trans isomerization steps of the labeled substrate, the cis conformation begins in a ground-state conformation in which the αC-H/D, and β$C\text{-}H/D_2$ bonds at serine can sterically interfere with the carbonyl of the proline ring. In the transition state, the steric interference is relieved, a loosening of the structure, which is more important for the C-H than the C-D substrate. Since the proline N is β to the Ser α-CH/D, the magnitude of the 2º KIE at serine is in agreement with the earlier results for cyclophilin[158]. Further experiments are necessary to confirm the identity of Pin1 residues that facilitate the formation of a hydrogen bond to the Pro-N during the rate-limiting step of proline cis and trans isomerization.

Chapter 7
Conclusions

Pin1 inhibition has been extensively studied as a viable approach for treating a large number of diseases, such as cancer and Alzheimer's disease, as well as organ transplant rejection, allergies, and asthma [92, 93, 94, 108, 109, 110, 111, 112]. In efforts to identify potential inhibitors of Pin1, two types of assays were used to identify inhibitors and/or ligands of Pin1. We developed the enzyme-linked enzyme binding assay (ELEBA) for the identification of Pin1 WW domain ligands from a compound library. For the ELEBA, a peptide (-VPRpTPV-) previously identified as specific for the Pin1 WW domain with a K_d value of 7.7 μM ± 3.3 was modified [32], and synthesized using solid phase peptide synthesis. The peptide was covalently immobilized in a pre-activated DNA-binding 96-well plate [90]. Commercially available Pin1 chemically conjugated to horseradish peroxidase (Pin1-HRP) was used for chemiluminescent detection of ligands that block the association of the WW domain with immobilized peptide[90].

Using the ELEBA, we measured binding constants for specific WW domain ligands, and screened a small WW domain compound library of 315 pSer–Pro peptidomimetic designed and synthesized by X. R. Chen and F. A. Etzkorn. Three ligands *cis*-D2, O2, and M18 were identified as the better WW domain ligands. Using the ELEBA, relative competitive K_d values for *cis*-D2, O2, and M18 were determined to be 263 ± 6.4, 206 ± 3.4, and 130 ± 3.0 μM, respectively. The K_d values for cis-D2, O2, and M18 were also measured using NMR by our collaborators, Jill Bouchard and Jeffrey Peng (University of Notre Dame). K_d values for *cis*-D2, O2, and M18 were determined to be 88 ± 8, 175 ± 21, and 108 ± 20 μM, respectively. NMR titrations studies were performed using the full-length Pin1 at different concentrations of ligands. Interestingly, chemical shift perturbation of Pin1 catalytic residues was not observed during the

titration studies, which indicates that ligands appear to bind selectively at the Pin1 WW domain. The ELEBA is a noncatalytic binding assay for the identification of ligands that bind to the Pin1 WW domain. The assay is fast, selective, and amenable to screening ligand libraries, with the potential for automation. The assay is advantageous over existing methods, because it selectively identifies compounds that bind to the Pin1 WW domain, it uses small quantities of reagents, and not antibodies, fluorescent labels, or radioactive labels are required. We would like to investigate further, the effect of the ligands *cis*-D2, O2, and M18 on Pin1 catalytic activity using our coupled-proteolytic continuous assay. The determination of the ligand mode of inhibition, if any, will provide the necessary evidence that the WW domain could be a regulatory site for Pin1, and allosteric inhibition could represent a viable approach for the inactivation and study of Pin1.

We utilized a proteolytic-discontinuous assay for the identification of Pin1 catalytic inhibitors. For the assay, we synthesized a chromogenic substrate, Suc–Ala–Glu–Pro–Phe–AMC. The substrate was synthesized in ten synthetic steps using solution-phase peptide synthesis on a large scale (3.0 g). Pin1 protein was purified from *E. coli* BL21-DE3. The traditional Pin1 continuous-catalytic assay was then adapted from 1.2 mL to a discontinuous assay in a 50 µL total volume in aqueous buffer. Using the proteolytic-discontinuous assay, we manually screened the small WW domain compound library of 315 pSer–Pro peptidomimetic. From the screening, ligands D20 and K7 decreased more than 90% Pin1 catalytic activity. We would like to investigate further the IC_{50} values of pure D20 and K7 using our proteolytic-continuous assay with 0.47 M LiCl·TFE.

For the investigation of the effect of Pin1 catalyzed cis-trans isomerization of c-Myc oncoprotein Thr58 and Ser62, I synthesized and characterized four peptides corresponding to the c-Myc sequence. Peptides Ac–LLPTPPLSPS–NH_2, Ac–LLPpT58PPLSPS–NH_2, Ac–

LLPTPPLpS62PS–NH_2, and Ac–LLPpT58PPLpS62PS–NH_2 were synthesized using solid phase peptide synthesis, purified by RP-HPLC, and characterized by NMR and LC-MS. NMR isomerization studies were performed by our collaborator Dr. Jeffrey Peng (University of Notre Dame). Preliminary data showed that Pin1 binds and isomerizes the Ac–LLPpT58PPLSPS–NH_2 at the pThr58. Recently, we purified more doubly phosphorylated Ac–LLPpT58PPLpS62PS–NH_2, since peptide precipitation with Pin1 was observed with the initial batch.

The secondary kinetic isotopic effect (2° KIE) to study the Pin1 catalytic mechanism of proline isomerization was measured. We synthesized and characterized Ac–Phe–Phe–pSer–Pro–Arg–*p*NA (unlabeled) and Ac–Phe–Phe–p[d_3]Ser–Pro–Arg–*p*NA (labeled) substrates. The ratio of k_H/k_D for unlabeled and [d_3]-labeled substrate gave a 2° KIE value of 1.34 ± 0.01. The magnitude of the SKIE value indicates that serine-carbonyl hybridization is not changing from sp^2 to sp^3, but suggests that the prolyl nitrogen rehybridizes from sp^2 to sp^3 in the rate-limiting step transition state. This result supports previous inhibitor, d_7-Pro labeled substrate and solvent 2° KIE results for Pin1, that suggest a twisted-amide mechanism assisted by a transient hydrogen bond in the transition state.

Appendix A

Supplementary Material for Enzyme-linked enzyme binding assay for Pin1 WW domain ligands

Characterization of Peptides

Characterization data for H–GGGGVPRpTPVGG–NH_2 **1**

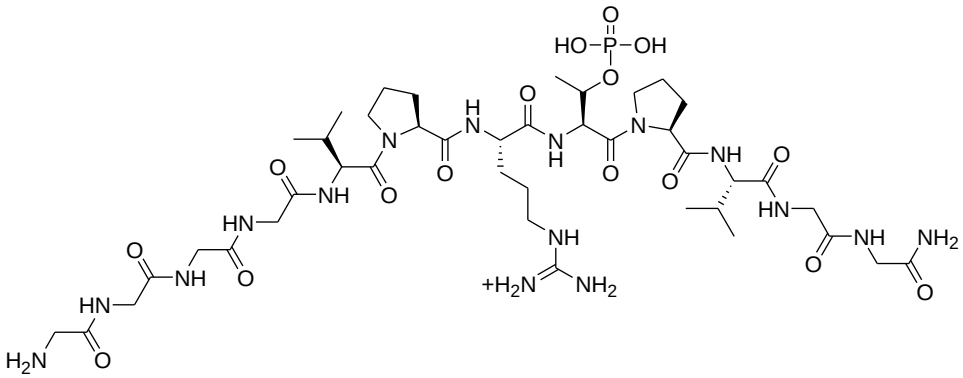

1

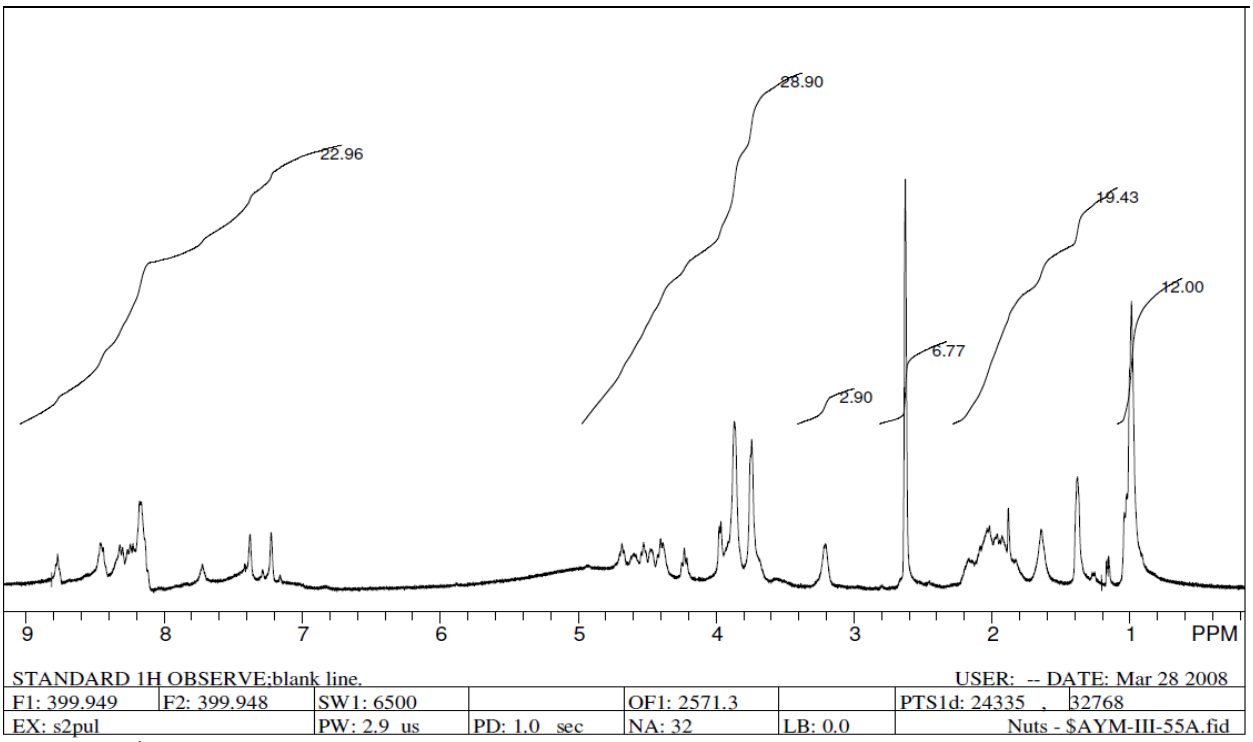

Fig. S1. ^{1}H NMR spectrum of ligand 1 in DMSO-d_6, some characteristic amide-protons exchange at 7-9 ppm, the six α-protons of the peptide core are observed at 4-5 ppm, and the valine methylenes were observed at 0.9-0.7 ppm.

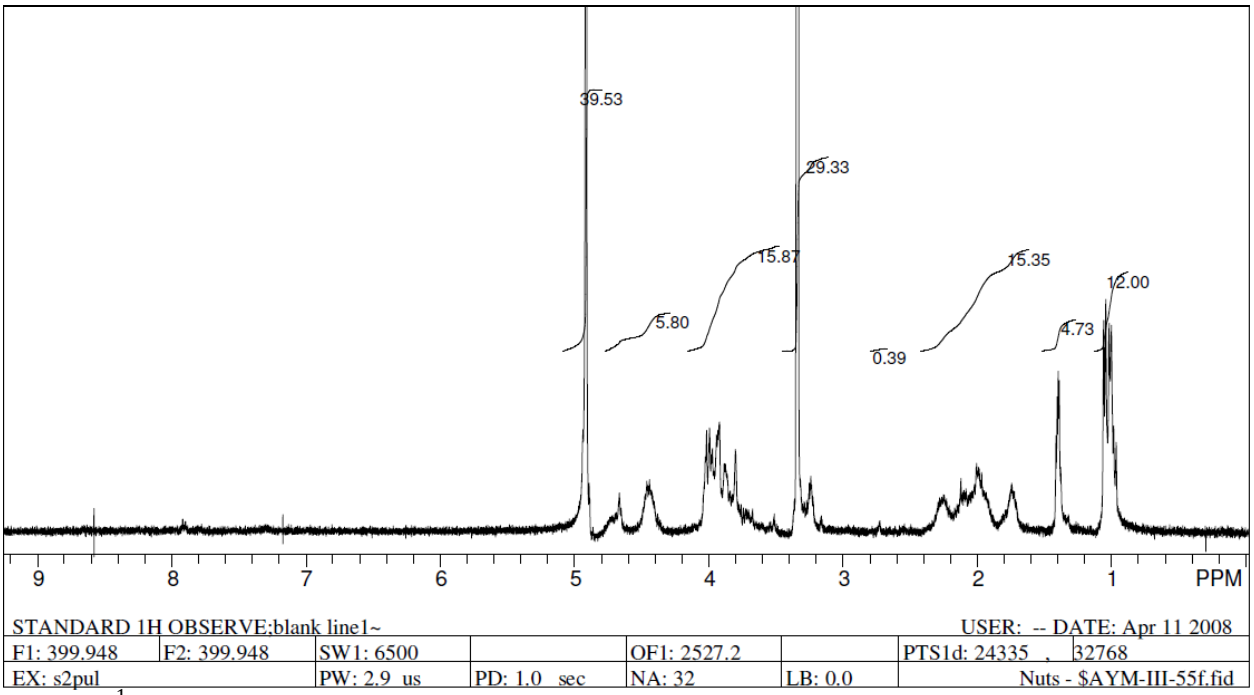

Fig. S2. ^{1}H NMR in CD_3OD of ligand **1**. The complete deprotection of the OBzl from phospho-Thr side chain was confirmed by the absence of aromatic protons at 7-9 ppm. The amide-protons were not observed at 7-9 ppm due to exchange. The six α-protons of the peptide core overlap at 4.8-4.4 ppm, and the two valine methylene doublets appear at 0.9-0.7 ppm.

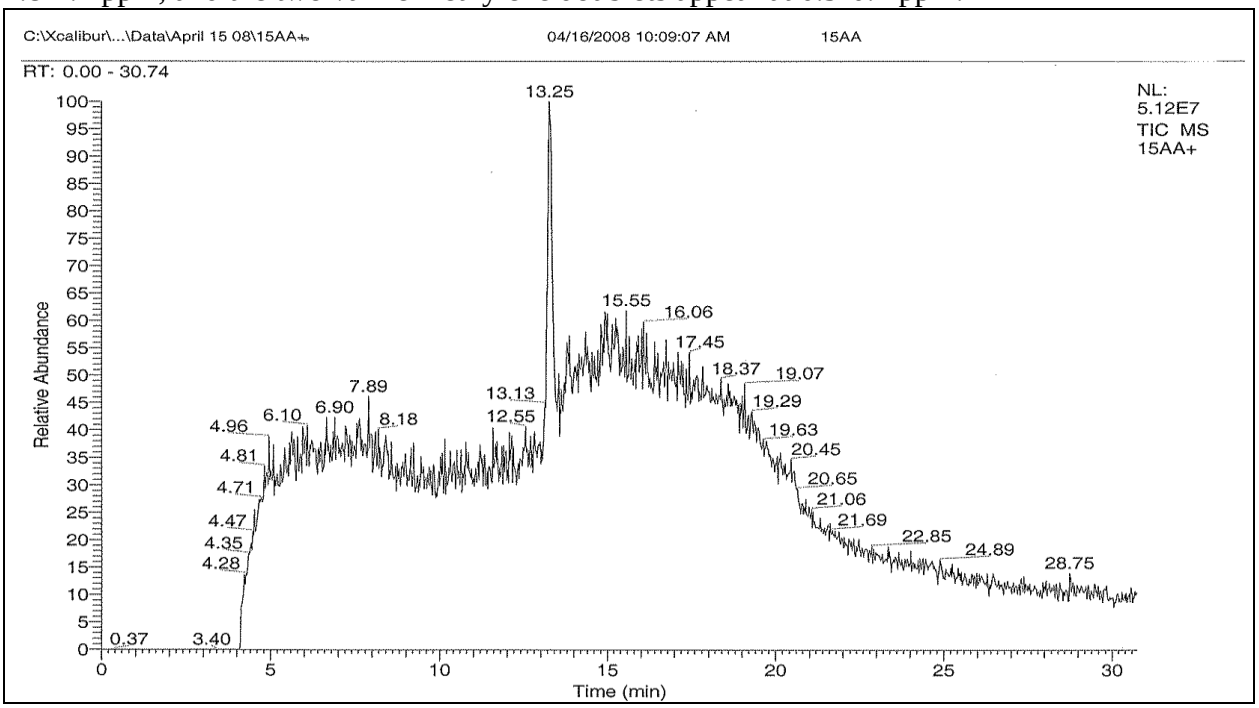

Fig. S3. LC-MS total ion chromatogram of ligand 1. The peak at 13.25 min had the correct molecular mass (See Fig. S4).

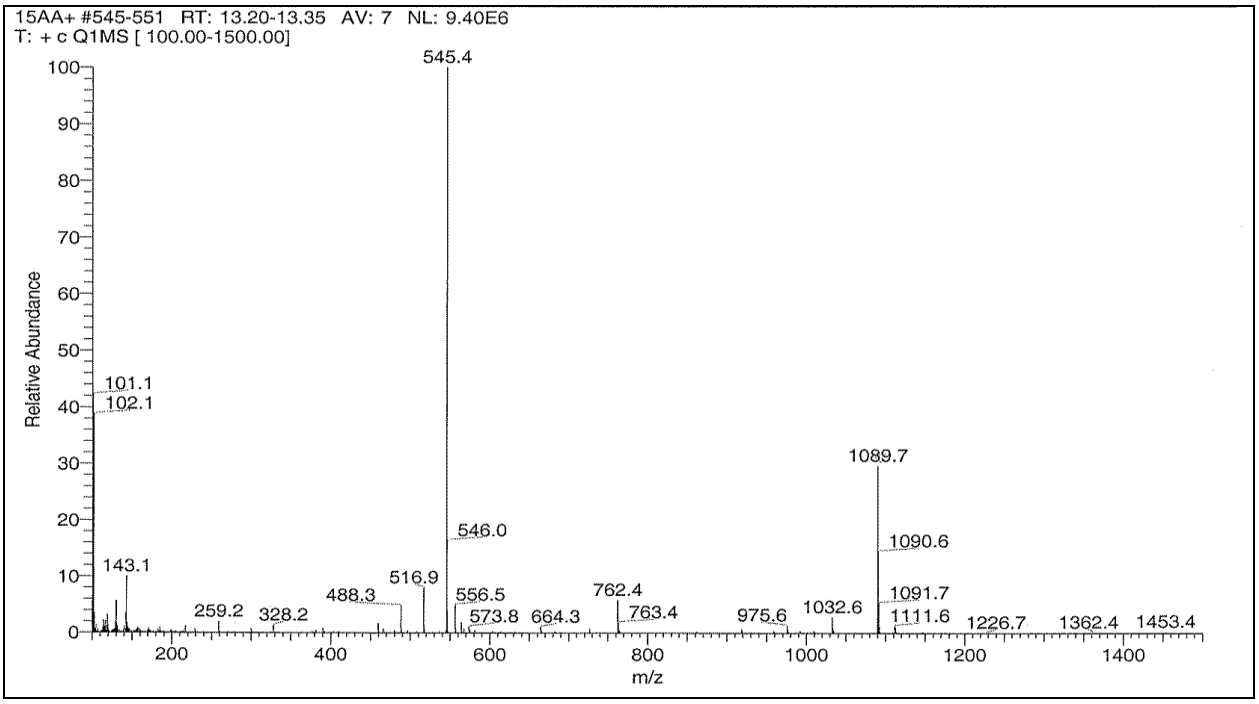

Fig. S4. MS with electrospray ionization (ESI+) showing the fragmentation pattern for ligand **1**. The LC peak from 13.20-13.35 min was selected for molecular ion detection, identifying [MH]+ = 1089.7 *m/z* and [MH]2+ = 545.4 *m/z*.

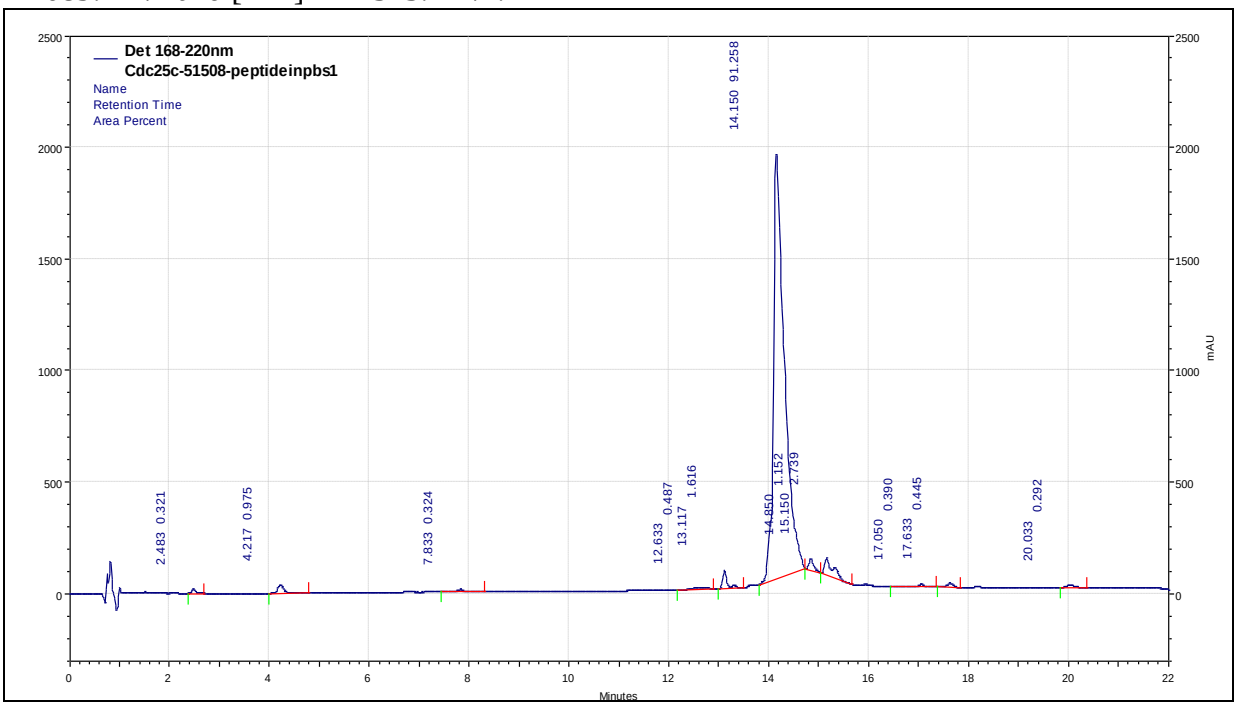

Fig. S5. Analytical HPLC of ligand 1 using a Waters C18 XBridgeTM 2.5 µm, 4.6 × 50 mm column, with 5% CH_3CN/H_2O for 2 min, then 5% to 50% gradient over 15 min showed a major peak at 14.2 min, 91.2% pure.

Analytical characterization of Fmoc–VPRpTPVGGGK–NH_2 **2**

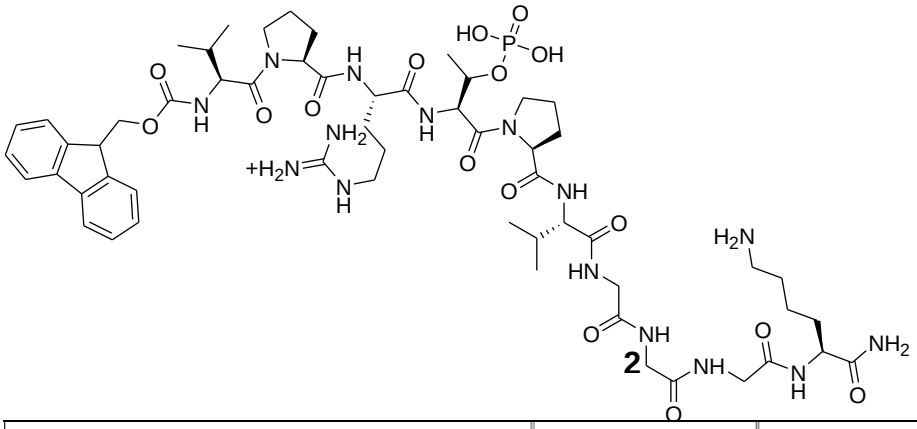

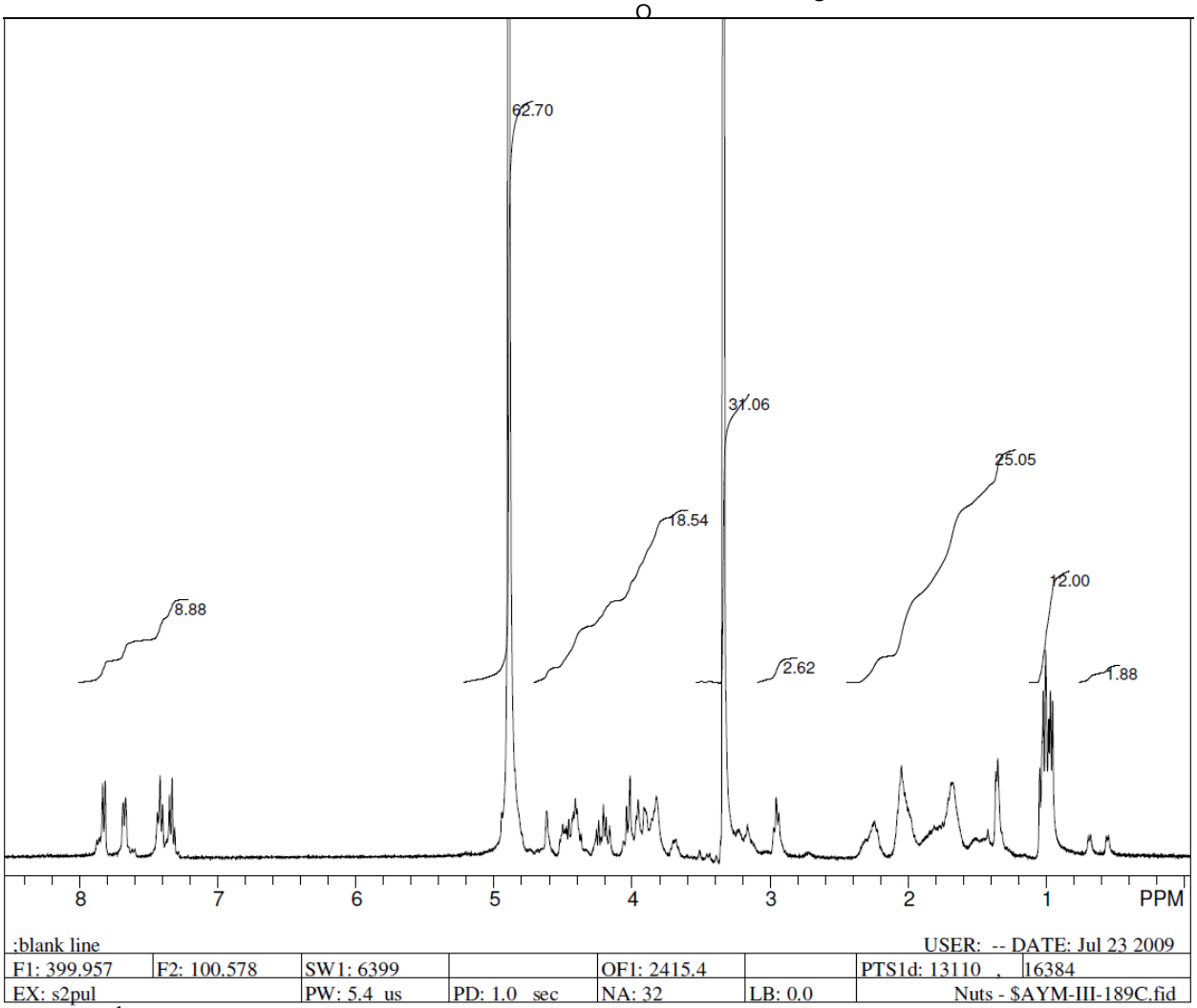

Fig. S6. ^{1}H NMR in CD_3OD of ligand **2**. The 13 α-protons of the peptide overlap at 4.8 - 3.6 ppm, aromatic protons of the Fmoc group were observed at 7-9 ppm, and the two valine methylene doublets appear at 0.9-0.7 ppm.

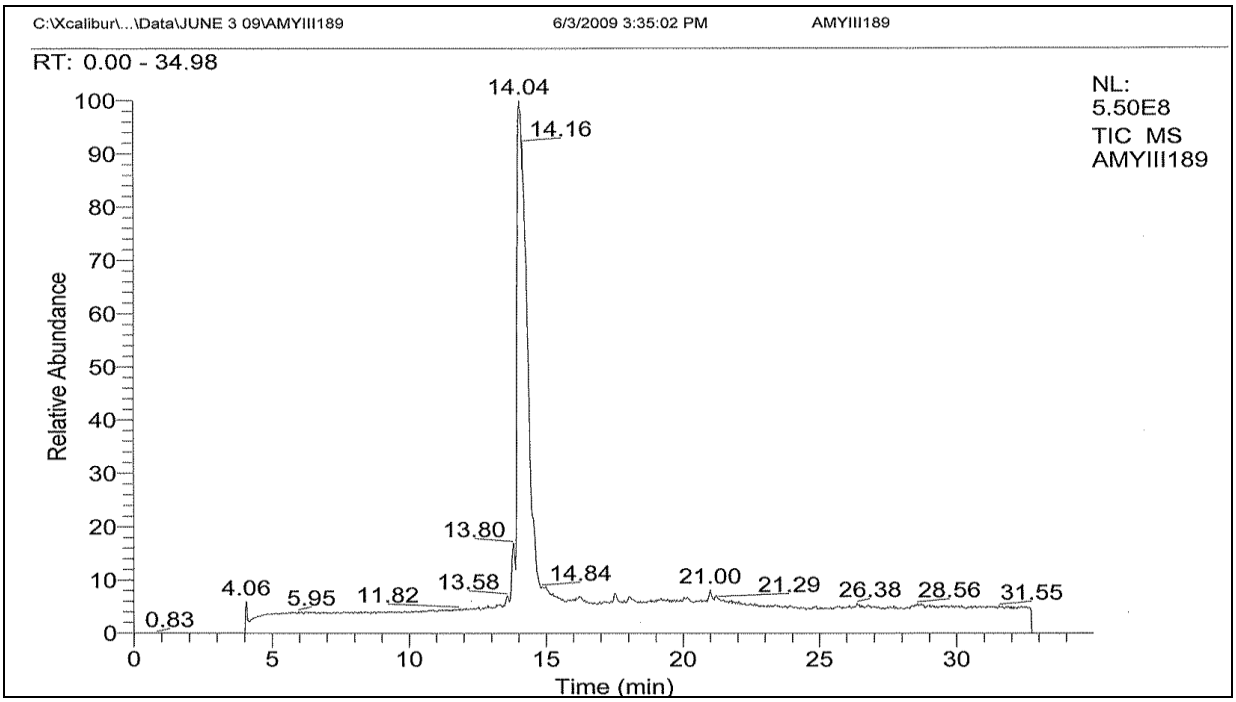

Fig. S7. LC-MS total ion chromatogram of ligand **2**. The peak at 14.04 min had the correct molecular mass (See Fig. S13).

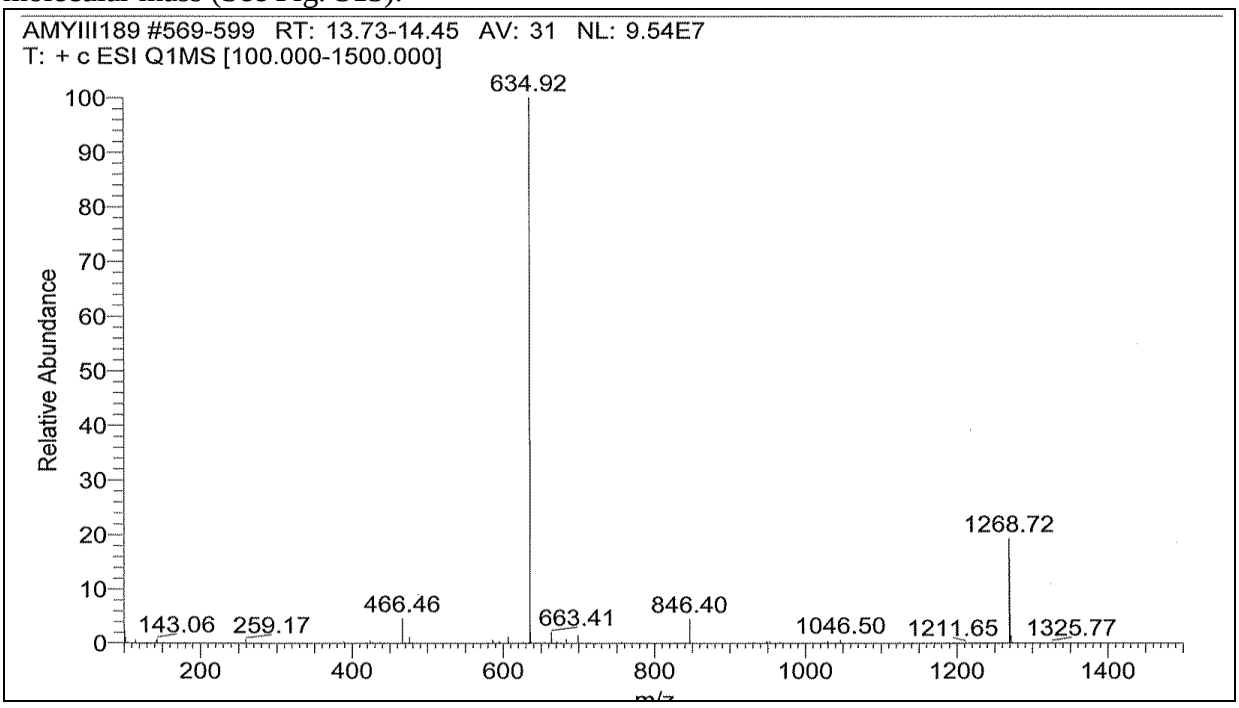

Fig. S8. MS with electrospray ionization (ESI+) showing the fragmentation pattern for ligand **2**. The LC peak from 13.73-14.45 min was selected for molecular ion detection, identifying [MH]+ = 1268.7 *m/z* and $[MH]^{2+}$ = 634.9 *m/z*.

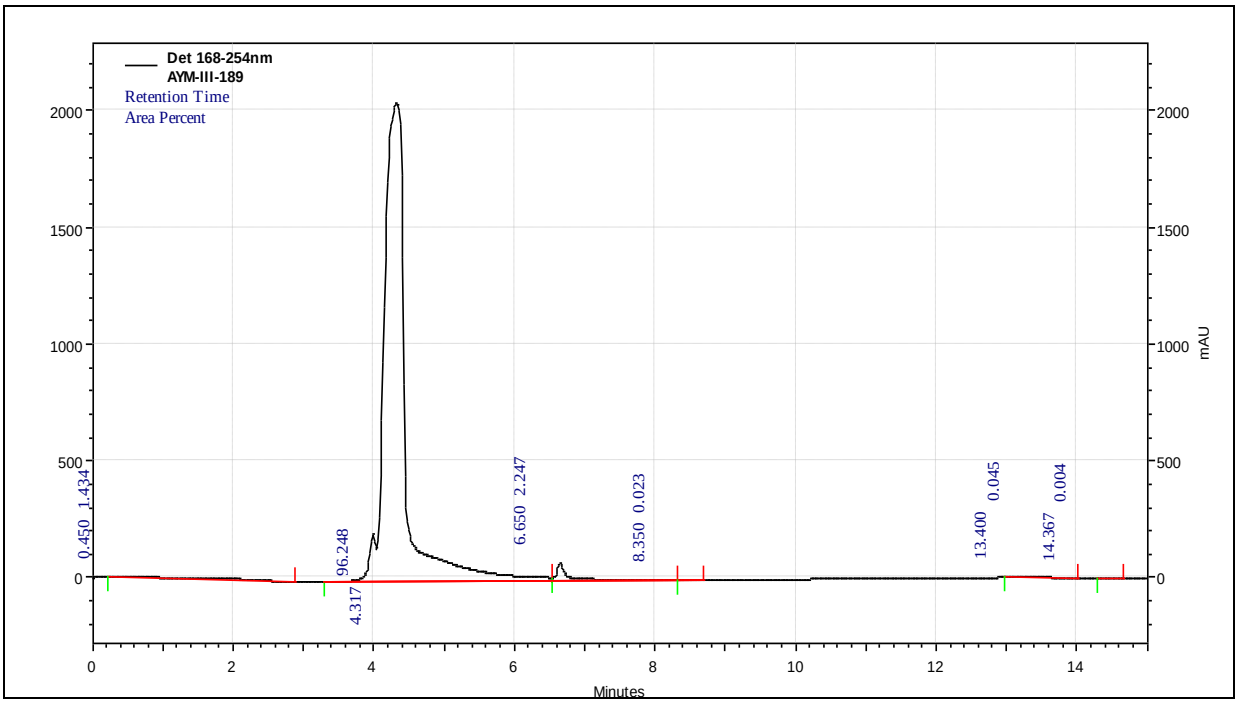

Fig. S9. Analytical HPLC of ligand **2** using an XBridgeTM BET130 3.5 µm C18 4.6 × 50 mm column, with 5% CH3CN/H2O for 2 min, then 5% to 80% gradient over 5 min, showed a major peak at 4.3 min, 96.2% pure.

Characterization data of Ac–VPRpTPV–NH_2 **3**

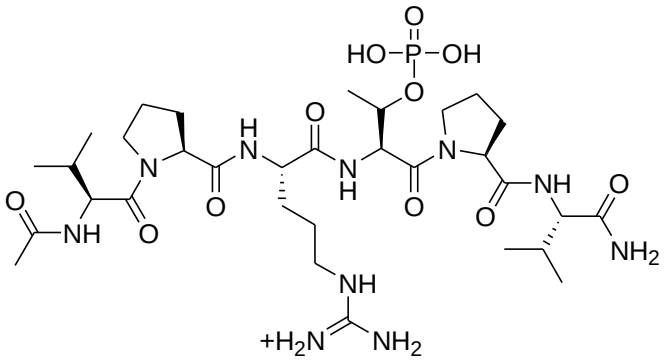

3

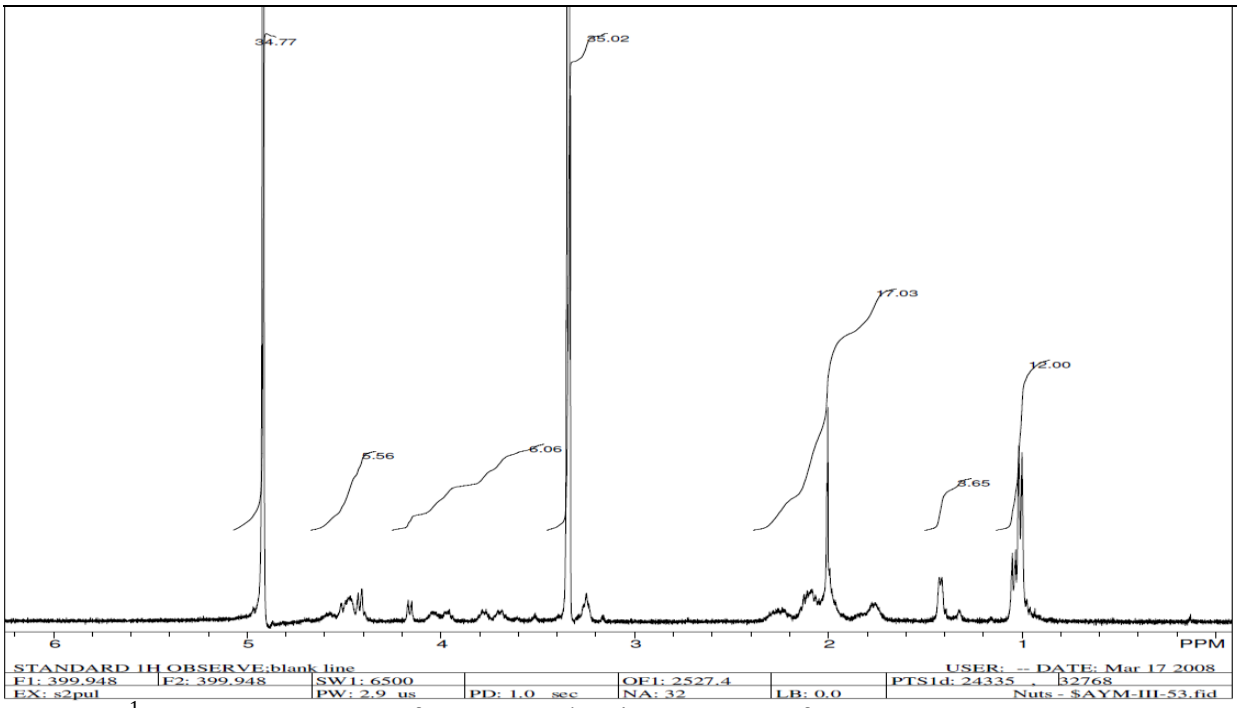

Fig. S10. ^{1}H NMR in CD_3OD of ligand **3**. The six α-protons of the peptide core overlap at 4.6-4.4 ppm, the β and γ-ethyl groups of the Arg side chain at 1.4-1.3 ppm, and the two valine methylene doublets appear at 1.0-0.9 ppm.

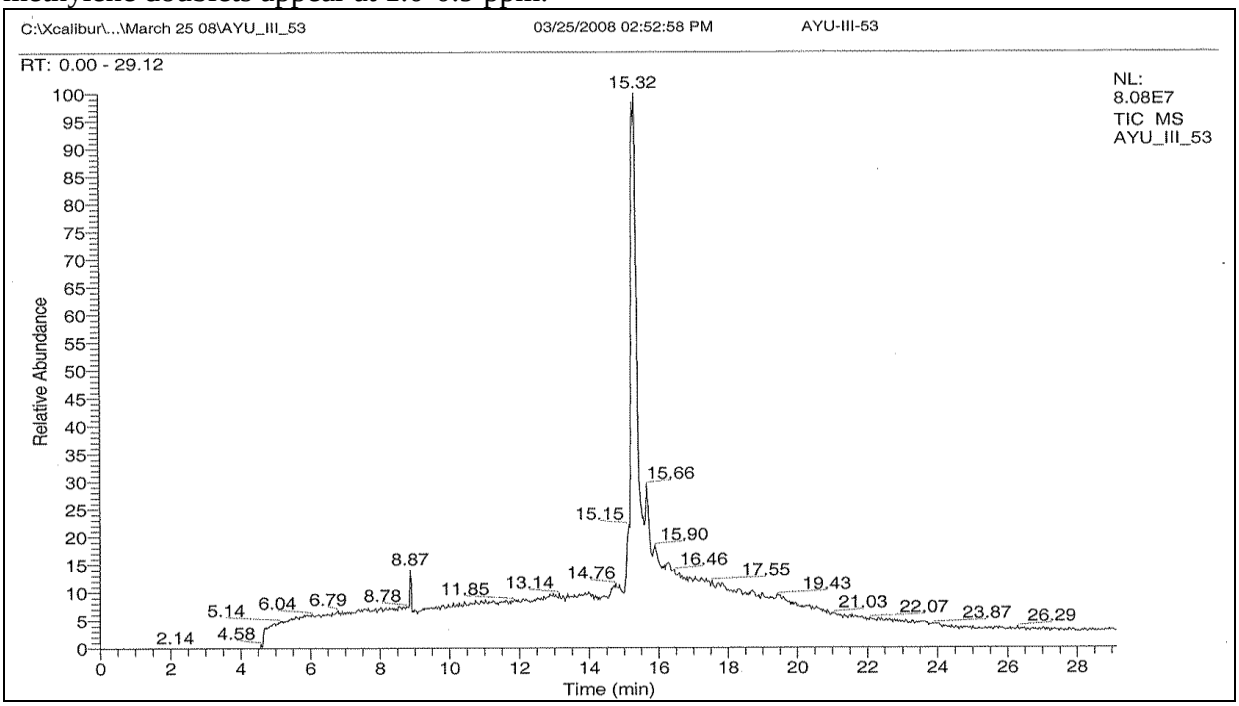

Fig. S11. LC-MS total ion chromatogram of ligand **3**. The peak at 15.32 min had the correct molecular mass (See Fig. S17).

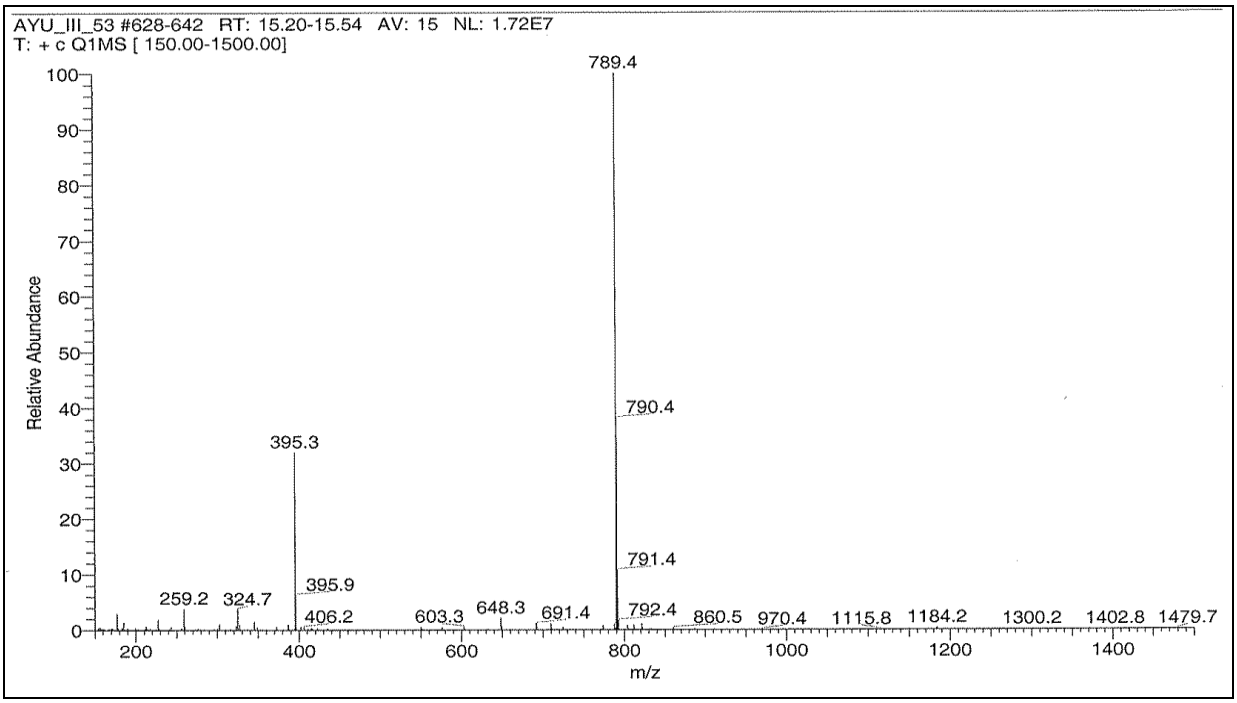

Fig. S12. MS with electrospray ionization (ESI+) showing the fragmentation pattern for ligand **3**. The LC peak from 15.20-15.54 min was selected for molecular ion detection, identifying [MH]+ = 789.4 *m/z* and [MH]2+ = 395.3 *m/z*.

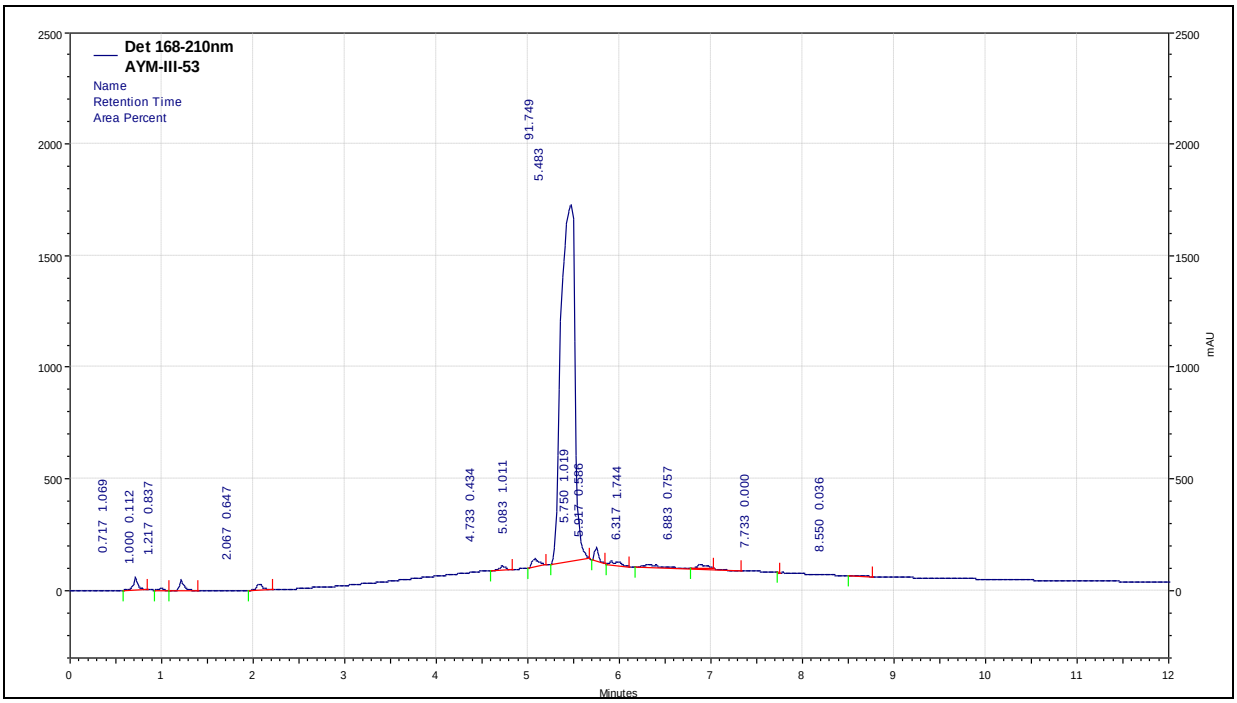

Fig. S13. Analytical HPLC of ligand **3** using a Waters C18 XBridgeTM 2.5 µm, 4.6 × 50 mm column, with 5% CH3CN/H2O for 2 min, then 5% to 60% gradient over 5 min, then 60% for 4.5 min, showed a major peak at 5.48 min, 91.7% pure.

Analytical characterization of Ac–LPTPPLSPS–NH_2 **4**

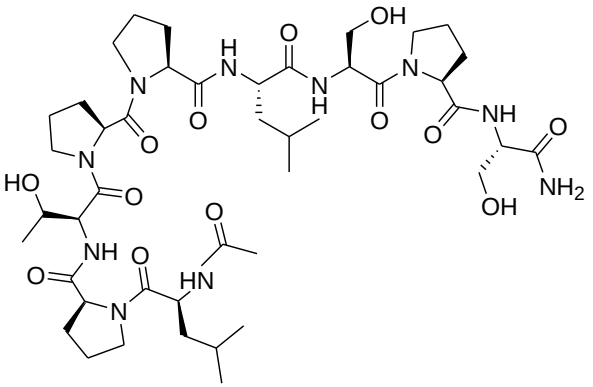

4

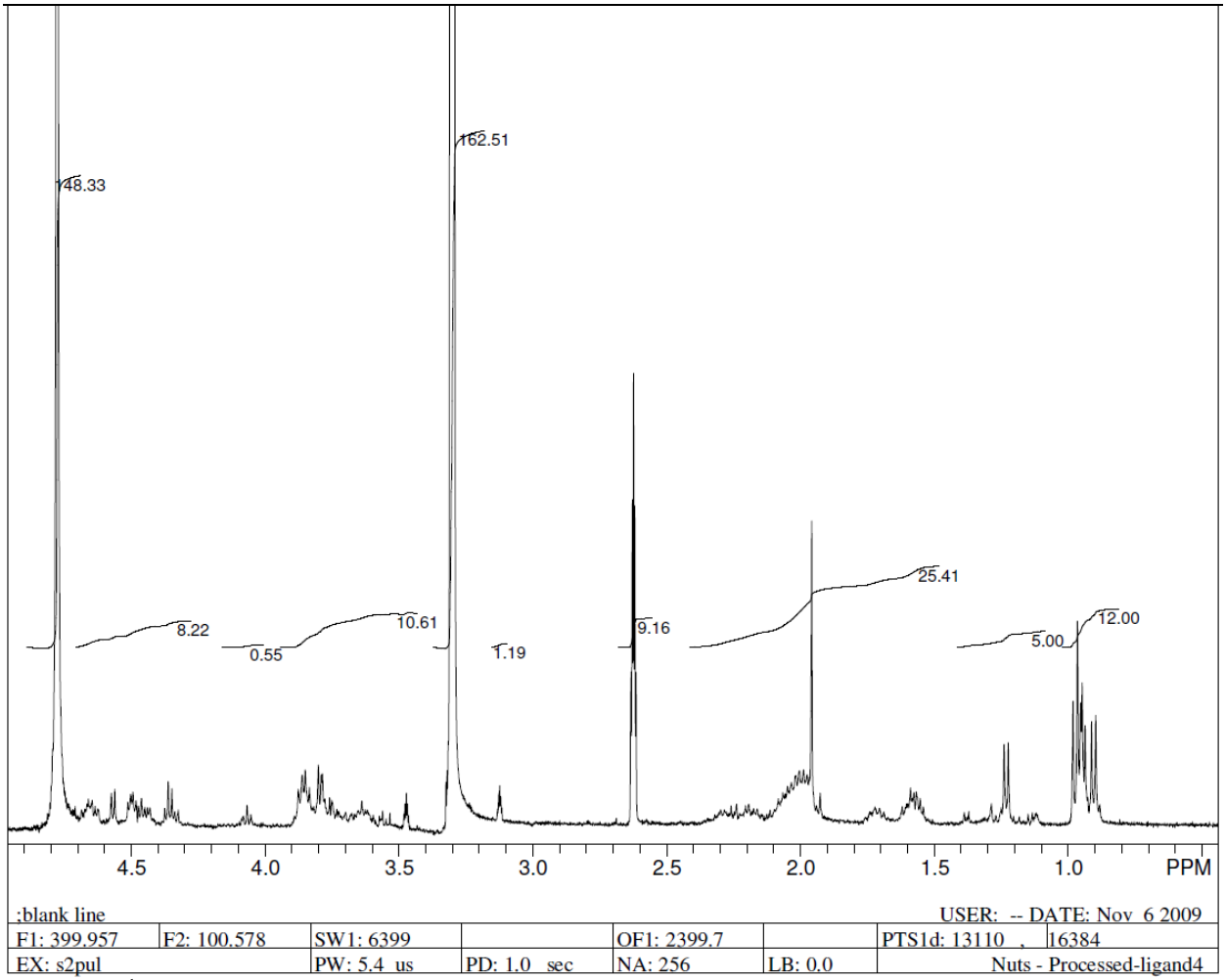

Fig. S14. ^{1}H NMR in CD_3OD: DMSO (4:1) of ligand **4**. Leucine side chains were observed at 0.9-0.7 ppm, protons of the nine α-protons of the peptide overlap at 4.9-4.0 ppm.

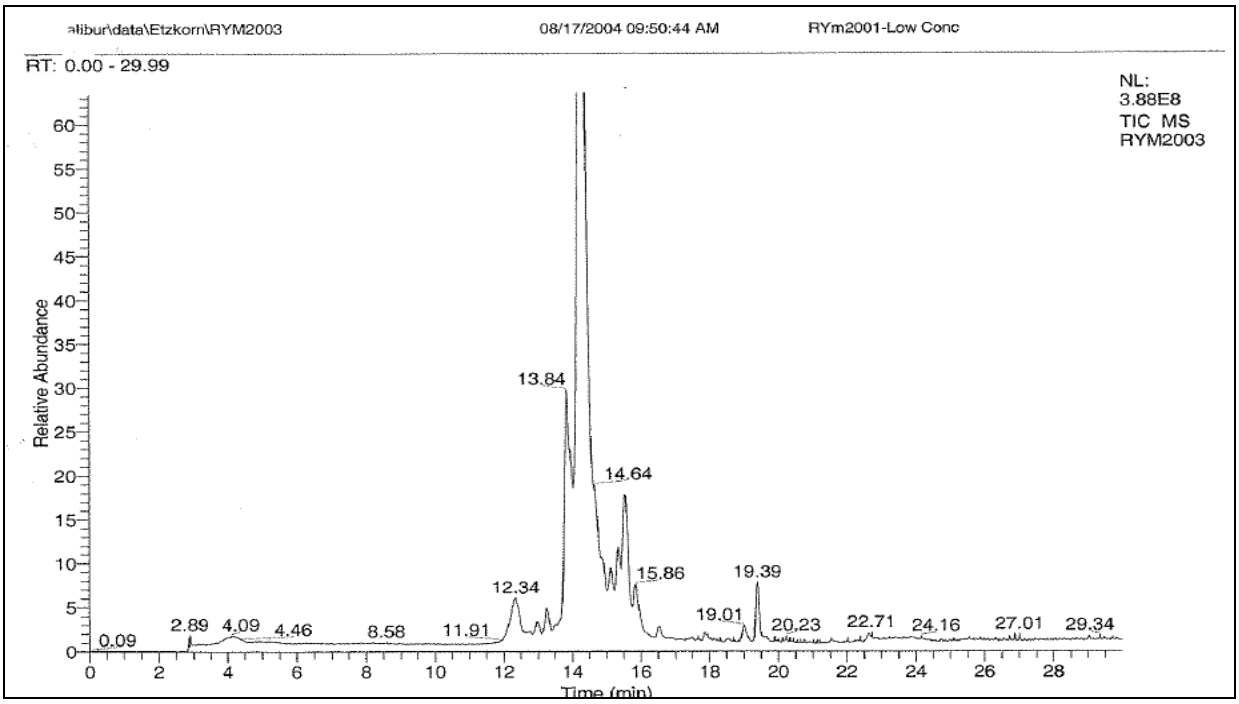

Fig. S15. LC-MS total ion chromatogram of crude ligand **4**. The peak at 13.75-14.5 min had the correct molecular mass (See Fig. S21 and S22).

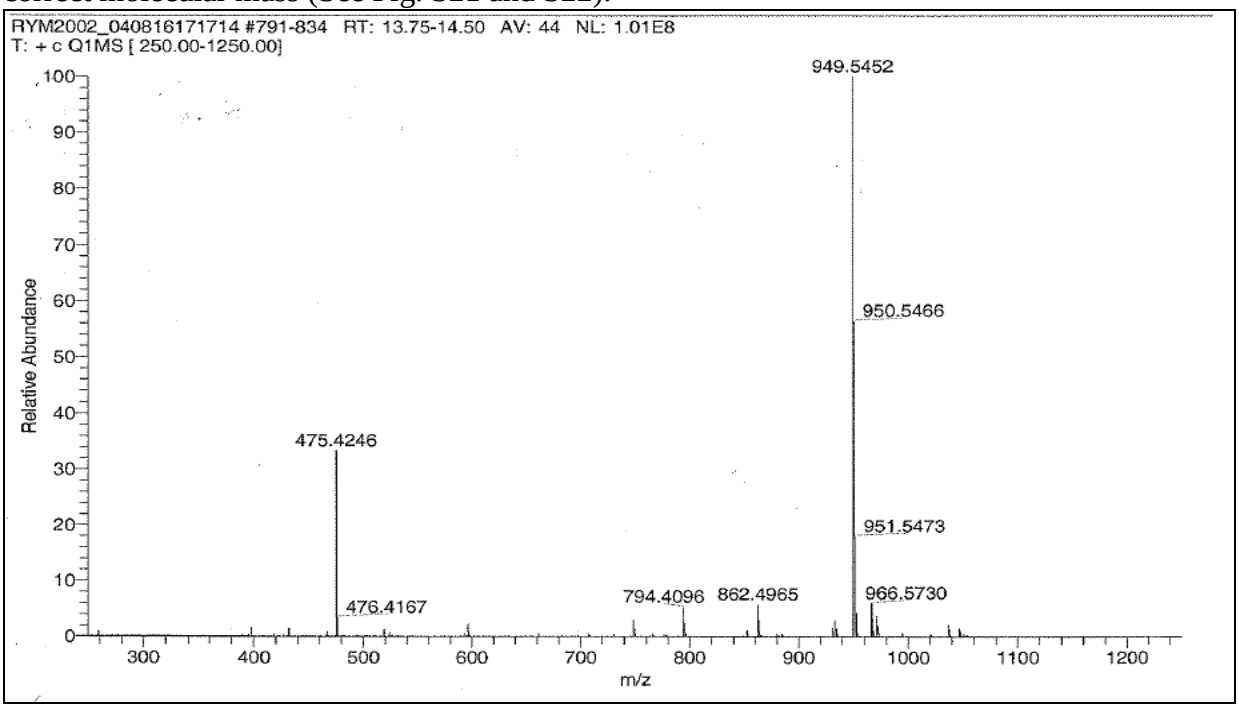

Fig. S16. MS with electrospray ionization (ESI+) showing the fragmentation pattern for ligand **4**. The LC peak from 13.75-14.50 min was selected for molecular ion detection, identifying [MH]+ = 949.54 *m/z* and [MH]2+ = 475.4 *m/z*.

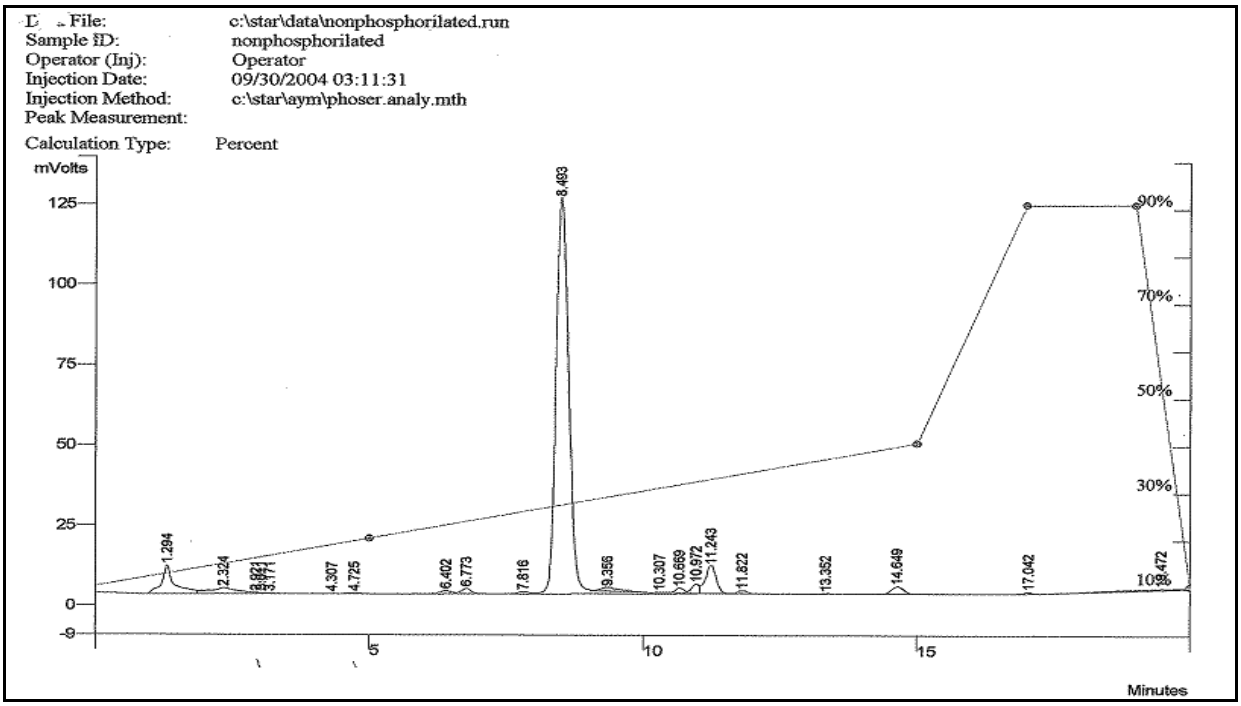

Fig. S17. Analytical HPLC of ligand 4 in using a linear gradient of 10% to 40% CH_3CN/H_2O over 15 min showed a major peak at 8.5 min, 84.5% pure.

Optimization of Pin1-HRP concentration

The Pin1-HRP concentration was varied to optimize conditions for the ELEBA. The plate was treated with 2.8 mM ligand 1 (100 µL/well) as described in Materials and Methods. For ELEBA assays, 200 pM of Pin1-HRP was chosen (Fig. S18).

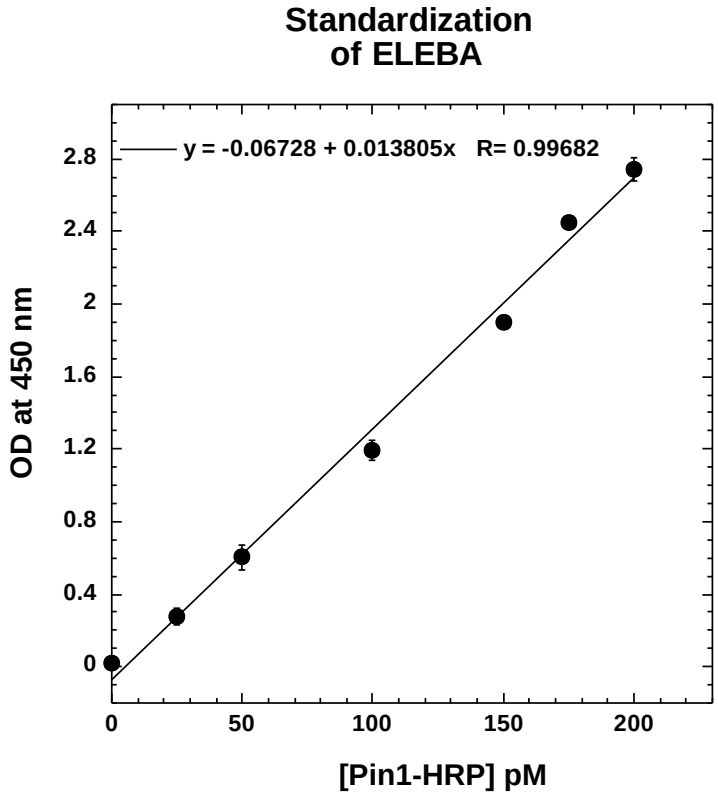

Fig. S18. Calibration curve to optimize Pin1–HRP concentrations. Assays were performed in duplicate with standard deviations shown as error bars. (Prepared with Kaleidagraph 4.3.)

Reuse of the 96-well microtiter plate with covalently bound ligand

The ability to reuse the 96-well plate with covalently bound NH_2–GGGGVPRpTPVGG–NH_2 **1** was tested. After one assay, the plate was rinsed with H_2O and wash buffer 3 times each. The plate was dried under high vacuum overnight, and the plate was treated with blocking buffer overnight before reassay. A decrease in sensitivity of ~17% in comparison with a new plate is probably a consequence of the quenching with 2N H_2SO_4 in the first assay. Strong acid treatment of the plate surface is likely to cause β-elimination of phosphate from Thr side chain. Nonspecific binding (NSB) remained similar for the new and the used plate (Fig. S19).

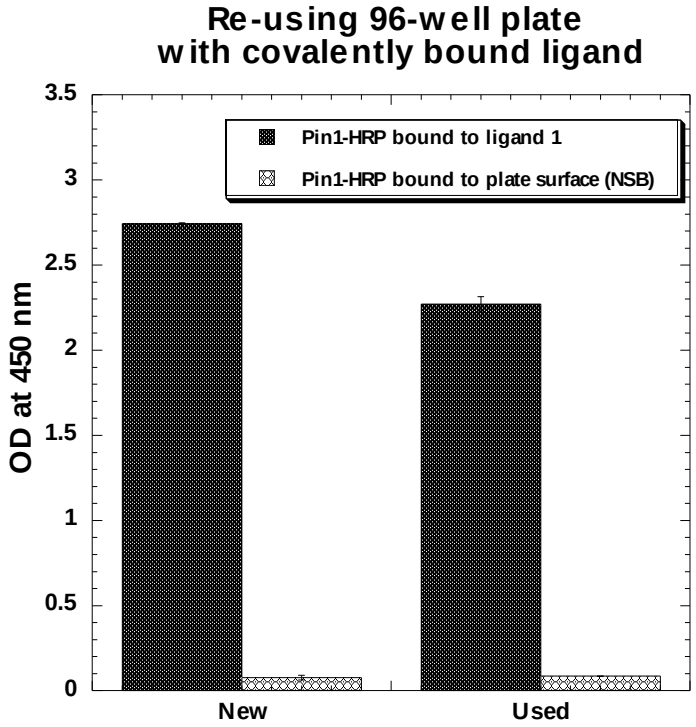

Fig. S19. 96-well DNA-BIND™ plate with covalently bound NH_2–GGGGVPRpTPVGG–NH_2 **1** after one assay to show re-usability of the plate. (Prepared with Kaleidagraph 4.3.)

Computer modeling of ligand 1

The Pin1 crystal structure in complex with the RNA Polymerase C-terminal domain-peptide (CTD) was obtained from the RCSB-Protein Data Bank (PDB ID: 1F8A) [32]. The peptide, H–GGGGVPRpTPVGG–NH_2 1, was built by mutating amino acids of the CTD-peptide sequence (chain C), partial charges were assigned with Gasteiger and Marsili, and the complex within an 8.0 Å radius of the ligand was minimized using the force field, Amber FF02, in a water dielectric field, with a gradient end point of 0.1 kcal/mol energy using SYBYL 8.1., Tripos, Inc. (Fig. S20).

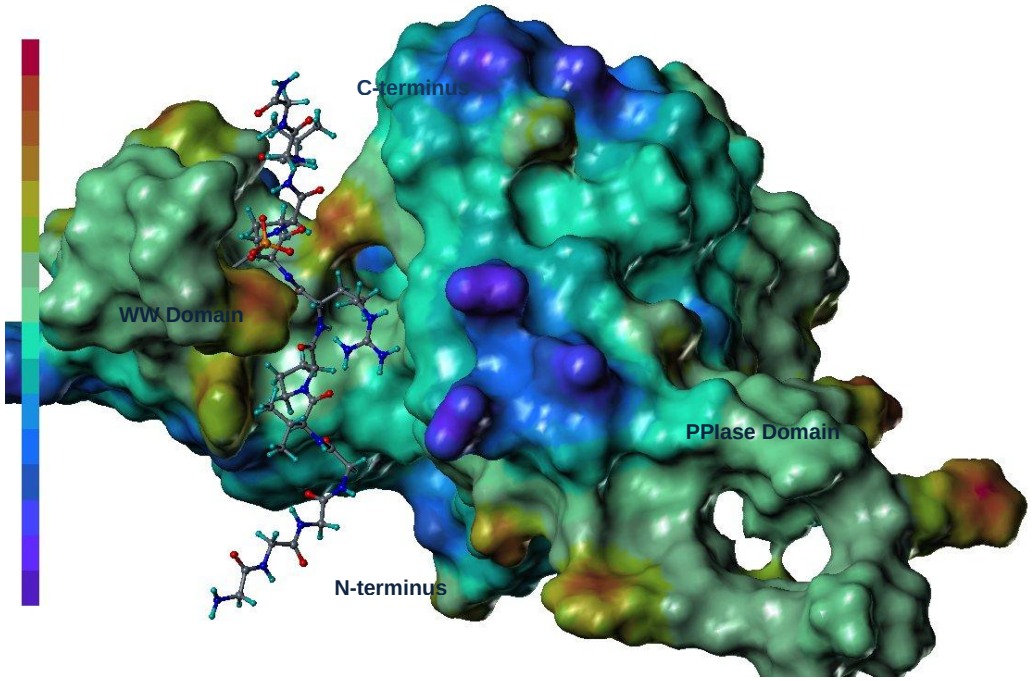

Fig. S20. Molecular model of Pin1 in complex with H–GGGGVPRpTPVGG–NH_2 **1**, and minimized using Sybyl 8.1.1 (Tripos, Inc.). The electrostatic potential (EP) of Pin1 surface indicates sites of attractive interactions with ligand **1** by matching opposite colors. The color ramp for EP ranges from red (most positive) to purple (most negative). The model showed that the glycine residues did not disrupt the binding of ligand **1** in the WW domain site of Pin1. (Prepared with Sybyl 8.1.)

Effect of buffers in the ELEBA

Three buffers commonly used in Pin1 catalysis assays were tested to investigate their effect on Pin1-HRP affinity for WW domain ligand 3 without NaCl (Fig. S21). Pin1–HRP was incubated with or without 130 μM of ligand 3 for 1 h at room temperature with orbital shaking. The buffers used in the ELEBA were tested at pH values ± 1 their respective pKa values, with 150 mM NaCl (Fig. S22). The most suitable buffer for the ELEBA was PBS with 150 mM NaCl at pH 7.3 to prevent Pin1–HRP nonspecific binding (NSB) with the plate surface.

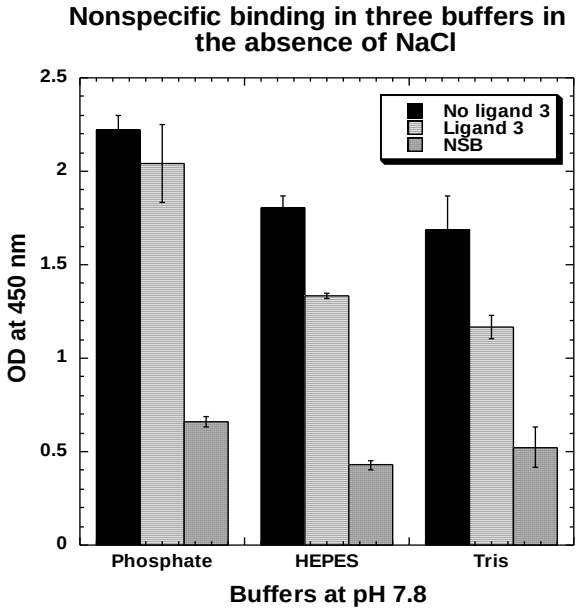

Fig. S21. Buffers commonly used in Pin1 catalysis assays were tested to investigate their effect on Pin1-HRP affinity for WW domain ligand **3** without NaCl. Pin1–HRP binding to covalently immobilized ligand **1**, with ligand **3** at 130 μM in solution, and nonspecific binding without ligand **1** on the plate, mean of N = 3 with standard deviation shown as error bars. (Prepared with Kaleidagraph 4.3.)

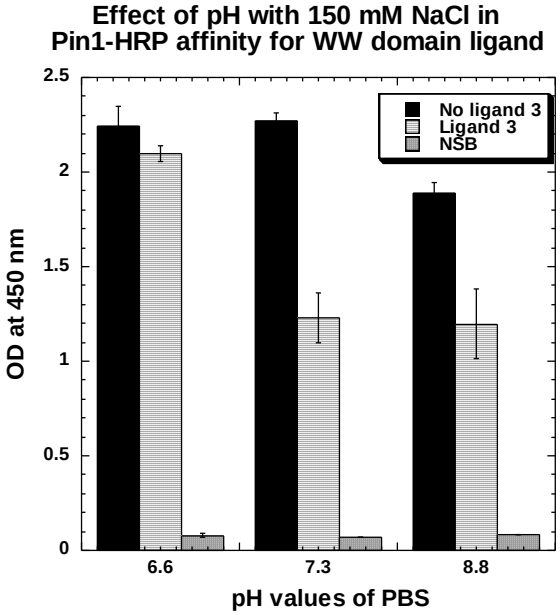

Fig. S22. The pH value of PBS buffer was optimized for Pin1-HRP binding to covalently immobilized ligand **1**, with ligand **3** at 130 μM in solution, and nonspecific binding without ligand **1** on the plate, mean of N = 3 with standard deviation shown as error bars. (Prepared with Kaleidagraph 4.3.)

Addendum: Additional experiments supporting the development of the ELEBA.

Analytical characterization of NH2–GGGGPPGpSPPGG–NH_2 **5**

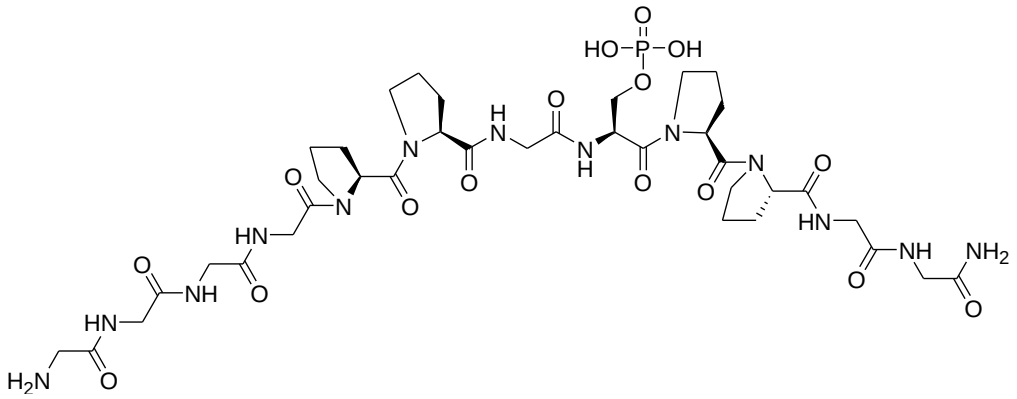

5

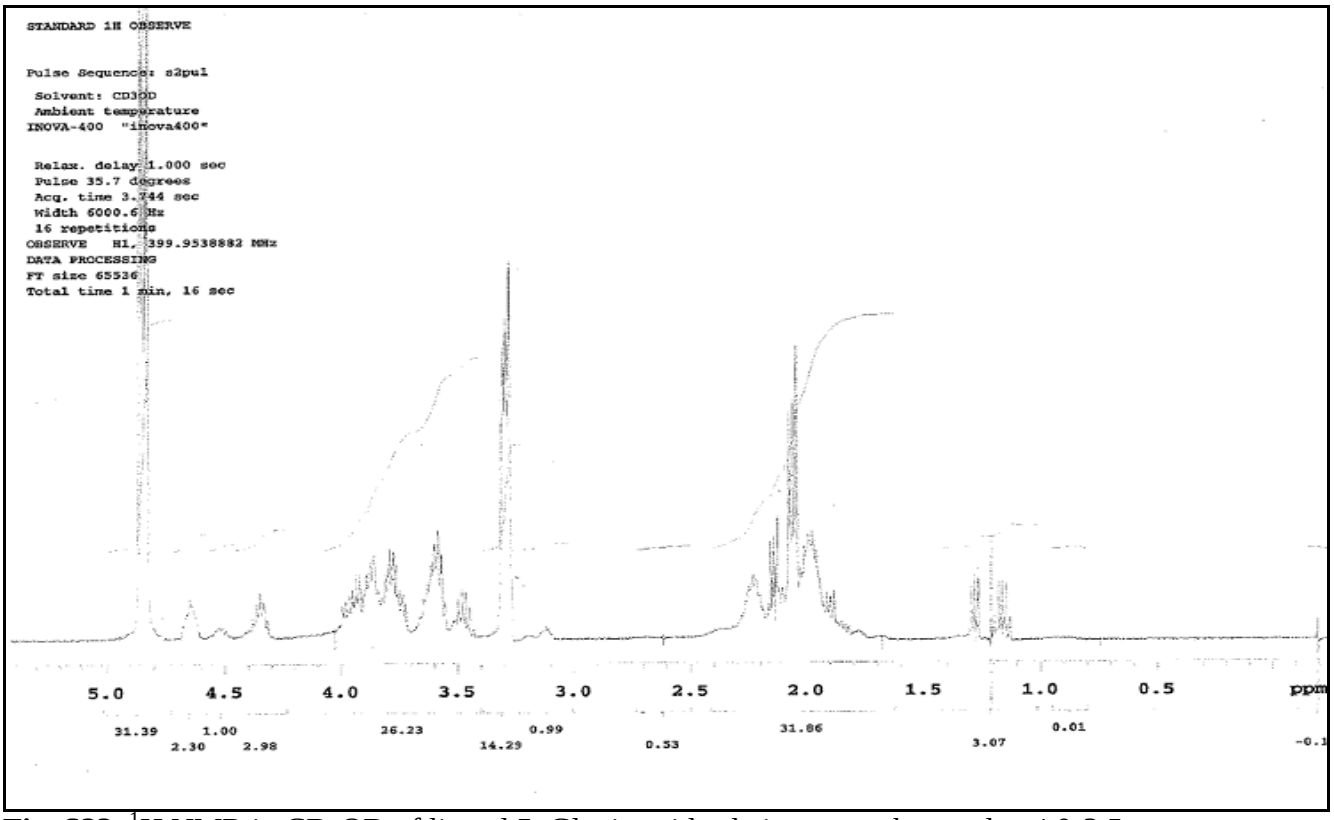

Fig. S23. ^{1}H NMR in CD_3OD of ligand **5**. Glycine side chains were observed at 4.0-3.5 ppm, protons of the five α-protons of the peptide at 4.9-4.5 ppm.

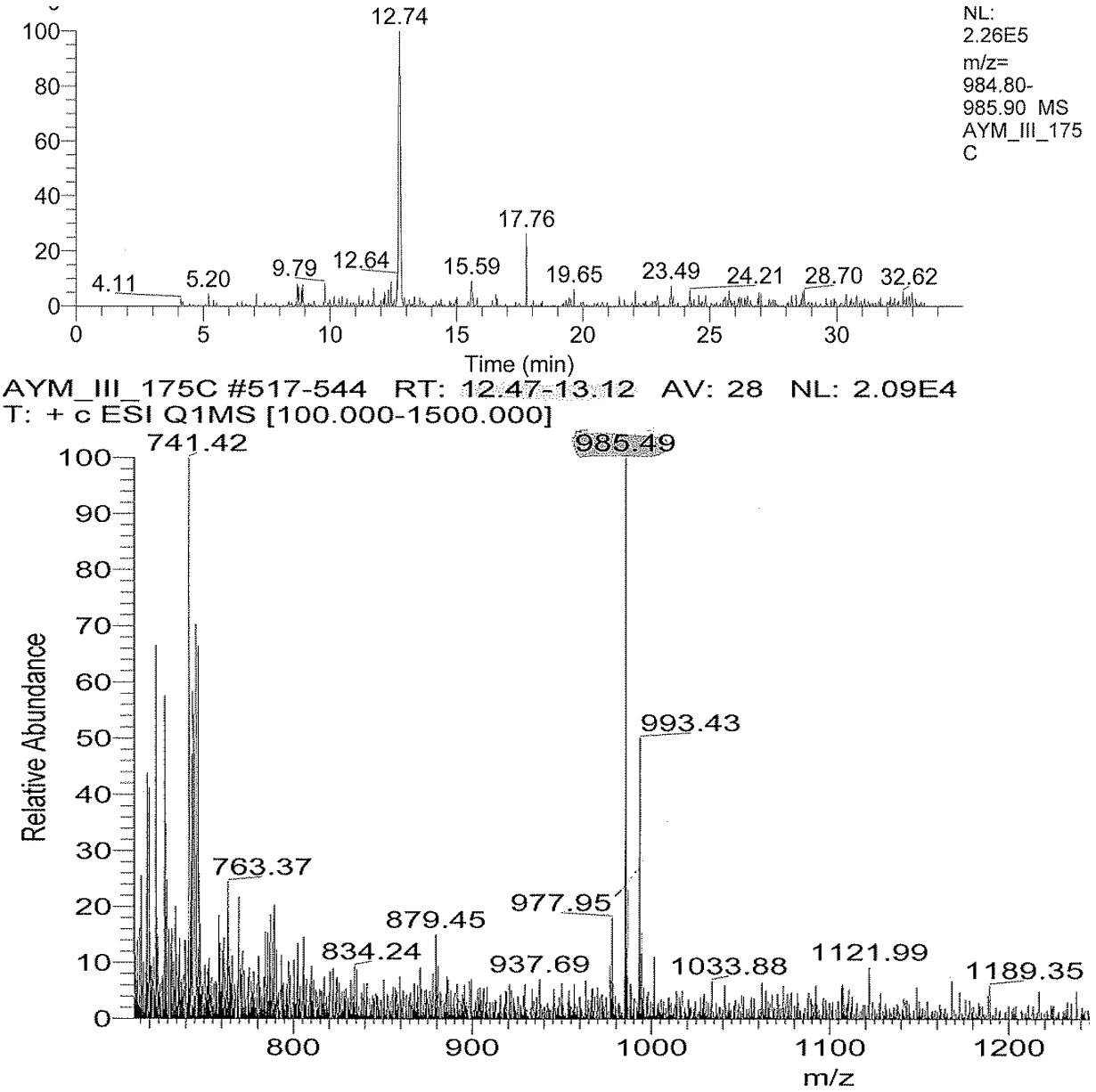

Fig. S24. MS with electrospray ionization (ESI+) showing the fragmentation pattern for ligand 5. The LC peak from 12.47-13.12 min was selected for molecular ion detection, identifying [MH]+ = 985.49 *m/z*.

Decreasing Pin1 affinity for ligands 1 and 2

To explore a weaker ligand, we synthesized NH_2–GGGGPPGpSPPGG–NH_2 (**5**), which corresponds to the cell cycle kinase Myt1 at the pSer416–Pro417 position. Fluorescence anisotropy has shown that the Pin1 WW domain binds the PPGpSPP sequence, with an affinity of 126 μM for the WW domain, and no detectable binding to the PPIase domain (Table 3.1). We

were unsuccessful in detecting UV-Vis absorption at 210 and 220 nm for ligand **5**. Therefore, we used crude peptide for plate immobilization according to the DNA-BIND™ microtiter plate specifications. The desired sequence was confirmed by LC-MS 14 min, calcd. for $C_{38}H_{60}N_{13}O_{16}P$ [M + H]+ *m/z* = 985.4, found *m/z* = 985.4(Fig. S24). The affinity of Pin1–HRP for ligand **5** was measured as described as for ligand **1** and **2** [90]. Results showed that the affinity of Pin1–HRP for the plate-linked ligand 5 was weak, as evidenced by the fact that the Pin1–HRP was removed from the plate during washing (Fig. S25).

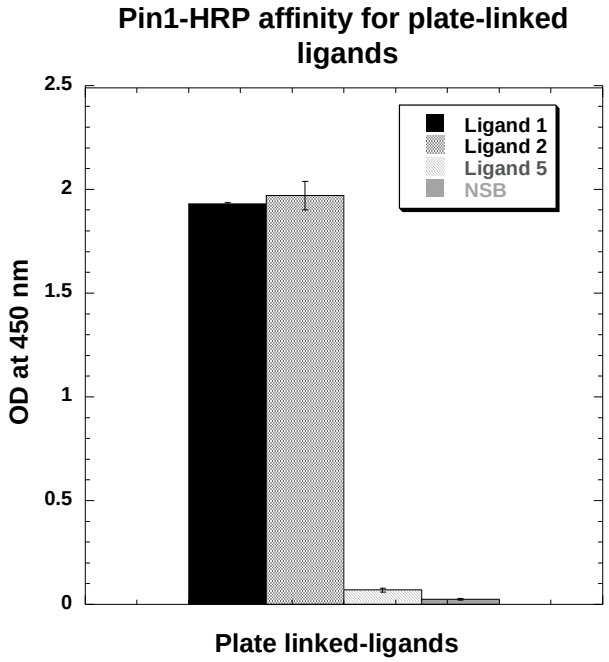

Fig. S25. Decreasing Pin1–HRP affinity for plate-linked ligand 1 and 2. Data for for N = 3 with standard deviations shown as error bars. (Prepared with Kaleidagraph 4.3.)

NMR binding studies for Ac–VPRpTPV–NH_2 , 3

We asked our collaborator, Jeffry Peng, University of Notre Dame to measure the K_d value for the Ac–VPRpTPV–NH_2 **3**. NMR titration was performed with the isolated Pin1 WW domain (ww6) in a 20 mM phosphate buffer containing 30 mM NaCl, and 0.03% NaN_3 pH 7.0 at 278K in a 700MHz NMR spectrophotometer. The K_d value was determined by fitting chemical-shift perturbations of 2D cross-peaks as a function of added peptide by using Arg14 as a reliable marker. A K_d value of 3.7 ± 0.3 μM was determined, indicating that peptides not labeled with a rhodamine flourophore were able to conserve the necessary elements to bind the Pin1 WW domain with high affinity, as previously reported (Fig. S26) [32, 126]. A direct comparison between currently-used methods for determining the dissociation constants for ligands binding to Pin1 and the ELEBA was not established due to the fact that ELEBA is a competitive-binding assay. In other words, since two ligands are competing for the same receptor-binding site, we do not determine a single ligand-receptor association or dissociation. The resulting 30-fold difference between ELEBA and NMR K_d values that we identified is likely due to different experimental conditions, such as ionic strength, pH, and buffer, as previously reported (Table S2.1) [41, 87, 127]. Moreover, ligands used for ELEBA are susceptible to pH and ionic strength changes because of the ionization state of the Arg guanidine and the phosphorylated-Thr. Indeed, previous experimental data have shown that Pin1 PPIase activity and binding affinity for phospho-substrates is affected by high ionic strength [25, 87].

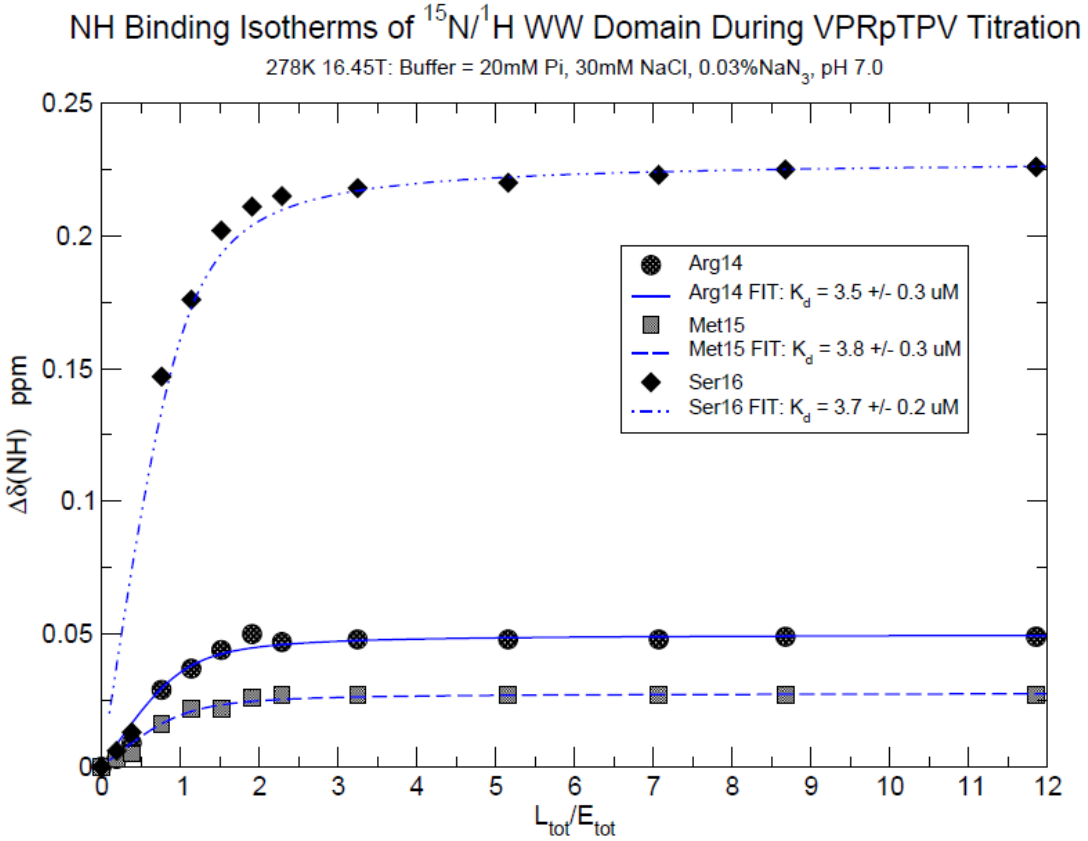

Fig. S26. NMR binding studies for Ac–VPRpTPV–NH_2, **3**. The backbone δ amide proton mobility of Arg14 was used to calculate the binding constant. Truncated WW domain (ww6): ligand 3 molar ratio titration curve.

Table S2.1. Binding affinities (K_d) for WW domain libraries screened by a variety of methods.

Peptides	K_d µM	Buffer	Method	Titration	Ref.
WFYpSPFLE (Pintide)	1	50 mM Hepes, 2% Glycerol, and 100 mM NaCl at pH 7.4	fluorescence polarization	Vary [WW domain] 0.1 µM of ligand	Lu et al. 1999[41]
WFYpSPFLE	44	25 mM HEPES·Na^+, 1 mM DTT, and 100 mM NaCl at pH 7.5	fluorescence anisotropy	Vary [WW domain]	Verdecia et al. 2000[32]
WFYpSPFLE	323	50 mM phosphate buffer, 5 mM DTT, 0.03% NaN_3, and 10% D2O/H_2O, 300K at pH 6.5	NMR	100 µM Pin1 0.5-2 mM ligand	Wu et al. 2009[127]
WFYpSPFLE	200-400	100 mM imidazole, 5 mM DTT, 100 mM NaCl 0.03% NaN3, and 10% D2O/H_2O, at pH 6.6	NMR	Vary WW domain (0.5, 0.2, 0.1, 0.05, and 0.02 mM)WW domain : ligand 1:4	Jacobs et al. 2003[88]
EQPLpTPVTDL (Cdc25C)	2.2	50 mM Hepes, 100 mM NaCl and 2% glycerol,295K, at pH 7.4	fluorescence polarization	Vary [WW domain] 0.1 µM of ligand	Lu et al. 1999[41]
EQPLpTPVTDL	8	30 mM imidazole-d_4, 0.03% NaN_3, 1 mM DTT-d_{10}, 30 mM NaCl, and 10% D_2O/H_2O, at pH 6.6	NMR	50 µM Pin1, 2 mM ligand	Peng et al. 2009[159]
EQPLpTPVTDL	120	30 mM imidazole-d_4, 0.03% NaN_3, 5 mM DTT-d_{10}, 30 mM NaCl and 10% D_2O/H_2O,, 295K, at pH 6.6	NMR	0.37 mM Pin1, 3 mM ligand	Namanja et al. 2007[27]
EQPLpTPVTDL	117	50 mM deuterated Tris.HCl, 100 mM NaCl, 285K, at pH 6.4	NMR	1 mM of WW domain with 0.0 to 4.5 mM ligand	Wintjen et al. 2000[87]
EQPLpTPVTDL	29	50 mM deuterated Tris.HCl, 285K, at pH 6.4,	NMR	1 mM of WW domain with 0.0 to 4.5 mM ligand	Wintjen et al. 2000[87]
rhodamine–VPRpTPV	7.7	25 mM HEPES·Na^+, 100 mM NaCl and 1 mM DTT, at pH 7.5	fluorescence anisotropy	Vary [WW domain]	Verdecia et al. 2000[32]
Ac–VPRpTPV–NH_2	3.6	20 mM phosphate, 30 mM NaCl and 0.03% NaN_3, 278K, at pH 7.0	NMR	Vary [WW domain] 31µM starting [ligand]	Peng et al. 2009 (Unpublished results)
Ac–VPRpTPV–NH_2	110	15 mM sodium phosphate, 2 mM potassium phosphate, and 150 mM NaCl, 298K, at pH 7.3	ELEBA	Vary [ligand] 200 pM Pin1-HRP	Mercedes et al. 2010 [90]
Ac–VPRpTPV–NH_2	NSB	15 mM sodium phosphate, 2 mM potassium phosphate, 298K, at pH 7.3	ELEBA	Vary [ligand] 200 pM Pin1-HRP	Mercedes et al. 2010 [90]
Fmoc–VPRpTPVGGK–NH_2	36	15 mM sodium phosphate, 150 mM NaCl and 2 mM potassium phosphate, 298K, at p3 7.4	ELEBA	Vary [ligand] 200 pM Pin1-HRP	Mercedes et al. 2010 [90]
rhodamine-YpSPTPSPS (CTD)	10	25 mM HEPES·Na^+, 100 mM NaCl, and 1 mM DTT, at pH 7.5	fluorescence anisotropy	Vary [WW domain]	Verdecia et al. 2000[32]
YpSPTPSPS	200	100 mM imidazole, 100 mM NaCl, 5 mM dithioerythritol, 0.03% NaN_3, and 10% D_2O/H_2O, 300K, at pH 6.6	NMR	Vary WW domain (0.5, 0.2, 0.1, 0.05, and 0.02 mM)WW domain : ligand 1:4	Jacobs et al. 2003[88]
WFYpSPFLE (Pintide)	1	50 mM Hepes, 2% Glycerol, and 100 mM NaCl at pH 7.4	fluorescence polarization	Vary [WW domain] 0.1 µM of ligand	Lu et al. 1999[41]
WFYpSPFLE	44	25 mM HEPES·Na^+, 1 mM DTT, and 100 mM NaCl at pH 7.5	fluorescence anisotropy	Vary [WW domain]	Verdecia et al. 2000[32]
WFYpSPFLE	323	50 mM phosphate buffer, 5 mM DTT, 0.03% NaN_3, and 10% D2O/H_2O, 300K at pH 6.5	NMR	100 µM Pin1 0.5-2 mM ligand	Wu et al. 2009[127]

Appendix B

Supplementary material for ELEBA for the screening of pSer–Pro ligand library

Primary screening of competitive binding of pSer–Pro dipeptides was measured at 600 μM with plate-linked Fmoc–VPRpTPVGGGK–NH_2 (L1). Acid N and P did not couple during the synthesis.

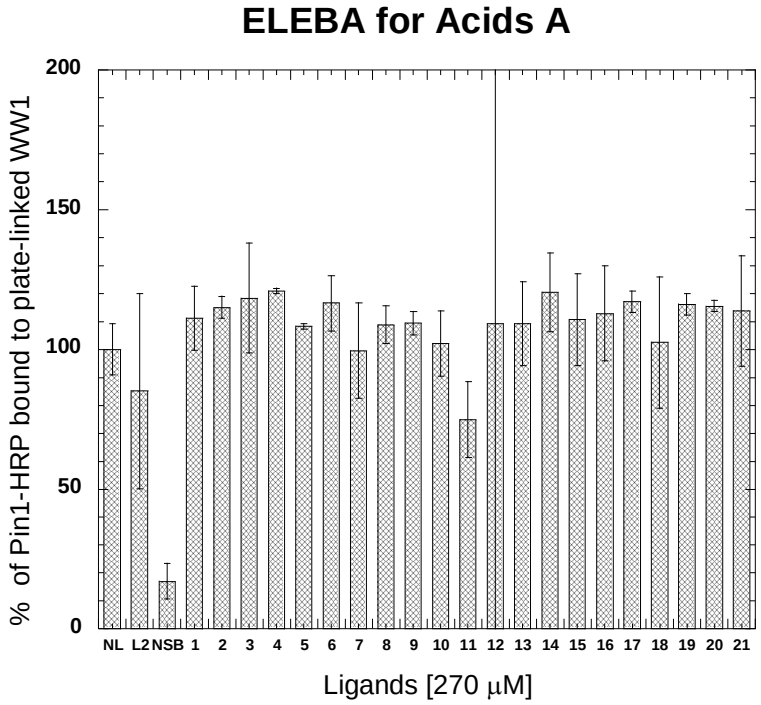

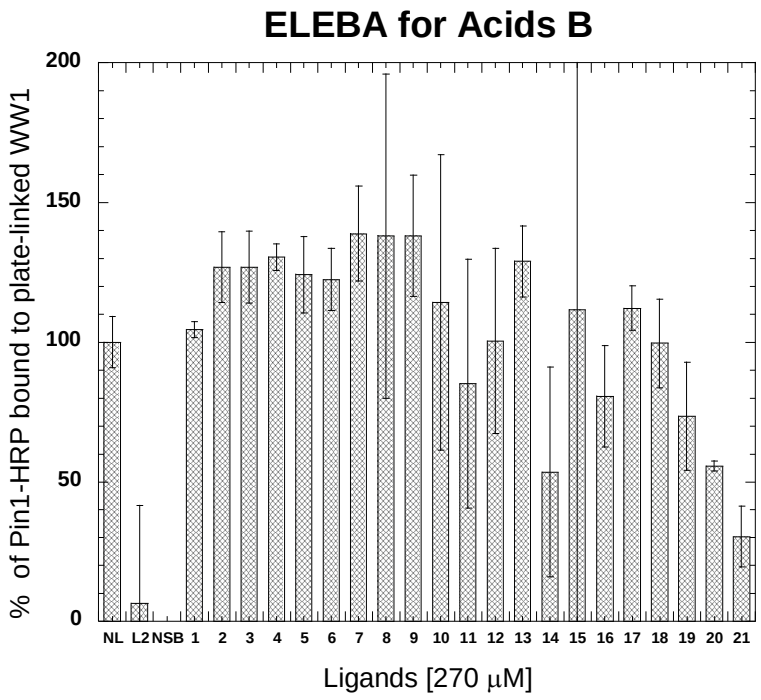
ELEBA for Acids B
% of Pin1-HRP bound to plate-linked WW1
200
150
100
50
0
NL L2 NSB 1 2 3 4 5 6 7 8 9 10 11 12 13 14 15 16 17 18 19 20 21
Ligands [270 μM]

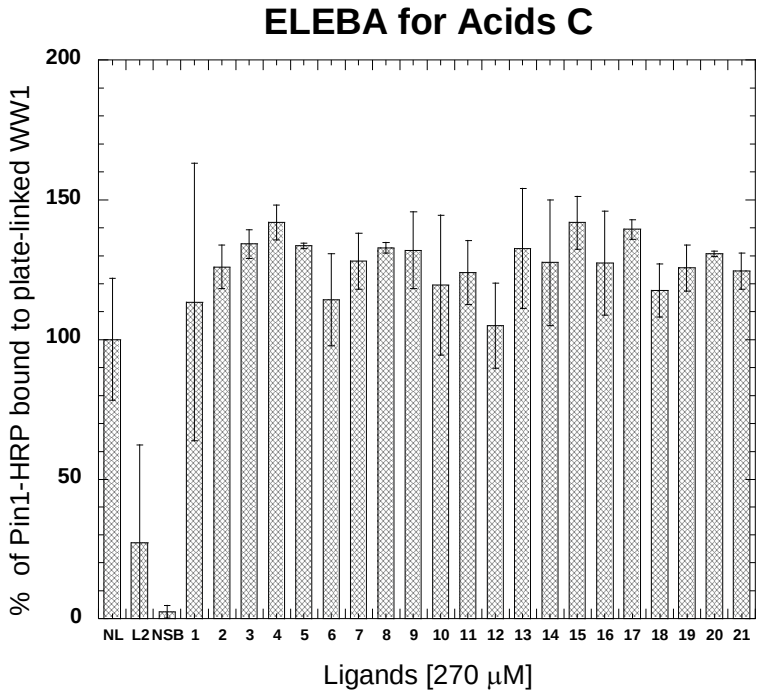
ELEBA for Acids C
% of Pin1-HRP bound to plate-linked WW1
200
150
100
50
0
NL L2 NSB 1 2 3 4 5 6 7 8 9 10 11 12 13 14 15 16 17 18 19 20 21
Ligands [270 μM]

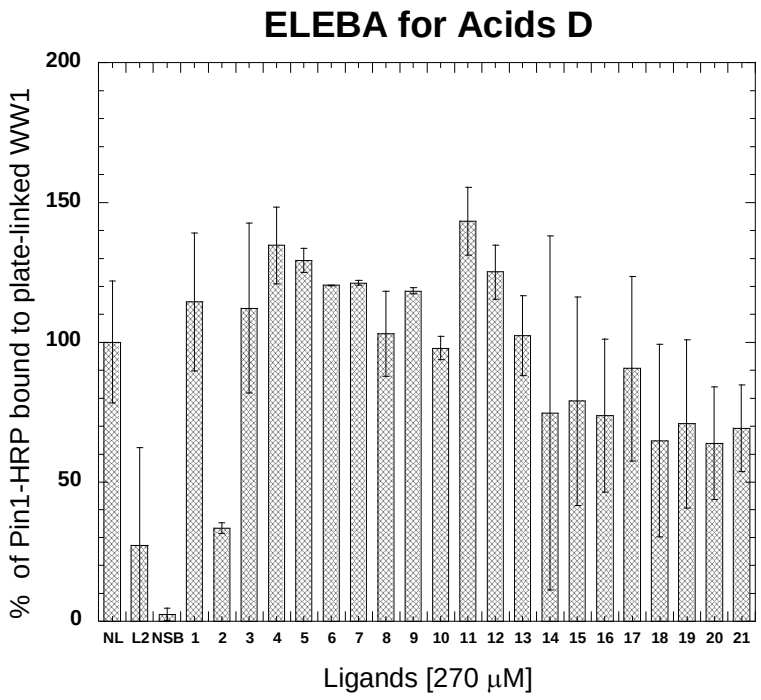
ELEBA for Acids D
% of Pin1-HRP bound to plate-linked WW1
200
150
100
50
0
NL L2 NSB 1 2 3 4 5 6 7 8 9 10 11 12 13 14 15 16 17 18 19 20 21
Ligands [270 μM]

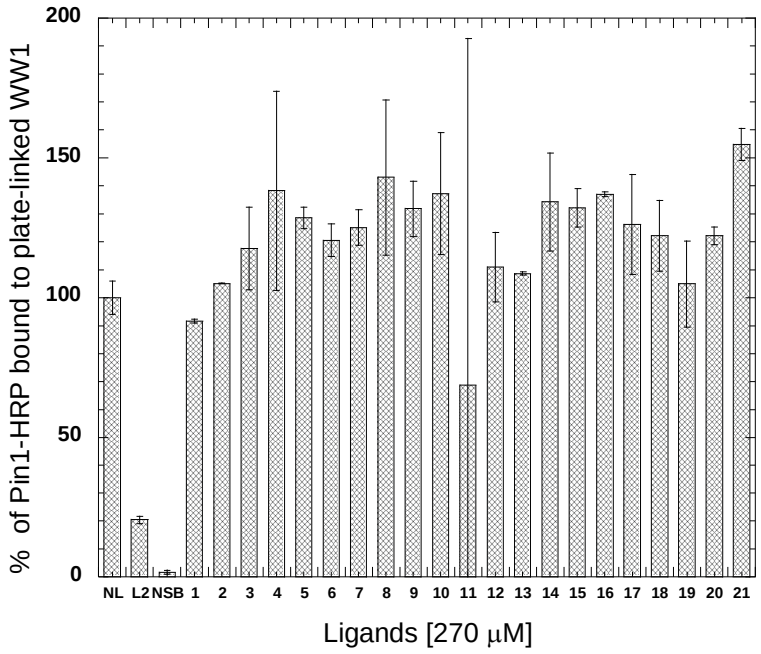
ELEBA for Acids E
% of Pin1-HRP bound to plate-linked WW1
200
150
100
50
0
NL L2 NSB 1 2 3 4 5 6 7 8 9 10 11 12 13 14 15 16 17 18 19 20 21
Ligands [270 μM]

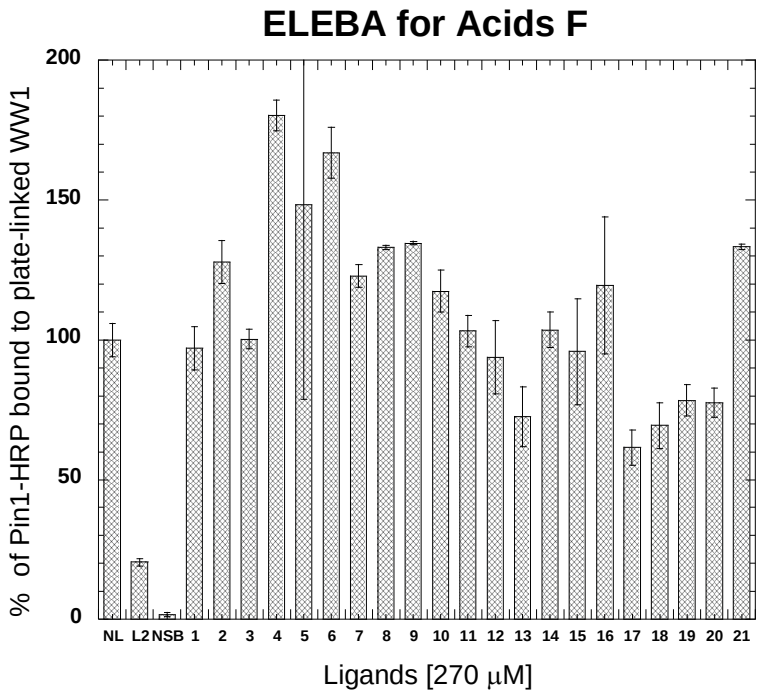
ELEBA for Acids F
% of Pin1-HRP bound to plate-linked WW1
200
150
100
50
0
NL L2 NSB 1 2 3 4 5 6 7 8 9 10 11 12 13 14 15 16 17 18 19 20 21
Ligands [270 μM]

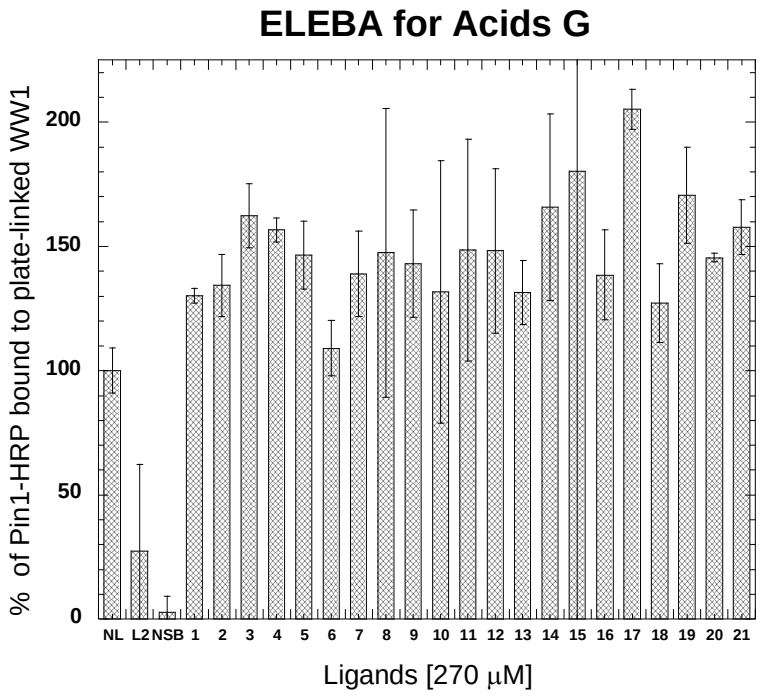
ELEBA for Acids G
% of Pin1-HRP bound to plate-linked WW1
200
150
100
50
0
NL L2 NSB 1 2 3 4 5 6 7 8 9 10 11 12 13 14 15 16 17 18 19 20 21
Ligands [270 μM]

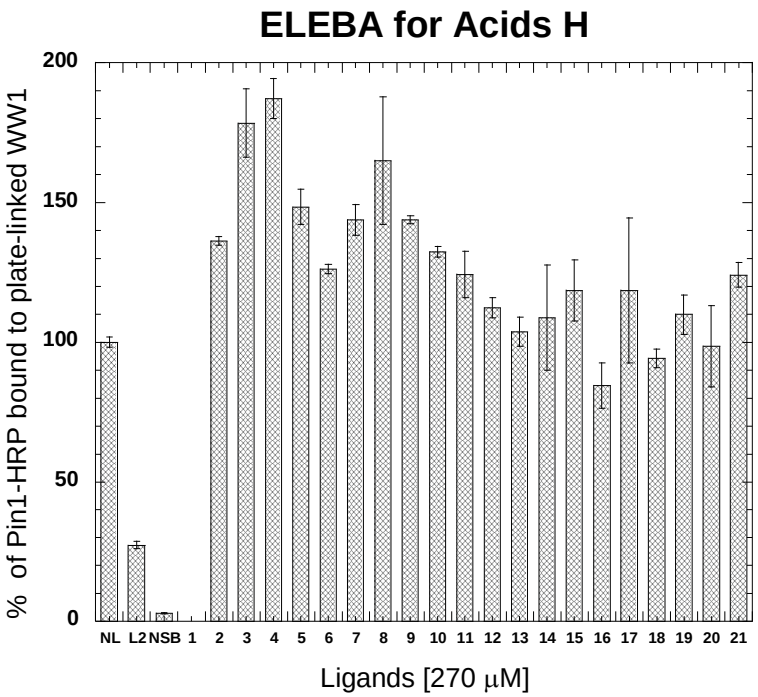
ELEBA for Acids H
% of Pin1-HRP bound to plate-linked WW1
200
150
100
50
0
NL L2 NSB 1 2 3 4 5 6 7 8 9 10 11 12 13 14 15 16 17 18 19 20 21
Ligands [270 μM]

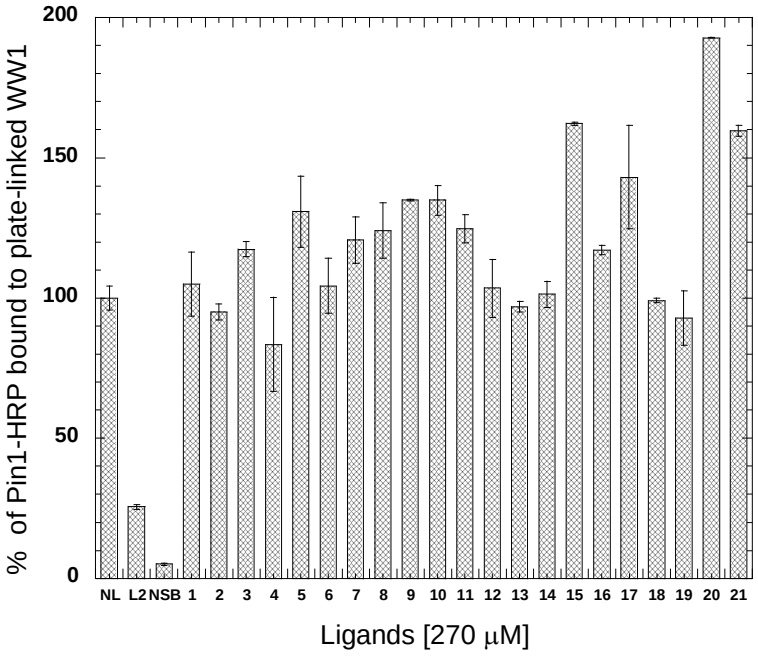
ELEBA for Acids I
% of Pin1-HRP bound to plate-linked WW1
200
150
100
50
0
NL L2 NSB 1 2 3 4 5 6 7 8 9 10 11 12 13 14 15 16 17 18 19 20 21
Ligands [270 μM]

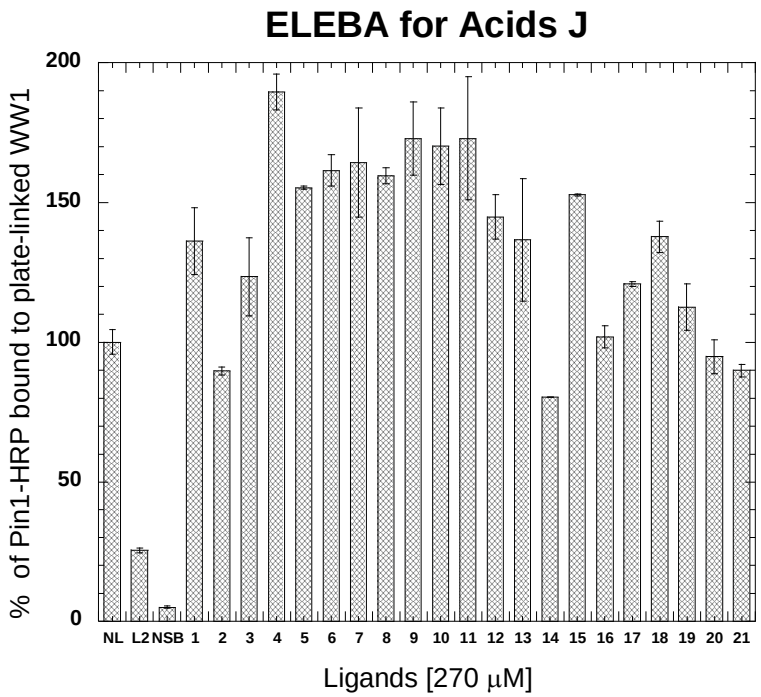
ELEBA for Acids J
% of Pin1-HRP bound to plate-linked WW1
200
150
100
50
0
NL L2 NSB 1 2 3 4 5 6 7 8 9 10 11 12 13 14 15 16 17 18 19 20 21
Ligands [270 μM]

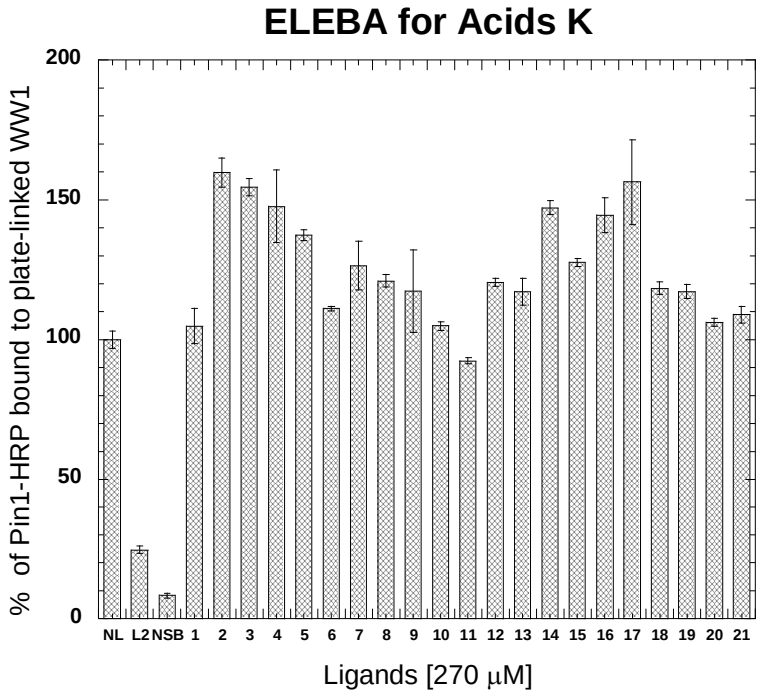
ELEBA for Acids K
% of Pin1-HRP bound to plate-linked WW1
200
150
100
50
0
NL L2 NSB 1 2 3 4 5 6 7 8 9 10 11 12 13 14 15 16 17 18 19 20 21
Ligands [270 μM]

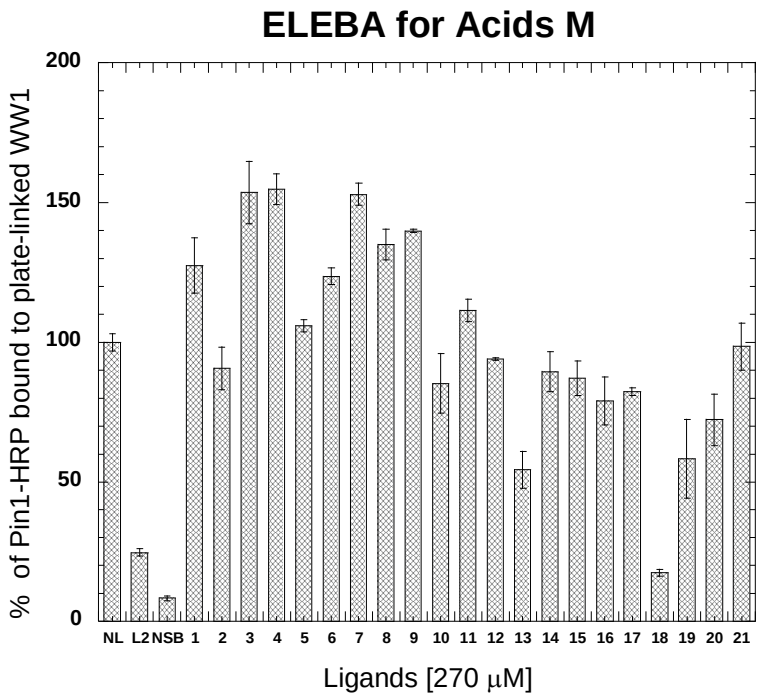
ELEBA for Acids M
% of Pin1-HRP bound to plate-linked WW1
200
150
100
50
0
NL L2 NSB 1 2 3 4 5 6 7 8 9 10 11 12 13 14 15 16 17 18 19 20 21
Ligands [270 μM]

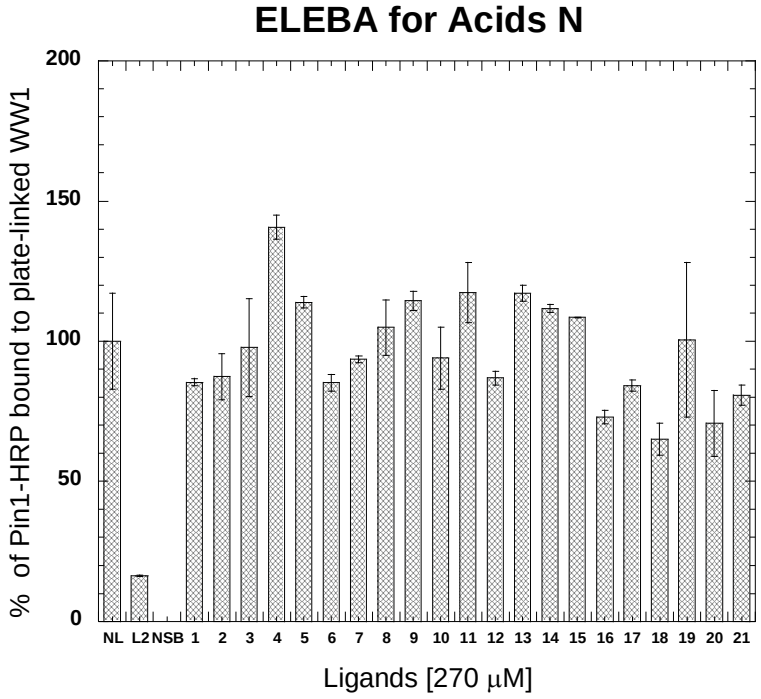
ELEBA for Acids N
% of Pin1-HRP bound to plate-linked WW1
200
150
100
50
0
NL L2 NSB 1 2 3 4 5 6 7 8 9 10 11 12 13 14 15 16 17 18 19 20 21
Ligands [270 μM]

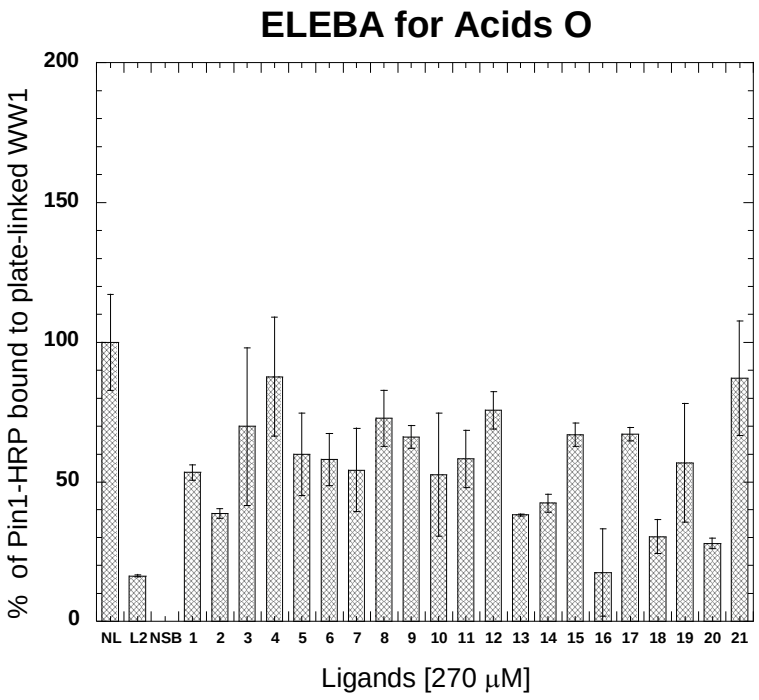
ELEBA for Acids O
% of Pin1-HRP bound to plate-linked WW1
200
150
100
50
0
NL L2 NSB 1 2 3 4 5 6 7 8 9 10 11 12 13 14 15 16 17 18 19 20 21
Ligands [270 μM]

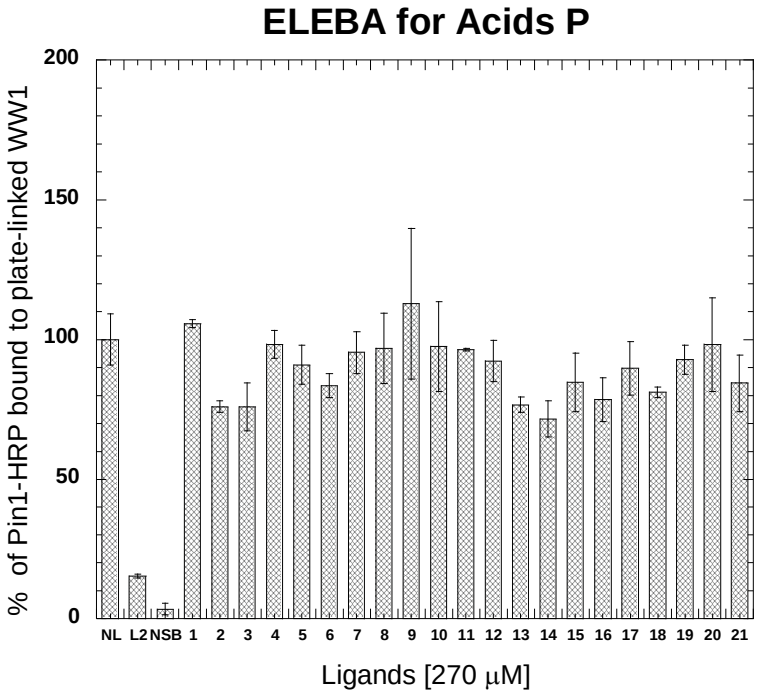
ELEBA for Acids P
% of Pin1-HRP bound to plate-linked WW1
200
150
100
50
0
NL L2 NSB 1 2 3 4 5 6 7 8 9 10 11 12 13 14 15 16 17 18 19 20 21
Ligands [270 μM]

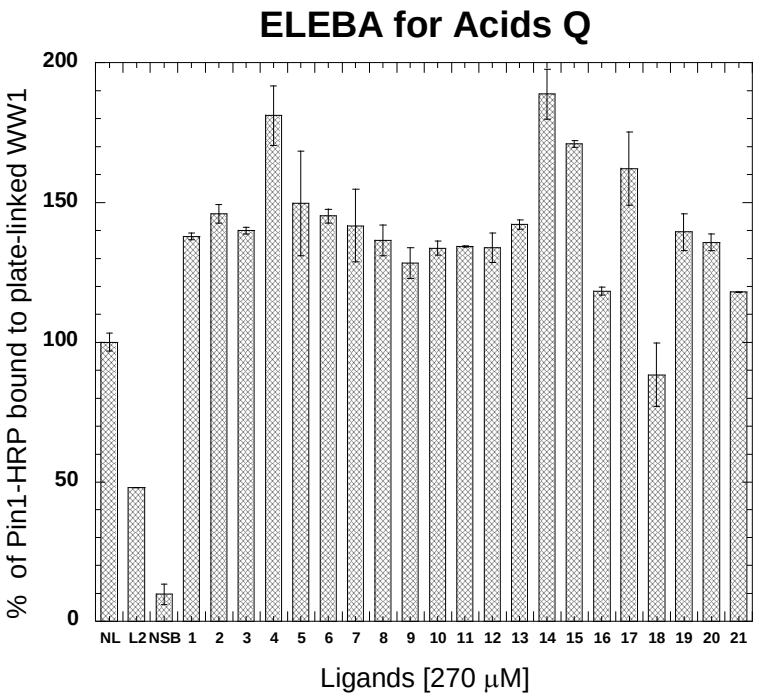
ELEBA for Acids Q
% of Pin1-HRP bound to plate-linked WW1
200
150
100
50
0
NL L2 NSB 1 2 3 4 5 6 7 8 9 10 11 12 13 14 15 16 17 18 19 20 21
Ligands [270 μM]

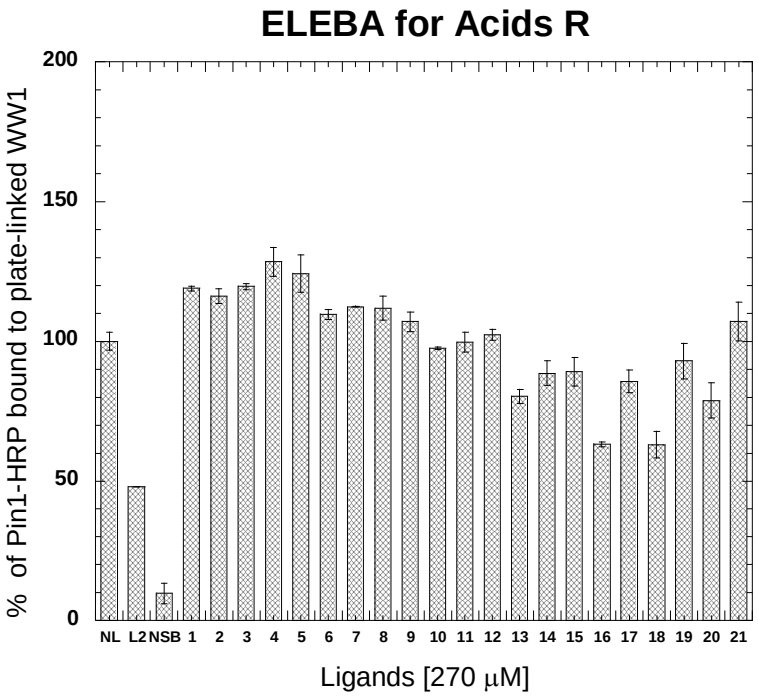
ELEBA for Acids R
% of Pin1-HRP bound to plate-linked WW1
200
150
100
50
0
NL L2 NSB 1 2 3 4 5 6 7 8 9 10 11 12 13 14 15 16 17 18 19 20 21
Ligands [270 μM]

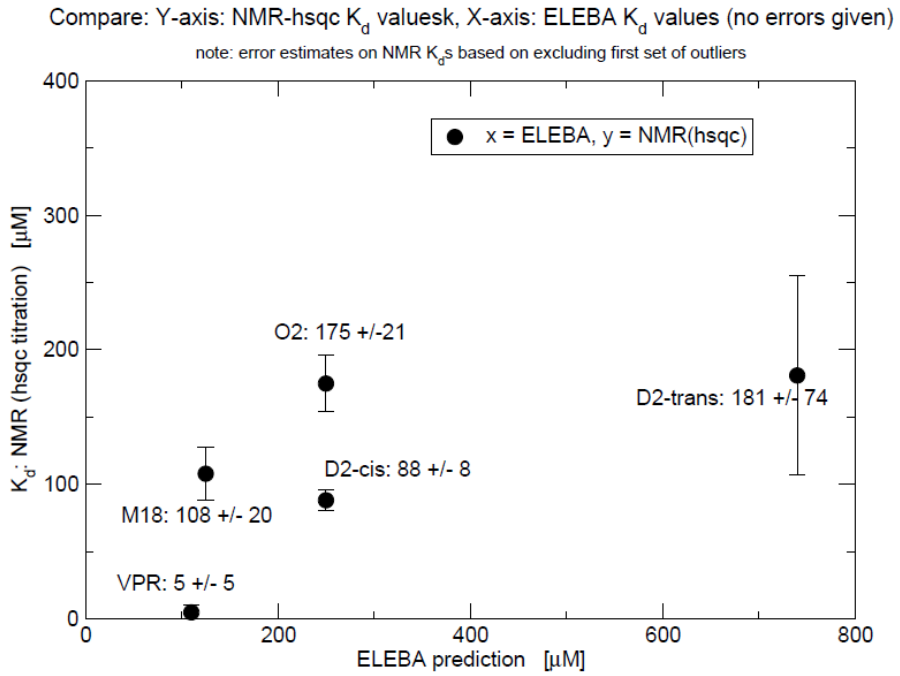

Fig.S27. The chemical shift perturbations demonstrate localized binding to the WW domain of Pin1. Eleven residues from the WW domain (K13, R14, M15, S16, G20, R21, A31, S32, Q33, W34, and E35) consistently reported perturbations upon ligand addition, versus one PPI residue (K132, Table S28). Data were obtained by Jill Bouchard and Jeffrey Peng (University of Notre Dame).

Residue	Pin1 + D2-cis		Pin1 + D2-trans		Pin1 + M18		Pin1 + O2		Pin1-WW + Ac-VPRpTPV-NH_2	
	Kd (µM)	Error (±)	Kd (µM)	Error (±)	Kd (µM)	Error (±)	Kd (µM)	Error (±)	Kd (µM)	Error (±)
K13	92.85	1.59	136.7	5.40	100.1	3.52	209.54	16.26	2.35	1.36
R14	76.38	1.86	144.78	9.55	56.86	2.86	164.52	15.03	3.16	0.48
M15	89.42	3.91	209.39	11.47	109.69	4.92	164.58	3.45	3.42	0.34
S16	85.04	1.64	204.88	4.93	101.06	3.24	209.85	7.46	2.54	1.65
G20	92.27	1.22	177.02	4.98	128.46	3.95	184.1	2.15	2.52	1.00
R21	97.7	1.03	202.67	9.00	9.72	-nan	167.09	2.77	3.27	0.66
A31	108.55	1.87	182.83	6.13	100.36	5.89	125	6.47	7.64	0.52
S32	89.93	1.33	182.91	6.14	102.45	3.82	188.88	3.04	6.07	0.31
Q33	86.33	1.45	228.16	11.79	33.16	3.51	175.16	2.15	3.09	0.64
W34	84.72	1.37	181.77	5.64	131.86	4.19	248.65	4.88	46.45	30.15
W34E	87.44	1.55	168.24	5.46	124.09	4.16	189.02	3.02	46.45	30.15
E35	82.75	1.52	166.55	3.99	11.15	1.11	180.79	3.09	10.45	6.91
K132	399.01	4.58	665.85	38.91	391.67	83.08	45.45	96.93	NA	NA
Global	88.3	8.0	181	74	108	20	175	21	5.0	5.5
ELEBA	250		740		125		250		110	

Fig.S28. Representative residues included those that consistently reported chemical shift perturbations across all titrations with ligands. Global K_d values are the average of all residue-specific K_d values, removing any outliers above 1 RMSD, and recalculating the remaining average. Data were obtained by Jill Bouchard and Jeffrey Peng (University of Notre Dame).

Appendix C

PPIase catalytic assay for the identification of Pin1 inhibitors

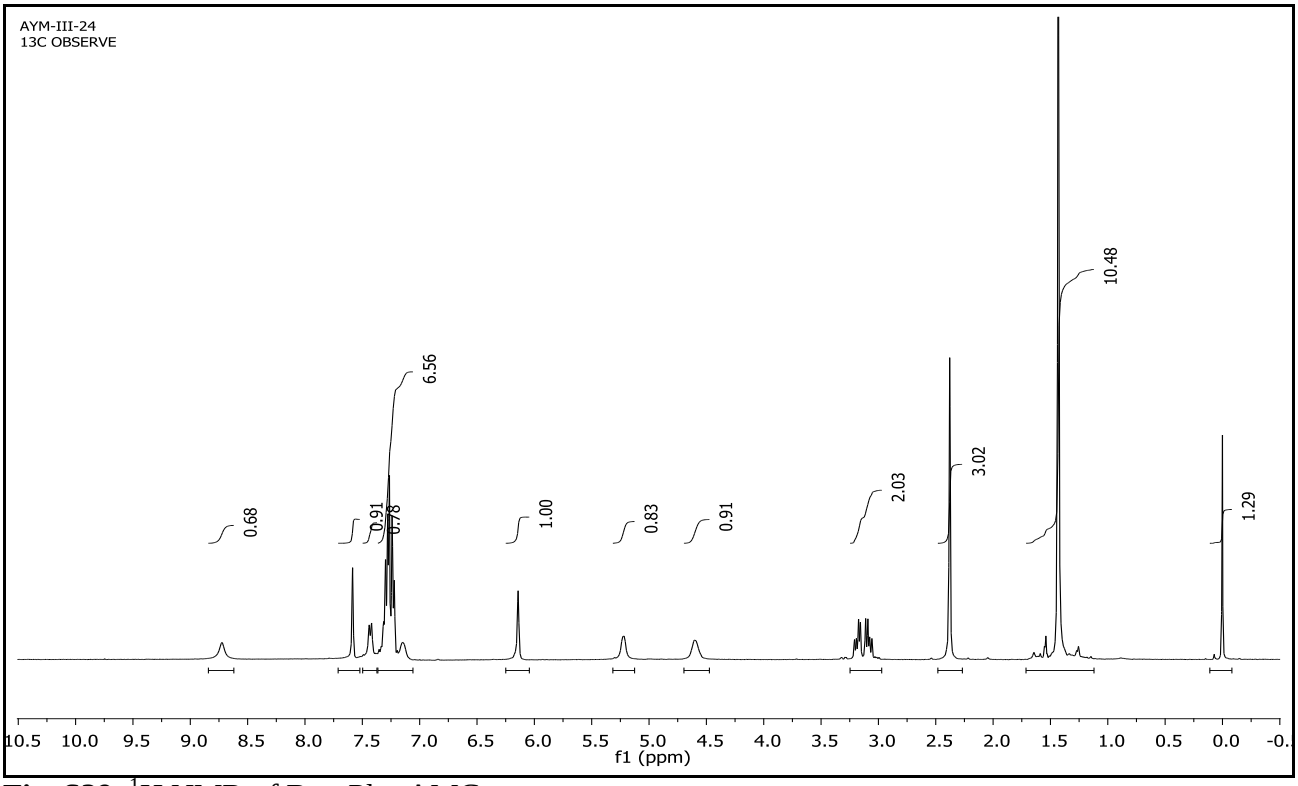

Fig. S29. ^{1}H NMR of Boc-Phe-AMC.

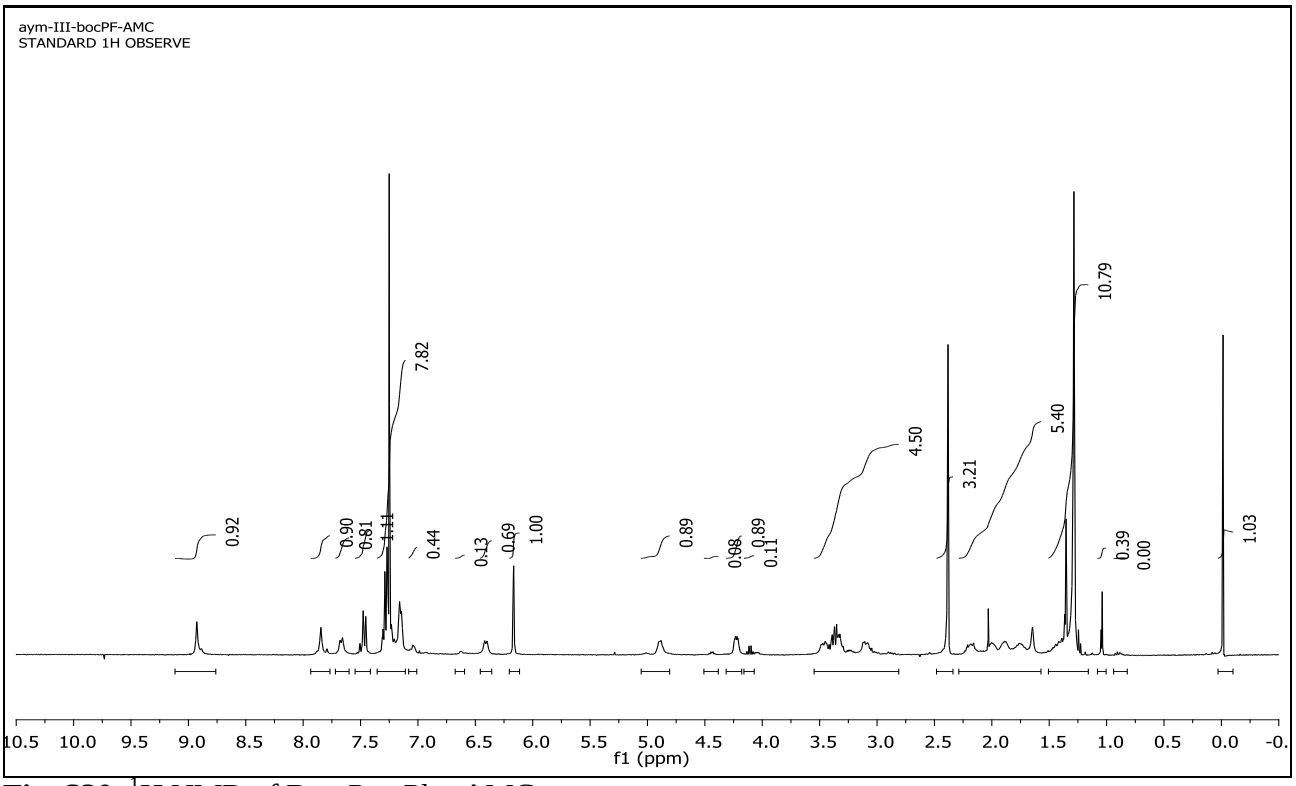

Fig. S30. ^{1}H NMR of Boc-Pro-Phe-AMC.

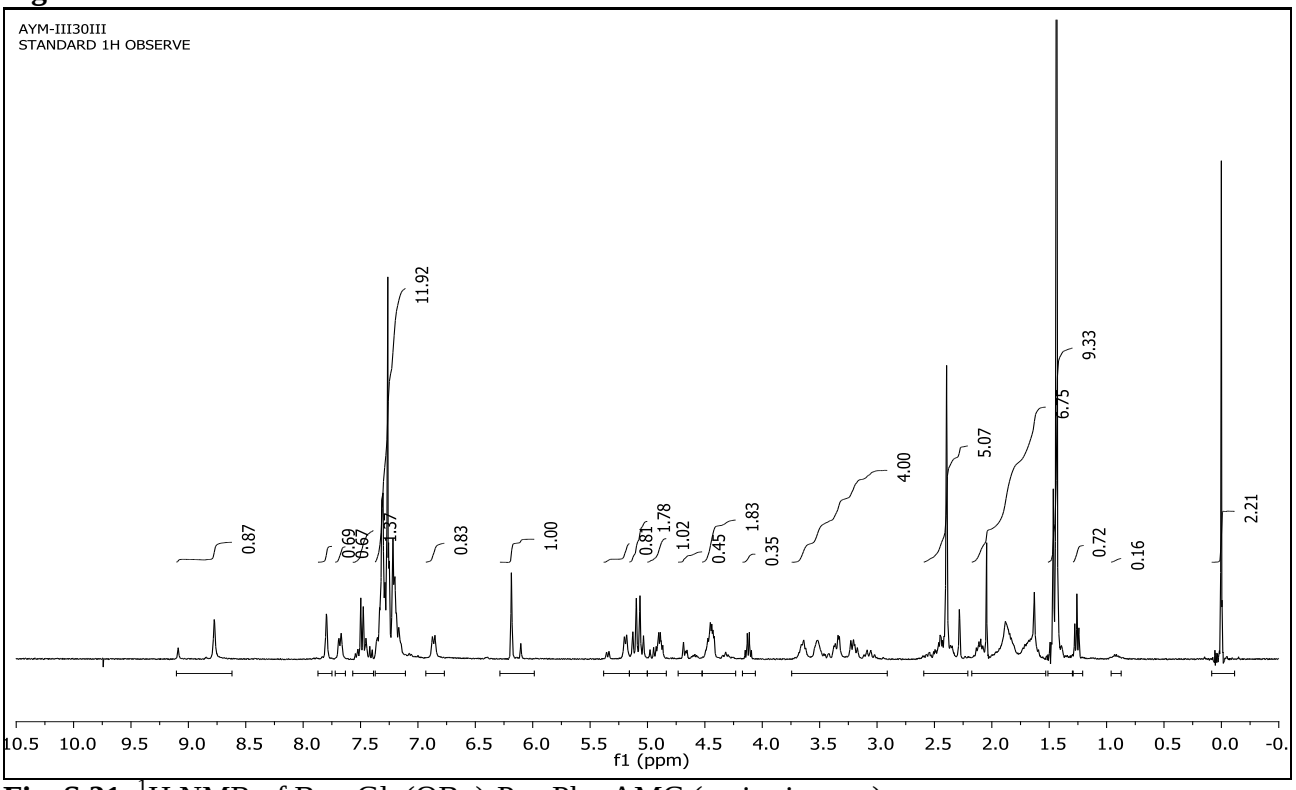

Fig. S.31. ^{1}H NMR of Boc-Glu(OBn)-Pro-Phe-AMC (major isomer).

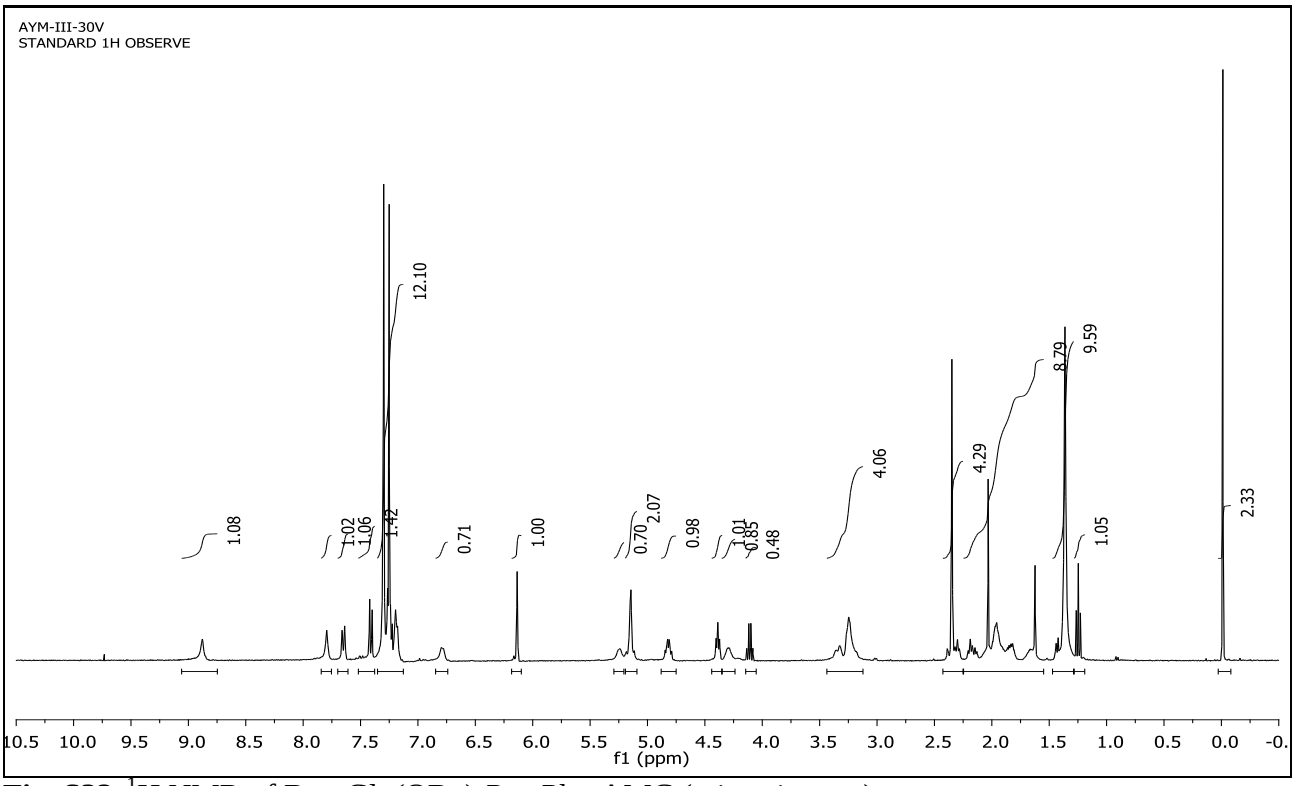

Fig. S32. ^{1}H NMR of Boc-Glu(OBn)-Pro-Phe-AMC (minor isomer).

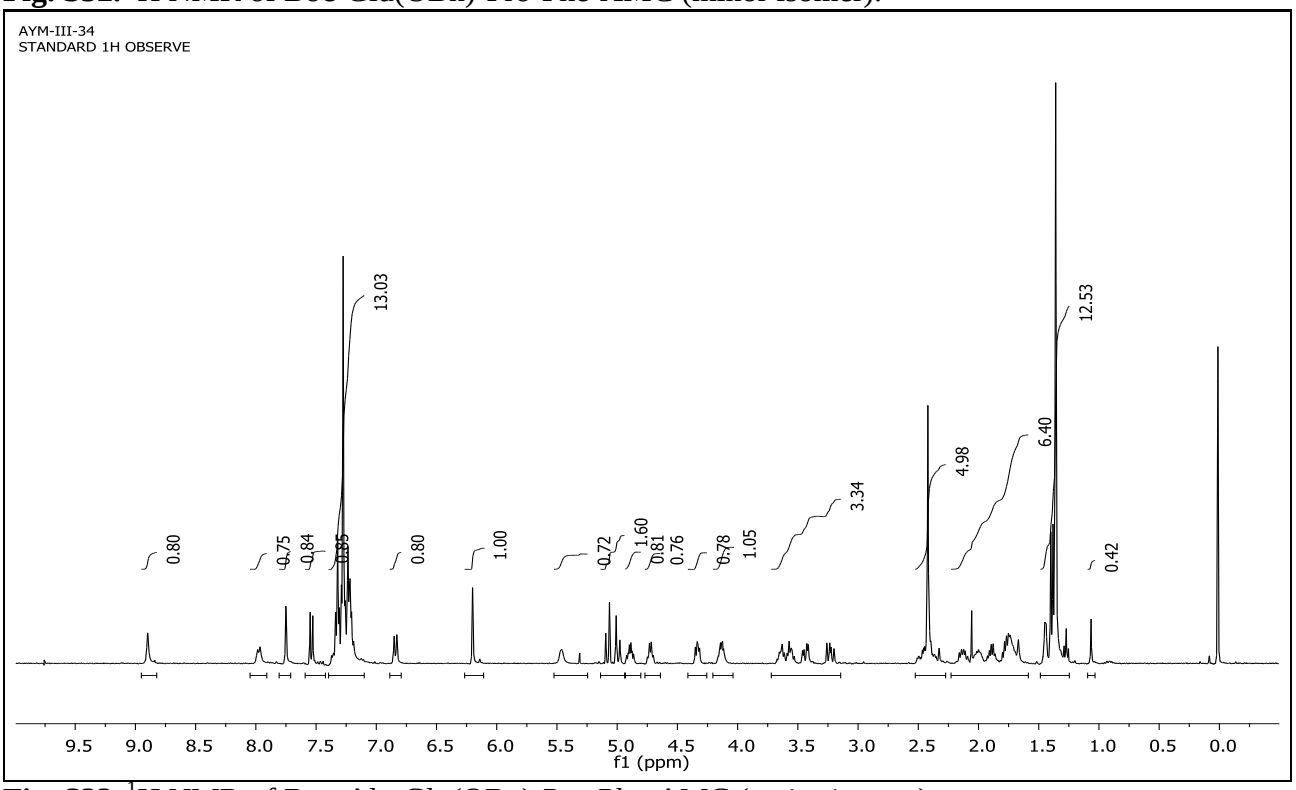

Fig. S33. ^{1}H NMR of Boc-Ala-Glu(OBn)-Pro-Phe-AMC (major isomer).

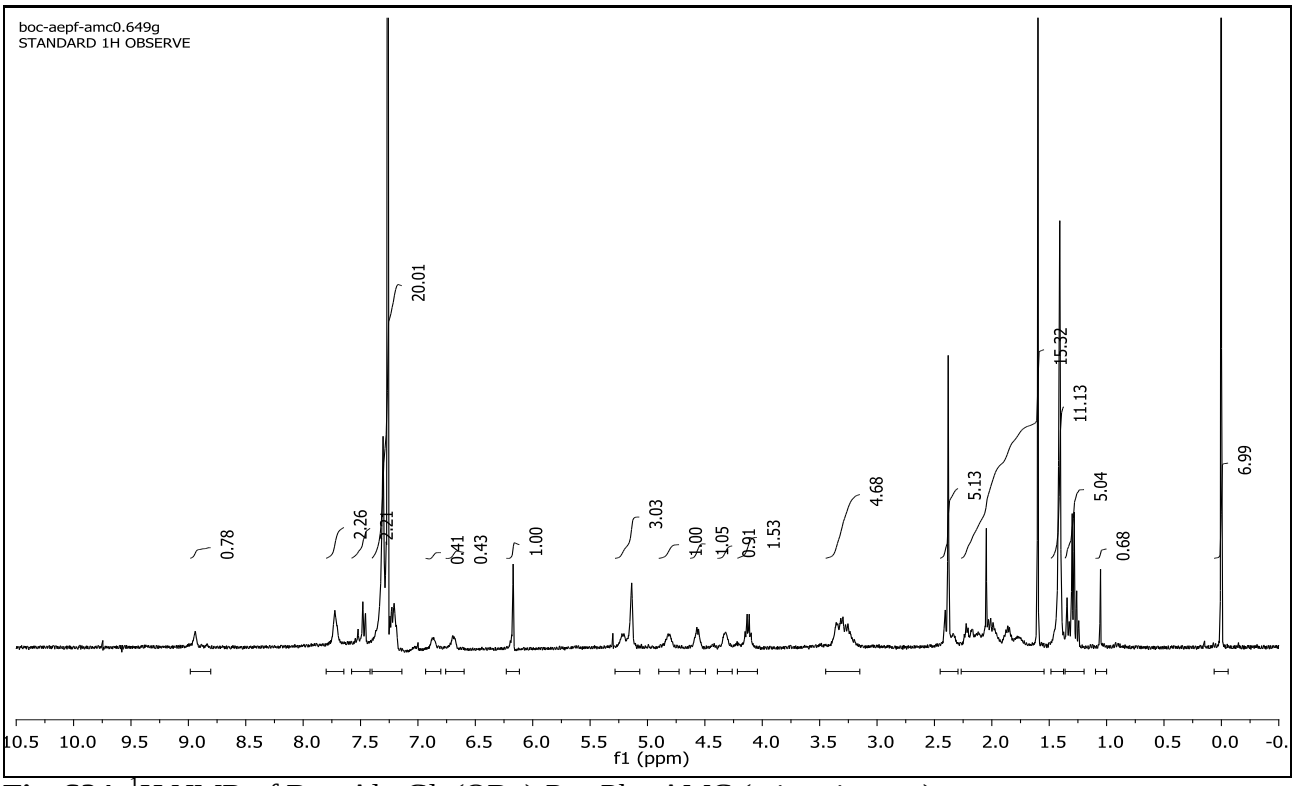

Fig. S34. [1]H NMR of Boc-Ala-Glu(OBn)-Pro-Phe-AMC (minor isomer).

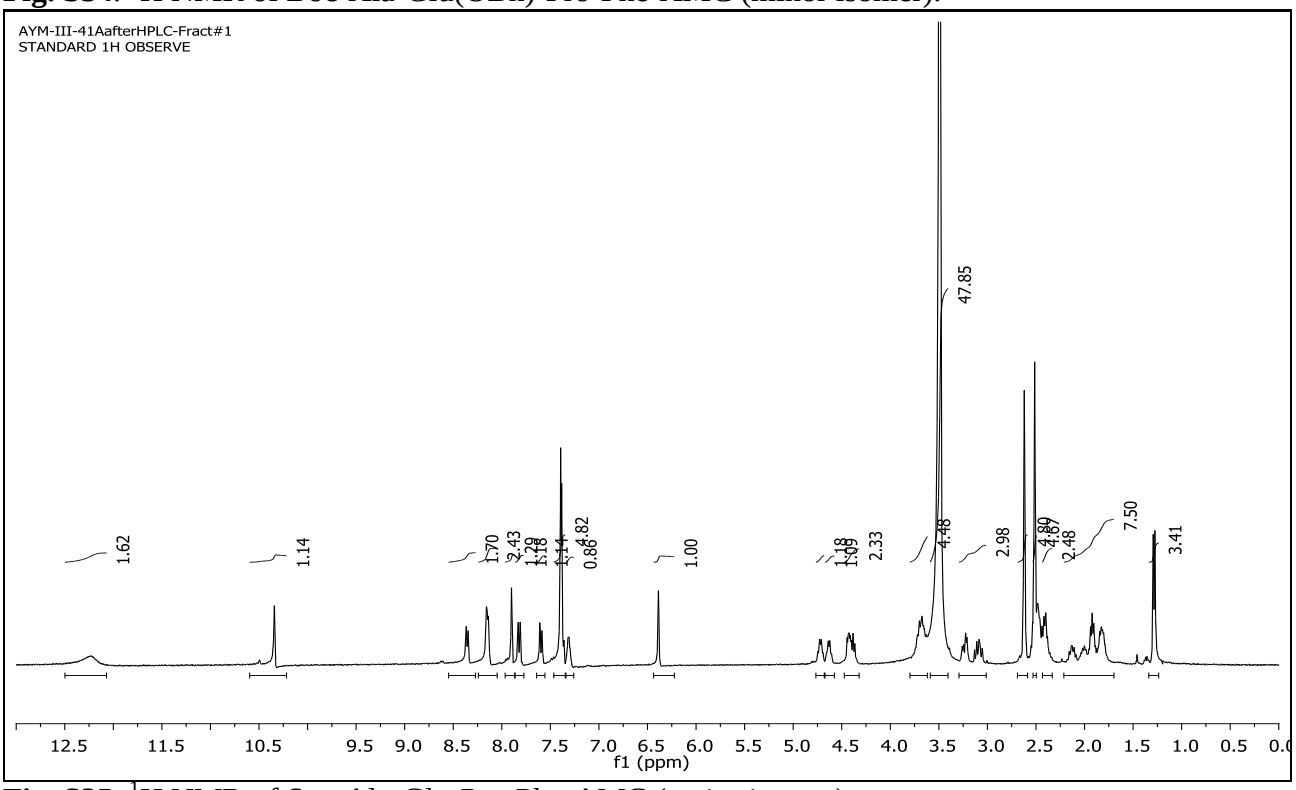

Fig. S35. [1]H NMR of Suc-Ala-Glu-Pro-Phe-AMC (major isomer).

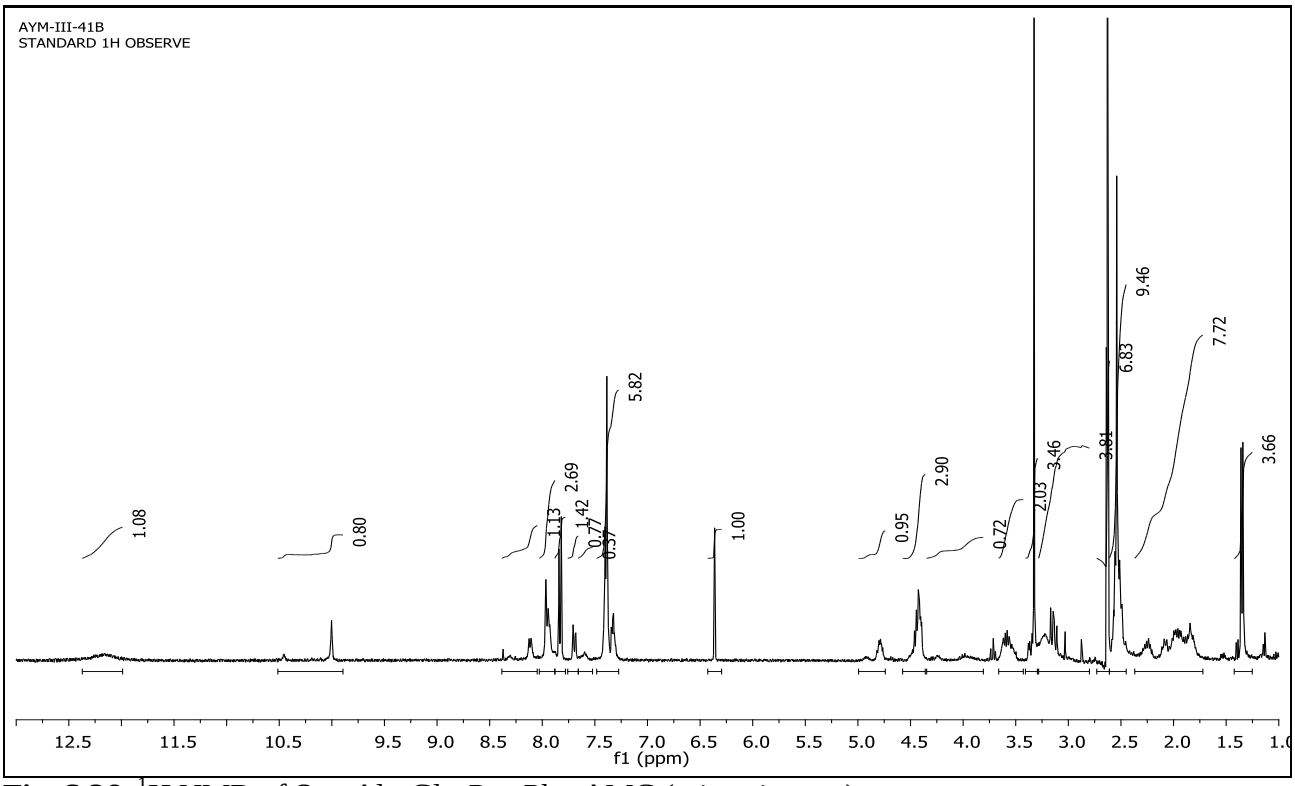

Fig. S.36. ^{1}H NMR of Suc-Ala-Glu-Pro-Phe-AMC (minor isomer).

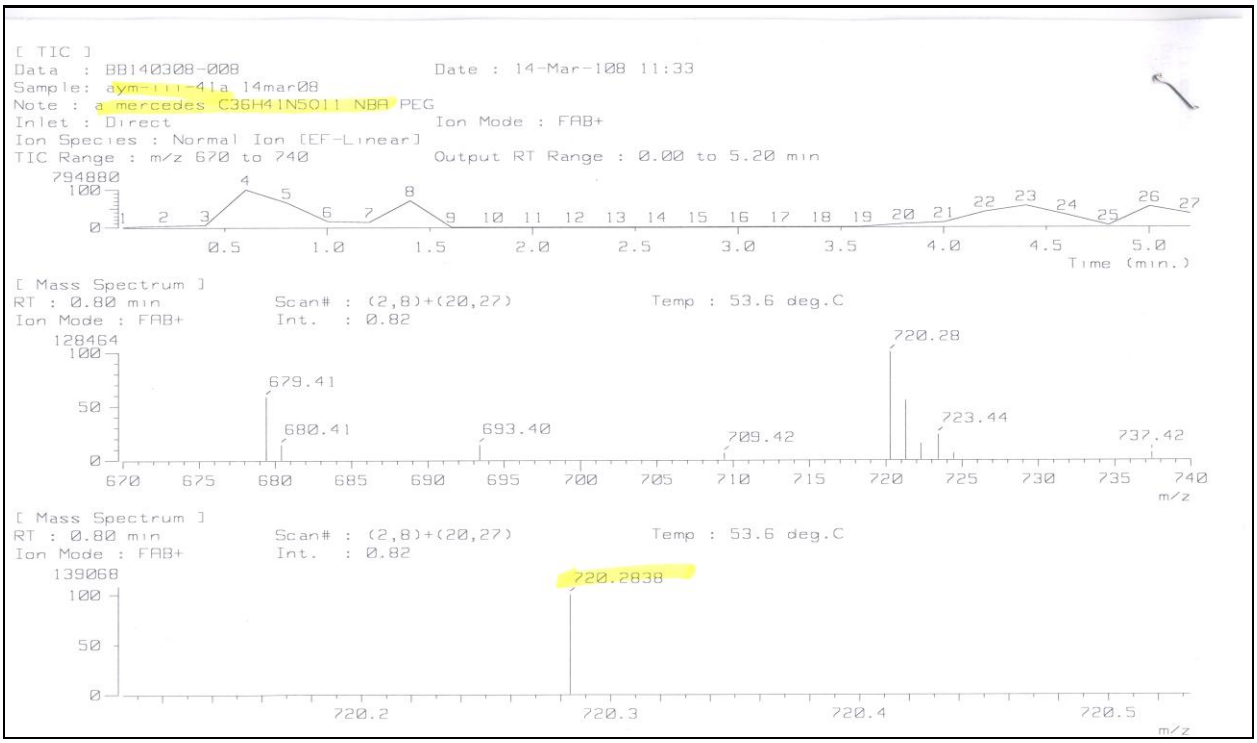

Fig. S37. FAB+ molecular ion detection for major isomer, calcd. for $C_{36}H_{41}N_{5O}11$ [M + H]+ *m/z* = 720.3, found *m/z* = 720.3.

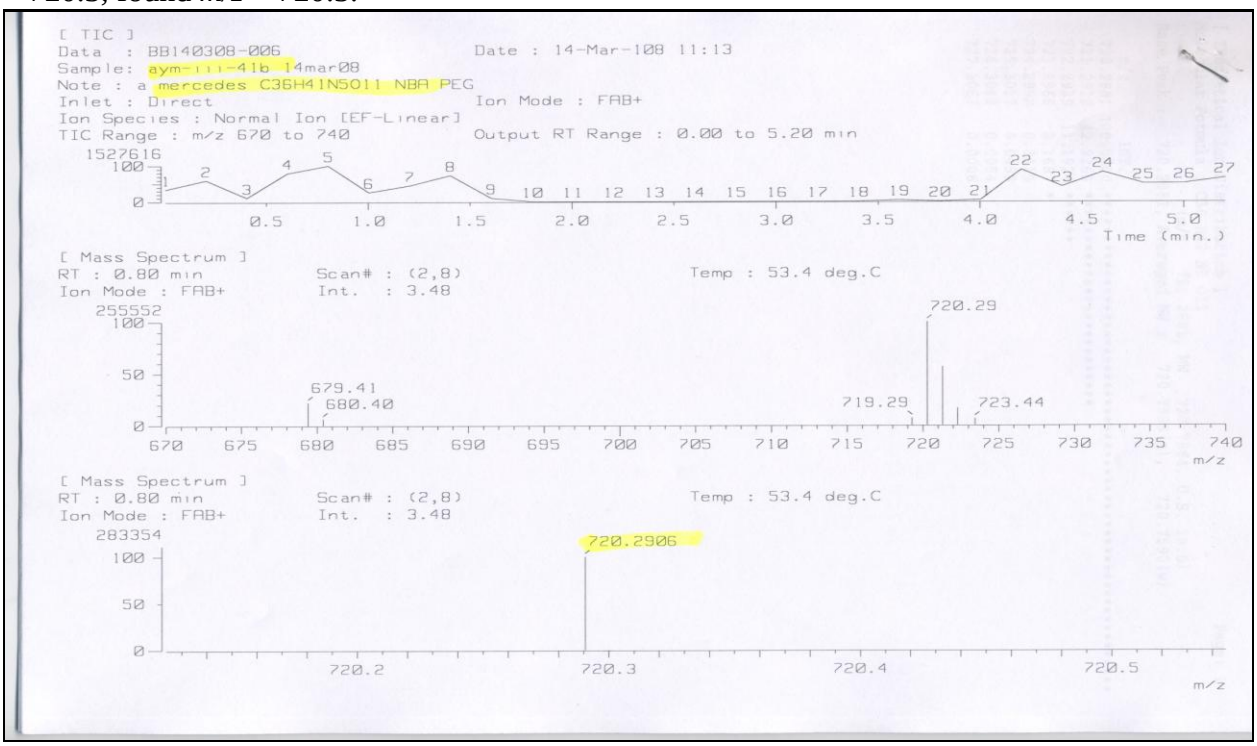

Fig. S38. FAB+ molecular ion detection for minor isomer, calcd. for $C_{36}H_{41}N_5O_{11}$ [M + H]+ *m/z* = 720.3, found *m/z* = 720.3.

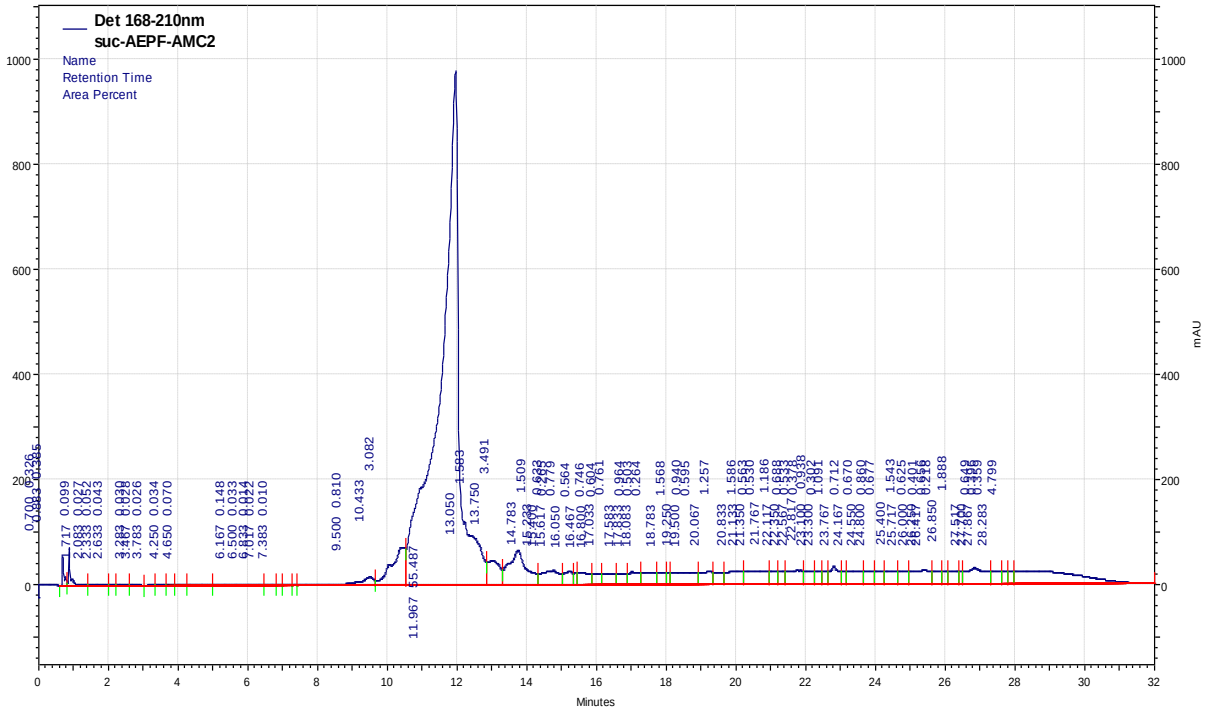

Fig. S39. Analytical HPLC, 1 single broad peak was observed for major isomer with retention time of 12.0 min.

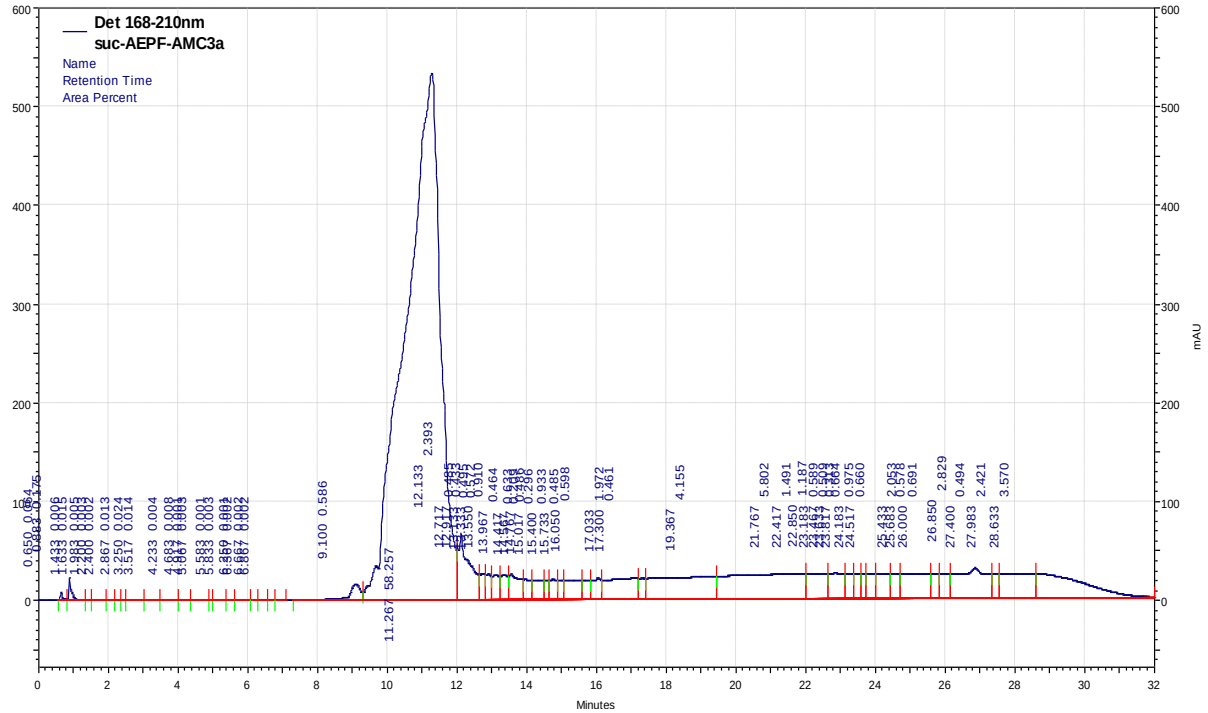

Fig. S40. Analytical HPLC, 1 single broad peak was observed for minor isomer with retention time of 11.2 min. Pin1 expression and quantification.

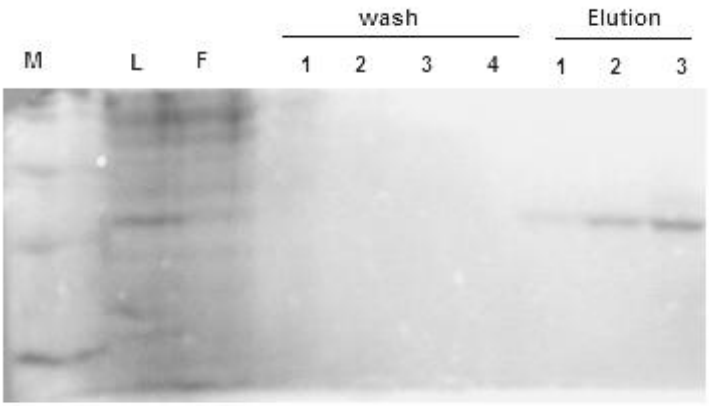

Fig. S41. SDS-PAGE image stained with Comasie Brillant Blue-G250: M =Molecular Weight Marker, L = lysate load, F = flow-through, lines 1-4 = washed with wash buffer (4 mL × 4, 0.5 mM Tris at pH 8.0). 1-3 = elution of His6–Pin1 with elution buffer (3 mL × 3, 250 mM imidazole, 500 mM NaCl, 20 mM Tris at pH 7.9).

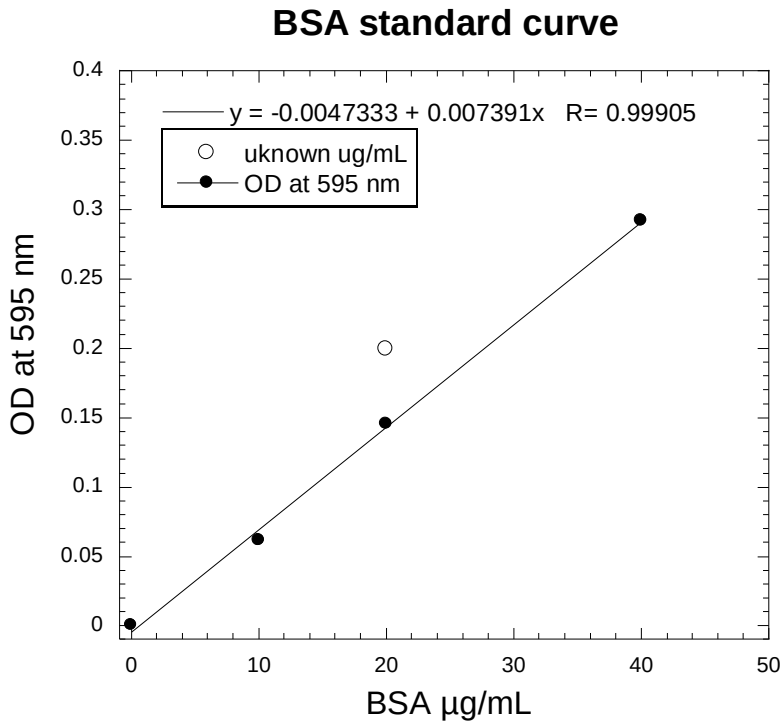

Fig. S42. Bradford Assay for the concentration determination of Pin1: standard curve was created with vary concentration of Bovine Serum Albumi (BSA, 3 mg/mL stock solution) in 250 µL of protein assay dye reagent (Bio-Rad, 500-0006) and volume was completed with water to a final volume 350. µL. The Absorbance was recorded at 595 nm. 1.2 mg/ mL of Pin1 was obtained in 4 mL of 20 mM HEPES with 100 mM NaCl at pH 7.5.

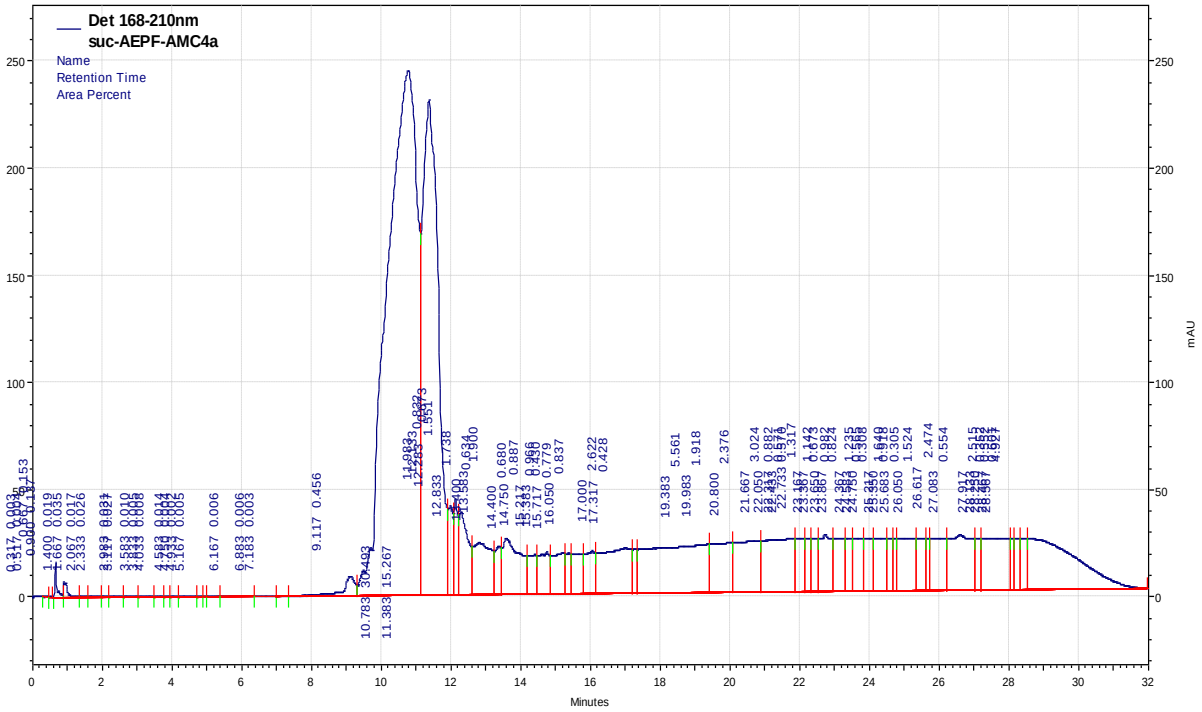

Fig. S43. Analytical HPLC co-injection of both isomers.

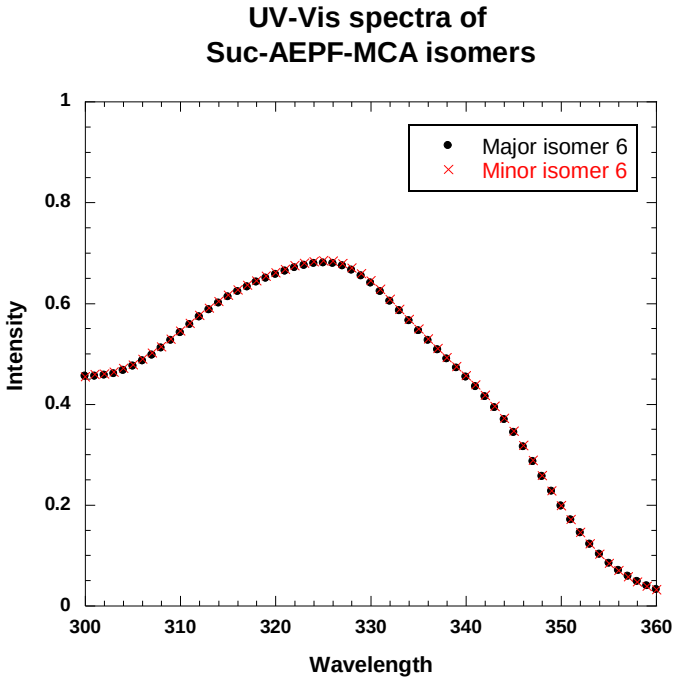

Fig. S44. UV-Vis spectra were measured to ensure the integrity of the AMC.

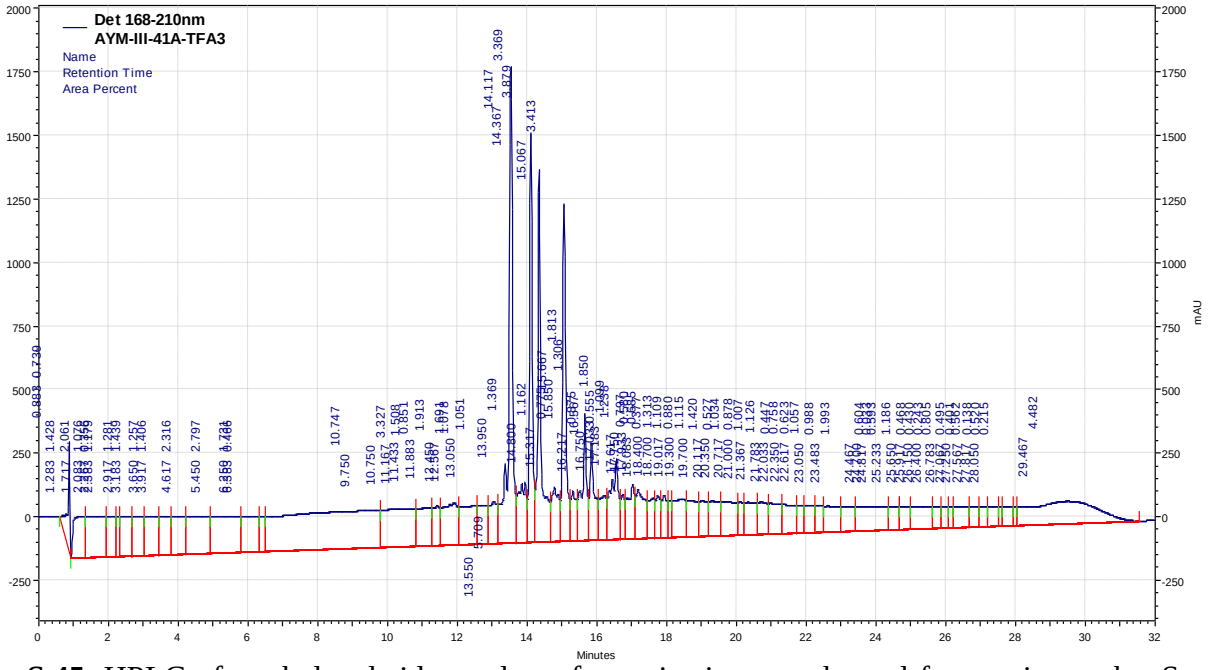

Fig S.45. HPLC of methylated-side products for major isomer, showed four major peaks. Suc-Ala-Glu-Pro-Phe-MCA at 13.5 min, ESI+ showed $[MH]^+$ = 720.3 *m/z*. Suc-Ala-Glu(OMe)-Pro-Phe-MCA and Suc(OMe)-Ala-Glu-Pro-Phe-MCA at 14.1 and 14.3 mins, ESI+ showed constitutional isomers with $[MH]^+$ = 734.3 *m/z*, respectively. Suc(OMe)-Ala-Glu(OMe)-Pro-Phe-AMC at 15.1 min, ESI^+ showed $[MH]^+$ = 770.3 *m/z*.

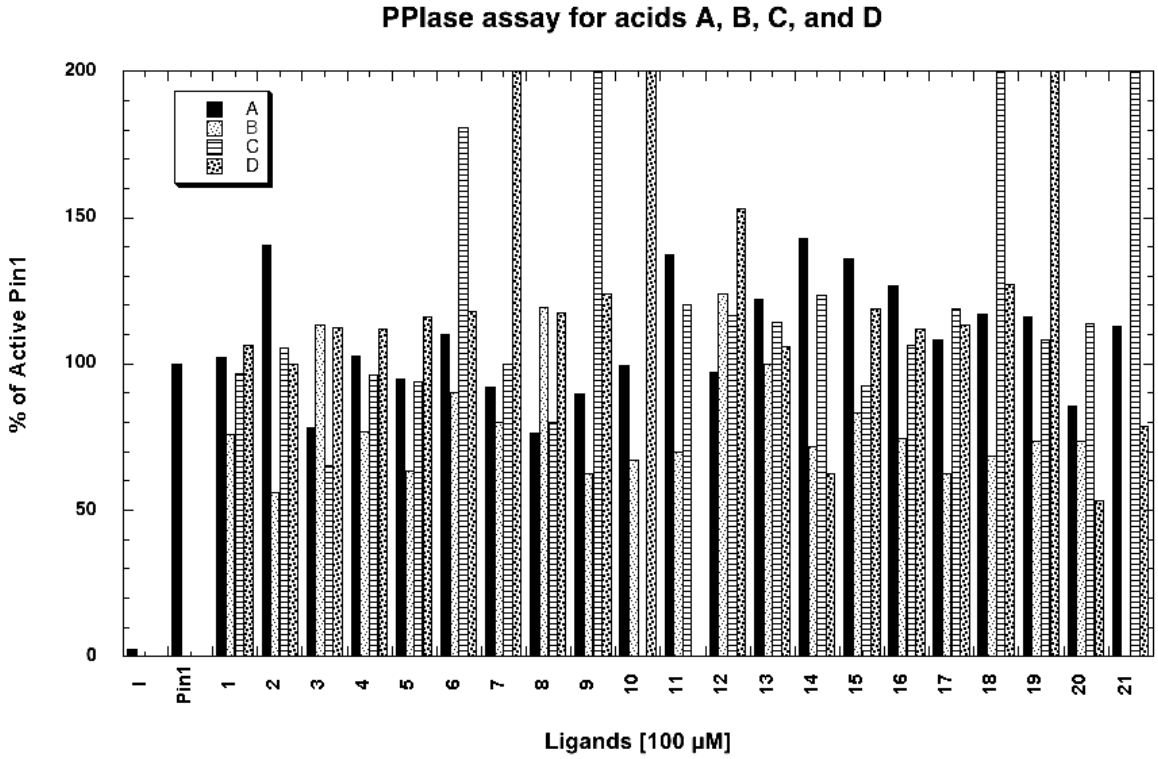

Fig. S46. Pin1 PPIase assay with 100 µM of pSer–Pro ligands, DMSO was used as negative control, and Fmoc-pS–Ψ[CH2N]–P–2-(3-indolyl)-ethylamine (I) was used as positive control.

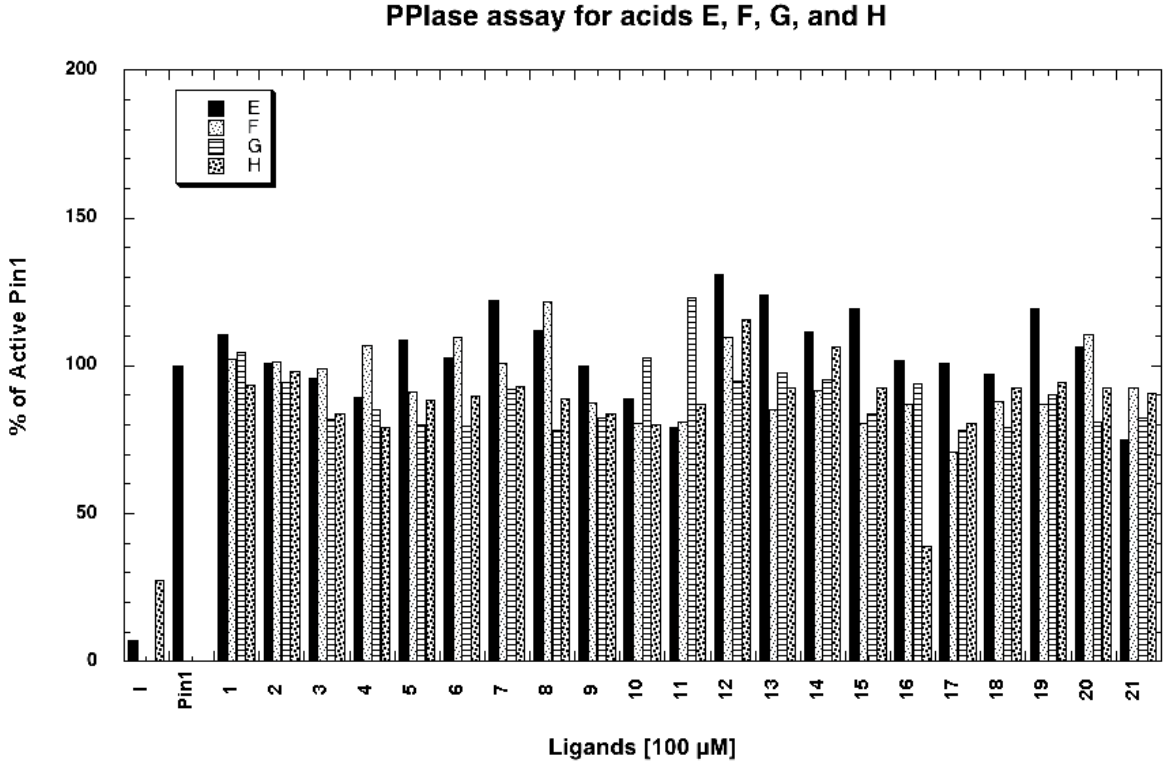

Fig. S47. Pin1 PPIase assay with 100 µM of pSer–Pro ligands, DMSO was used as negative control, and Fmoc-pS–Ψ[CH2N]–P–2-(3-indolyl)-ethylamine (I) was used as positive control.

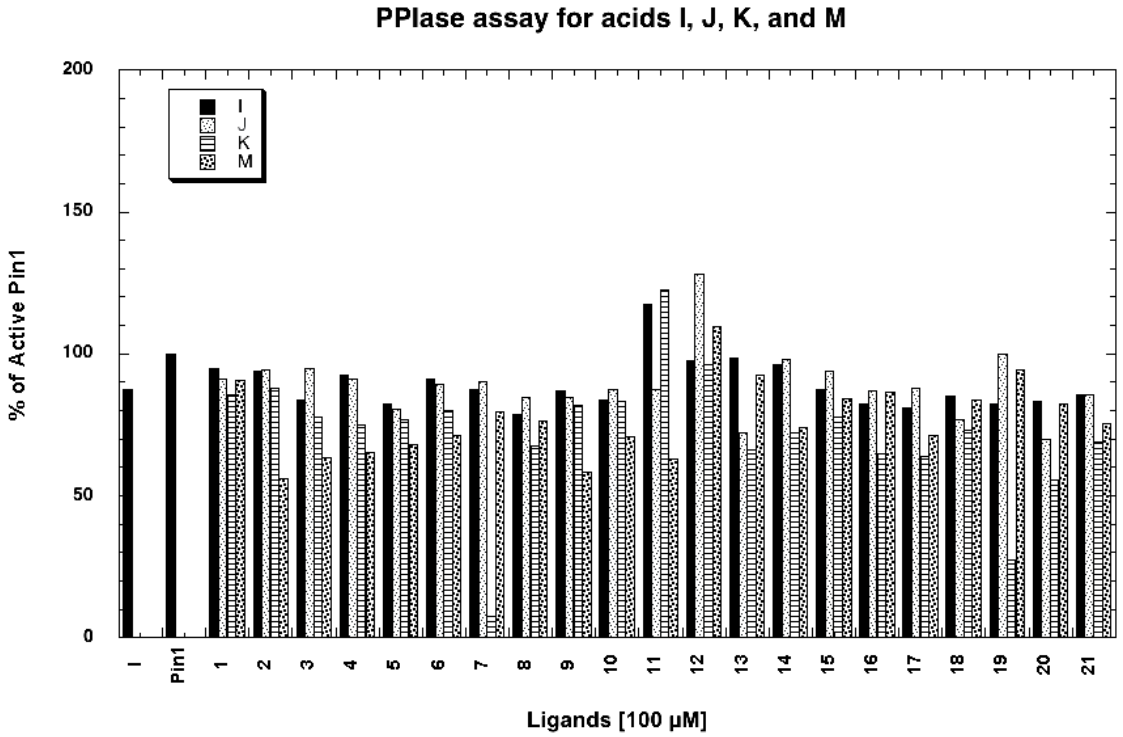

Fig. S48. Pin1 PPIase assay with 100 µM of pSer–Pro ligands, DMSO was used as negative control, and Fmoc-pS–Ψ[CH_2N]–P–2-(3-indolyl)-ethylamine (I) was used as positive control.

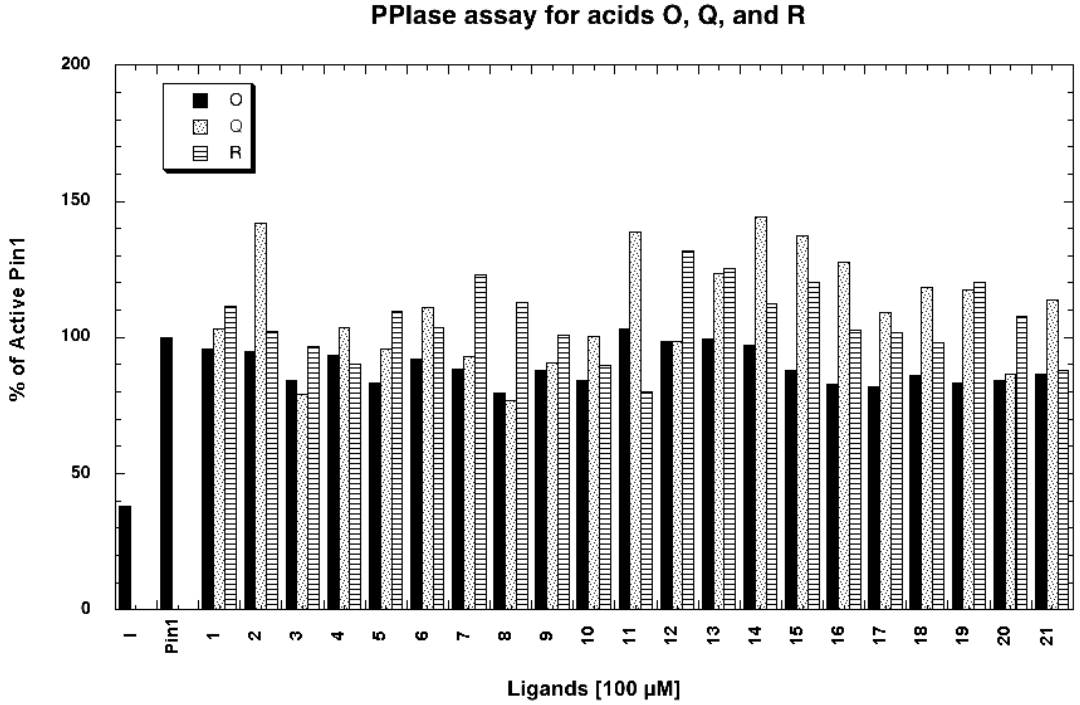

Fig. S49. Pin1 PPIase assay with 100 µM of pSer–Pro ligands, DMSO was used as negative control, and Fmoc-pS–Ψ[CH_2N]–P–2-(3-indolyl)-ethylamine (I) was used as positive control.

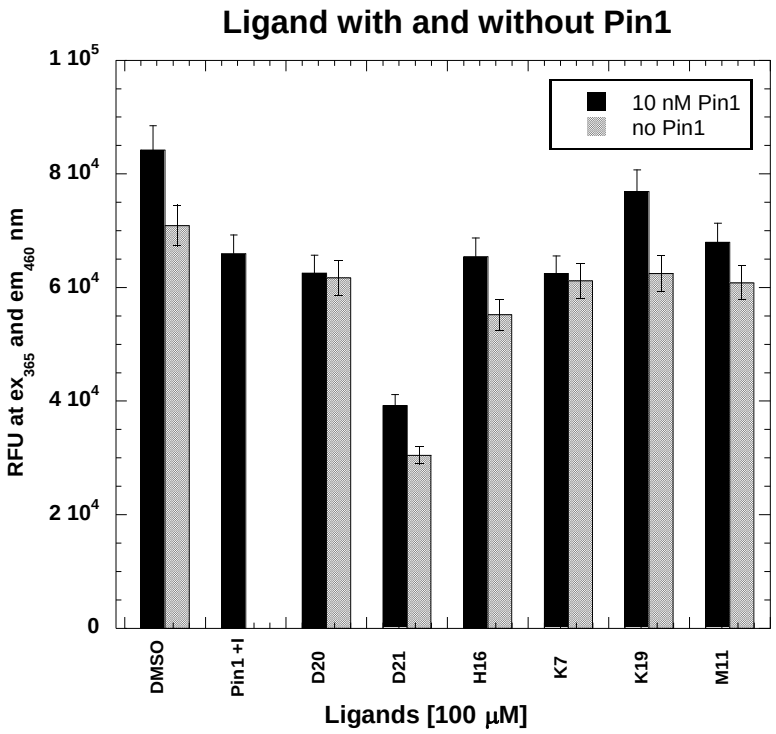

Fig. S50. Raw data of 100 μM pSer–Pro ligands with aromatic moieties for the measurement of possible signal interferance at Em_{365}/Ex_{460} nm. DMSO was used as negative control, and new Fmoc-pS–Ψ[CH_2N]–P–2-(3-indolyl)-ethylamine (NI) was used as positive control.

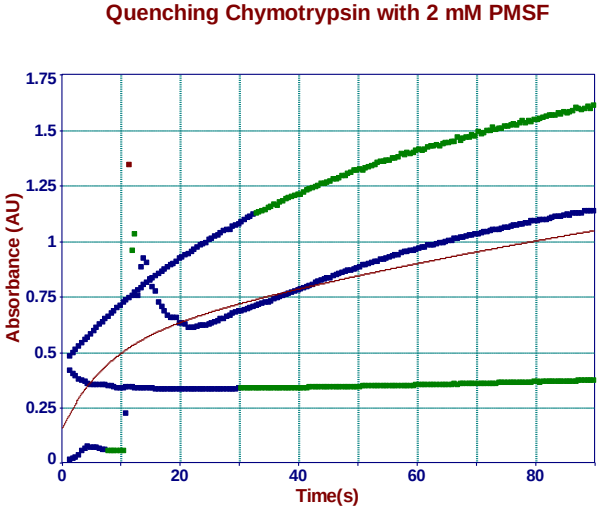

Fig. S51. Quenching chymotrypsin with 2 mM phenylmethanesulfonylfluoride (PMSF) in 100% 2-propanol. No PMSF added (Top curve). PMSF partially inactivated chymotrypsin by pipetting up and down of the quenching solution (middle curve). PMSF inactivated chymotrypsin instantly with the proper mixing of the sample by inversion of the cuvette three times (bottom curve).

Appendix D

Nuclear magnetic resonance studies of Pin1 with ligands

Ligands characterization

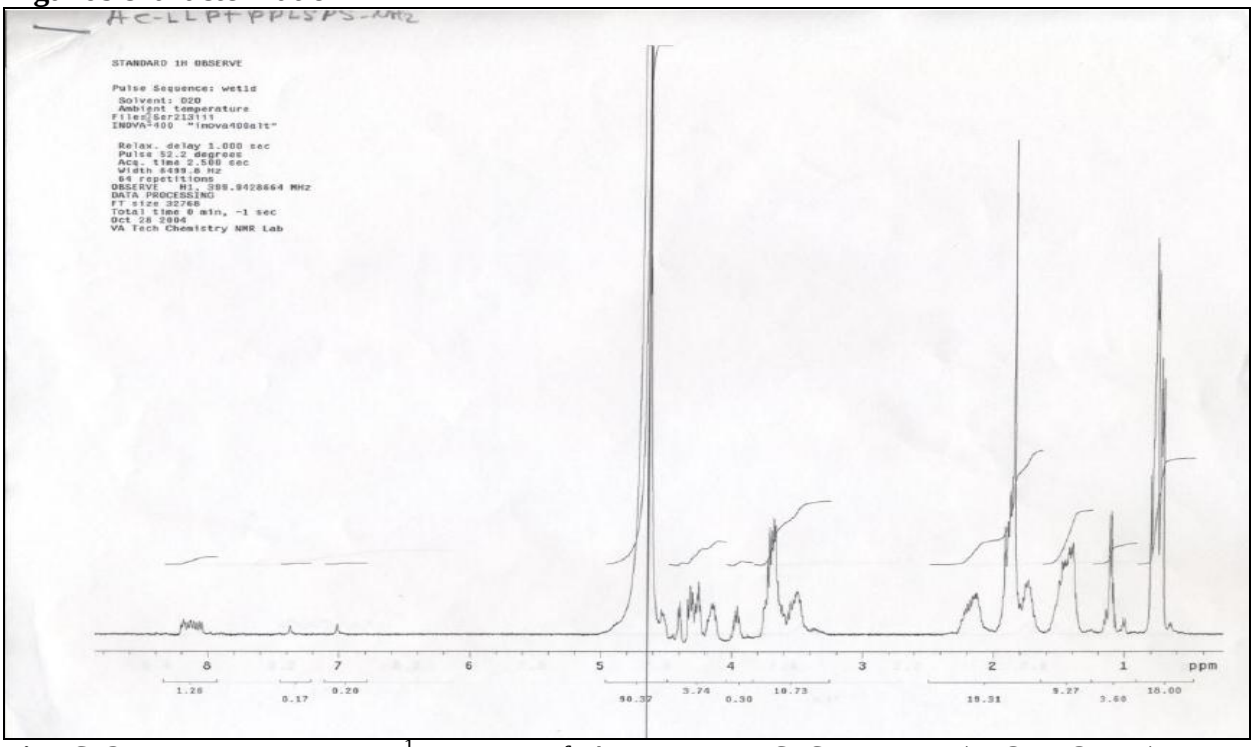

Fig. S52. Water-suppression ^{1}H NMR of Ac–LLPTPPLSPS–NH_2 in (D_2O:H_2O 1:1), some characteristic amide-protons exchange at 7-8.5 ppm, the α-protons of the peptide core are observed at 4-5 ppm, and the leucine methyls were observed at 0.9-0.7 ppm.

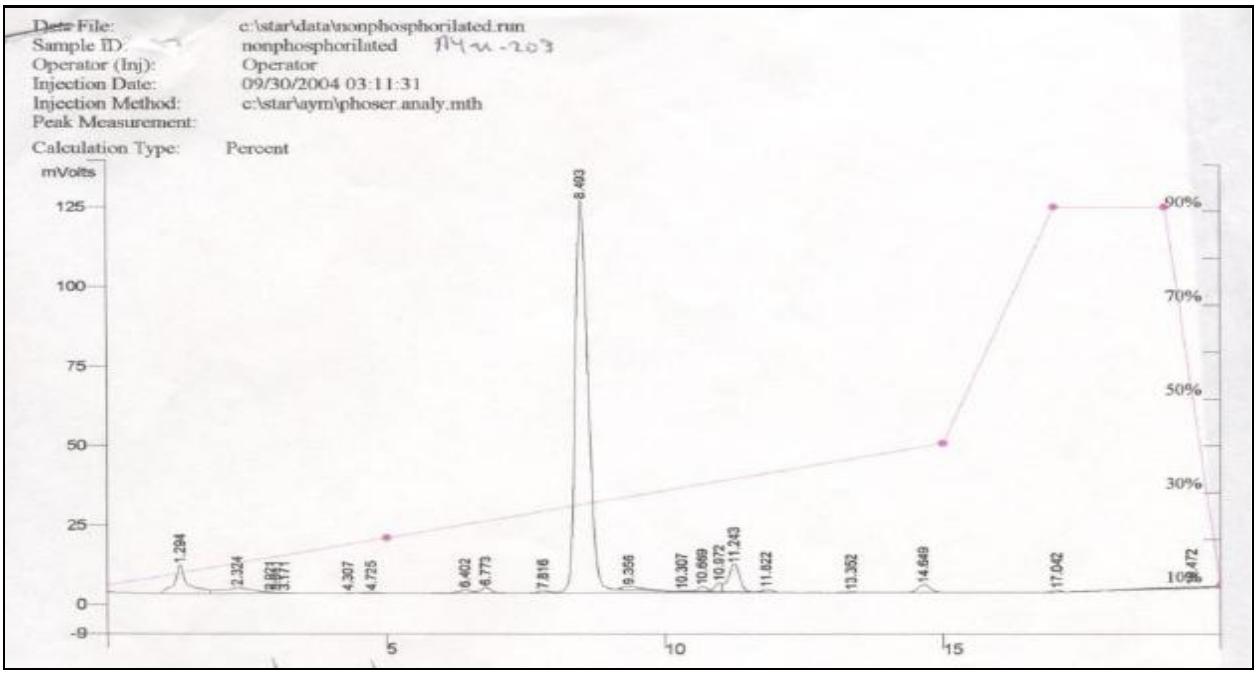

Fig. S53. RP-HPLC of Ac–LLPTPPLSPS–NH_2 with 0.1% TFA in 10 to 35% CH_3CN/H_2O gradient over 15 min showed a major peak at 8.5 min.

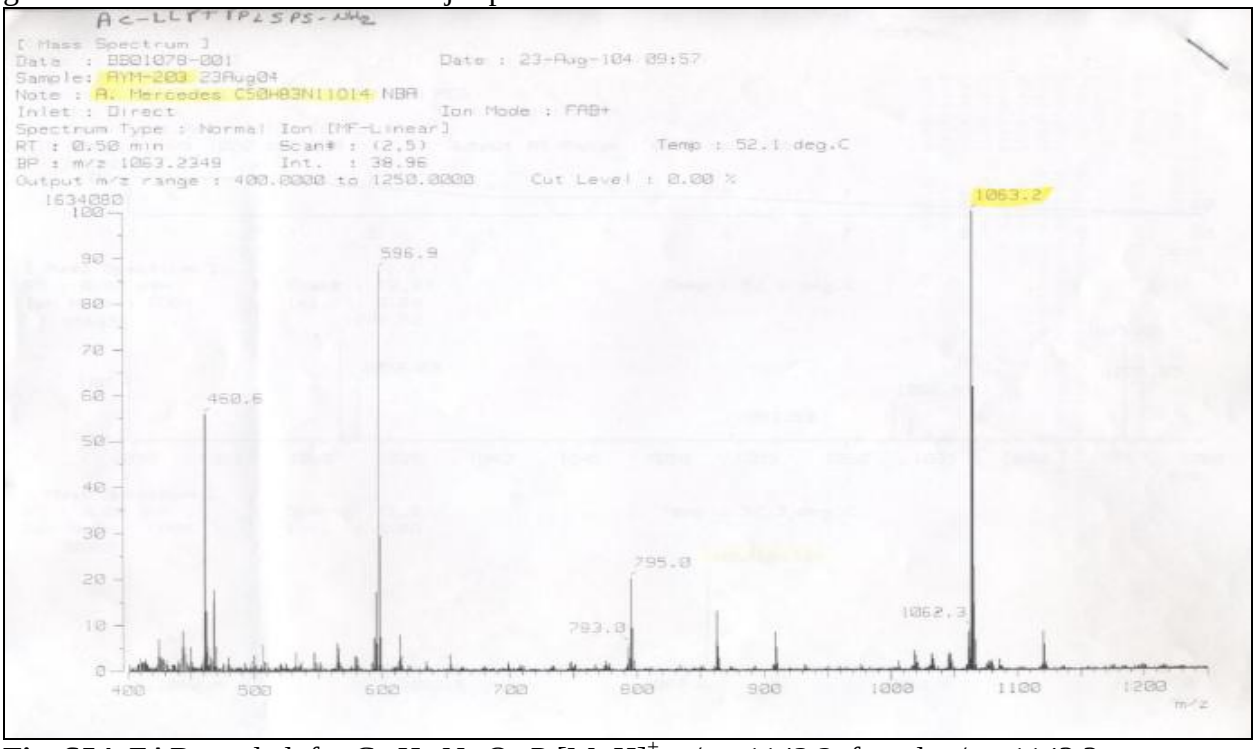

Fig. S54. FAB+, calcd. for $C_{50}H_{84}N_{11}O_{17}P$ $[M+H]^+$ *m/z* = 1142.2, found *m/z* = 1143.3.

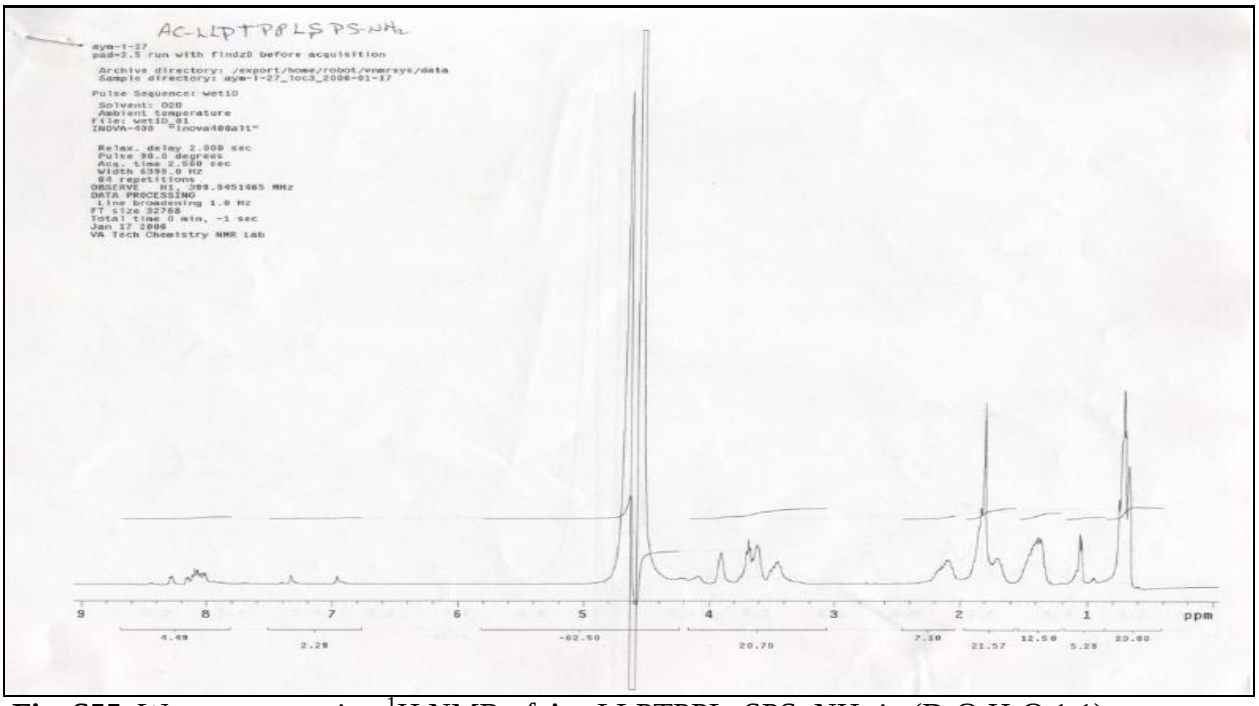

Fig. S55. Water-suppression ^{1}H NMR of Ac–LLPTPPLpSPS–NH_2 in (D_2O:H_2O 1:1), some characteristic amide-protons exchange at 6.9-8.5 ppm, the α-protons of the peptide core are observed at 3-4 ppm, and the leucine methyls were observed at 0.9-0.7 ppm.

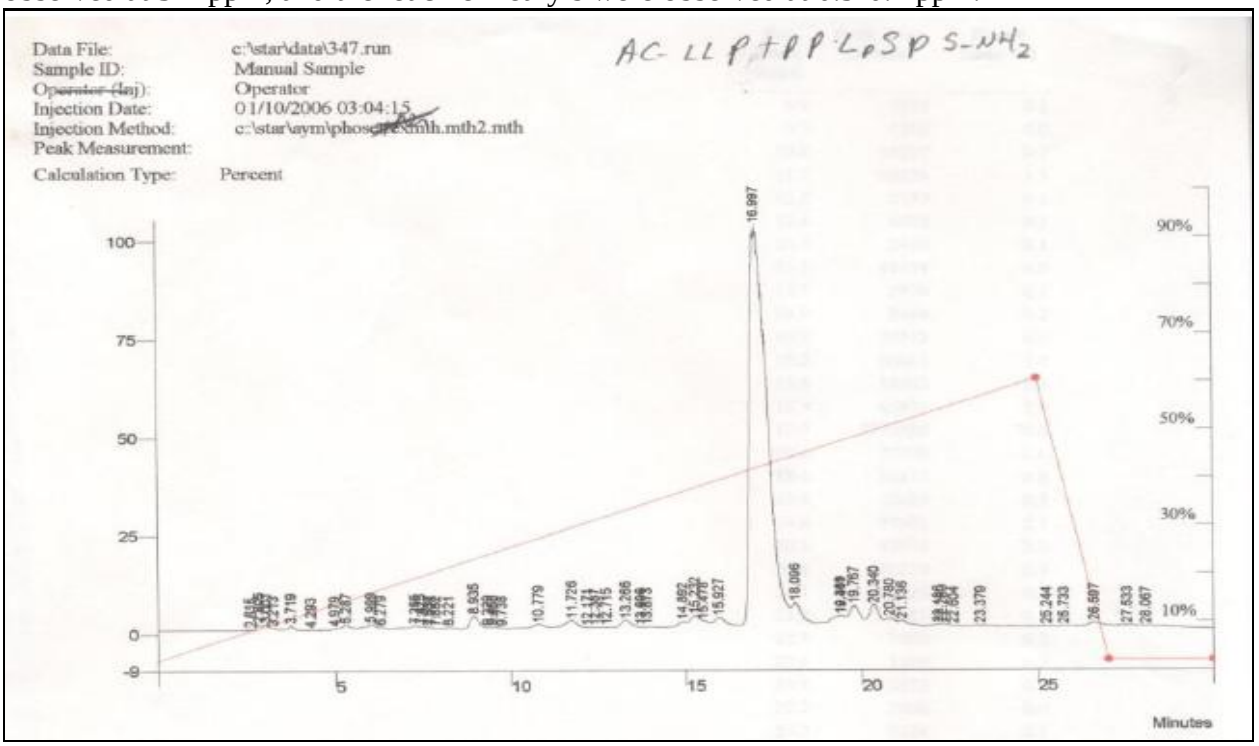

Fig. S56. RP-HPLC of Ac–LLPTPPLSPS–NH2 with 0.1% TFA in 10 to 55% CH_3CN/H_2O gradient over 26 min showed a major peak at 17 min.

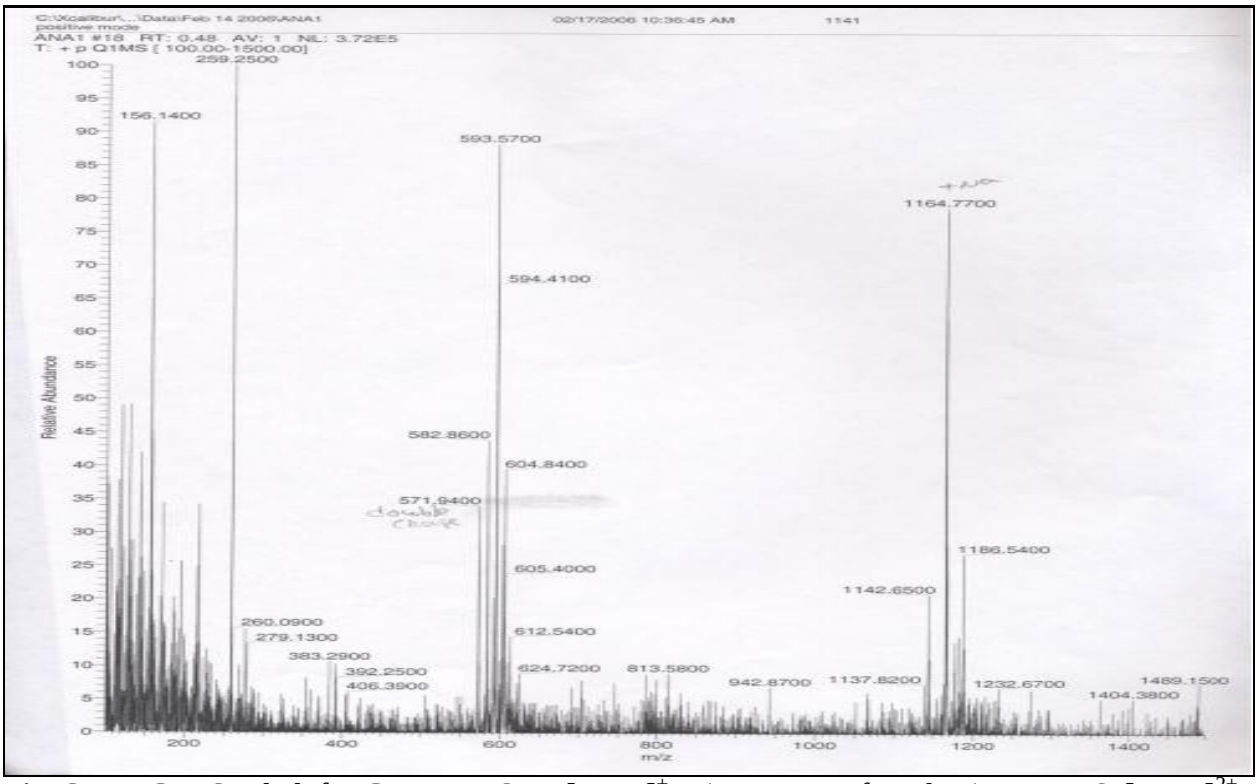

Fig. S57. LC-MS calcd. for $C_{50}H_{84}N_{11}O_{17}P$ $[M+H]^+$ *m/z* = 1142.2, found *m/z* = 1142.6, $[M+H]^{2+}$ *m/z* = 1164.7, $[M+Na]^+$ *m/z* = 571.9.

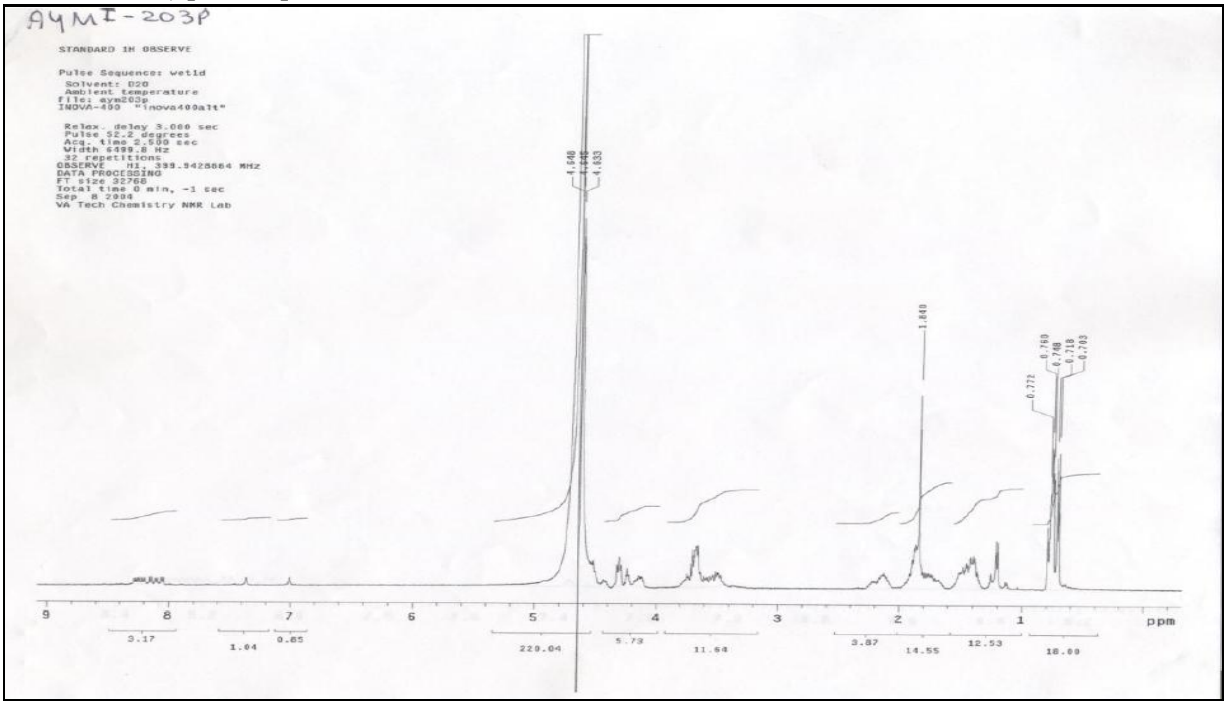

Fig. S58. Water-suppression 1H NMR of Ac–LLPpTPPLSPS–NH2 in (D2O:H2O 1:1), some characteristic amide-protons exchange at 7-8.5 ppm, the α-protons of the peptide core are observed at 4.3-5 ppm, and the leucine methyls were observed at 0.9-0.7 ppm.

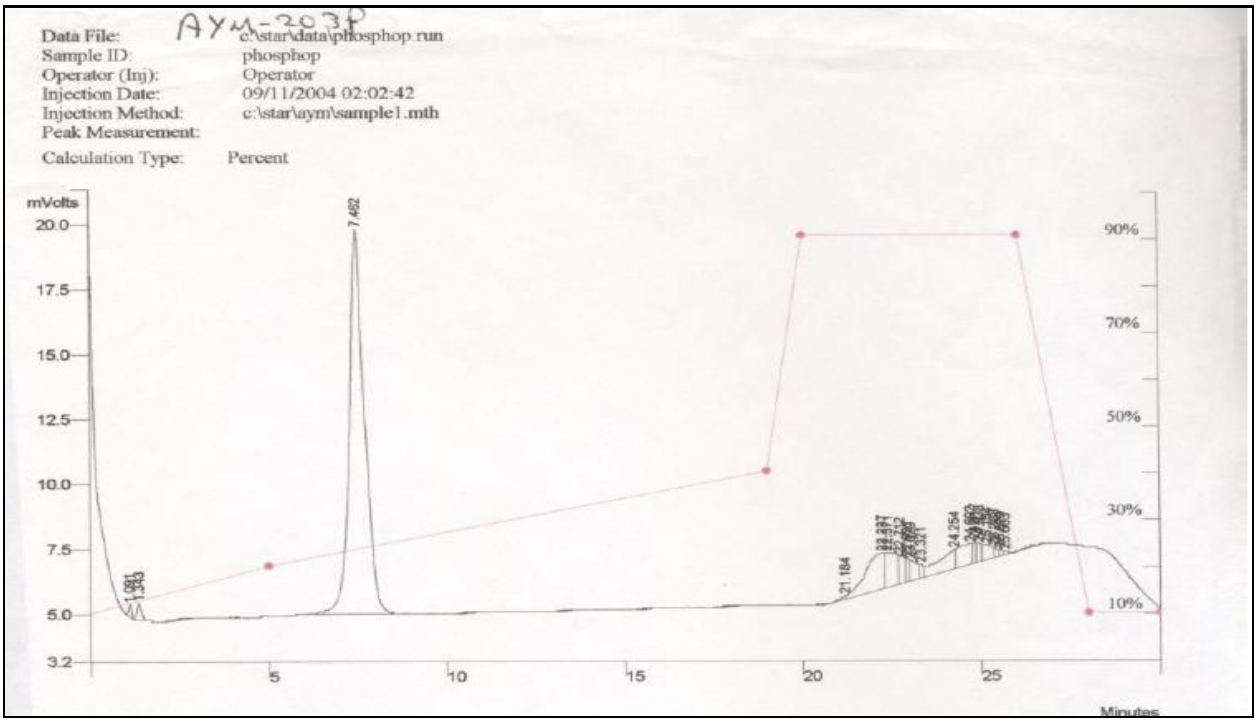

Fig. S59. RP-HPLC of Ac–LLpPTPPLSPS–NH_2 with 0 in 10 to 30% CH_3CN/H_2O gradient over 12 min showed a major peak at 7.5 min.

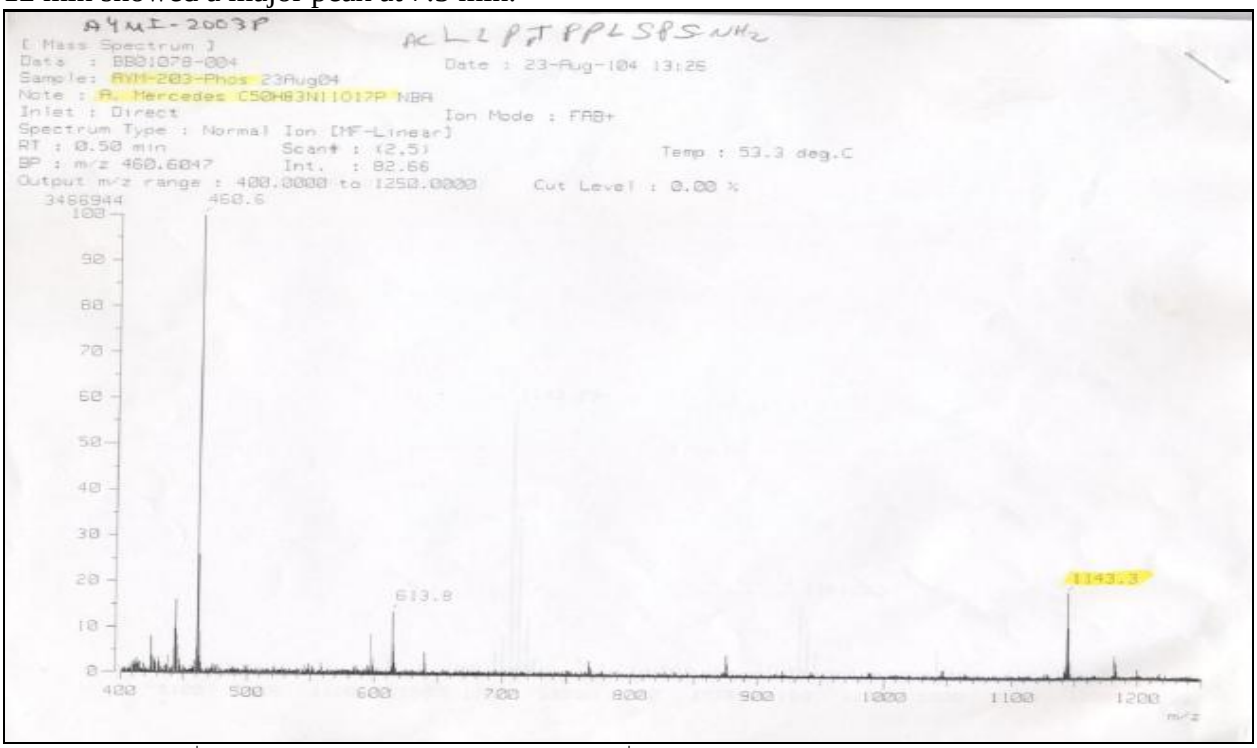

Fig. S60. FAB^+, calcd. for $C_{50}H_{84}N_{11}O_{17}P$ $[MH]^+$ *m/z* = 1143.2, found *m/z* = 1143.3.

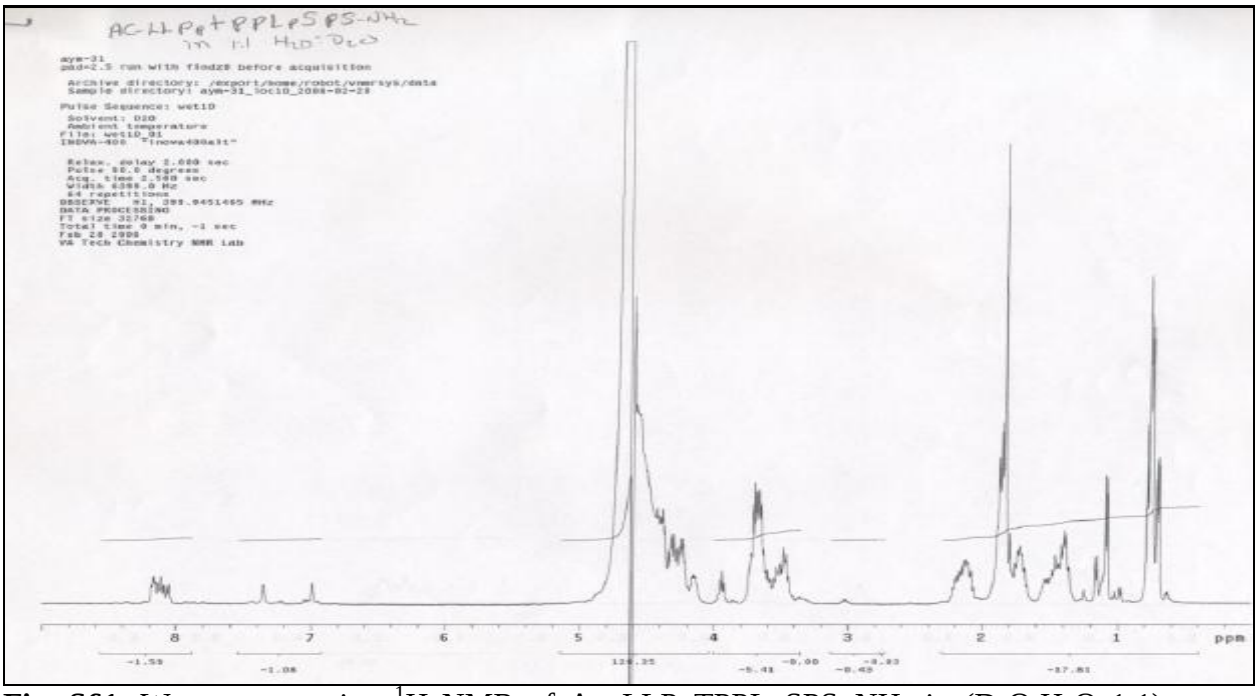

Fig. S61. Water-suppression ^{1}H NMR of Ac–LLPpTPPLpSPS–NH_2 in (D_2O:H_2O 1:1), some characteristic amide-protons exchange at 7-8.5 ppm, the α-protons of the peptide core are observed at 3.8-5 ppm, and the leucine methyls were observed at 0.9-0.7 ppm.

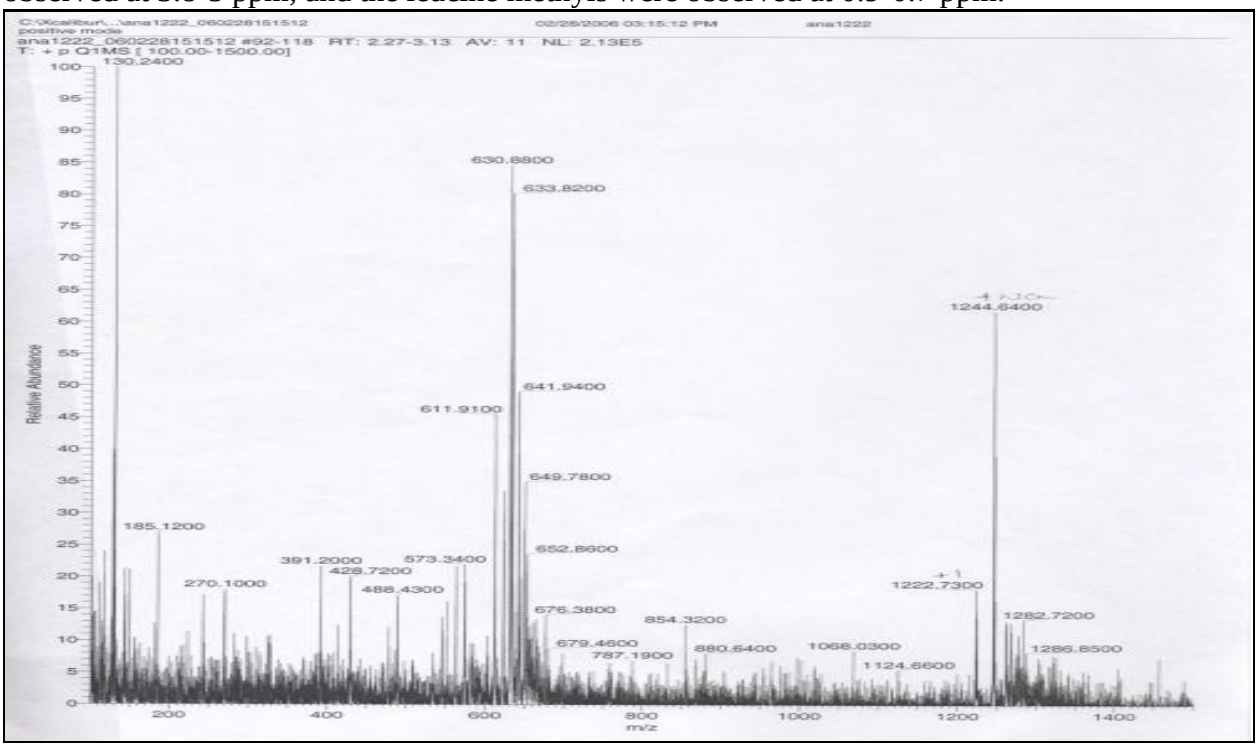

Fig. S62. LC-MS calcd. for C50H85N11O20P2 [M+H]+ *m/z* = 1221.5, found *m/z* = 1222.7, [M+H]2+ *m/z* = 1244.6, [M+Na]+ *m/z* = 611.3.

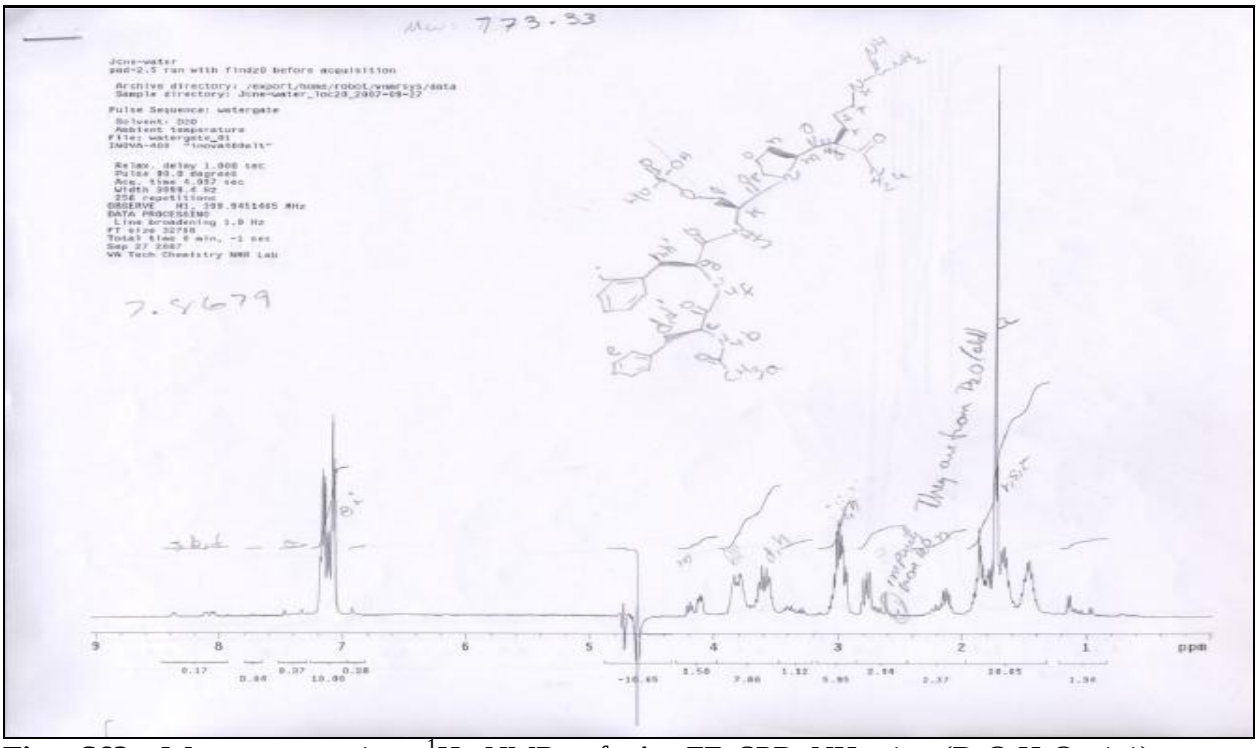

Fig. S63. Water-suppression ^{1}H NMR of Ac–FFpSPR–NH_2 in (D_2O:H_2O 1:1), some characteristic aromatic-protons of phenylalanine at 7.3 ppm, the α-protons of the peptide core are observed at 4-5 ppm.

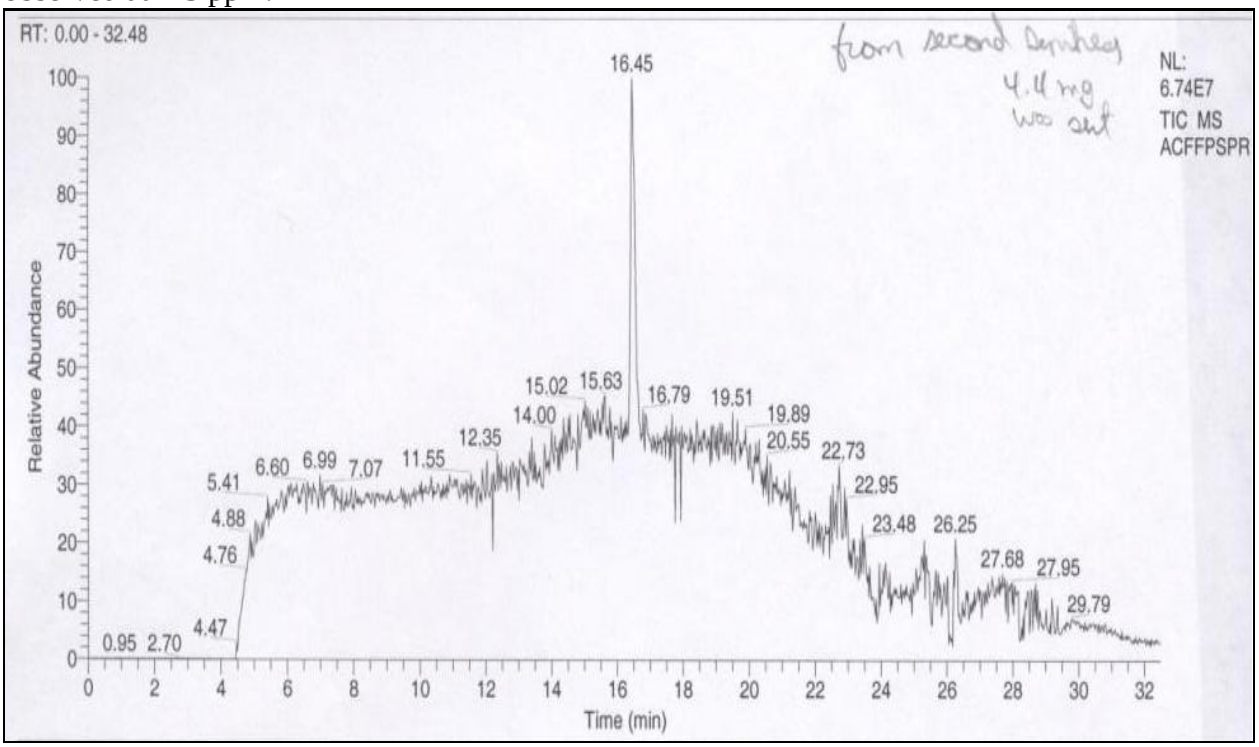

Fig. S64. LC-MS total ion chromatogram of Ac–FFpSPR–NH_2. The peak at 16.45 min had the correct molecular mass (See Fig. S65).

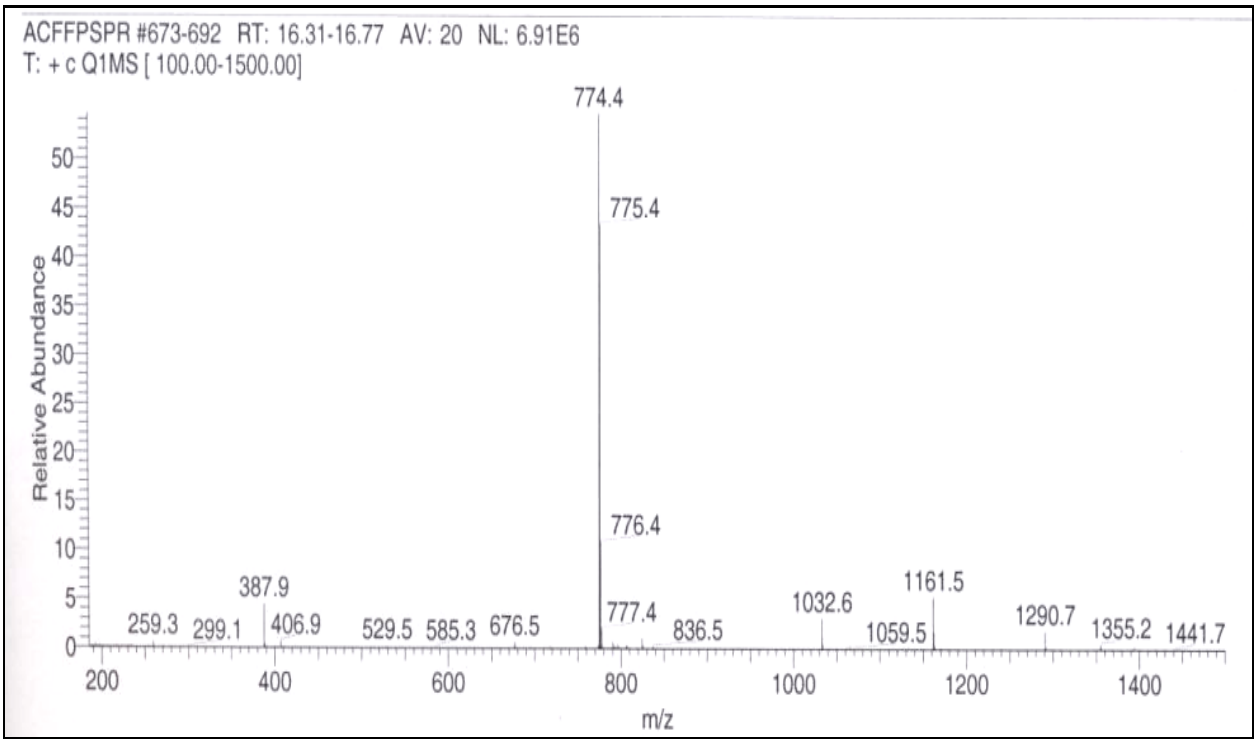

Fig. S65. LC-MS calcd. for $C_{34}H_{48}N_9O_{10}P$ [M+H]+ *m/z* = 774.3, found *m/z* = 774.4[89].

Appendix E

Toward the understanding of Pin1 catalytic mechanism by using kinetic isotopic effect studies

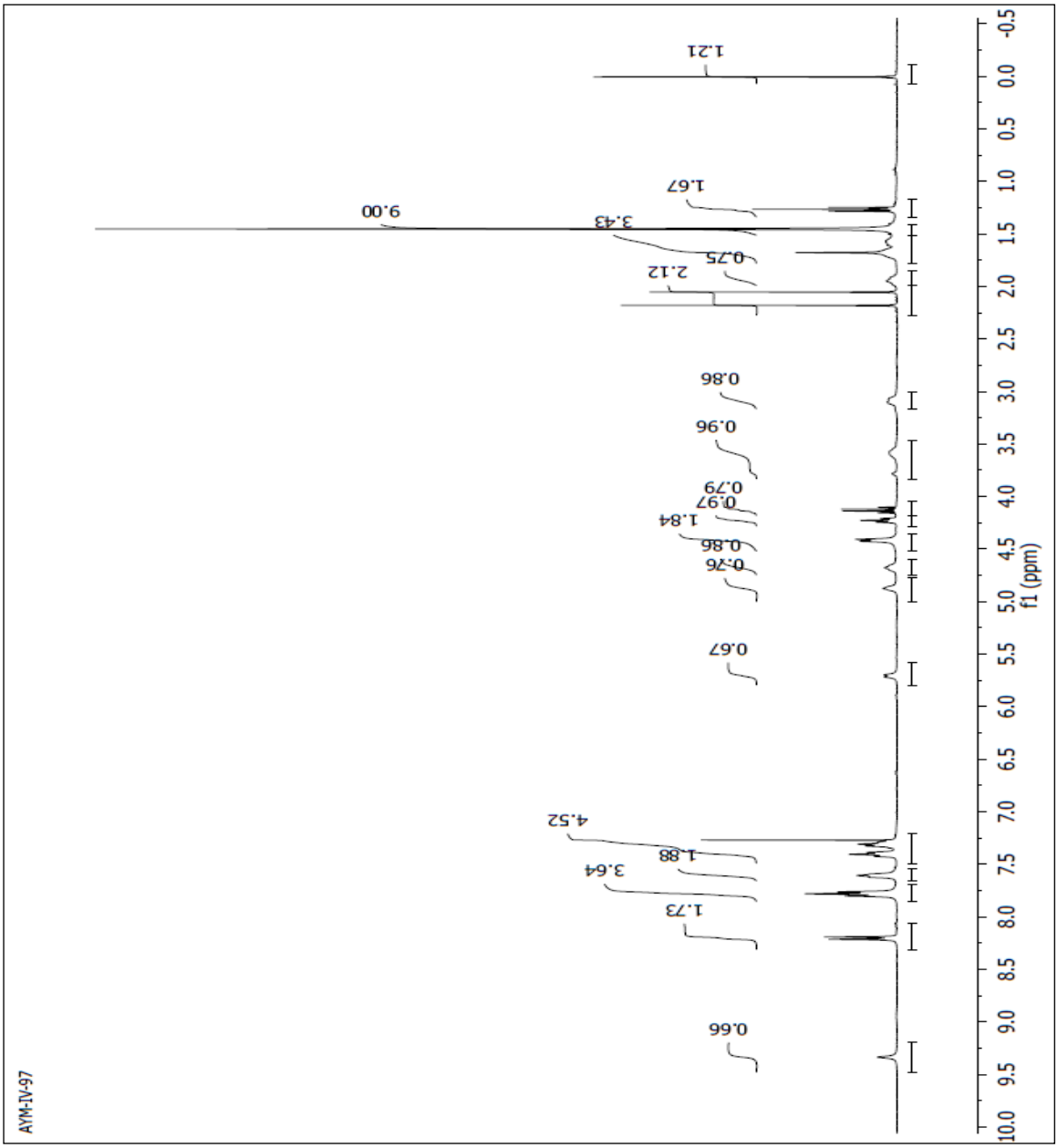

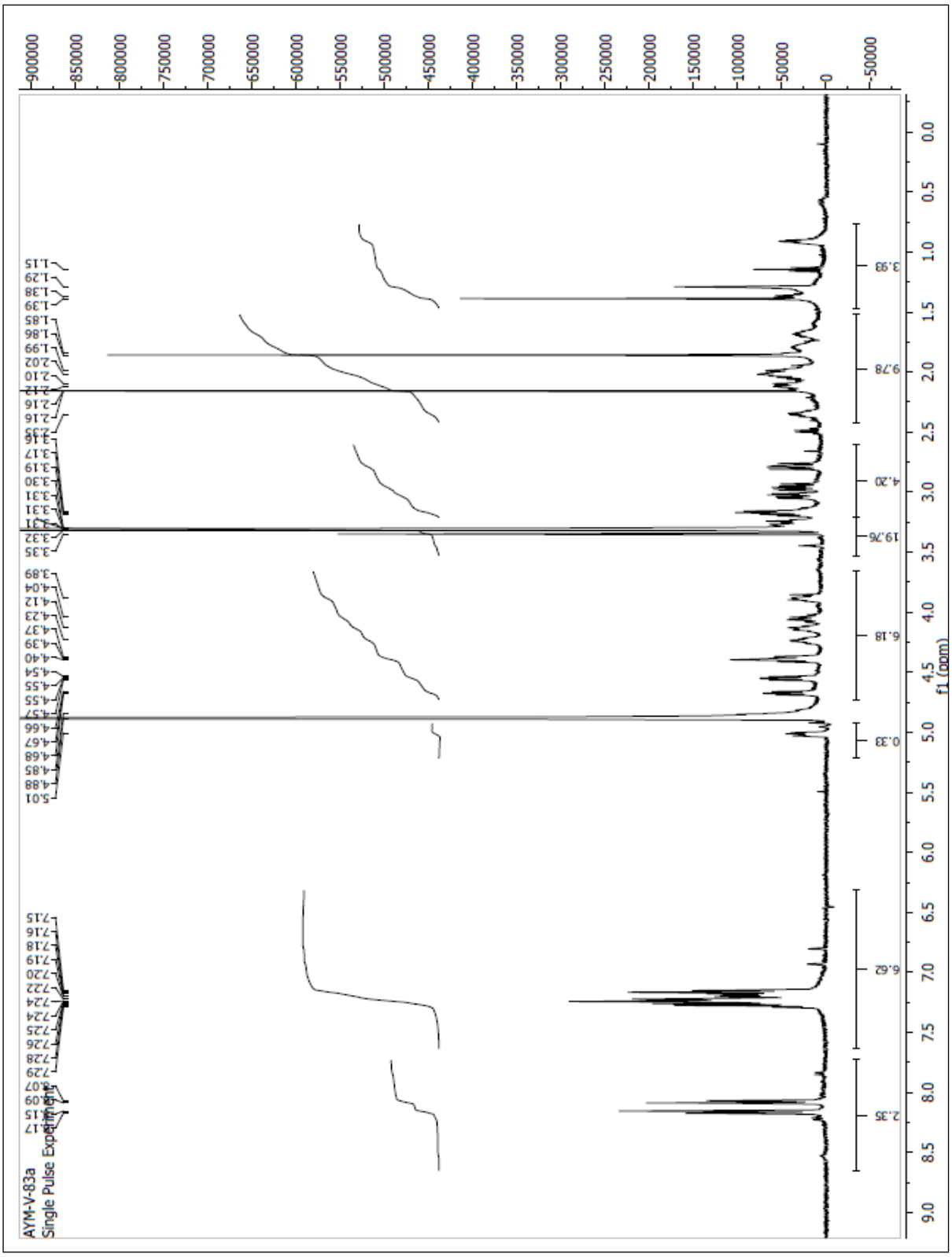
AYM-V-83a
Single Pulse Exp
f1 (ppm)

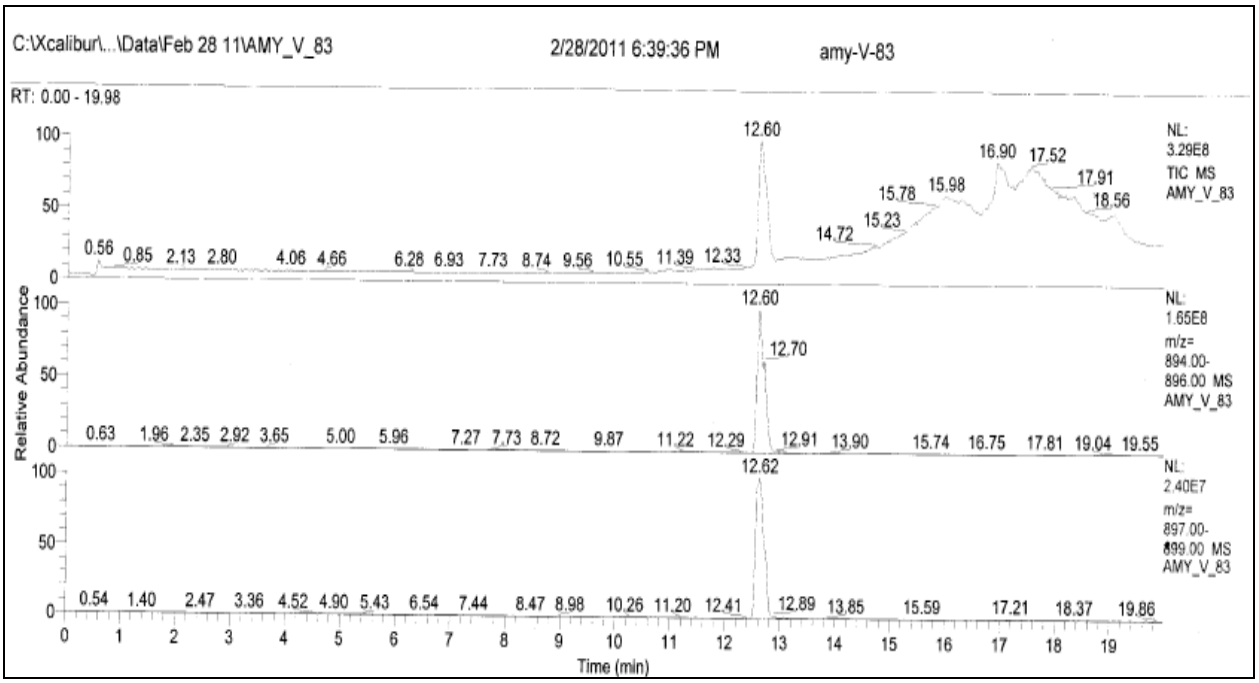

Fig. S.68. LC-MS total ion chromatogram Ac–Phe–Phe–pSer–Pro–Arg–*p*NA. The peak at 12.60 min had the correct molecular mass (See Fig. S69).

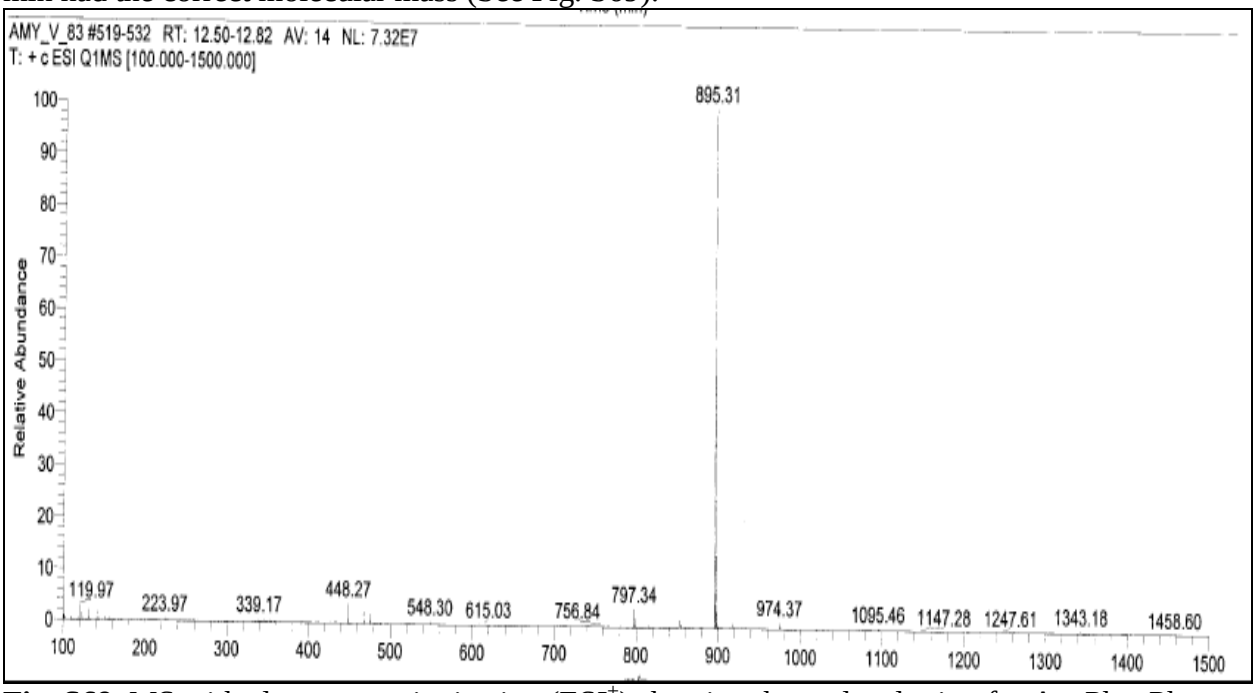

Fig. S69. MS with electrospray ionization (ESI^+) showing the molecular ion for Ac–Phe–Phe–pSer–Pro–Arg–*p*NA. The LC peak from 12.6 min was selected for molecular ion detection, identifying $[MH]^+$ = 895.3 *m/z*.

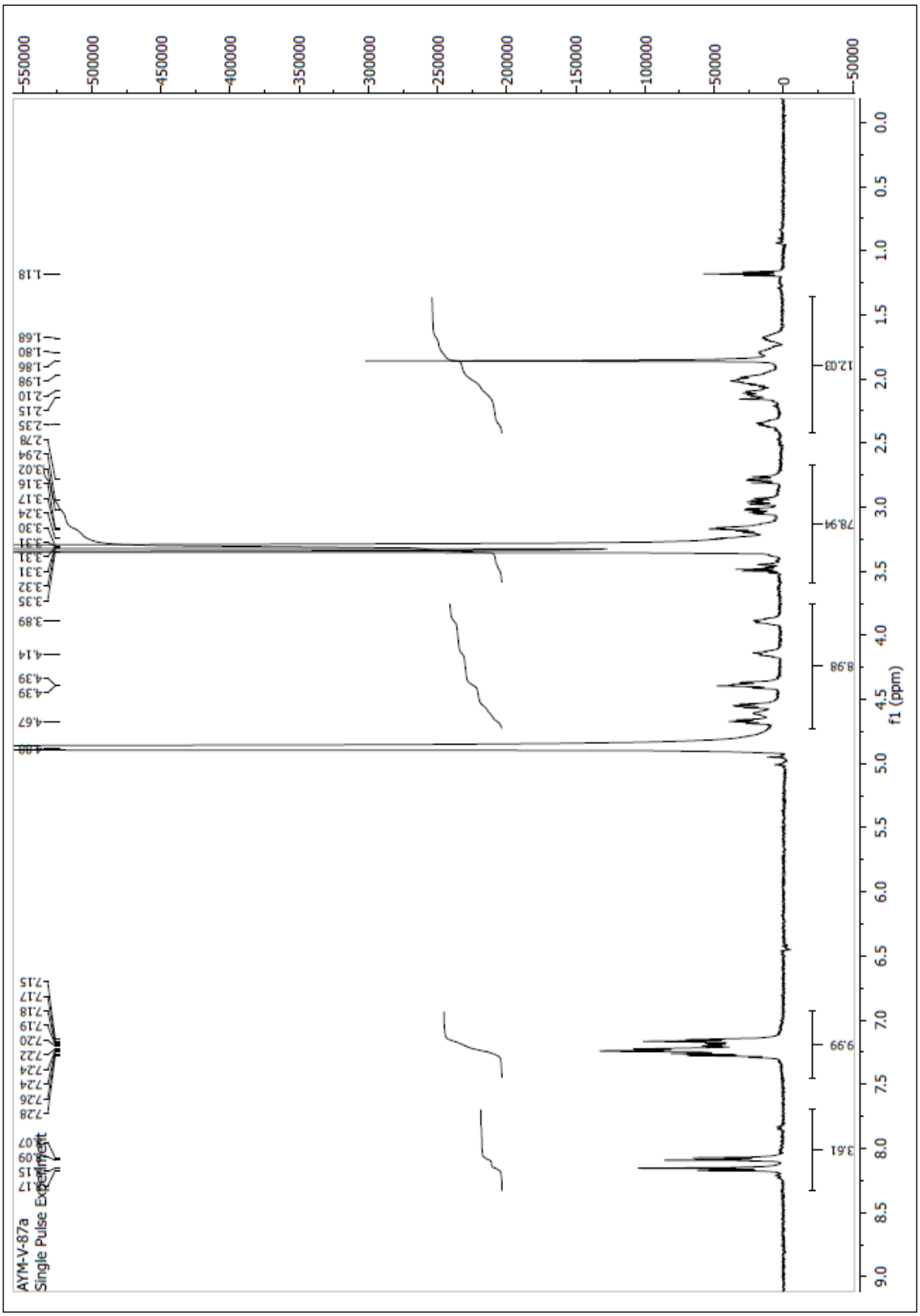
AYM-V-87a
Single Pulse Experiment
f1 (ppm)
12.03
78.94
8.98
9.99
3.61

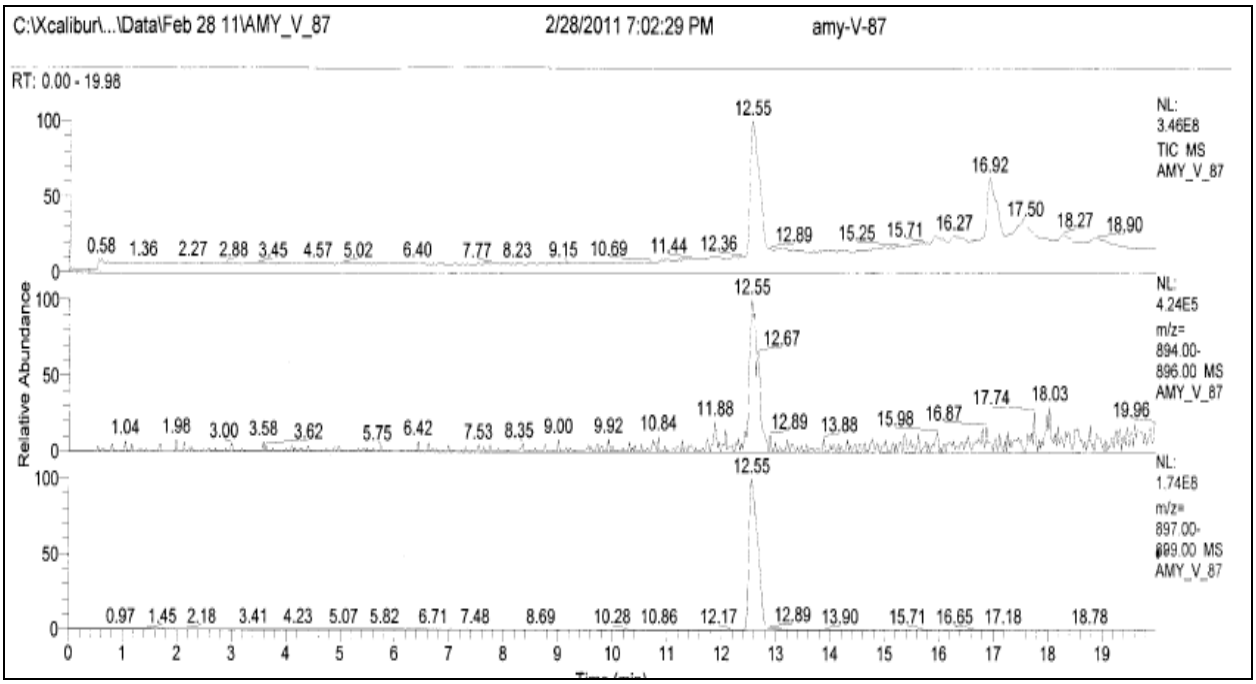

Fig. S.71. LC-MS total ion chromatogram Ac–Phe–Phe–p[d_3]Ser–Pro–Arg–*p*NA. The peak at 12.55 min had the correct molecular mass (See Fig. S72).

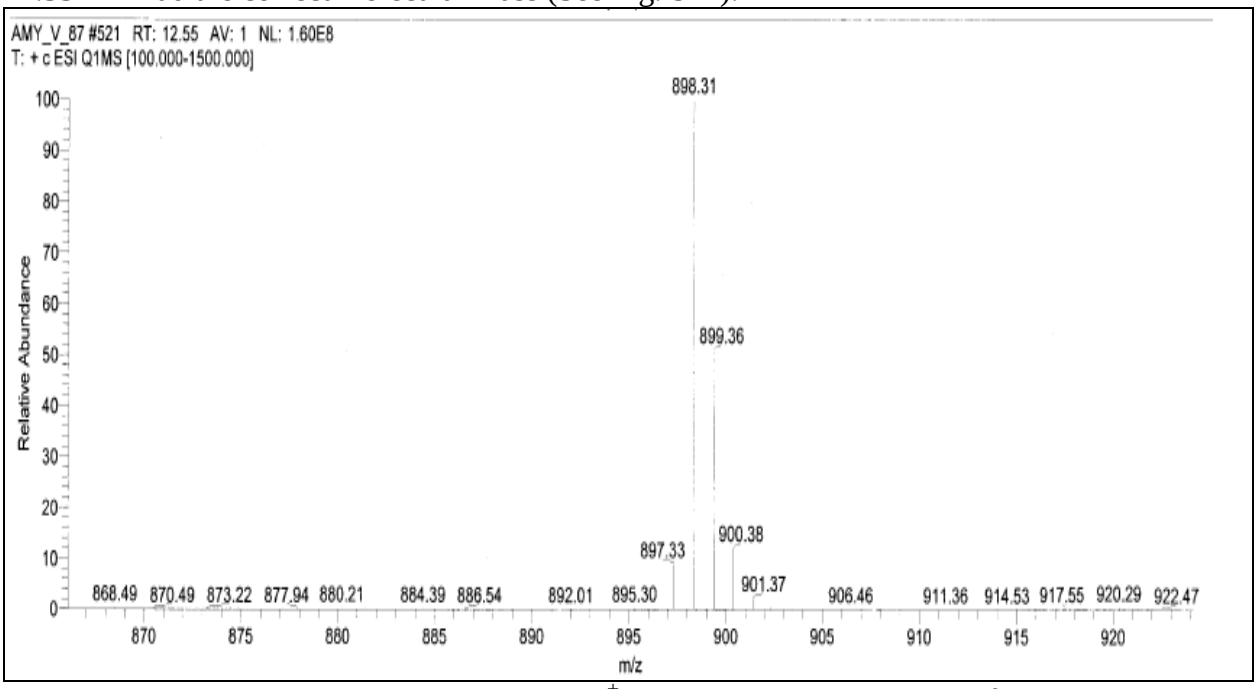

Fig. S72. MS with electrospray ionization (ESI^+) showing the molecular ion for Ac–Phe–Phe–p[d_3]Ser–Pro–Arg–*p*NA. The LC peak from 12.55 min was selected for molecular ion detection, identifying $[MH]^+$ = 898.3 *m/z*.

References

[1] L. Pauling, and R.B. Corey, Configurations of Polypeptide Chains With Favored Orientations Around Single Bonds: Two New Pleated Sheets. *Proc Natl Acad Sci U S A* **37** (1951) 729-740.

[2] A.S. Edison, Linus Pauling and the planar peptide bond. *Nat Struct Biol* **8** (2001) 201-202.

[3] T. Drakenberg, K.I. Dahlqvist, and A. Forsen, Effect of Lithium Ion on the Torsional Barrier in Amides. *J. Phys. Chem.* **76** (1972) 2178-2183.

[4] F.X. Schmid, Protein folding. Prolyl isomerases join the fold. *Curr Biol* **5** (1995) 993-994.

[5] C. Dugave, Cis-Trans Isomerization in Biochemistry, ISBN: 9783527609499 *Wiley-VCH Verlag GmbH & Co. KGaA* (2006).

[6] G. Fischer, H. Bang, and C. Mech, [Determination of enzymatic catalysis for the cis-trans-isomerization of peptide binding in proline-containing peptides. *Biomed Biochim Acta* **43** (1984) 1101-1111.

[7] P.O. Freskgard, N. Bergenhem, B.H. Jonsson, M. Svensson, and U. Carlsson, Isomerase and chaperone activity of prolyl isomerase in the folding of carbonic anhydrase. *Science* **258** (1992) 466-468.

[8] C. Schiene-Fischer, J. Habazettl, F.X. Schmid, and G. Fischer, The hsp70 chaperone DnaK is a secondary amide peptide bond cis-trans isomerase. *Nat Struct Biol* **9** (2002) 419-424.

[9] J.J. Siekierka, S.H. Hung, M. Poe, C.S. Lin, and N.H. Sigal, A cytosolic binding protein for the immunosuppressant FK506 has peptidyl-prolyl isomerase activity but is distinct from cyclophilin. *Nature* **341** (1989) 755-757.

[10] J.U. Rahfeld, A. Schierhorn, K. Mann, and G. Fischer, A novel peptidyl-prolyl cis/trans isomerase from Escherichia coli. *FEBS Lett* **343** (1994) 65-69.

[11] K.P. Lu, S.D. Hanes, and T. Hunter, A human peptidyl-prolyl isomerase essential for regulation of mitosis. *Nature* **380** (1996) 544-547.

[12] S.K. Swanson, T. Born, L.D. Zydowsky, H. Cho, H.Y. Chang, C.T. Walsh, and F. Rusnak, Cyclosporin-mediated inhibition of bovine calcineurin by cyclophilins A and B. *Proc Natl Acad Sci U S A* **89** (1992) 3741-3745.

[13] F.A. Etzkorn, Chang, Z. Y., Stolz, L. A., and Walsh, C. T., Cyclophilin residues that affect noncompetitive inhibition of the protein serine phosphatase activity of calcineurin by the cyclophilin.cyclosporin A complex. *Biochemistry* **33** (1994) 2380-2388.

[14] K. Dolinski, S. Muir, M. Cardenas, and J. Heitman, All cyclophilins and FK506 binding proteins are, individually and collectively, dispensable for viability in Saccharomyces cerevisiae. *Proc Natl Acad Sci U S A* **94** (1997) 13093-13098.

[15] L.D. Zydowsky, F.A. Etzkorn, H.Y. Chang, S.B. Ferguson, L.A. Stolz, S.I. Ho, and C.T. Walsh, Active site mutants of human cyclophilin A separate peptidyl-prolyl isomerase activity from cyclosporin A binding and calcineurin inhibition. *Protein Sci* **1** (1992) 1092-1099.

[16] R.E. Handschumacher, M.W. Harding, J. Rice, R.J. Drugge, and D.W. Speicher, Cyclophilin: a specific cytosolic binding protein for cyclosporin A. *Science* **226** (1984) 544-547.

[17] A. Galat, Peptidylprolyl cis/trans isomerases (immunophilins): biological diversity--targets--functions. *Curr Top Med Chem* **3** (2003) 1315-1347.

[18] D.A. Butterfield, H.M. Abdul, W. Opii, S.F. Newman, G. Joshi, M.A. Ansari, and R. Sultana, Pin1 in Alzheimer's disease. *J Neurochem* **98** (2006) 1697-1706.

[19] S. Barik, Immunophilins: for the love of proteins. *Cell Mol Life Sci* **63** (2006) 2889-2900.

[20] T. Maruyama, and M. Furutani, Archaeal peptidyl prolyl cis-trans isomerases (PPIases). *Front Biosci* **5** (2000) D821-836.

[21] K.P. Lu, G. Finn, T.H. Lee, and L.K. Nicholson, Prolyl cis-trans isomerization as a molecular timer. *Nat Chem Biol* **3** (2007) 619-629.

[22] J.S. Fraser, M.W. Clarkson, S.C. Degnan, R. Erion, D. Kern, and T. Alber, Hidden alternative structures of proline isomerase essential for catalysis. *Nature* **462** (2009) 669-673.

[23] S. Szep, S. Park, E.T. Boder, G.D. Van Duyne, and J.G. Saven, Structural coupling between FKBP12 and buried water. *Proteins* **74** (2009) 603-611.

[24] R. Ranganathan, K.P. Lu, T. Hunter, and J.P. Noel, Structural and functional analysis of the mitotic rotamase Pin1 suggests substrate recognition is phosphorylation dependent. *Cell* **89** (1997) 875-886.

[25] M. Schutkowski, A. Bernhardt, X. Zhou, M. Shen, R. Jens-Ullrich, K.P. Lu, and G. Fischer, Role of Phosphorylation in Determining the Backbone Dynamics of the Serine/Threonine-Proline Motif and Pin1 Substrate Recognition. *Biochemistry* **37** (1998) 5566-5575.

[26] M.B. Yaffe, M. Schutkowski, M. Shen, X.Z. Zhou, P.T. Stukenberg, J.U. Rahfeld, J. Xu, J. Kuang, M.W. Kirschner, G. Fischer, L.C. Cantley, and K.P. Lu, Sequence-specific and phosphorylation-dependent proline isomerization: a potential mitotic regulatory mechanism. *Science* **278** (1997) 1957-1960.

[27] A.T. Namanja, T. Peng, J.S. Zintsmaster, A.C. Elson, M.G. Shakour, and J.W. Peng, Substrate recognition reduces side-chain flexibility for conserved hydrophobic residues in human Pin1. *Structure* **15** (2007) 313-327.

[28] E. Bayer, S. Goettsch, J.W. Mueller, B. Griewel, E. Guiberman, L.M. Mayr, and P. Bayer, Structural analysis of the mitotic regulator hPin1 in solution: insights into domain architecture and substrate binding. *J Biol Chem* **278** (2003) 26183-26193.

[29] C. Guo, X. Hou, L. Dong, E. Dagostino, S. Greasley, R. Ferre, J. Marakovits, M.C. Johnson, D. Matthews, B. Mroczkowski, H. Parge, T. Vanarsdale, I. Popoff, J. Piraino, S. Margosiak, J. Thomson, G. Los, and B.W. Murray, Structure-based design of novel human Pin1 inhibitors (I). *Bioorg Med Chem Lett* **19** (2009) 5613-5616.

[30] C. Lufei, and X. Cao, Nuclear import of Pin1 is mediated by a novel sequence in the PPIase domain. *FEBS Lett* **583** (2009) 271-276.

[31] C.D. Behrsin, M.L. Bailey, K.S. Bateman, K.S. Hamilton, L.M. Wahl, C.J. Brandl, B.H. Shilton, and D.W. Litchfield, Functionally important residues in the peptidyl-prolyl isomerase Pin1 revealed by unigenic evolution. *J Mol Biol* **365** (2007) 1143-1162.

[32] M.A. Verdecia, M.E. Bowman, K.P. Lu, T. Hunter, and J.P. Noel, Structural basis for phosphoserine-proline recognition by group IV WW domains. *Nat Struct Biol* **7** (2000) 639-643.

[33] G.A. Petsko, and D. Ringe, Protein Structure and function, ISBN: 1405119225. *New Science Press* (2004).

[34] M. Sudol, P. Bork, A. Einbond, K. Kastury, T. Druck, M. Negrini, K. Huebner, and D. Lehman, Characterization of the mammalian YAP (Yes-associated protein) gene and its role in defining a novel protein module, the WW domain. *J Biol Chem* **270** (1995) 14733-14741.

[35] T.S. Keshava Prasad, R. Goel, K. Kandasamy, S. Keerthikumar, S. Kumar, S. Mathivanan, D. Telikicherla, R. Raju, B. Shafreen, A. Venugopal, L. Balakrishnan, A. Marimuthu, S. Banerjee, D.S. Somanathan, A. Sebastian, S. Rani, R. S., C.J. Kishore, S. Kanth, M. Ahmed, M.K. Kashyap, R. Mohmood, Y.L. Ramachandra, V. Krishna, B.A. Rahiman, S. Mohan, P. Ranganathan, S. Ramabadran, R. Chaerkady, and A. Pandey, Human Protein Reference Database--2009 update. *Nucleic Acids Res.* **37** (2009) 767-772.

[36] P.A. Dalby, R.H. Hoess, and W.F. DeGrado, Evolution of binding affinity in a WW domain probed by phage display. *Protein Sci* **9** (2000) 2366-2376.

[37] L. Otte, U. Wiedemann, B. Schlegel, J.R. Pires, M. Beyermann, P. Schmieder, G. Krause, R. Volkmer-Engert, J. Schneider-Mergener, and H. Oschkinat, WW domain sequence activity relationships identified using ligand recognition propensities of 42 WW domains. *Protein Sci* **12** (2003) 491-500.

[38] H. Linn, K.S. Ermekova, S. Rentschler, A.B. Sparks, B.K. Kay, and M. Sudol, Using molecular repertoires to identify high-affinity peptide ligands of the WW domain of human and mouse YAP. *Biol Chem* **378** (1997) 531-537.

[39] K.S. Ermekova, N. Zambrano, H. Linn, G. Minopoli, F. Gertler, T. Russo, and M. Sudol, The WW domain of neural protein FE65 interacts with proline-rich motifs in Mena, the mammalian homolog of Drosophila enabled. *J Biol Chem* **272** (1997) 32869-32877.

[40] M. Sudol, K. Sliwa, and T. Russo, Functions of WW domains in the nucleus. *FEBS Lett* **490** (2001) 190-195.

[41] P. Lu, X.Z. Zhou, M. Shen, and K.P. Lu, Function of WW Domains as Phosphoserine- or Phosphothreonine-binding Modules. *Science* **283** (1999) 1325-1329.

[42] M. Shen, P.T. Stukenberg, M.W. Kirschner, and K.P. Lu, The essential mitotic peptidyl-prolyl isomerase Pin1 binds and regulates mitosis-specific phosphoproteins. *Genes Dev* **12** (1998) 706-720.

[43] M. Jäger, M. Dendle, A.A. Fuller, and J.W. Kelly, A cross-strand Trp Trp pair stabilizes the hPin1 WW domain at the expense of function. *Protein Sci* **10** (2007) 2306-2313.

[44] M. Jager, Y. Zhang, J. Bieschke, H. Nguyen, M. Nendle, M.E. Bowman, J.P. Noel, M. Gruebele, and J.W. Kelly, Structure-function-folding relationship in a WW domain. *Proc Natl Acad Sci U S A* **103** (2006) 10648-10653.

[45] M. Jager, H. Nguyen, M. Dendle, M. Gruebele, and J.W. Kelly, Influence of hPin1 WW N-terminal domain boundaries on function, protein stability, and folding. *Protein Sci* **16** (2007) 1495-1501.

[46] Y. Zhang, S. Fussel, U. Reimer, M. Schutkowski, and G. Fischer, Substrate-based design of reversible Pin1 inhibitors. *Biochemistry* **41** (2002) 11868-11877.

[47] S.H. Chao, A.L. Greenleaf, and D.H. Price, Juglone, an inhibitor of the peptidyl-prolyl isomerase Pin1, also directly blocks transcription. *Nucleic Acids Res* **29** (2001) 767-773.

[48] M.C. Galas, P. Dourlen, S. Begard, K. Ando, D. Blum, M. Hamdane, and L. Buee, The peptidylprolyl cis/trans-isomerase Pin1 modulates stress-induced dephosphorylation of Tau in neurons. Implication in a pathological mechanism related to Alzheimer disease. *J Biol Chem* **281** (2006) 19296-19304.

[49] G.G. Xu, and F.A. Etzkorn, Convergent synthesis of alpha-ketoamide inhibitors of Pin1. *Org Lett* **12** 696-699.

[50] O.E. Schroeder, E. Carper, J.J. Wind, J.L. Poutsma, F.A. Etzkorn, and J.C. Poutsma, Theoretical and experimental investigation of the energetics of cis-trans proline isomerization in peptide models. *J Phys Chem A* **110** (2006) 6522-6530.

[51] M.L. Bailey, B.H. Shilton, C.J. Brandl, and D.W. Litchfield, The dual histidine motif in the active site of Pin1 has a structural rather than catalytic role. *Biochemistry* **47** (2008) 11481-11489.

[52] G.E. Wiederrecht, FA, Immunophilins. In Immunosuppressants. *Perspectives in Drug Discovery and Design series; ESCOM Science* **2** (1994) 57-84.

[53] J. Fanghanel, Enzymatic catalysis of the peptidyl-prolyl bond rotation: are transition state formation and enzyme dynamics directly linked? *Angew Chem Int Ed Engl* **42** (2003) 490-492.

[54] Y. Zhang, S. Daum, D. Wildemann, X.Z. Zhou, M.A. Verdecia, M.E. Bowman, C. Lucke, T. Hunter, K.P. Lu, G. Fischer, and J.P. Noel, Structural basis for high-affinity peptide inhibition of human Pin1. *Chem Biol* **2** (2007) 320-328.

[55] T. Ikura, K. Kinoshita, and N. Ito, A cavity with an appropriate size is the basis of the PPIase activity. *Protein Eng Des Sel* **21** (2008) 83-89.

[56] R.T. Williams, L. Wu, D.A. Carbonaro-Hall, V.T. Tolo, and F.L. Hall, Identification of a novel cyclin-like protein in human tumor cells. *J Biol Chem* **268** (1993) 8871-8880.

[57] L. Hengst, V. Dulic, J.M. Slingerland, E. Lees, and S.I. Reed, A cell cycle-regulated inhibitor of cyclin-dependent kinases. *Proc Natl Acad Sci U S A* (1994) 5291-5295.

[58] N.J. Wells, N. Watanabe, T. Tokusumi, W. Jiang, M.A. **91**Verdecia, and T. Hunter, The C-terminal domain of the Cdc2 inhibitory kinase Myt1 interacts with Cdc2 complexes and is required for inhibition of G(2)/M progression. *J Cell Sci* **112** (Pt 19) (1999) 3361-3371.

[59] M. Bedin, M.G. Catelli, L. Cabanie, A.M. Gaben, and J. Mester, Indirect participation of Hsp90 in the regulation of the cyclin E turnover. *Biochem Pharmacol* **77** (2009) 151-158.

[60] K.P. Lu, Y.C. Liou, and X.Z. Zhou, Pinning down proline-directed phosphorylation signaling. *Trends Cell Biol* **12** (2002) 164-172.

[61] R. Pang, J. Yuen, M.F. Yuen, C.L. Lai, T.K. Lee, K. Man, R.T. Poon, S.T. Fan, C.M. Wong, I.O. Ng, Y.L. Kwong, and E. Tse, PIN1 overexpression and beta-catenin gene mutations are distinct oncogenic events in human hepatocellular carcinoma. *Oncogene* **23** (2004) 4182-4186.

[62] A. Basu, M. Das, S. Qanungo, X.J. Fan, G. DuBois, and S. Haldar, Proteasomal degradation of human peptidyl prolyl isomerase pin1-pointing phospho Bcl2 toward dephosphorylation. *Neoplasia* **4** (2002) 218-227.

[63] N. Pathan, C. Aime-Sempe, S. Kitada, S. Haldar, and J.C. Reed, Microtubule-targeting drugs induce Bcl-2 phosphorylation and association with Pin1. *Neoplasia* **3** (2001) 70-79.

[64] K.P. Lu, F. Suizu, X.Z. Zhou, G. Finn, P. Lam, and G. Wulf, Targeting carcinogenesis: a role for the prolyl isomerase Pin1? *Mol Carcinog* **45** (2006) 397-402.

[65] F. De Nicola, T. Bruno, S. Iezzi, M. Di Padova, A. Floridi, C. Passananti, G. Del Sal, and M. Fanciulli, The prolyl isomerase Pin1 affects Che-1 stability in response to apoptotic DNA damage. *J Biol Chem* **282** (2007) 19685-19691.

[66] M.M. Messenger, R.B. Saulnier, A.D. Gilchrist, P. Diamond, G.J. Gorbsky, and D.W. Litchfield, Interactions between protein kinase CK2 and Pin1. Evidence for phosphorylation-dependent interactions. *J Biol Chem* **277** (2002) 23054-23064.

[67] K.J. Stanya, Y. Liu, A.R. Means, and H.Y. Kao, Cdk2 and Pin1 negatively regulate the transcriptional corepressor SMRT. *J Cell Biol* **183** (2008) 49-61.

[68] A. Ryo, A. Hirai, M. Nishi, Y.C. Liou, K. Perrem, S.C. Lin, H. Hirano, S.W. Lee, and I. Aoki, A suppressive role of the prolyl isomerase Pin1 in cellular apoptosis mediated by the death-associated protein Daxx. *J Biol Chem* **282** (2007) 36671-36681.

[69] M. Li, P.T. Stukenberg, and D.L. Brautigan, Binding of phosphatase inhibitor-2 to prolyl isomerase Pin1 modifies specificity for mitotic phosphoproteins. *Biochemistry* **47** (2008) 292-300.

[70] W. Liu, H.D. Youn, X.Z. Zhou, K.P. Lu, and J.O. Liu, Binding and regulation of the transcription factor NFAT by the peptidyl prolyl cis-trans isomerase Pin1. *FEBS Lett* **496** (2001) 105-108.

[71] J. He, A.G. Lau, M.B. Yaffe, and R.A. Hall, Phosphorylation and cell cycle-dependent regulation of Na+/H+ exchanger regulatory factor-1 by Cdc2 kinase. *J Biol Chem* **276** (2001) 41559-41565.

[72] E. Yeh, M. Cunningham, H. Arnold, D. Chasse, T. Monteith, G. Ivaldi, W.C. Hahn, P.T. Stukenberg, S. Shenolikar, T. Uchida, C.M. Counter, J.R. Nevins, A.R. Means, and R. Sears, A signalling pathway controlling c-Myc degradation that impacts oncogenic transformation of human cells. *Nat Cell Biol* **6** (2004) 308-318.

[73] J. Ma, H.K. Arnold, M.B. Lilly, R.C. Sears, and A.S. Kraft, Negative regulation of Pim-1 protein kinase levels by the B56beta subunit of PP2A. *Oncogene* **26** (2007) 5145-5153.

[74] P.J. Lu, X.Z. Zhou, Y.C. Liou, J.P. Noel, and K.P. Lu, Critical role of WW domain phosphorylation in regulating phosphoserine binding activity and Pin1 function. *J Biol Chem* **277** (2002) 2381-2384.

[75] E.L. Reineke, M. Lam, Q. Liu, Y. Liu, K.J. Stanya, K.S. Chang, A.R. Means, and H.Y. Kao, Degradation of the tumor suppressor PML by Pin1 contributes to the cancer phenotype of breast cancer MDA-MB-231 cells. *Mol Cell Biol* **28** (2008) 997-1006.

[76] M.K. Dougherty, J. Muller, D.A. Ritt, M. Zhou, X.Z. Zhou, T.D. Copeland, T.P. Conrads, T.D. Veenstra, K.P. Lu, and D.K. Morrison, Regulation of Raf-1 by direct feedback phosphorylation. *Mol Cell* **17** (2005) 215-224.

[77] V. Brondani, Q. Schefer, F. Hamy, and T. Klimkait, The peptidyl-prolyl isomerase Pin1 regulates phospho-Ser77 retinoic acid receptor alpha stability. *Biochem Biophys Res Commun* **328** (2005) 6-13.

[78] P. Dourlen, K. Ando, M. Hamdane, S. Begard, L. Buee, and M.C. Galas, The peptidyl prolyl cis/trans isomerase Pin1 downregulates the Inhibitor of Apoptosis Protein Survivin. *Biochim Biophys Acta* **1773** (2007) 1428-1437.

[79] Y.X. Xu, and J.L. Manley, Pin1 modulates RNA polymerase II activity during the transcription cycle. *Genes Dev* **21** (2007) 2950-2962.

[80] S.B. Lavoie, A.L. Albert, and M. Vincent, Unexpected roles of the peptidyl-prolyl cis/trans isomerase Pin1. *Med Sci (Paris)* **19** (2003) 1251-1258.

[81] K.P. Lu, Phosphorylation-dependent prolyl isomerization: a novel cell cycle regulatory mechanism. *Prog Cell Cycle Res* **4** (2000) 83-96.

[82] G. Lippens, I. Landrieu, and C. Smet, Molecular mechanisms of the phospho-dependent prolyl cis/trans isomerase Pin1. *FEBS Lett* **274** (2007) 5211-5222.

[83] G. Fischer, T. Tradler, and T. Zarnt, The mode of action of peptidyl prolyl cis/trans isomerases in vivo: binding vs. catalysis. *FEBS Lett* **426** (1998) 17-20.

[84] S.I. Reed, E. Bailly, V. Dulic, L. Hengst, D. Resnitzky, and J. Slingerland, G1 control in mammalian cells. *J Cell Sci Suppl* **18** (1994) 69-73.

[85] K. Okamoto, and N. Sagata, Mechanism for inactivation of the mitotic inhibitory kinase Wee1 at M phase. *Proc Natl Acad Sci U S A* **104** (2007) 3753-3758.

[86] P.T. Stukenberg, and M.W. Kirschner, Pin1 acts catalytically to promote a conformational change in Cdc25. *Mol Cell* **7** (2001) 1071-1083.

[87] R. Wintjens, J.M. Wieruszeski, H. Drobecq, P. Rousselot-Pailley, L. Buee, G. Lippens, and I. Landrieu, 1H NMR study on the binding of Pin1 Trp-Trp domain with phosphothreonine peptides. *J Biol Chem* **276** (2001) 25150-25156.

[88] D.M. Jacobs, K. Saxena, M. Vogtherr, P. Bernado, M. Pons, and K.M. Fiebig, Peptide binding induces large scale changes in inter-domain mobility in human Pin1. *J Biol Chem* **278** (2003) 26174-26182.

[89] A.T. Namanja, X.J. Wang, B. Xu, A.Y. Mercedes-Camacho, B.D. Wilson, K.A. Wilson, F.A. Etzkorn, and J.W. Peng, Toward flexibility-activity relationships by NMR spectroscopy: dynamics of Pin1 ligands. *J Am Chem Soc* **132** (2010) 5607-5609.

[90] A.Y. Mercedes-Camacho, and F.A. Etzkorn, Enzyme-linked enzyme-binding assay for Pin1 WW domain ligands. *Anal Biochem* **402** (2010) 77-82.

[91] X.Z. Zhou, O. Kops, A. Werner, P.J. Lu, M. Shen, G. Stoller, G. Kullertz, M. Stark, G. Fischer, and K.P. Lu, Pin1-dependent prolyl isomerization regulates dephosphorylation of Cdc25C and tau proteins. *Mol Cell* **6** (2000) 873-883.

[92] G. Ayala, D. Wang, G. Wulf, A. Frolov, R. Li, J. Sowadski, T.M. Wheeler, K.P. Lu, and L. Bao, The prolyl isomerase Pin1 is a novel prognostic marker in human prostate cancer. *Cancer Res* **63** (2003) 6244-6251.

[93] L. Bao, A. Kimzey, G. Sauter, J.M. Sowadski, K.P. Lu, and D.G. Wang, Prevalent overexpression of prolyl isomerase Pin1 in human cancers. *Am J Pathol* **164** (2004) 1727-1737.

[94] S. Esnault, Z.J. Shen, and J.S. Malter, Pinning down signaling in the immune system: the role of the peptidyl-prolyl isomerase Pin1 in immune cell function. *Crit Rev Immunol* **28** (2008) 45-60.

[95] Q. Ding, L. Huo, J.Y. Yang, W. Xia, Y. Wei, Y. Liao, C.J. Chang, Y. Yang, C.C. Lai, D.F. Lee, C.J. Yen, Y.J. Chen, J.M. Hsu, H.P. Kuo, C.Y. Lin, F.J. Tsai, L.Y. Li, C.H. Tsai, and M.C. Hung, Down-regulation of myeloid cell leukemia-1 through inhibiting Erk/Pin 1 pathway by sorafenib facilitates chemosensitization in breast cancer. *Cancer Res* **68** (2008) 6109-6117.

[96] M. Fukuchi, Y. Fukai, M. Sohda, T. Miyazaki, M. Nakajima, T. Inose, N. Tanaka, K. Tsukada, H. Kato, and H. Kuwano, Expression of the prolyl isomerase Pin1 is a useful indicator of sensitivity to chemoradiotherapy in advanced esophageal squamous cell carcinoma. *Oncol Rep* **21** (2009) 853-859.

[97] H.D. Campbell, G.C. Webb, S. Fountain, and I.G. Young, The human PIN1 peptidyl-prolyl cis/trans isomerase gene maps to human chromosome 19p13 and the closely related PIN1L gene to 1p31. *Genomics* **44** (1997) 157-162.

[98] G.M. Wulf, A. Ryo, G.G. Wulf, S.W. Lee, T. Niu, V. Petkova, and K.P. Lu, Pin1 is overexpressed in breast cancer and cooperates with Ras signaling in increasing the transcriptional activity of c-Jun towards cyclin D1. *EMBO J* **20** (2001) 3459-3472.

[99] A. Ryo, Y.C. Liou, K.P. Lu, and G. Wulf, Prolyl isomerase Pin1: a catalyst for oncogenesis and a potential therapeutic target in cancer. *J Cell Sci* **116** (2003) 773-783.

[100] G.M. Wulf, Y.C. Liou, A. Ryo, S.W. Lee, and K.P. Lu, Role of Pin1 in the regulation of p53 stability and p21 transactivation, and cell cycle checkpoints in response to DNA damage. *J Biol Chem* **277** (2002) 47976-47979.

[101] T.H. Lee, A. Tun-Kyi, R. Shi, J. Lim, C. Soohoo, G. Finn, M. Balastik, L. Pastorino, G. Wulf, X.Z. Zhou, and K.P. Lu, Essential role of Pin1 in the regulation of TRF1 stability and telomere maintenance. *Nat Cell Biol* **11** (2009) 97-105.

[102] P.J. Lu, G. Wulf, X.Z. Zhou, P. Davies, and K.P. Lu, The prolyl isomerase Pin1 restores the function of Alzheimer-associated phosphorylated tau protein. *Nature* **399** (1999) 784-788.

[103] J. Lim, M. Balastik, T.H. Lee, K. Nakamura, Y.C. Liou, A. Sun, G. Finn, L. Pastorino, V.M. Lee, and K.P. Lu, Pin1 has opposite effects on wild-type and P301L tau stability and tauopathy. *J Clin Invest* **118** (2008) 1877-1889.

[104] N.Y. Lee, H.K. Choi, J.H. Shim, K.W. Kang, Z. Dong, and H.S. Choi, The prolyl isomerase Pin1 interacts with a ribosomal protein S6 kinase to enhance insulin-induced AP-1 activity and cellular transformation. *Carcinogenesis* **30** (2009) 671-681.

[105] M.M. Zita, I. Marchionni, E. Bottos, M. Righi, G. Del Sal, E. Cherubini, and P. Zacchi, Post-phosphorylation prolyl isomerisation of gephyrin represents a mechanism to modulate glycine receptors function. *Embo J* **26** (2007) 1761-1771.

[106] J.W. Hong, M.S. Ryu, and I.K. Lim, Phosphorylation of serine 147 of tis21/BTG2/pc3 by p-Erk1/2 induces Pin-1 binding in cytoplasm and cell death. *J Biol Chem* **280** (2005) 21256-21263.

[107] P. Rudrabhatla, Y.L. Zheng, N.D. Amin, S. Kesavapany, W. Albers, and H.C. Pant, Pin1-dependent prolyl isomerization modulates the stress-induced phosphorylation of high molecular weight neurofilament protein. *J Biol Chem* **283** (2008) 26737-26747.

[108] K. Takahashi, C. Uchida, R.W. Shin, K. Shimazaki, and T. Uchida, Prolyl isomerase, Pin1: new findings of post-translational modifications and physiological substrates in cancer, asthma and Alzheimer's disease. *Cell Mol Life Sci* **65** (2008) 359-375.

[109] S. Esnault, L.A. Rosenthal, Z.J. Shen, C.J. Westmark, R.L. Sorkness, and J.S. Malter, Thymic stromal lymphopoietin expression in allergic pulmonary inflammation is Pin1-dependent. *J Allergy Clin Immunol* **121** (2008) 1289-1290.

[110] K. Watashi, M. Khan, V.R. Yedavalli, M.L. Yeung, K. Strebel, and K.T. Jeang, Human immunodeficiency virus type 1 replication and regulation of APOBEC3G by peptidyl prolyl isomerase Pin1. *J Virol* **82** (2008) 9928-9936.

[111] Z.J. Shen, S. Esnault, L.A. Rosenthal, R.J. Szakaly, R.L. Sorkness, P.R. Westmark, M. Sandor, and J.S. Malter, Pin1 regulates TGF-beta1 production by activated human and murine eosinophils and contributes to allergic lung fibrosis. *J Clin Invest* **118** (2008) 479-490.

[112] K. Inoue, H. Takano, and Y. Kumagai, Pin1 blockade in asthma by naphthoquinone? *J Allergy Clin Immunol* **121** (2008) 1064; author reply 1065.

[113] T. Uchida, M. Takamiya, M. Takahashi, H. Miyashita, H. Ikeda, T. Terada, Y. Matsuo, M. Shirouzu, S. Yokoyama, F. Fujimori, and T. Hunter, Pin1 and Par14 peptidyl prolyl isomerase inhibitors block cell proliferation. *Chem Biol* **10** (2003) 15-24.

[114] X.J. Wang, B. Xu, A.B. Mullins, F.K. Neiler, and F.A. Etzkorn, Conformationally locked isostere of phosphoSer-cis-Pro inhibits Pin1 23-fold better than phosphoSer-trans-Pro isostere. *J Am Chem Soc* **126** (2004) 15533-15542.

[115] Y.S. Zhang, Inhibitors targeting the enzymatic activity and biological function of Pin1. *Mini-Reviews in Organic Chemistry* **1** (2004) 359-366.

[116] D. Wildemann, F. Erdmann, B.H. Alvarez, G. Stoller, X.Z. Zhou, J. Fanghanel, M. Schutkowski, K.P. Lu, and G. Fischer, Nanomolar inhibitors of the peptidyl prolyl cis/trans isomerase Pin1 from combinatorial peptide libraries. *J Med Chem* **49** (2006) 2147-2150.

[117] S. Zhao, and F.A. Etzkorn, A phosphorylated prodrug for the inhibition of Pin1. *Bioorg Med Chem Lett* **17** (2007) 6615-6618.

[118] L. Hennig, C. Christner, M. Kipping, B. Schelbert, K.P. Rucknagel, S. Grabley, G. Kullertz, and G. Fischer, Selective inactivation of parvulin-like peptidyl-prolyl cis/trans isomerases by juglone. *Biochemistry* **37** (1998) 5953-5960.

[119] C. Fila, C. Metz, and P. van der Sluijs, Juglone inactivates cysteine-rich proteins required for progression through mitosis. *J Biol Chem* **283** (2008).

[120] M. Braun, A. Hessamian-Alinejad, B.F. de Lacroix, B.H. Alvarez, and G. Fischer, Novel spiroannulated 3-benzofuranones. synthesis and inhibition of the human peptidyl prolyl cis/trans isomerase Pin1. *Molecules* **13** (2008) 995-1003.

[121] T. Liu, Y. Liu, H.Y. Kao, and D. Pei, Membrane permeable cyclic peptidyl inhibitors against human Peptidylprolyl Isomerase Pin1. *J Med Chem* **53** (2010) 2494-2501.

[122] S. Daum, F. Erdmann, G. Fischer, B. Feaux de Lacroix, A. Hessamian-Alinejad, S. Houben, W. Frank, and M. Braun, Aryl indanyl ketones: efficient inhibitors of the human peptidyl prolyl cis/trans isomerase Pin1. *Angew Chem Int Ed Engl* **45** (2006) 7454-7458.

[123] S. Daum, C. Lucke, D. Wildemann, and C. Schiene-Fischer, On the benefit of bivalency in Peptide ligand/pin1 interactions. *J Mol Biol* **374** (2007) 147-161.

[124] C. Smet, W.J. M., L. Buee, I. Landrieu, and G. Lippens, Regulation of Pin1 peptidyl-prolyl cis/trans isomerase activity by its WW binding module on a multi-phosphorylated peptide of Tau protein. *FEBS Lett* **579** (2005) 4159-4164.

[125] G.G. Xu, and F.A. Etzkorn, Pin1 as an anticancer drug target. *Drug News Perspect* **22** (2009) 399-407.

[126] C. Smet, J.F. Duckert, J.M. Wieruszeski, I. Landrieu, L. Buee, G. Lippens, and B. Deprez, Control of protein-protein interactions: structure-based discovery of low molecular weight inhibitors of the interactions between Pin1 WW domain and phosphopeptides. *J Med Chem* **48** (2005) 4815-4823.

[127] B. Wu, M.F. Rega, J. Wei, H. Yuan, R. Dahl, Z. Zhang, and M. Pellecchia, Discovery and binding studies on a series of novel Pin1 ligands. *Chem Biol Drug Des* **73** (2009) 369-379.

[128] W.Q. Liu, M. Vidal, N. Gresh, B.P. Roques, and C. Garbay, Small peptides containing phosphotyrosine and adjacent alphaMe-phosphotyrosine or its mimetics as highly potent inhibitors of Grb2 SH2 domain. *J Med Chem* **42** (1999) 3737-3741.

[129] E. Kaiser, R.L. Colescott, C.D. Bossinger, and P.I. Cook, Color test for detection of free terminal amino groups in the solid-phase synthesis of peptides. *Anal Biochem* **34** (1970) 595-598.

[130] T. Vojkovsky, Detection of secondary amines on solid phase. *Pept Res* **8** (1995) 236-237.

[131] S. Steinberg, and J.L. Bada, Diketopiperazine formation during investigations of amino acid racemization in dipeptides. *Science* **213** (1981) 544-545.

[132] J.K. Wang, J.L. Li, M.L. Li, D. Hua, and H.M. Chen, Assay of DNA-binding proteins with a dsDNA-coupled plate. *Clin Biochem* **39** (2006) 167-175.

[133] G.G. Xu, and F.A. Etzkorn, Design and synthesis of amine and ketone inhibitors of Pin1. *Abstract. 235th ACS Nat. Mtg., New Orleans, LA, US, April 6-10* (2008) BIOL-057.

[134] X.R. Chen, and F.A. Etzkorn, Three stereoisomers of Ac-pSer-Y[(Z)CH=C]-Pip-2-(2-naphthyl)ethylamine as inhibitors of Pin1. *Abstracts of Papers, 238th ACS National Meeting, Washington, DC, US, August 16-20, 2009* (2009) ORGN-286.

[135] P.J. Munson, LIGAND: a computerized analysis of ligand binding data. *Methods Enzymol* 92 (1983) 543-576.

[136] A. Lal, S.R. Haynes, and M. Gorospe, Clean Western blot signals from immunoprecipitated samples. *Mol Cell Probes* **19** (2005) 385-388.

[137] D. Horakova, M. Rumlova, I. Pichova, and T. Ruml, Luminometric method for screening retroviral protease inhibitors. *Anal Biochem* **345** (2005) 96-101.

[138] M.B. Yaffe, and S.J. Smerdon, PhosphoSerine/threonine binding domains: you can't pSERious? *Structure* **9** (2001) R33-38.

[139] N.G. Bowery, Allosteric Receptor Modulation in Drug Targeting, ISBN: 9780824727918. (2006).

[140] A.C. Foster, and J.A. Kemp, Glutamate- and GABA-based CNS therapeutics. *Curr Opin Pharmacol* **6** (2006) 7-17.

[141] M.A. Enoch, The role of GABA(A) receptors in the development of alcoholism. *Pharmacol Biochem Behav* **90** (2008) 95-104.

[142] G. Fischer, H. Bang, E. Berger, and A. Schellenberger, Conformational specificity of chymotrypsin toward proline-containing substrates. *Biochim Biophys Acta* **791** (1984) 87-97.

[143] J.L. Kofron, P. Kuzmic, V. Kishore, E. Colon-Bonilla, and D.H. Rich, Determination of kinetic constants for peptidyl prolyl cis-trans isomerase by an improved spectroscopy assay. *Biochemistry* **30** (1991) 6127-6134.

[144] M. Zimmerman, E. Yurewicz, and G. Patel, A New Fluorogenic Substrate for Chymotrypsin *Anal Biochemistry* **70** (1976) 258-262.

[145] A. Hamzé, J. Martinez, and J.F. Hernandez, Solid-Phase Synthesis of Arginine-Containing Peptides and Fluorogenic Substrates Using a Side-Chain Anchoring Approach. *J. Org. Chem.* **69** (2004) 8394–8402.

[146] B.S. Jursic, and P.K. Patel, Cyclodextrin assisted enantiomeric recognition of benzo[de]isoquinoline-1,3-dione derived amino acids. *Tetrahedron* **61** (2005) 919-926.

[147] T. Mori, M. Hidaka, Y.C. Lin, I. Yoshizawa, T. Okabe, S. Egashira, H. Kojima, T. Nagano, M. Koketsu, M. Takamiya, and T. Uchida, A dual inhibitor against prolyl isomerase

Pin1 and cyclophilin discovered by a novel real-time fluorescence detection method. *Biochem Biophys Res Commun* **406** (2011) 439-443.

[148] T. Mori, S. Itami, T. Yanagi, Y. Tatara, M. Takamiya, and T. Uchida, Use of a real-time fluorescence monitoring system for high-throughput screening for prolyl isomerase inhibitors. *J Biomol Screen* **14** (2009) 419-424.

[149] A.J. Potter, S. Ray, L. Gueritz, C.L. Nunns, C.J. Bryant, S.F. Scrace, N. Matassova, L. Baker, P. Dokurno, D.A. Robinson, A.E. Surgenor, B. Davis, J.B. Murray, C.M. Richardson, and J.D. Moore, Structure-guided design of alpha-amino acid-derived Pin1 inhibitors. *Bioorg Med Chem Lett* **20** (2010) 586-590.

[150] I. Landrieu, C. Smet, J.M. Wieruszeski, A.V. Sambo, R. Wintjens, L. Buee, and G. Lippens, Exploring the molecular function of PIN1 by nuclear magnetic resonance. *Curr Protein Pept Sci* **7** (2006) 179-194.

[151]H.K. Arnold, X. Zhang, C.J. Daniel, D. Tibbitts, J. Escamilla-Powers, A. Farrell, S. Tokarz, C. Morgan, and R.C. Sears, The Axin1 scaffold protein promotes formation of a degradation complex for c-Myc. *EMBO J* **28** (2009) 500-512.

[152] J. Jeener, B.H. Meier, P. Bachmann, and R.R. Ernst, Investigation of exchange processes by two-dimensional NMR spectroscopy. *J Chem Phys* **71** (1979) 4546-4553.

[153] O. Heikkinen, R. Seppala, H. Tossavainen, S. Heikkinen, H. Koskela, P. Permi, and I. Kilpelainen, Solution structure of the parvulin-type PPIase domain of Staphylococcus aureus PrsA--implications for the catalytic mechanism of parvulins. *BMC Struct Biol* **9** (2009) 17.

[154] W.W. Cleland, Use of isotope effects to elucidate enzyme mechanisms. *CRC Crit Rev Biochem* **13** (1982) 385-428.

[155] W.W. Cleland, The use of isotope effects to determine enzyme mechanisms. *J Biol Chem* **278** (2003) 51975-51984.

[156] M.O. Doublet, A. Olomucki, A. Baici, and P.L. Luisi, Investigations on the kinetic mechanism of octopine dehydrogenase. 2. Location of the rate-limiting step for enzyme turnover. *Eur J Biochem* **59** (1975) 185-191.

[157] R.L. Stein, Mechanism of enzymatic and nonenzymatic prolyl cis-trans isomerization. *Adv Protein Chem* **44** (1993) 1-24.

[158] R.K. Harrison, and R.L. Stein, Substrate specificities of the peptidyl prolyl cis-trans isomerase activities of cyclophilin and FK-506 binding protein: evidence for the existence of a family of distinct enzymes. *Biochemistry* **29** (1990) 3813-3816.

[159] J.W. Peng, B.D. Wilson, and A.T. Namanja, Mapping the dynamics of ligand reorganization via 13CH3 and 13CH2 relaxation dispersion at natural abundance. *J Biomol NMR* **45** (2009) 171-183.